



**HAL**  
open science

# The Intersection of Metabolism and Neural Crest Cell Development

Nioosha Nekooie Marnany

► **To cite this version:**

Nioosha Nekooie Marnany. The Intersection of Metabolism and Neural Crest Cell Development. Human health and pathology. Université Paris-Est Créteil Val-de-Marne - Paris 12, 2022. English. NNT : 2022PA120066 . tel-04505814

**HAL Id: tel-04505814**

**<https://theses.hal.science/tel-04505814>**

Submitted on 15 Mar 2024

**HAL** is a multi-disciplinary open access archive for the deposit and dissemination of scientific research documents, whether they are published or not. The documents may come from teaching and research institutions in France or abroad, or from public or private research centers.

L'archive ouverte pluridisciplinaire **HAL**, est destinée au dépôt et à la diffusion de documents scientifiques de niveau recherche, publiés ou non, émanant des établissements d'enseignement et de recherche français ou étrangers, des laboratoires publics ou privés.

Ecole doctorale Sciences de la vie et de la santé

Thèse de Doctorat, spécialité : Biologie cellulaire et moléculaire

Team “Biology of the neuromuscular system” – Headed by Frederic RELAIX – INSERM U955/IMRB,  
Faculté de Santé, Créteil, France

## **The Intersection of Metabolism and Neural Crest Cell Development**

**Nioosha NEKOOIE MARNANY**

Dirigée par Sylvie DUFOUR et co-dirigée par Jean-Loup DUBAND

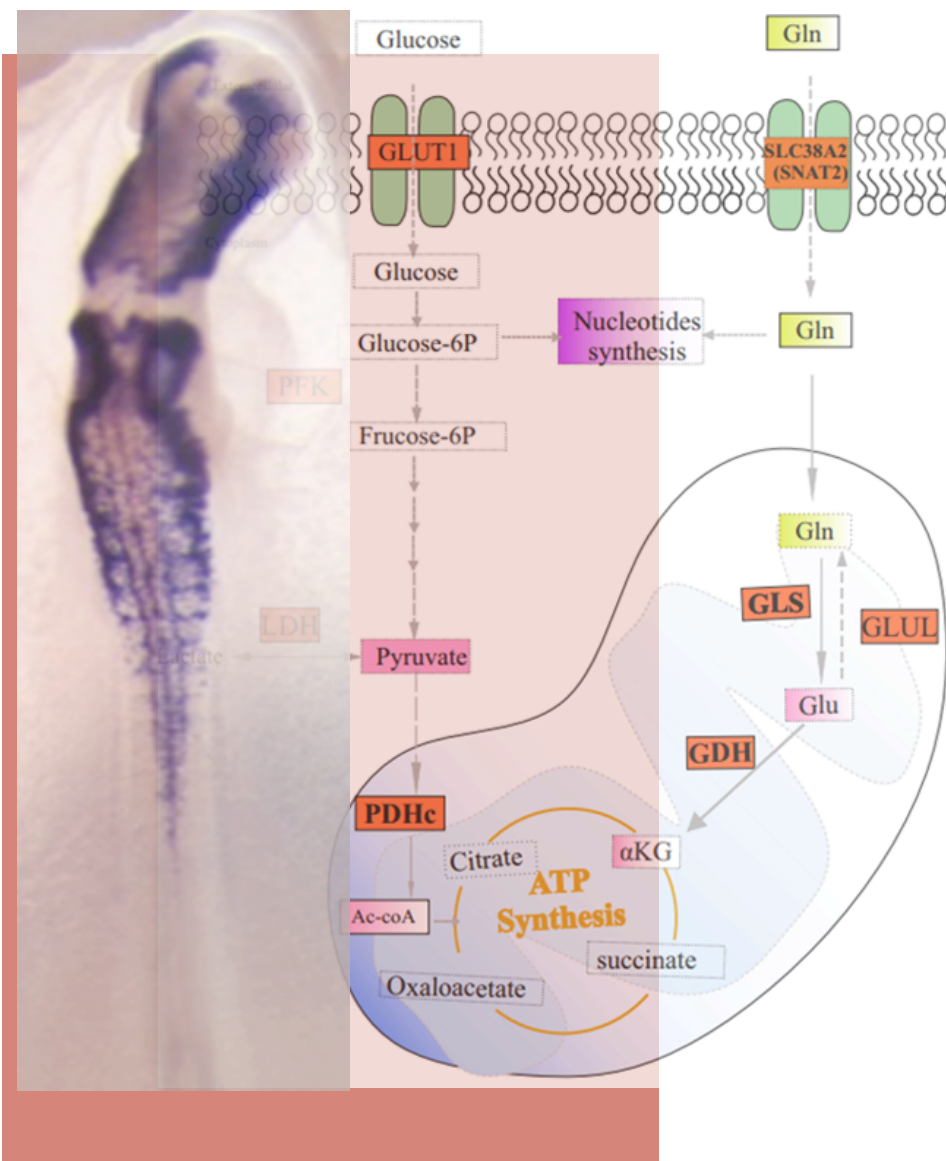
### **JURY :**

Chantal THIBERT	Rapportrice
Julien COURCHET	Rapporteur
Sophie CREUZET	Examinatrice
Roberta FORESTI	Examinatrice
Jean-Loup DUBAND	Co-directeur de thèse
Sylvie DUFOUR	Directrice de thèse

**Soutenue publiquement le 7 octobre 2022**

## The Intersection of Metabolism and Neural Crest Cell Development

Nioosha NEKOOIE MARNANY



## Summary

Metabolism as a keystone of stem cells' fate not only supplies demands for energy and precursor molecules but also has roles in chromatin remodeling. In vertebrate embryos, neural crest (NC) cells constitute a remarkable population of embryonic progenitors, which upon delamination from dorsal neural tube, extensive migration and differentiation give rise to both neural/neuronal and mesenchymal derivatives. The developmental potential of NC cells necessitates epigenetic remodeling and environmental cues. Accordingly, the intersection of metabolism and NC plasticity will provide critical insights into the regulation of NC cell identity and development. Thus, I intended to figure out the metabolism role in the developmental aspect of one sub-population of NC cells, trunk type. The first part of my study resulted in a general view of the metabolic impacts on all developmental NC steps. I evidenced that glucose oxidation is a pivotal metabolic profile governing NC delamination, adhesion, migration, proliferation, maintenance of stemness, and widespread differentiation. Given the incidence of G1/S transition upon EMT in trunk NC cells, the inhibition of pentose phosphate pathway (PPP) was unable to influence the NC delamination, suggesting a metabolic adaptation to maintain developmental steps and survival. Hence, In the next step, I sought to appreciate how metabolic pathways integrate into the NC delamination. The rewiring of glycolysis pathway under PPP suppression in delaminating stage provided support for multi metabolic pathways recruited by NC progenitors in response to the metabolic stress. My study also elucidated the metabolic reprogramming from PPP to glucose oxidation in trunk NC cells, aligned with delaminating to migratory transition of these cells. Additionally, besides glucose, glutamine had a prominent role in pluripotent acquisition and delamination of NC progenitors that triggers the nuclear localization of glutaminase (GLS) upon EMT step. Therefore, the nuclear GLS localization of pre-migratory NC cells in delaminating stage suggests the gene regulatory function for GLS. Altogether, my results indicated the intersection of metabolism and NC reprogramming from pluripotent step to the NC commitment, defined respectively by promoted PPP and nuclear localization of GLS to glucose based OXPHOS phenotype with cytoplasmic GLS localization. Moreover, the possible interaction between GLS and B-catenin fostered the new concept about the contribution of GLS to Wnt signaling, holding promise for understanding the etiology of many neurocristopathies.

*Key words: neural crest cells, pluripotency, delamination, metabolism, glutaminase, OXPHOS, EMT*

## Acknowledgment

My life in France has been a real milestone involving enormous felicity, upset, forward and reverse. Looking back, I find myself among sympatric and supportive persons who tried to provide my success and relief. I would like to express my deepest appreciation to my excellent mentors, Dr. Sylvie Dufour and Dr. Jean-Loup Duband for their invaluable patience, support, and feedback. It was November 2017 when I joined équipe 6 of IMRB as a master2 student. The board of this group was comprised of Dr. Sylvie Dufour as the head and her assistant Dr. Jean-Loup Duband, as well as two other junior researchers: Dr. Redouane Fodil and Dr. Sophie Fereol. I felt warmly welcomed by them which facilitated my integration into the group. During my internship, Sylvie and Jean-Loup tried to introduce me an unknown world of embryonic biology inspiring me to effort for granting 3 years award of “*école doctorale*”. Two awesome mentors with two different views of thinking and support made it possible for me to thrive. Jean-Loup was shrewd in his advice. He encouraged me to express myself, my ideas and fight for that. We had wonderful discussions on diverse subjects from philosophy, politics, fiction, books, and movies during the time interval of experiments. Sylvie also helped me to be more creative and independent. Her precise attention to details provoked me to have a scientific view. I have been privileged to have these insightful mentors who supported me in all aspects of my life as like as my parents. Thanks should also go to Redouane and Sophie who were in charge of supportive engineer in our group besides of directing their projects. Redouane helped me by software programming to be able to track crazy cells (Neural crest cells). So you can imagine how we feel as a family member.

In 2020 our team merged to team “Biology of the neuromuscular system” group headed by Pr. Frederic Relaix. It was a great chance for me to attend the lab meetings of that group and obtain more information about different research subjects. I’m extremely grateful to Pr. Frédéric Relaix for his continuous support that covering of the whole project was impossible without his financial support during these years. I am also thankful to Lila Bendameche who helped me a lot with the signing of my contracts and renting a residence in Paris or the countryside.

I would like to extend my sincere thanks to Pr. Roberta Foresti and Dr. Roberto Motterlini who were our collaborators in the project. The amazing discussions we have had since 2017 made me interested more and more in metabolism and motivated me to follow this field for my future. Sharp and brilliant ideas of Roberta evoked me to be insightful and pay attention to the details.

I also could not have undertaken this journey without my defense committee, who generously provided knowledge and expertise. I appreciate Dr. Chantal Thibert, Dr. Julien Courchet, Dr. Sophie Creuzet and Pr. Roberta Foresti as the president of committee.

Words cannot express my gratitude to my parents whom I owe for my life. They trained me to fend for myself and be liberal regardless of community customs. Last, many thanks to my brothers: Ali and Aras, my friends: Atena, Guitti, Maziar, Nazli, Hossein, Negar, Kamran, Shahla and Pooja who try to make me happy and joyful.

# Table of Contents

I. Introduction .....	1
Forewords .....	2
Background .....	4
1) Metabolism: An Important Player in Cellular Fate .....	5
1.1) Bioenergetic function of cellular metabolism.....	5
1.2) Metabolic signaling function .....	12
1.2.a) <i>Metabolites as rate-limiting substrates for epigenetic and post translational modifications</i> .....	12
1.2.b) <i>Post-translational modification (PTM)</i> .....	18
1.3) Non-canonical moonlighting functions of metabolic enzymes.....	19
2) Mechanical Cues: an Intermediate between Metabolism and Cell Fitness.....	21
3) The Emerging Roles of Metabolism during Development .....	24
3.1) Metabolism and pluripotent stem cell (PSC) in context .....	27
3.2) Nutrient Availability and PSC .....	33
4) Neural Crest Cells .....	35
A brief overview of neural crest development .....	37
4.1) The Neural Crest Gene Regulatory Network .....	40
4.2) Migratory Neural Crest Cells .....	48
4.3) Metabolic Regulation of NC Development .....	50
Objective .....	51
II. Results.....	52
Part A: Neural crest Development Relies on Glucose Oxidation .....	53
1. Multiple Metabolic Pathways are Mobilized during Trunk NC Dispersion .....	55
2. Nutrient Availability Affects Trunk NC Dispersion .....	57
3. Metabolic Profiling of NCC Reveals a Typical OXPHOS Signature during Migration .....	60
4. Expressions of Glucose Transporter and Glycolysis Enzymes are Regulated at the Time of Migration ...	65
5. Glucose Metabolism Regulates Expression of EMT Genes during Delamination .....	67
6. Glucose Metabolism is Crucial for Locomotion .....	69
7. Glucose Metabolism Coordinates Substrate and Cell Adhesions .....	72
8. Glucose Metabolism is Required for Sustained Proliferation .....	74
9. Fate Decision is Dictated by Exogenous Nutrient Inputs .....	76

Part B: Nuclear Translocation of Glutaminase (GLS) Aligned with Metabolic Remodeling Steers Neural Crest Delamination .....	80
1. Metabolic Remodeling Incorporates into the Transition from Delamination to Migration Steps of Neural Crest Development: .....	82
2. Glucose Metabolism Modulates Metabolic States during Neural Crest Development .....	87
3. Glutamine Plays a Profound Role in NC Production: .....	91
4. GLS has a Non-Enzymatic Function to Support NC Production: .....	95
5. Nuclear Expression of GLS in NC Cells .....	99
6. Contribution of GLS to Wnt Signaling .....	102
III. Discussion and Perspective .....	105
Part A: Neural Crest Development Relies on Glucose Oxidation .....	106
Part B: Nuclear Translocation of Glutaminase (GLS) Aligned with Metabolic Remodeling Steers Neural Crest Delamination .....	111
Postface .....	115
IV. Materials and Methods.....	116
Reagents .....	117
Cell Culture .....	117
Cellular Bioenergetic Analyses .....	119
Seahorse analysis .....	119
Presens analysis .....	120
Intracellular ATP and lactate measurement .....	120
Intracellular glutamine and glutamate measurement .....	120
Fluorescence Labeling of NCC Cultures .....	121
In Situ Hybridizations for mRNA Detection on NCC Primary Cultures and Whole Mount Embryos ....	122
RNA Quantification by Quantitative RT-PCR Analyses .....	123
Whole mount immunolabeling .....	125
Cell Proliferation Assay .....	125
Cell Locomotion Assays .....	126
Proximity Ligations Assay (PLA) .....	126
Statistical Methods.....	127
References .....	128
V. Annex.....	142
Establishing primary cultures of trunk neural crest cells (first paper) .....	143

Glucose oxidation and nutrient availability drive neural crest cells development (submitted version-Part A of result) .....	168
Résumé .....	210
Abstract.....	211

## Table of Figures

### I. Introduction

Fig. 1. An overview of glucose metabolism .....	6
Fig. 2. Glucose and glutamine are critical inputs in major anabolic pathways.....	8
Fig. 3. The per capita energy consumption of people across the countries.....	11
Fig. 4. Metabolic regulation of chromatin marks .....	17
Fig. 5. Metabolic Enzymes Moonlighting in the Nucleus. ....	20
Fig. 6. ECM mechanosensing and mechanotransduction mechanisms. ....	23
Fig. 7. Graded glycolytic activity in the presomitic mesoderm .....	26
Fig. 8. Transitions between human pluripotent stem cell (PSC) states.....	29
Fig. 9. The neural crest is a multipotent cell population .....	36
Fig. 10. Molecular players involved in EMT.....	39
Fig. 11. GRN module controlling the formation of the neural plate border .....	42
Fig. 12. A GRN controls neural crest formation.....	44
Fig. 13. Bmp/Wnt signaling regulates trunk neural crest cell delamination .....	47

### II. Results

#### Part A

Fig. 1. Multiple metabolic pathways are mobilized during trunk NCC dispersion. ....	57
Fig. S1. Effect of the metabolic inhibitors on NC dispersion .....	59
Fig. S2. Characterization of NCC locomotory capacity (A- B) .....	60
Fig. 2. Metabolic profiling of NCC reveals a typical OXPHOS signature .....	62
Fig. S3. Morphological features of mitochondria networks in NCC cultured .....	64
Fig. 3. Expressions of glucose transporter and glycolytic enzymes .....	66
Fig. 4. Glucose Metabolism Regulates Expression of EMT Genes. ....	68
Fig. 5. Glucose Metabolism is crucial for NCC locomotion(A-E) .....	70
Fig. S2. Characterization of NCC locomotory capacity (C, D) .....	72

Fig. 5 (F-I) Glucose Metabolism coordinates substrate and cell adhesions. ....	73
Fig. 6. Glucose metabolism is required for NCC sustained proliferation .....	75
Fig. 7. Glucose metabolism is required for NCC pluripotency .....	77
Fig. 8. NCC fate decision is biased by exogenous nutrient inputs .....	79

## Part B

Fig. 1. Integration of metabolic profiles into NC development .....	83
Fig. S1. Drawing figure of NT dissection and mitostress (García-Castro <i>et al.</i> ) .....	85
Fig. 2. Role of glucose metabolism in NC development .....	88
Fig. S1. Glycolytic capacity and 6-AN effect (D-F) .....	90
Fig. 3. Pivotal role of glutamine in NC delamination .....	92
Fig. S2. The effect of glutamine or glucose deprivation .....	93
Fig. 4. Putative non-enzymatic role of GLS in NC delamination .....	96
Fig. S3. Glutamate effect on NC identity .....	98
Fig. 5. Nuclear localization of GLS in delaminating NC cells .....	100
Fig. 6. Model for intersection of metabolism and NC development .....	101
Fig. 7. Putative contribution of GLS in Wnt signaling .....	103

اسرار ازل را نه تو دانی و نه من

این حل معما نه تو دانی و نه من

هست از پس پرده گفتگوی من و تو

چون پرده برافتاد نه تو مانی و نه من

خیام

**“The secrets eternal neither you know nor I**

**And answer to the riddle neither you know nor I**

**Behind the veil there is much talk about us, why**

**When the veil falls, neither you remain nor I”.**

**Khayyam<sup>1</sup>**

---

<sup>1</sup> Khayyam (1048- 1131) was an Iranian astronomer, astrologer, physician, philosopher, and mathematician: he made outstanding contributions in algebra. His poetry is better known in the West than any other non-Western poet. He compiled astronomical tables and contributed to calendar reform and discovered a geometrical method of solving cubic equations by intersecting a parabola with a circle.

# **I. Introduction**

## Foreword

The world has encountered global energy problems in recent years. The link between energy access and greenhouse gas emissions has recently received the most attention from experts, which compromises our natural environment as a consequence of climate change. In addition, hundreds of millions of people have no access to sufficient energy entirely. Nevertheless, the war in Europe has exerted a negative influence over energy transition since February 2022, leading to the emergence of a true energy crisis in the world (Turnbull, 2021) (<https://ourworldindata.org/worlds-energy-problem>).

Energy fuels many such services. Thus, 'energy system' harnesses resources and subsequently transforms them into 'energy carriers' utilized in appliances and machinery to provide those services. Indeed, at one end of the system, there are the primary energy resources, like coal, crude oil, uranium, wind, and others. On the other end, there are energy services, such as lighting, heating, motive power, telecommunication, IT, and others. Energy services widely range from providing motive power and heat in industries, communications technology in commerce, to appliances in households. Therefore, the development of the socio-economy is impossible without energy services. To align with this aim, we require affordable and accessible energy services to meet actual needs. On the other hand, sustainable development relies on the energy system, which in turn, impacts and interacts with the economy, environment, and society (Giovannucci *et al.*, 2012).

To solve the current energy problems, two strategies are required: 1) Maximize energy efficiency and minimize energy use, and 2) Develop new sources of clean energy to target both greenhouse gas emissions and energy access of people (Chu, 2008). But the main factors like the technology change, the population, and economic growth, altogether enhance global energy consumption. Moreover, polarized and politicized views typically dominate the energy debate at national, regional and global levels (Giovannucci *et al.*, 2012). Therefore, the key question rises about how we can tackle the current energy crisis to access affordable and sustainable energy for the whole world.

Blaise Pascal, a French scientist, inventor, and philosopher, has the famous book called “*Les Pensées*” which brings us between the infinitely large and infinitively small worlds: “compared to the universe, human is infinitely small. However, compared to *un ciron*, humans are infinitely large”. So, it would be insightful to follow the ideas of B. Pascal and increase the resolution of our observation to probe the solvation of energy problems at the cellular level as the journey into the inner world.

The aim of my thesis was in the frame of the above considerations, and I sought to investigate the energy services at the neural crest cells population as appliances. Thus, here, we follow two general topics: Metabolism in charge of cellular ‘energy-system’ and neural crest cells as the end-user of energy.

## Background

At the cellular level, similarly, the development of tissues and organs is not possible without energy suppliers. Cellular survival and growth are tightly dependent on metabolism, a chemical process, which shares similarities with “energy-carrier,” and converts nutrients to energy in cells as end-use appliances. Thus, cells necessitate catabolizing nutrients to generate ATP and reducing equivalents (NADH, FADH<sub>2</sub>) to sustain the basic cellular process. In addition, anabolic metabolisms convert nutrients into macromolecules like nucleic acids, lipids, and proteins, required for cell growth and proliferation. The growth of a unicellular organism is directly linked to nutrient availability, illustrated by a special cross-link between metabolism and cellular fitness (Vander Heiden *et al.*, 2009). This condition changes in a multicellular organism (metazoan) that cells must cooperate to share relatively constant nutrient supplies; and consequently, it leads to highly regulated metabolism by time and space to match context-dependent cellular demands (Vander Heiden and Deberardinis, 2017). Of note, either unicellular or multicellular, organisms must develop many mechanisms to sense and respond to food. Thus “metabolic signaling” is comprised of biochemical, physiological, and developmental pathways responsive to such cues (Blackstone, 2006).

First, let us start with the usual nutrients and energy production for cells.

## 1) Metabolism: An Important Player in Cellular Fate

### 1.1) Bioenergetic function of cellular metabolism

The bioenergetic function of metabolism is characterized by canonical metabolic activities to provide energy and/or cellular building blocks. Cells rely on two processes to produce energy in the form of ATP: glycolysis and oxidative phosphorylation (OXPHOS). Glucose is a fundamental substrate for central carbon metabolism driving both processes. The glycolysis pathway initiates the catalyzation of glucose through a series of cytosolic enzymes, eventually yielding two molecules of pyruvate (Fig 1). Through this enzymatic pathway, four net molecules ATP and two net molecules NADH are generated from each glucose molecule. Pyruvate, the end product of glycolysis, can be used in two ways: under anaerobic conditions, pyruvate is reduced to lactate that can be excreted to extracellular space, while under aerobic conditions pyruvate can deviate from reduction and go to the mitochondria where it is oxidatively decarboxylated into acetyl-CoA by pyruvate dehydrogenase complex (PDH) accompanied by generation of one NADH molecule (Fig 1). Acetyl-CoA then fulfils the Krebs cycle (TCA cycle), located inside the mitochondria. From each acetyl-CoA that gets into the TCA cycle, three molecules of NADH, one flavin adenine dinucleotide (FADH<sub>2</sub>) (part of the succinate dehydrogenase enzyme (SDH)), and one molecule of guanosine triphosphate (GTP) are produced. In the end, each glucose molecule generates four molecules of ATP, ten molecules of NADH, and two reduced FADH<sub>2</sub> (Pereira *et al.*, 2014). Consequently, OXPHOS as a critical pathway enables electrons donated from NADH and FADH<sub>2</sub> to flow down reduction potential gradients in the electronic transition chain (ETC) through the embedded inner mitochondrial membrane with protons, developing an electrochemical gradient. The transport of protons back across the membrane into the mitochondrial matrix is performed by ATP synthase, which links proton transport with ATP synthesis. Therefore, OXPHOS is a more efficient pathway to produce 36 ATP molecules per glucose versus 4 ATP molecules from glycolysis alone (Perestrelo *et al.*, 2018; Tsogtbaatar *et al.*, 2020). In addition to its role in energy production, glycolysis and the TCA cycle provide intermediates for other molecular pathways (Fig 1) (Pereira *et al.*, 2014; Miyazawa, Hidenobu and Aulehla, Alexander, 2018). On the other hand, it should be noted that many cells carry out

aerobic glycolysis (Warburg effect), using TCA mostly for precursor production not for ATP generation. This particular metabolic state, characterized by enhanced glycolytic pathway regardless of oxygen presence, can efficiently provide the metabolic demands for production of macromolecules, such as nucleic acids required for proliferation. Thus, it is reasonable that cells with excessive proliferation, including cancer cells and stem cells, present high rate of glycolysis as their metabolic phenotype (Vander Heiden *et al.*, 2009).

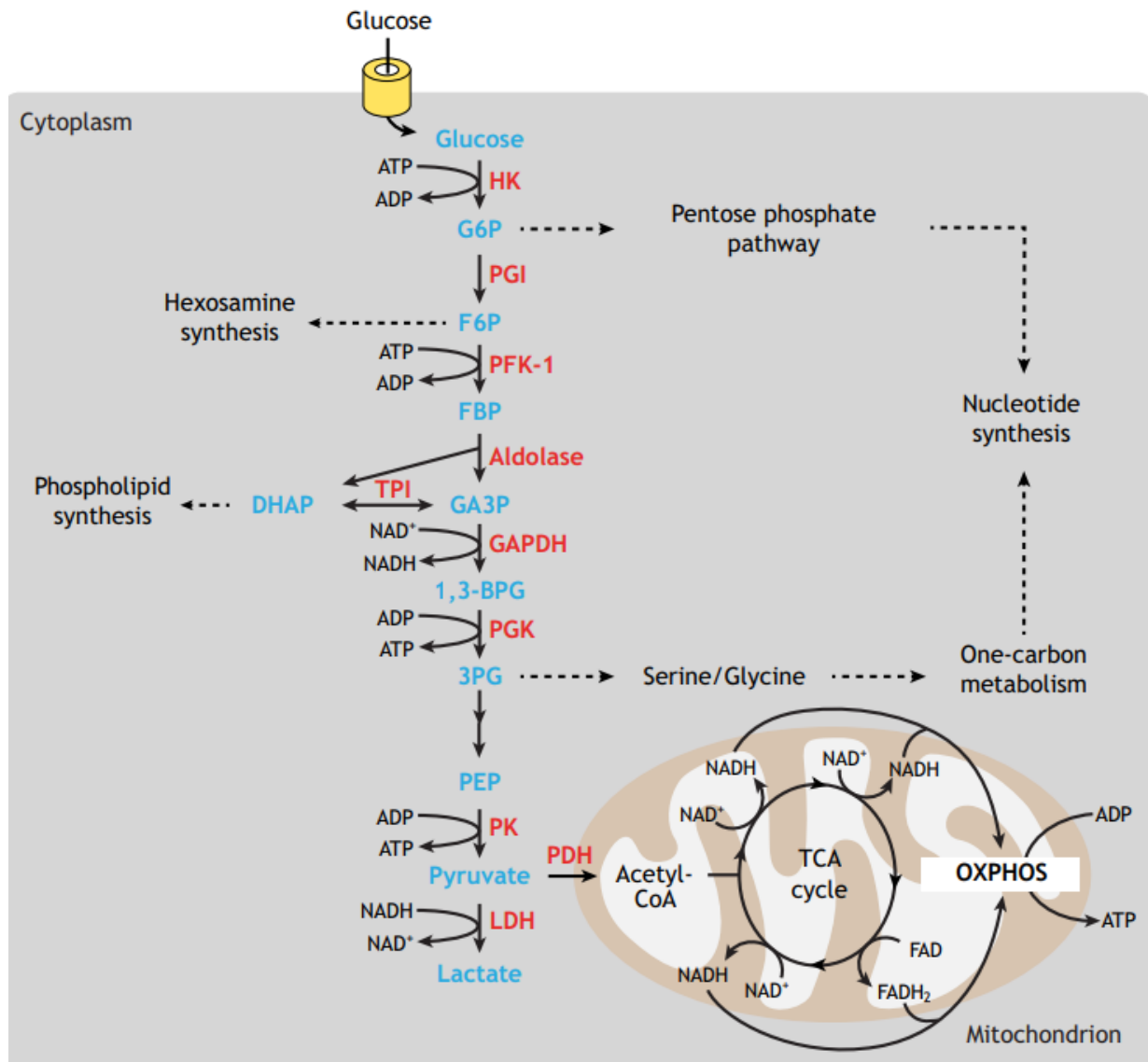


**Fig. 1. An overview of glucose metabolism.** Glucose, transported into cells via glucose transporters, is catabolized in a series of enzymatic reactions and eventually it terminates with pyruvate production. Pyruvate is then either converted into lactate or transported into mitochondria and metabolized into acetyl-CoA, fueling the TCA cycle. NADH and FADH<sub>2</sub>, produced through glycolysis and the TCA cycle, are used by the mitochondrial electron transport chain for generating a proton gradient, which drives OXPHOS for ATP production. Glycolytic metabolites (shown in blue) also feed into metabolic pathways that branch from glycolysis. These include the pentose phosphate pathway, the one-carbon metabolism pathway, and the hexosamine and phospholipid synthesis pathways. Enzymes are shown in red. 1,3-BPG, 1,3-bisphosphoglyceric acid; 3PG, 3-phosphoglyceric acid; DHAP, dihydroxyacetone phosphate; F6P, fructose 6-phosphate; G6P, glucose 6-phosphate; GA3P, glyceraldehyde 3-phosphate; HK, hexokinase; PEP, phosphoenolpyruvic acid; PGI, phosphoglucose isomerase; PK, pyruvate kinase; TPI, triose phosphate isomerase (Miyazawa, Hidenobu and Aulehla, Alexander, 2018).

**Glucose and Glutamine are crucial substrates for cells:** To build the biomass blocks, proliferative cells need to have raw materials for macromolecular synthesis. For this aim, they increase the uptake and catabolism of nutrients to generate the nucleic acids, lipids and proteins required for proliferation. Among nutrients, glucose and glutamine are the major sources of energy and reducing equivalents needed to assemble metabolic building blocks into macromolecules (Fig 2)(Fan *et al.*, 2013). Indeed, these two nutrients are representatives of gas and oil, known as fundamental sources of socio-economy, in the cellular system.

Beside ATP and NAD(P)H generation, glucose and glutamine provide precursors for biogenesis of non-essential amino acids required to sustain the synthesis of proteins. Additionally, glucose supplies ribose, and glutamine supplies essential sources of reduced nitrogen for nucleic acid biosynthesis. Moreover, de-novo lipid biosynthesis is contingent on production of glucose-derived acetyl-coA as the primary source of carbon, whereas the protein biosynthesis constructing most of cellular biomass is provided by combination of direct amino acid uptake and de novo synthesis of non-essential amino acids from glucose and glutamine. Therefore, a fundamental feature of proliferative cells in culture relies on the central role of glucose and glutamine in supporting anabolic growth (Hosios *et al.*, 2016; Intlekofer, A. M. and Finley, L. W., 2019). It is worth noting that different cellular demands and restricted available nutrients in metazoan cells force bioenergetic activity to be tightly regulated by time and space.

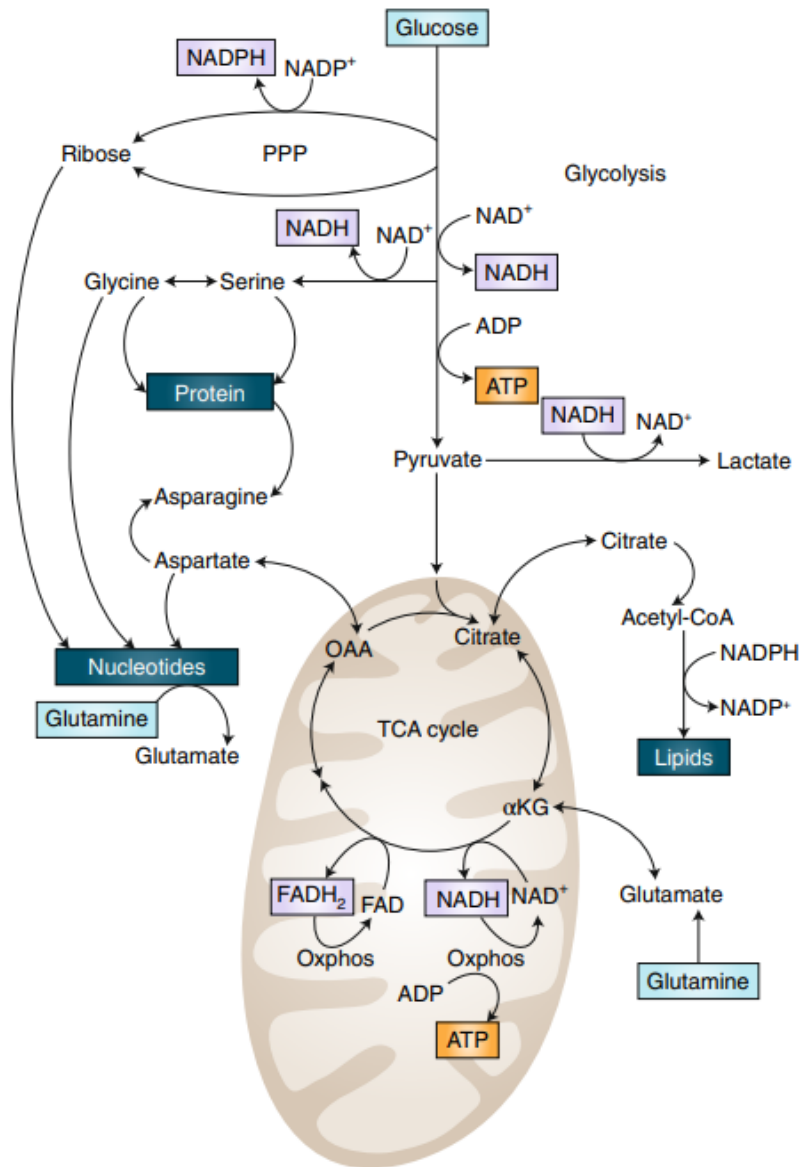


**Fig. 2. Glucose and glutamine are critical inputs in major anabolic pathways.** In proliferating cells, glucose and glutamine (blue) are taken up from the extracellular environment and catabolized through major metabolic pathways, including glycolysis, the pentose-phosphate pathway and the TCA cycle, and they provide the reducing equivalents (purple) and high energy carriers (ATP, red) required to synthesize major macromolecules. A subset of the non-essential amino acids synthesized from glucose and glutamine are shown. Reducing equivalents (NADH and FADH<sub>2</sub>) in the mitochondria fuel the electron-transport chain and enable synthesis of ATP through OXPHOS. TCA cycle intermediates such as citrate and oxaloacetate (OAA, converted to aspartate) likewise contribute to lipid and nucleotide biosynthesis, respectively (Intlekofer, A. M. and Finley, L. W., 2019).

**Metabolic regulation in time and space:** The energy metabolism dynamically alters in both aspects of time and space across intracellular or tissue levels, generating a new concept that metabolic activity is not homogenous within and between cells, against the general view of metabolism. A well-known example of dynamically metabolic activity is the brain where glucose metabolism is compartmentalized between neurons and astrocytes. The constant degradation

of an enzyme 6-phosphofructo-2-kinase/ fructose-2,6-bisphosphatase-3 (PFKB3) in neurons which is responsible to produce a potent allosteric activator of a key glycolytic enzyme phosphofructokinase 1 (PFK-1) causes a lower glycolytic activity of those cells rather than astrocytes (Herrero-Mendez, Angel *et al.*, 2009). A key interesting point is an intelligently metabolic compartmentalization between neurons and astrocytes. Such heterogeneous metabolic actions eventually generate a gradient of lactate, the end-product of glycolysis, from astrocytes to neurons that result in flowing lactate from astrocytes toward neurons (Mächler *et al.*, 2016). In neurons, lactate plays as an energy resource for ATP production through oxidation in the TCA cycle. The lactate shuttle between neurons and astrocytes displays an intelligent glucose utilization where neurons govern anabolic metabolism through pentose phosphate pathway (PPP) (Fig 1). In this condition, they maintain cellular redox balance due to NADPH production; and subsequently, they grab another extracellular source of energy (lactate) from their neighbors (Herrero-Mendez, Angel *et al.*, 2009). In other words, neurons indicate an economical and efficient energy utilization to meet both anabolic and bioenergetic demands.

The high-resolution approaches recently enabled the assessment of metabolic compartmentalization between mouse embryo and uterus through the midgestation period which is another example of such spatiotemporally regulated metabolism (Solmonson *et al.*, 2022). The isotope tracing leads to deciphering the diverse carbohydrate metabolism between embryo and placenta in the midgestation period. This period is identified by vascular maturation in the placenta and embryo, which leads to enhanced transfer of nutrients and oxygen from maternal circulation as fetal erythropoiesis. Interestingly, midgestation is a metabolically dynamic period in both placenta and embryo. Given the divergent cellular composition and functions, metabolomic distinctions caused the metabolic transition between gestational day (GD) 10.5 and GD11.5 in both tissues (Solmonson *et al.*, 2022). Indeed, purine and pyrimidine metabolisms are the most activated pathways in the embryo between GD10.5 and GD11.5, whereas, in the placenta, nitrogen and amino acid metabolism are in abundance that may be routed in a possible role of arginine in stimulating placental-fetal blood flow. Moreover, distinct transport kinetics for different nutrients vary from maternal blood to placenta and embryo. It is evidenced by rapid glucose transfer from maternal circulation to both embryo and placenta, while glutamine follows a slow pattern of transfer in embryo relative to placenta. Overall,

prominent consumption of maternal glutamine and glucose caused the rapid glucose-dependent purine synthesis (PPP) in embryos compared with placenta and ultimately distinct pattern of metabolic labeling between these tissues (Solmonson *et al.*, 2022).

On the large scale, if we compare spatiotemporal regulation of metabolism in organisms with the total energy consumption in the world, we can find a different pattern of total energy consumption across countries. It can reflect differences in population size that countries with lots of people inevitably consume more energy than tiny ones. But, if we measure the energy consumption per person, we reach another pattern that indicates a distinct consumption pattern of per capita energy in rich versus poor countries (Fig 3) (<https://ourworldindata.org/energy-production-consumption>). These data far demonstrate that polarized and politicized view typically dominate on energy debates that is really far from intelligent compartmentalization of metabolites in organs or cellular states.

## Energy use per person, 2020

Energy use not only includes electricity, but also other areas of consumption including transport, heating and cooking.

Our World  
in Data

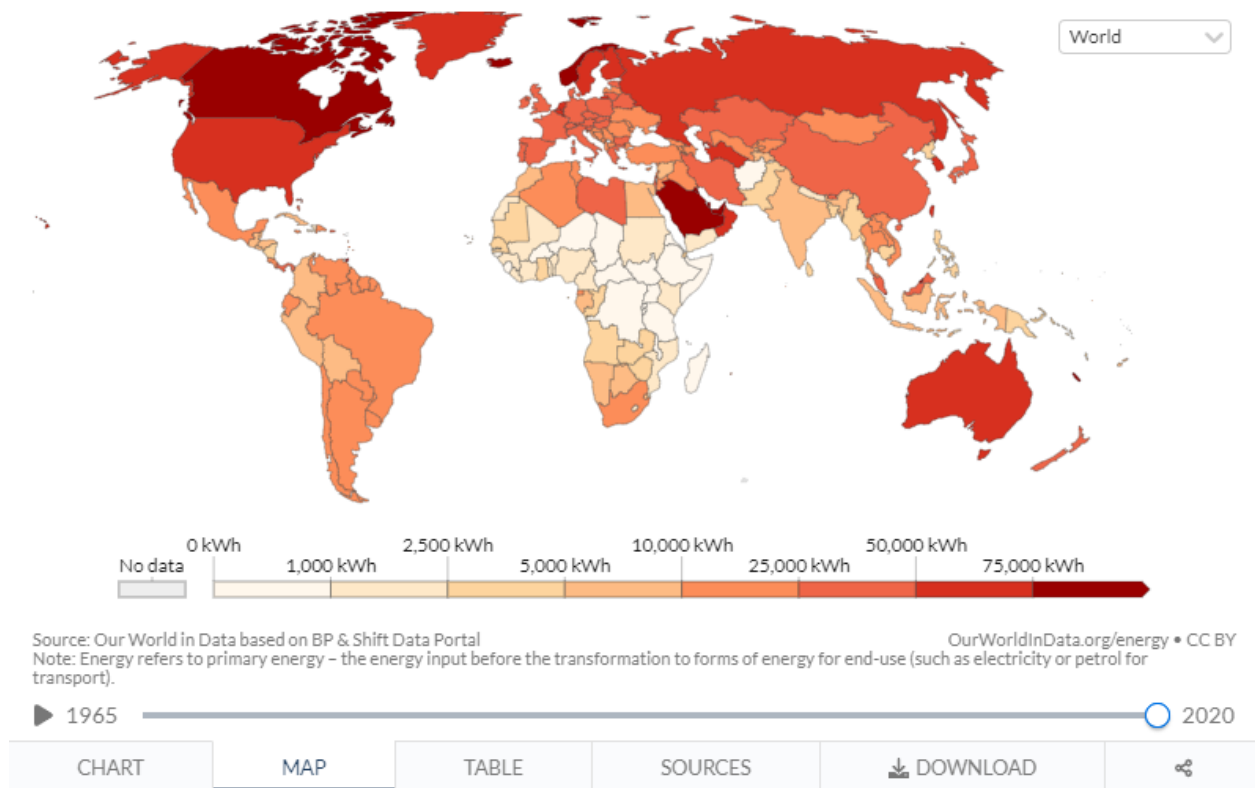


**Fig. 3. The per capita energy consumption of people across the countries.** The largest energy consumers include Iceland, Norway, Canada, the United States, and wealthy nations in the Middle East such as Oman, Saudi Arabia and Qatar. The average person in these countries consumes as much as 100 times more than the average person in some of the poorest countries. In fact, the true differences between the richest and poorest might be even greater. We do not have high-quality data on energy consumption for many of the world's poorest countries. This is because they often use very little commercially-traded energy sources (such as coal, oil, gas, or grid electricity) and instead rely on traditional biomass – crop residues, wood and other organic matter that is difficult to quantify. This means we often lack good data on energy consumption for the world's poorest (<https://ourworldindata.org/energy-production-consumption>).

## **1.2) Metabolic signaling function**

A key question emerging here is that how cells can regulate and sense their metabolic demands. Until now it has been argued that cells exploit some signaling pathways to enhance nutrient uptake and promote anabolic metabolic pathways, known as gatekeepers of anabolic metabolism. Indeed, growth factors activate receptor tyrosine-kinases engaging signaling pathways, in which Ras and phosphatidylinositol 3-kinase are involved and consequently activate downstream effectors like MEK (protein kinase kinase)/ERK, AKT and mTOR. Ultimately the activation of these signaling pathways results in lipid, protein and nucleic acid synthesis (Stine *et al.*, 2015; Intlekofer, A. M. and Finley, L. W., 2019). In addition, cells are endowed with energy sensor called AMP-activated protein kinase (AMPK) that senses energy stress by low ATP/AMP ratio, inducing enhanced catabolic and precluded anabolic pathways (Perestrelo *et al.*, 2018). These cellular signaling pathways are beyond the scope of my thesis work; and will not be further detailed here.

Beyond canonical functions including bioenergetic and anabolic roles (Fig. 2), metabolism regulates the cellular processes at various levels, ranging from effects on epigenetic modifications and post-translational modifications (PTM), to the regulation of mRNA transcription/translation and signaling pathways. In addition to known mechanisms, such as the activation of redox signaling by reactive oxygen species (ROS), an emerging view emphasizes the roles of metabolites as rate-limiting substrates for epigenetic modifications and PTM. Furthermore, it is increasingly understood that metabolic enzymes also play non-bioenergetic 'moonlighting' functions, non-enzymatic nuclear roles of glycolytic enzymes (Boukouris *et al.*, 2016). These non-canonical signaling functions of metabolism can establish intriguing and direct links between distant cellular processes (Miyazawa, Hidenobu and Aulehla, Alexander, 2018).

### ***1.2.a) Metabolites as rate-limiting substrates for epigenetic and post translational modifications***

Dynamic alterations in concentration of several key intermediate metabolites, which reflects the spatiotemporal regulation of metabolic activity, impacts downstream of biochemical reactions via protein post-translational modifications or by altering epigenetic markers. We first focus on

epigenetic modification. The emerging evidence has indicated that DNA and histone modifications may be particularly responsive to metabolic inputs through allosteric mechanisms of substrates affecting enzyme activity. As such, histone acetylation and lactylation as well as methylation of both DNA and histone can be considered as the direct influence of metabolites on cell fate decisions through altering chromatin modifications (Su *et al.*, 2016; Miyazawa, Hidenobu and Aulehla, Alexander, 2018; Cable *et al.*, 2021; Dai *et al.*, 2021). In addition, an intimate connection between metabolism and cellular environment accompanied by spatiotemporal regulations of metabolism proposes a precise level of regulatory function of metabolism, which integrate environment and genes expression to translate into cellular fates. For this purpose, substrates, metabolic enzymes, and their products exhibit fundamental roles in cellular programming.

### **1.2-a.1) Histone acetylation**

Histone acetylation generally provides chromatin accessibility and activates gene transcription (Tessarz and Kouzarides, 2014). Accordingly, several enzymes modulate chromatin modification, such as histone acetyltransferases (HAT) which mediates the transfer of acetyl groups from acetyl-CoA to histones. In contrast, histone deacetylases (HDAC) remove acetyl marks from histone (Fig. 4). Acetyl-CoA serves as the main source of acetyl group in the cells, derived from pyruvate, acetate, fatty acids or amino acids in mitochondria, and supports the function of TCA cycle. Despite its abundant production in the mitochondria, it is unable to diffuse across the mitochondrial membrane and then it is out of access for histone modifications (Sivanand *et al.*, 2018). Alternatively, acetyl-CoA and oxaloacetate condensed into mitochondria underly citrate production, which can pass out of the mitochondria. Citrate breaks into acetyl-CoA and oxaloacetate under ATP-citrate lyase (Khacho *et al.*) activity in the cytosol, thereby the source of acetylation and lipid biosynthesis becomes revived in the cytosol. In addition to cytosolic ACL, nuclear localization of ACL and PDH provide together the localized sources of acetyl-CoA in the nucleus for histone modification, indicating subcellular level of metabolic regulation to facilitate histone acetylation (Wellen *et al.*, 2009; Miyazawa, Hidenobu and Aulehla, Alexander, 2018). Hence, acetyl-CoA represents not only an important substrate for energy production via TCA

cycle, but its localization and concentration also impact the degree of epigenetic modifications, providing an intriguing link between cellular metabolic state, epigenetics and gene expression (Cai *et al.*, 2011). For instance, the pronounced activation of glycolysis coincides with T-cell activation through enhanced glucose-derived citrate and subsequent histone acetylation levels (Wang *et al.*, 2011; Peng *et al.*, 2016). In addition, under hypoxia stress, the source of acetyl-CoA production changes due to limitation of glucose-derived citrate, thus, acyl-CoA synthase short-chain family member 2 (ACSS2) substitutes acetate for cytosolic acetyl-CoA production. Subsequently, tumours growing in-vivo rely on high consumption of acetate and ACSS2 action to sustain acetyl-CoA production, lipid synthesis and histone acetylation (Comerford *et al.*, 2014; Schug *et al.*, 2014). Additionally, nuclear translocation of ACSS2 in response to oxygen and nutrient limitation may play a key role in maintaining histone acetylation (Comerford *et al.*, 2014; Bulusu, Tumanov, *et al.*, 2017).

### **1.2-a.2) Methylation of histones and DNA**

Methylation of specific histone residues can either activate or repress transcription, whereas DNA methylation results in transcriptional repression (Berger, 2007). Thus, the balance between histone and DNA methylation is another critical factor for gene expression, regulated by relative rate of deposition and removal of methyl marks (Plass *et al.*, 2013), which can be regulated at metabolic level.

**S-adenosylmethionine:** Methyltransferase enzymes catalyze the transfer of methyl groups from S-adenosylmethionine (SAM) to lysine and arginine residues on histones and cytosine nucleotides in DNA. Intracellular SAM pools are dependent on both cellular import of methionine through amino acid transporters and the methionine cycle, which revive the homocysteine resulted from methyltransferase reactions through the methionine regeneration (Su *et al.*, 2016) (Fig. 4). Then, re-methylation of homocysteine is contingent on one-carbon donation from folate cycle, which in turn is intimately related to serine and glycine metabolism (Su *et al.*, 2016). According to the link between amino acids metabolism and methylation,

alteration in any metabolic inputs largely influence histone and DNA methylation, leading ultimately to cell reprogramming.

Many oncogenic lesion regulate and enhance uptake and/ or synthesis of amino acids involved in SAM metabolism, which in turn impact methylation patterns in cancer and stem cells (Denicola *et al.*, 2015; Kottakis *et al.*, 2016). For example, in lung cancer models, increased expression of methionine transporter LAT1 mounts intracellular SAM pools, thereby underlying the sustain activity of methyltransferase (EZH2)(Dann *et al.*, 2015).

***α-ketoglutarate:*** Despite of passive removal of methyl markers from DNA and histones during cell division or nucleosome turnover, the enzymatic removal of methyl marks plays a critical role in the regulation of methylation status in cancers and stem cells (Plass *et al.*, 2013; Intlekofer, A. M. and Finley, L. W. S., 2019). The lysine-specific demethylase enzymes catalyze the removal of some histone marks in a flavin-dependent oxidative reaction. Demethylation reactions are performed by the large family of αKG-dependent dioxygenases, including the Jumonji-domain-containing histone demethylases (JHDM) and the ten-eleven-translocation enzymes which mediate the iterative oxidation and demethylation of methylated cytosines in DNA (Losman and Kaelin, 2013). Thus, availability of αKG, succinate and fumarate accompanied by contribution of ferrous iron and oxygen altogether modulate activities of these enzymes (Fig. 4). Collectively, dynamic interplay among metabolic pathways that ties production and consumption of oncometabolites (αKG, succinate, fumarate and 2- hydroxyglutarate (2-HG) influences the activity of αKG-dependent dioxygenases (Intlekofer, A. M. and Finley, L. W., 2019). For example, in myeloid leukemia stem cells, overexpression of the enzyme branched-chain amino acid transaminase 1 (BCAT1) contributes to oncogenesis through direct effects on αKG levels. Specifically, BCAT1 depletes intracellular αKG, thus resulting in impaired TET enzyme activity, DNA hypermethylation and blockade of normal myeloid cells (Raffel *et al.*, 2017).

***Antagonists of α-ketoglutarate:*** Beside αKG-dependent dioxygenases, isocitrate dehydrogenase enzymes (IDH1/2) is another metabolic regulation of chromatin, which catalyzes interconversion of isocitrate and αKG in an NADP(H)-dependent manner in TCA cycle. Mutation

at specific arginine residue located in active site of IDH 1/2 results in a neomorphic enzyme activity, which reduces  $\alpha$ KG to structurally similar metabolite 2-hydroxyglutarate (2-HG) (Ward *et al.*, 2010). Thus, 2-HG works as a competitive inhibitor of  $\alpha$ KG-dependent dioxygenases and exogenous 2-HG induces many of the oncogenic effects of IDH mutations (Fig. 4) (Losman *et al.*, 2013), which promotes hypermethylation of DNA and repressive histone marks (Lu *et al.*, 2012). Furthermore, 2-HG function is not confined only to DNA and histone modification, but it can also modulate epitranscriptome (the chemical modification of RNA) by inhibiting an  $\alpha$ KG-dependent RNA demethylase (Su *et al.*, 2018). Intriguingly, under hypoxia condition resulting from malate dehydrogenase or elevated activity of lactate dehydrogenase (Bertero *et al.*), wild-type IDH produces 2-HG and thus influences histone methylation (Intlekofer *et al.*, 2015).

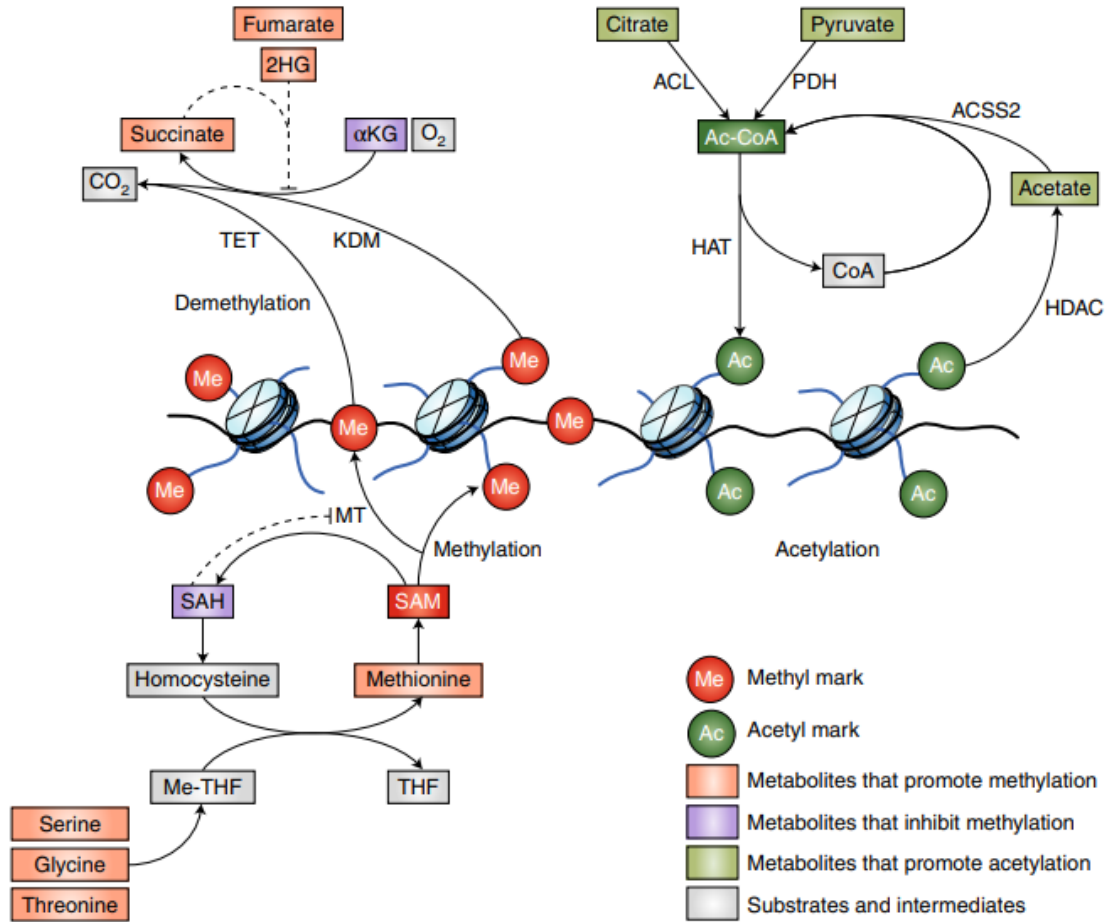


**Fig. 4. Metabolic regulation of chromatin marks.** Methyltransferase (MT) enzymes transfer methyl (Me) groups from SAM to histones and DNA. Methylation reactions generate S-adenosylhomocysteine as a product; SAH inhibits methylation reactions, thus making MT activity responsive to the relative ratio of SAM/SAH. Methionine is the direct precursor of SAM, and methionine pools are regulated by both cellular uptake (not shown) and the methionine cycle, which regenerates methionine from homocysteine. The methionine cycle is intimately connected to the folate cycles, in which serine, glycine and (in mouse PSCs) threonine provide one-carbon units to tetrahydrofolate (THF) for transfer to homocysteine. Lysine demethylases (KDM) and TET enzymes catalyze demethylation of histones and DNA, respectively, by using  $\alpha$ KG, oxygen and ferrous iron (not shown) as substrates. Succinate, fumarate and 2HG are competitive inhibitors of lysine demethylase and TET enzymes, thereby promoting accumulation of methyl marks. Histone acetyltransferases (HAT) transfer acetyl (Ac) groups from acetyl-CoA (Ac-CoA) to histones. Ac-CoA derives from cytosolic and/or nuclear citrate, pyruvate and acetate, which are substrates for the acetyl-CoA-generating enzymes ACL, pyruvate dehydrogenase (PDH) or ACSS2. Moreover, class I, II and IV histone deacetylase (HDAC) reactions generate acetate as a product, which can be captured by nuclear ACSS2 and used to regenerate Ac-CoA (Intlekofer, A. M. and Finley, L. W., 2019).

### **1.2-a.3) Histone lactylation**

Histone lactylation is a new epigenetic mark identified recently, which contributes to chromatin modification in cancer cells (Zhang, D. *et al.*, 2019). It is considered as the glycolytic switch in cancer cells resulting from lactate accumulation in nucleoprotein, reflecting the exogenous and endogenous lactate levels. Both histone acetylation and lactylation are rivals for lysine residues of histone. Of these, whether pyruvate selects reduction or oxidation reaction as the outlet of glycolysis can determine cancer cells' fate towards malignancy (excessive proliferation) or not. Histone lactylation has recently received the most attention as a novel therapeutic opportunity against cancer (Dai *et al.*, 2021).

### **1.2-b) post-translational modification (PTM)**

Metabolites can also exhibit particular roles in PTM, representing another regulation level of cellular signaling and cell behaviour. Hexosamine biosynthetic pathway (HBP) contributing to almost all central carbon metabolic pathways is a well-known example of PTM. As a branch of glycolysis, HBP generates UDP-GlcNAc with the contribution of glutamine, glucose, acetyl-CoA and UTP, a key substrate for protein glycolysis (De Queiroz *et al.*, 2019). The role of “metabolic sensors” has been attributed to UDP-GlcNAc due to similarity in cellular metabolic state and its levels. It acts as a substrate for O-GlcNAcylation transferring UDP-GlcNAc to serine or threonine residue at proximal to phosphorylation sites, which competes with phosphorylation and finally influences cell signaling (Bond and Hanover, 2015).

Other examples of PTM are poly-glutamylated and acetylated microtubules in neural stem cells and neural development. As such, the stability level of cytoskeleton is fundamental in those cells to affect neuronal migration under Notch pathway. Indeed, activation of Notch signaling in primary cortical neurons enhances  $\alpha$ -tubulin acetylation and poly-glutamylated that reflect microtubules stability, resulting in cytoskeleton remodeling and neuronal migration (Bonini *et al.*, 2017).

### 1.3) Non-canonical moonlighting functions of metabolic enzymes

Moonlighting enzymes are generally defined as those that exhibit additional non-metabolic functions by enhancing functional options for cells without change in numbers of genes that need to be replicated and transcribed (Boukouris *et al.*, 2016; Miyazawa, Hidenobu and Aulehla, Alexander, 2018). Notably, all glycolytic enzymes have been found in nuclear localization, proposing the high potential flexibilities in functions of those located in the nucleus (Fig. 5). For example, the embryonic isoform of pyruvate kinase, known as PKM2, follows both canonical and non-canonical functions in nucleus. On one hand, PKM2 contributes to PDH and HAT to generate acetyl-CoA pools in the nucleus and facilitates histone acetylation. In another hand, it represents several non-canonical functions, ranging from phosphorylation and methylation of histone H3 to being co-transcription factors such as HIF-1 and Oct4 (Li *et al.*, 2015; Boukouris *et al.*, 2016). In addition, PKM2 satisfies metabolic demands for biomass production due to facilitation of glycolytic intermediates into auxiliary glucose metabolisms such as PPP and one carbon metabolism (Anastasiou *et al.*, 2012; Miyazawa, Hidenobu and Aulehla, Alexander, 2018). Concomitantly, nuclear PKM2 upon growth factor stimulation interacts with B-catenin, enhancing expression of cyclin D1 and Myc that ultimately leads to cell cycle progression and glycolysis. Therefore, the contribution of PKM2 in genes expression (moonlighting function) forms a positive loop between glycolysis and growth factor signaling (Yang *et al.*, 2012; Miyazawa, Hidenobu and Aulehla, Alexander, 2018).

The link between moonlighting and canonical functions is inevitable and reciprocal. For instance, glyceraldehyde-3-phosphate dehydrogenase (GAPDH), an  $\text{NAD}^+$ -dependent dehydrogenase, acts as nuclear transcriptional co-factor, which connects with Oct-1 dependent on  $\text{NAD}^+/\text{NADH}$  ratio in the cells. Thus, the GAPDH and Oct-1 complex promotes expression of histone H2B during S-phase of cell cycle, when PPP enhances NADH production. This example provides the link between metabolic and moonlighting functions. Thus, the metabolic activity directly effects on the ability of metabolic enzymes to engage in their moonlighting function (Zheng *et al.*, 2003). In addition, GAPDH influences translation of proteins due to its RNA-binding properties. It binds to the 3'-UTR of interferon  $\gamma$  (IFN $\gamma$ ) RNA and thereby blocks its translation. Upon T-cell activation followed by increased glycolysis, GAPDH engages in glycolysis due to binding to  $\text{NAD}^+$ , which influences its preference to bind to 3'-UTR of IFN $\gamma$  mRNA and

enhances IFN $\gamma$  translation (Chang *et al.*, 2013), pointing to another example of the link between metabolic state and post-translational regulation.

Given the diverse functions of metabolism ranging from bioenergetic and biosynthesis to moonlighting, it is worth noting how metabolism incorporates into embryonic development. Therefore, we need to know how metabolism integrates extrinsic (biochemical stimuli) and intrinsic cues (cellular pathways), focusing firstly on its interaction with adhesion molecules and mechanical cues and then going to the embryonic level.

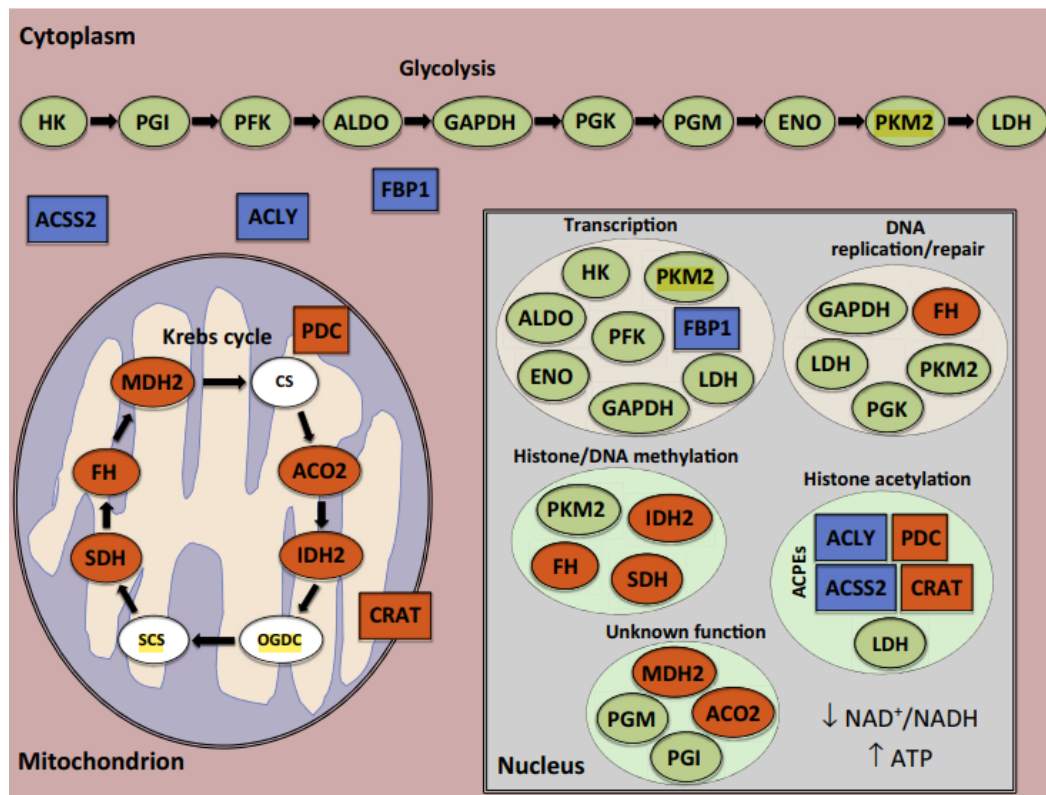


**Fig. 5. Metabolic Enzymes Moonlighting in the Nucleus.** Cytoplasmic glycolytic and non-glycolytic (blue) and mitochondrial enzymes are known to translocate into the nucleus. While all the essential glycolytic enzymes are found in the nucleus, only some Krebs cycle enzymes have been described in the nucleus (orange) whereas others have not (white filling). In the nucleus, the translocated enzymes have been grouped together according to their proposed nuclear function, whether canonical (i.e., production of a metabolite with secondary effects in nuclear functions) or non-canonical (i.e., a kinase function, participation in a transcription complex). Abbreviations: ACLY, ATP citrate lyase; ACO2, aconitase 2; ACPEs, acetyl-CoA-producing enzymes; ACSS2, acetyl-CoA synthetase short-chain family member 2; ALDO, fructose bisphosphate aldolase; CRAT, carnitine acetyltransferase; CS, citrate synthase; ENO, enolase; FBP1, fructose-1,6-bisphosphatase; FH, fumarate hydratase; GAPDH, glyceraldehyde 3-phosphate dehydrogenase; HK, hexokinase; IDH2, isocitrate dehydrogenase 2; LDH, lactate dehydrogenase; MDH2, malate dehydrogenase 2; OGDC,  $\alpha$ -ketoglutarate dehydrogenase; PDC, pyruvate dehydrogenase complex; PFK, phosphofructokinase; PGI, phosphoglycerate isomerase; PGK, phosphoglycerate kinase; PGM, phosphoglycerate mutase; PKM2, pyruvate kinase M2; SCS, succinyl-CoA synthetase; SDH, succinate dehydrogenase (Boukouris *et al.*, 2016).

## 2) Mechanical Cues: an Intermediate between Metabolism and Cell Fitness

Mechanotransduction is a cellular process that converts mechanical stimuli to biochemical signals, regulating cell fate. Therefore, change in mechanical cues of cell environment including extracellular matrix (ECM) mechanics, stiffness, topography, and physical forces such as stress, tension, and compression can be transmitted, through protein-protein interactions, between ECM and the cell or between neighboring cells, which ultimately influences cell fitness (Lacroix *et al.*, 2015). Indeed, transmembrane cadherins and integrins are a bridge between two cells or between cells and ECM, respectively, and are parts of mechanotransduction machinery. Integrins are defined as both force transmitters and mechanosensors (Fig. 6a). The link between ECM and the actin cytoskeleton is mediated by the focal adhesion machinery, forming a mechanical transduction platform inside of cells that leads to regulation of actomyosin structure and force transmission to the nucleus through LINK complex (Fig 6a)(Sheehy and Parker, 2011; Lacroix *et al.*, 2015) and activating numerous signaling cascades.

The response of cells to extracellular forces is typically contingent on a quick reinforcement of mechanosensitive structures, such as cell-cell and cell-ECM adhesions; and cytoskeleton in turn coordinates itself with mechanical forces (Fig. 6b)(Perestrelo *et al.*, 2018; Romani *et al.*, 2021). Thus, different biological effects emerge through forces applied at different adhesions (cell-ECM and cell-cell). The elastic property of ECM leads to tension forces acting on cells embedded in it and causes cellular reflects. For example, mechanostress can impact on glycolytic enzyme level such as PFK. As such, PFK level increases on stiff ECM mediated by stress fibers clamping ubiquitin ligase (TRIM21). Conversely, due to lack of stress fibers on soft ECM, TRIM2 is able to degrade PFK and reduce glycolysis. Studies of a mouse model with collagen IV deficiency showed that architectural changes in ECM trigger modification of cytoskeleton tension and consequently remodeling muscle metabolism by decreased glycolysis (De Palma *et al.*, 2013). Indeed, the intersection of metabolism and mechanics provides a physical and biochemical connections to external environment of cells, which empowers them to move and adopt different shapes (Evers *et al.*, 2021). Moreover, mechanotransduction pathways such as Yes-

associated protein 1 (YAP) and transcriptional co-activator with PDZ-binding motif (TAZ) (YAP/TAZ) complexes or the myocardin-related transcription factors (MRTFs) control cell fate and behavior through regulation of gene expression. Thus, YAP/TAZ are the well-known cell mechanosensor that has a role in cellular polarization, migration and organ growth. Indeed, ECM stiffness in malignant cancers promotes glycolysis and proliferation mediated by YAP/TAZ that regulate levels of PFK and GLUT3 glucose transporter combined with generation of glutamine-derived aspartate (Perestrelo *et al.*, 2018; Bertero *et al.*, 2019; Romani *et al.*, 2021). Another example is related to the post translational modification of cytoskeleton in neural stem cells and neural development explained briefly in PTM part

Altogether, it is obvious that metabolism and mechanics are intertwined to meet not only the energy demands for cytoskeleton rearrangement but also maintain normal function of mitochondria through their proper localization mediated by interaction with cytoskeleton (Perestrelo *et al.*, 2018). Mechanical cues have recently been recognized and accepted as important cues that work together with biochemical cues to regulate cell fate (Perestrelo *et al.*, 2018).

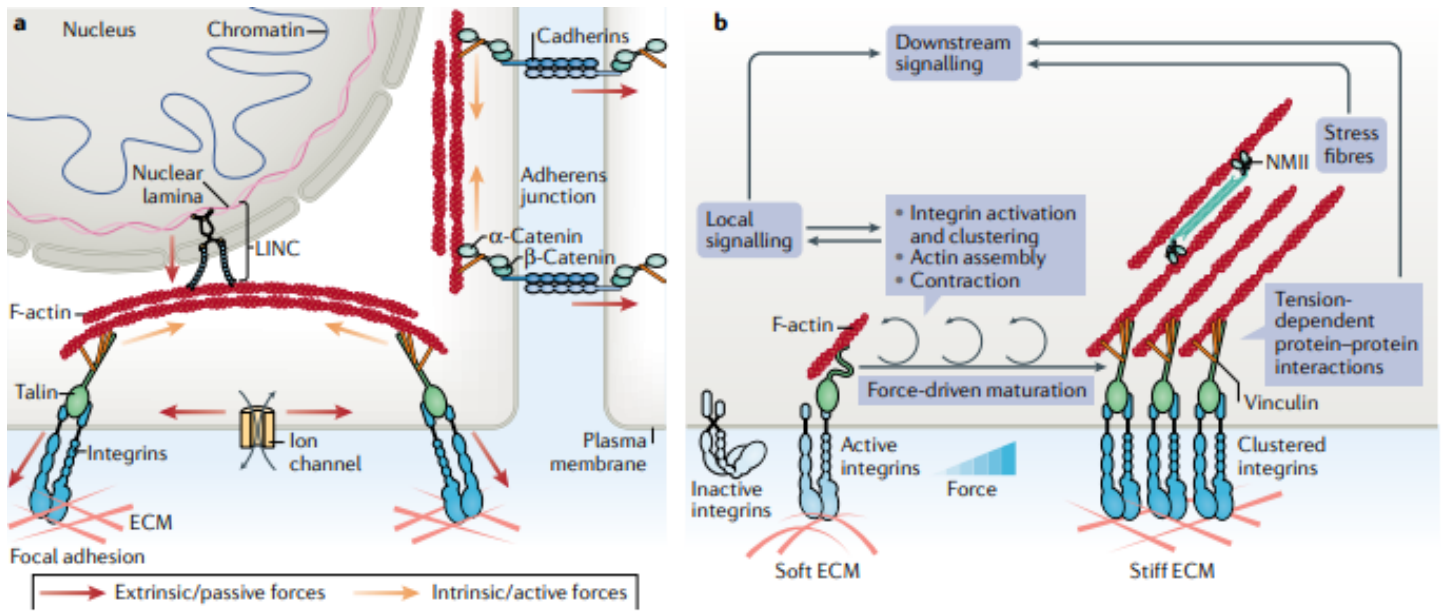


**Fig. 6. ECM mechanosensing and mechanotransduction mechanisms.** a | Mechanisms of force propagation in cells. Cells experience various forces, including those associated with sensing the viscoelastic properties of the extracellular matrix (ECM) at cell–ECM contacts, pulling forces exerted by neighbouring cells at cell–cell contacts and a plethora of tissue-level forces, such as shear, compression and stretch that result from, for example, tissue rearrangements or systemic functions (blood flow, breathing, body movements). These extrinsic forces propagate to the actin cytoskeleton through adhesion complexes (focal adhesions and adherens junctions). Actin is also coupled to the nuclear envelope via linker of nucleoskeleton and cytoskeleton (LINC) complexes that bridge cytoplasmic actin with nuclear lamins, potentially propagating extrinsic forces to chromatin. This may influence chromatin dynamics, epigenetics and gene transcription, and also DNA damage/repair mechanisms. Cells can in turn produce intrinsic force on cell–ECM and cell–cell contacts by active contraction of the actin cytoskeleton. Extrinsic forces can also propagate within the plasma membrane, controlling the activity of mechanoresponsive ion channels. b | Cells respond to extracellular resisting forces by reinforcing their adhesion complexes and by activating downstream signalling pathways. In the case of focal adhesions, the initial activation and binding of integrins to the ECM can occur in the presence of low resisting forces (soft ECM), leading to the formation of transient focal points where the intracellular domain of integrin is loosely attached to F-actin. The recruitment of adaptor and local signalling proteins promotes integrin clustering, assembly of thicker actin bundles and their contraction via non-muscle myosin II (NMII), which in the presence of extracellular resisting forces (stiff ECM) enables the build-up of increasing internal tension. Key force-bearing proteins such as talin undergo force-induced conformation changes which promotes the local recruitment of other proteins to reinforce the linkage to actin, such as vinculin, and regulates local signalling to provide a positive feedback leading to further growth and reinforcement of the focal adhesions. Multiple mechanisms then contribute to regulate downstream signalling pathways mediating the biological responses to ECM-derived mechanical cues (Romani *et al.*, 2021).

### 3) The Emerging Roles of Metabolism during Development

Until now, we found the mechanistical links between spatiotemporal regulation of metabolism and distinct cellular programs. In other words, reciprocal functions of metabolic enzymes such as canonical and signaling functions are modulated by both their substrates and products mediated by their direct sense of the supply and demand of fuel and nutrients. Thus, the ability of metabolic enzyme to both sense metabolites availability and cell reprogramming is an efficient way to provide adaptive responses of cells (Boukouris *et al.*, 2016). Align with nutrient availability and metabolic gradients, another question emerges how metabolic enzymes, pathways, and products affect multiple aspects of developmental steps which rely on the integration of both genotype and environmental cues.

During the first half of the 20<sup>th</sup> century, developmental biology studies revealed striking connections between metabolic activity and developmental processes with remarkable spatiotemporal regulation of metabolic activities (Child, 1941). By evidence of varying carbon sources in defined in-vitro culture conditions, analyses of nutritional requirements in early chick embryos showed that different metabolic processes underly the formation and maintenance of the two germ layer derivatives (Spratt Jr, 1950; Miyazawa, Hidenobu and Aulehla, Alexander, 2018). But descriptions of metabolic mechanisms to provide insight into cause-consequence relationships were neglected in pioneer studies. The accumulating evidence suggests the rewiring of cellular metabolic state is associated with the progression of embryonic development. However, the timely regulation of intrinsic and extrinsic cues to induce metabolic changes is still elusive in developing embryos (Miyazawa, Hidenobu and Aulehla, Alexander, 2018).

**Temporal control of metabolism during embryonic development:** Aerobic glycolysis (Warburg effect) is widely observed in developing embryos, similar to proliferating cancer cells (Miyazawa *et al.*, 2017; Oginuma, Masayuki *et al.*, 2017). The assessed spatiotemporal pattern of metabolism highlighted a glycolysis gradient along the embryonic rostro-caudal axis during formation of somites in vertebrates, evidencing a spatiotemporal regulation of metabolic activities within the presomitic mesoderm (PSM) (Fig.7). PSM represents a dynamic model where new somites appear at the anterior end of the PSM and neuromesodermal progenitors (NMPs) arise from the posterior tail bud; thus, the cells proliferate throughout the PSM and definitely require the regulated metabolic activities (Hubaud and Pourquié, 2014; Oginuma, Masayuki *et al.*, 2017). The use of mass-labeled glucose and a reporter mouse line for a Förster resonance energy transfer (FRET)-based pyruvate sensor enabling to probe metabolic profile reveal a gradient of glycolysis within the PSM. Cells in its posterior part, identified as more undifferentiated cells, exhibit higher glycolytic activity than those in the anterior PSM. Moreover, the uniform rate of cell proliferation across the PSM postulates that high glycolysis in the posterior region is not linked to cell proliferation activity. Likewise, the similar metabolic signature observed in in-vitro two-dimensional segmentation points to an intrinsic program related to metabolic regulation in the PSM (Bulusu, Prior, *et al.*, 2017). In addition, glycolytic activity was shown to be coupled with growth factor signaling. As such, graded fibroblast growth factor (FGF) signaling controls the expression of glycolytic enzymes, while subsequently the boosted glycolytic activity in turn induces another signaling pathway, the Wingless/Integrated (WNT) signaling pathway (Oginuma, Masayuki *et al.*, 2017). Excitingly, manipulation of glycolytic activities favors differentiation of NMP at the expense of mesodermal fate (Oginuma, Masayuki *et al.*, 2017; Miyazawa, Hidenobu and Aulehla, Alexander, 2018).

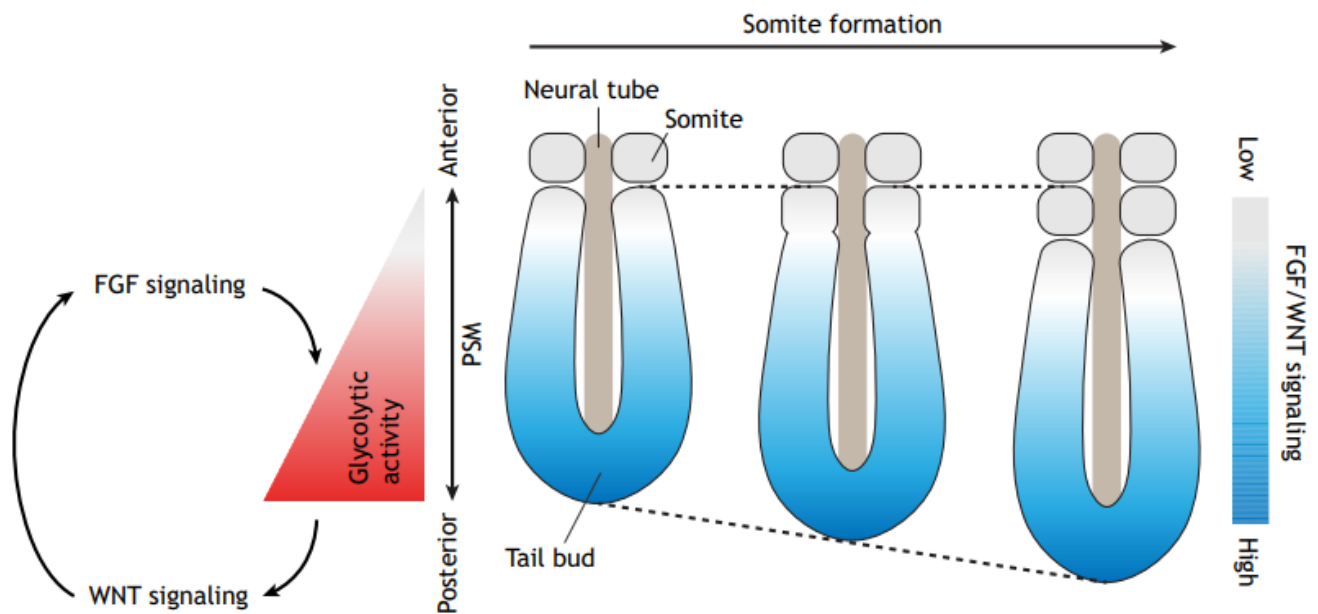


**Fig. 7. Graded glycolytic activity in the presomitic mesoderm during vertebrate somite formation.** A posterior-to-anterior gradient of glycolytic activity is found in the PSM of vertebrate embryos during somite formation and axis elongation. The metabolic gradient correlates with FGF- and WNT-signaling gradients in the PSM. FGF signaling regulates glycolytic activity, which in turn increases WNT-signaling activity. This constitutes a closed regulatory network with reciprocal feedback between growth factor signaling and glycolytic activity (Oginuma, Masayuki *et al.*, 2017; Miyazawa, Hidenobu and Aulehla, Alexander, 2018).

Altogether, the rewiring of metabolic states is coordinated with embryonic development and metabolic activities are regulated by intrinsic programs. Since cellular metabolic state relies on substrate availability, a key question is how the confluence of intrinsic and extrinsic cues occurs to regulate timely induction of metabolic transition during development. Thus, the investigation of metabolic activity at cellular level initially is required to tackle this issue, which is discussed below.

### 3.1) Metabolism and pluripotent stem cell (PSC) in context

Considering the link between cellular metabolic states and substrate availability, changes associated with the growing embryo trigger metabolic transitions. For example, the change in oxygen availability during embryonic development induces metabolic rewiring, which during implantation enhances glycolysis under reduction of local oxygen due to HIFs stabilization. However, after implantation when maternal oxygen supply increases, the predominance of OXPHOS occurs accompanied by environmental changes (Miyazawa *et al.*, 2017). For this type of metabolic programming, an intrinsic developmental program is required to adapt to extrinsic environmental changes in coordination with development. It has been further supported by in-vitro culture. Excitingly, under atmospheric oxygen conditions, again, embryonic stem cell (ESC) and epiblast stem cells (EpiSC), representative of pre- and post-implantation in culture respectively, exhibit different metabolic signatures, which indicate a higher glycolytic activity mediated by HIFs in late developmental stage (Zhou *et al.*, 2012). This result confirms what extent to metabolic phenotype is regulated by intrinsic cues rather than extrinsic environmental change.

Studies on pre-implantation embryos cultured in chemically defined media showed that certain nutrients alone (such as lactate, glutamine and pyruvate), without growth factors, have the capacity to induce cell identity transitions to support pre-implantation of embryos (Summers and Biggers, 2003). This result proposes that the presence of specific niche nutrients could initiate pluripotent stem cells (PSC) fate and not just support a pre-established PSC fate (Lu *et al.*, 2021). Moreover, specific nutrients influence the fate-specifying transition programs, enzymes-mediated chromatin change, and nutrient-sensitive signaling to retain pre-established pluripotency/self-renewal and differentiation fates (Baksh and Finley, 2021). Therefore, the same nutrients can either initiate or support PSC fates with different effects that depend on the context, such as the state of pluripotency, differentiation cues, culture media, and timed nutrient addition or deprivation (Lu *et al.*, 2021).

To realize the mechanically regulatory function of metabolism during embryonic development, it is required to initially obtain a comprehensive view of both metabolic phenotypes and intrinsic cellular patterns responsive to environmental changes in proliferative cells like cancers

or stem cells. Therefore, studying proliferative cells helps us to gain an understanding view from embryonic development by the impact of changing the medium-supply nutrients on proliferation, lineage specification and differentiation. I will briefly focus on the variety of metabolic phenotypes in various stages of stem cells.

***Pluripotent stem cell fate in utero and in-vitro:*** Pluripotency describes the developmental capacity of a cell to form the three primary germ layers, which in turn can give rise to all cell types of the adult body. Normal embryogenesis is highly dependent on proliferation and differentiation of PSC. After fertilization of oocyte with a sperm cell, which generates the zygote, embryogenesis begins as the consequence of zygote-derived totipotent and PSC cells. Subsequently, PSC has the potential to produce all embryonic lineages (Chazaud and Yamanaka, 2016; Perestrelo *et al.*, 2018; Tsogtbaatar *et al.*, 2020), providing an ideal model system to study not only the intersection of proliferation, differentiation and metabolism in the early embryo, but also in regenerative medicine and tissue engineering (Lu *et al.*, 2021).

The need for a better understanding of early embryonic development due to the transient nature of this type of cell led scientists to look for in vitro models to capture the pluripotent states at distinct stages of cell pluripotency, commitment, and differentiation. Thus, different cell populations have been successfully isolated: PSC can be isolated from inner cell mass (ICM) of pre-implantation epiblast (embryonic stem cells, ESC) or early post-implantation epiblast (epiblast stem cell (EpiSC)) (Perestrelo *et al.*, 2018; Intlekofer, A. M. and Finley, L. W., 2019; Tsogtbaatar *et al.*, 2020). PSC are unable to represent a single fixed stage, but, instead, a gradient of cellular phenotypes from “naïve” PSC, which shares molecular characteristics with cells of ICM in early blastocyst, to the “primed” PSC, which exhibits similarities to post-implantation epiblast cells (Fig 8). Of consideration, the core pluripotency genes represented in PSCs are Oct4, Nanog and Sox2, which will be progressively downregulated in blastocytes upon emerging of three germ layers during gastrulation (Tsogtbaatar *et al.*, 2020; Lu *et al.*, 2021).

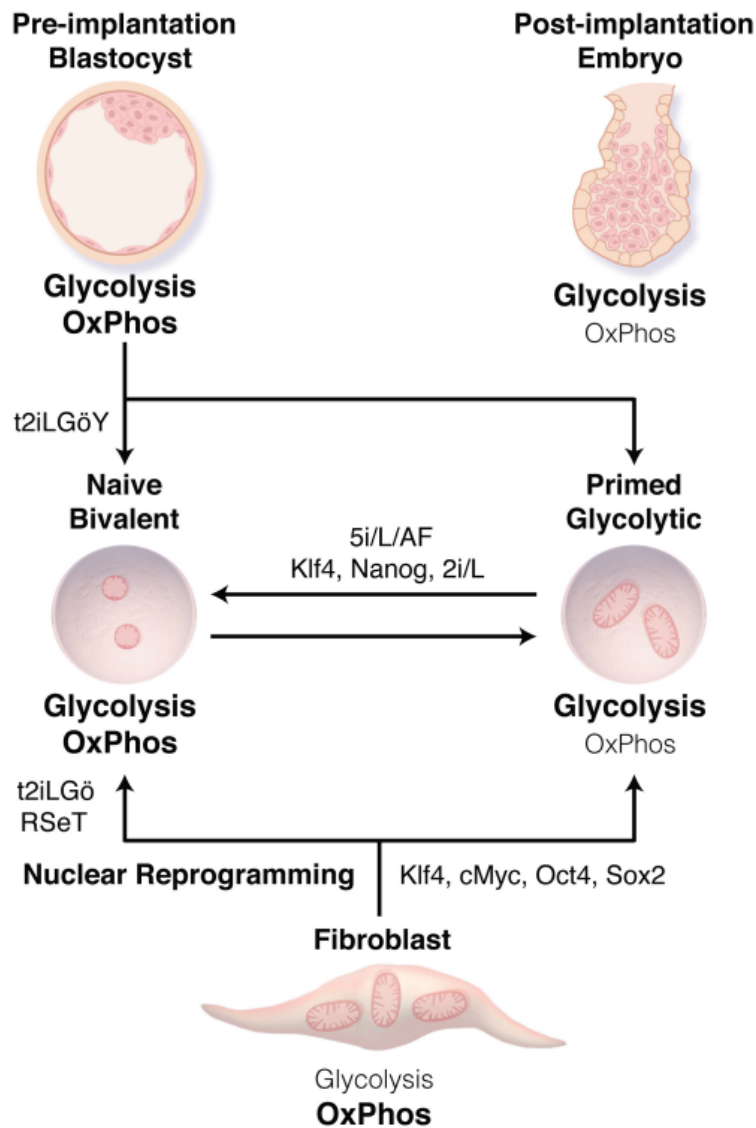


**Fig. 8. Transitions between human pluripotent stem cell (PSC) states.** Human embryonic stem cells derived from the inner cell mass of the blastocyst or through nuclear reprogramming traditionally display a primed state associated with bivalent metabolism using both glycolysis and OXPHOS. Methods have now been developed to derive naïve PSCs or to transition cells from the primed to naïve state, resulting in a transition from bivalent metabolism to nearly exclusively glycolysis. These metabolic preferences reflect those of the related stage during embryonic development (Tsogetbaatar *et al.*, 2020).

Therefore, naïve PSCs have the capacity to give rise to all germ layers and contribute to chimaeras, whereas primed PSCs represent a more committed developmental stage aligned with retaining pluripotency (Martello and Smith, 2014). Accordingly, the exogenous cues present in the culture medium influence PSC state, resulting in coaxing into either naïve or primed state (Weinberger *et al.*, 2016). Moreover, these cellular models have led to the recognition of transcription factors networks that govern the balance for maintenance of each developmental state (Perestrelo *et al.*, 2018). How convergence of metabolism and different transcription factors regulates cellular phenotype remains controversial. But the successful in-vitro isolation of PSC provided the opportunity to distinguish between metabolic alteration, which is align with differences in growth and proliferation to support cell-type specific fate decision (Intlekofer, A. M. and Finley, L. W., 2019; Tsogtbaatar *et al.*, 2020). Therefore, comparing different cell states resulted in the discovery of metabolism as a keystone in stem cell fate (Perestrelo *et al.*, 2018), supporting the concept that early metabolic alterations are critical to regulate epigenetics and cell identity (Intlekofer, A. M. and Finley, L. W., 2019; Tsogtbaatar *et al.*, 2020). Indeed, cells constantly adapt metabolic states in response to nutrient availabilities, extracellular signals, reprogramming and differentiation cues, inducing alterations in concentrations of key intermediate metabolites (Tsogtbaatar *et al.*, 2020). The key question is how metabolic pathways influence PSC identity or how modulated metabolism supports training of pluripotency.

***Glycolysis in PSC:*** High glycolytic flux is the common metabolic feature of various stem cells, which is critical for the acquisition and maintenance of pluripotency. The preferential utilization of glycolysis over OXPHOS may be routed in potential benefits of glycolytic metabolism. For instance, incomplete glucose oxidation enables stem cells to conserve carbon mass required for biosynthesis of cellular components (Lunt and Vander Heiden, 2011; Tsogtbaatar *et al.*, 2020). Moreover, due to reducing ROS production, this metabolic pathway helps to preserve the genomic integrity of PSC from subsequent damage of nuclear and mitochondrial DNA, as well as oxidation of proteins and lipids. This metabolic phenotype rapidly becomes reversible so that glycolytic flux decreases early during PSC differentiation (Moussaieff *et al.*, 2015; Cliff *et al.*, 2017; Intlekofer, A. M. and Finley, L. W., 2019), and reprogramming of somatic cells to

pluripotent state is contingent on re-acquisition of glycolytic phenotypes (Fig. 8) (Panopoulos *et al.*, 2012).

Despite glycolytic flux as a hallmark of pluripotency, the relative contributions of glycolysis versus OXPHOS vary in all stages of PSC. Indeed, The primed pluripotent state is almost exclusively glycolytic, whereas naïve PSC display a bivalent metabolic phenotype with a higher reliance on OXPHOS besides lactate production (Fig. 8) (Theunissen *et al.*, 2014; Cha *et al.*, 2017; Tsogtbaatar *et al.*, 2020). This metabolic preference in naïve PSC can reflect substrate availability and metabolic regulation during development. Indeed, early embryo firstly presents high rate of OXPHOS due to pyruvate supplied by ovarian follicle and glycolysis progressively emerges upon glucose usage during development (Tsogtbaatar *et al.*, 2020). In other words, due to increased expression of glucose transporters, glycolysis progressively is raised during embryonic development.

Core pluripotency transcription factors may directly regulate metabolic pathways. For example, Oct4 binds to encoding genes, such as *hexokinase (HK)* and *PKM2*, and consequently promotes glycolysis (Kim *et al.*, 2015a). In addition, a binding site of Sox2, Oct4 and Nanog has been recognized at GLUT1 enhancer, inducing both GLUT1 expression and downstream glycolytic flux in ESC (Yu *et al.*, 2019). C-Myc known as a strong driver of glycolysis in both naïve and primed pluripotent states targets PKM2 and LDHA, which subsequently leads to elevated glycolysis (Cao *et al.*, 2015).

During the transition between the naïve and primed state, numbers of upstream regulators influence the metabolic phenotype. The famous example of this regulation is related to HIF1 $\alpha$  driving glycolytic phenotype in prime state through nodal signaling (Zhou *et al.*, 2012). Ras has been also implicated in induction of transition from naïve to primed pluripotency through stimulation of glycolysis and epithelial-mesenchymal transition marked by an increase in N-cadherin (Altshuler *et al.*, 2018; Tsogtbaatar *et al.*, 2020). The pyruvate metabolisms are differently controlled in naïve versus primed stages of PSC by pyruvate dehydrogenase kinase (PDK), which regulates pyruvate-derived lactate production. Indeed, upon primed PSC stage, the pyruvate derives more towards lactate production mediated by HIF-1 $\alpha$ , which induces expression of PDK underlying phosphorylation and inhibition of PDH (Mathieu and Ruohola-

Baker, 2017). Collectively, these results support an idea that glycolysis is pivotal to both maintenance and acquisition of pluripotency and transition between naïve and primed PSC.

**Controversial benefits of glycolysis:** PSC are highly reliant on exogenous glucose and glutamine to proliferate in culture. In this condition, aerobic glycolysis as a hallmark of rapidly proliferative cells provides a major paradox, which is discarding most glucose carbons as lactate regardless of oxygen presence (Intlekofer, A. M. and Finley, L. W., 2019). Based on primary hypothesis, defective mitochondrial respiration drives conversion of pyruvate to lactate. However, it has been disproven in both cancer cells and normal cells (Deberardinis and Chandel, 2016). Indeed, this pioneer hypothesis is supported by the notably distinct quantity and morphology of mitochondria in PSC compared with their differentiated counterparts, including tendency of PSC to have fewer mitochondria per cell, and immature morphology of mitochondria marked by sparse cristae (Prigione *et al.*, 2010; Zhou *et al.*, 2012). Nevertheless, PSC are not defective in mitochondria-substrate oxidation; and respiratory complex are fully functional in these cells (Zhang *et al.*, 2011). Therefore, PSC consequently have flexibility to engage in either oxidation or glycolytic programs depending on nutrient availability (Zhou *et al.*, 2012; Zhang *et al.*, 2018). For example, PSC, even under basal conditions, engage in glutamine oxidation to sustain bioenergetics and enhance respiration, as a common feature in naïve state of PSC (Zhang *et al.*, 2016). Collectively, the aerobic glycolysis characterization of PSC and other proliferative cell types is not the consequence of a defect in mitochondrial function. In lack of knowledge from origin or consequences of aerobic glycolysis in PSC, it is difficult to attribute any particular benefit or function to aerobic glycolysis in retaining or maintenance of pluripotency (Intlekofer, A. M. and Finley, L. W., 2019). However, it has been recently suggested that aerobic glycolysis may arise in part as a secondary consequence of the metabolic requirements of proliferative cells rather than as a primary driver of proliferation. In fact, the conversion of pyruvate to lactate occurs when cytosolic NADH/NAD<sup>+</sup> ratio rises, which results from rapid consumption of NAD<sup>+</sup> in oxidative reactions of nucleotide production (Vander Heiden and Deberardinis, 2017). Therefore, the potential benefit of aerobic glycolysis is controversial and requires more studies.

### 3.2) Nutrient Availability and PSC

The binary functions of metabolites as substrates driving both regulatory and anabolic processes raises the possibility that utilization of nutrients targeted for cell proliferation might inherently influence the metabolites availability for other non-anabolic purposes (Intlekofer, A. M. and Finley, L. W. S., 2019). The notably high nuclear-to cytoplasmic ratio in PSC indicates rapid proliferation in these cells, relying on nucleotide biosynthesis for proliferative maintenance (Setoguchi *et al.*, 2016). Thus, the metabolic convergence of proliferation and cell-fate regulation particularly occurs in stem cells, which fulfills acquisition of both rapid proliferation and differentiation into specific cell type (Intlekofer, A. M. and Finley, L. W. S., 2019).

Considering the nutrient availability required for cell proliferation and other non-anabolic purposes, the inherent flexibility of metabolic networks enables cells to exert multiple mechanisms to fight against nutrient stress. The fundamental feature of proliferative cells in culture depends on the central role of glucose and glutamine to support all anabolic growth demands (Boroughs and Deberardinis, 2015; Intlekofer, A. M. and Finley, L. W., 2019).

Accumulating evidence suggests subtle differences in how different PSC types use nutrients. For example, naïve PSC in both human and mouse exhibit high consumption of glucose and glutamine, which leads to extensive production of lactate and higher basal respiration than the primed counterpart (bivalent metabolism). Another metabolic characterization of naïve ground-state ESC is their ability in de-novo generation of glutamine from glucose-derived carbons, enabling PSC at this state to proliferate in absence of glutamine. Moreover, human naïve PSC indicate more glycolysis than primed PSC, while the opposite trend occurs in mouse PSC (Zhou *et al.*, 2012; Gu *et al.*, 2016; Intlekofer, A. M. and Finley, L. W., 2019). The extent to which these metabolic differences arise from variations in cell size, proliferation rate and culture conditions rather than functional differences remains an open question. Simply culturing the same cell type in different medium conditions can elucidate how cells engage metabolic pathways to fulfil anabolic demand (Intlekofer, A. M. and Finley, L. W. S., 2019). However, emerging evidence suggests that PSC may exhibit metabolic diversity, even under routine culture conditions.

Indeed, driving the normally metastable and heterogenous population of naïve mouse ESC into homogenous ground state of pluripotency increases the contribution of glucose oxidation through TCA cycle (Carey *et al.*, 2015). Therefore, since PSC identity is intimately linked to culture conditions, these metabolic differences could also result from/or contribute to the establishment of different functional states (Weinberger *et al.*, 2016; Intlekofer, A. M. and Finley, L. W., 2019).

Moreover, short term glutamine withdrawal increases expression of Oct4 and Sox2 as core pluripotent transcription factors and subsequently eliminate cells with a high reliance on glutamine oxidation via TCA cycle (Vardhana *et al.*, 2019). On the other hand, long-term glutamine withdrawal leads to more oxidative PSC to die from a reduction in TCA cycle activity and OXPHOS. Therefore, glutamine withdrawal provide a strategy to eliminate PSC based on their state (Tohyama *et al.*, 2016; Lu *et al.*, 2021). These results suggest that the same nutrient(s) can either initiate or support PSC fates, with differential effects that depend on the context, such as the state of pluripotency, differentiation cues, culture media conditions, and timed nutrient addition or deprivation (Lu *et al.*, 2021).

Collectively, there is no single model of metabolism for PSC whose transient nature comprises a spectrum of cell identities or states; and consequently, the extent of metabolic trend shifts toward a dominant context of PSC population to supply their metabolic demands.

Concerning to intricate metabolic signature of PSC, we need more to study and probe into metabolic diversity in different types of PSC to better understand embryonic development. Of these, neural crest (NC) cells are considered as one of amazing types of PSC, exhibiting different steps through development, which provides a range of transient stages of primed PSC. Therefore, an exciting and fundamental question is how the convergence of metabolism and genes regulatory networks (GRN) activities regulates the different steps of NC development. But firstly, I will introduce this fascinating population. Let's view NC cells as "end-user" of energy.

#### 4) Neural Crest Cells

NC cells are notable for their ability to migrate extensively and differentiate into numerous derivatives in higher vertebrates (Fig. 9A-E). These amazing cells have been identified for the first time in 1868 by Wilhelm His, described as a band of cells residing between the neural tube and epidermis that later migrate laterally to form the spinal ganglion (His, 1868). By evolutionary view, NC is thought to have been crucial for the origin and diversification of vertebrates (Gans and Northcutt, 1983). They have been referred as the 'fourth germ layer' that generates a great interest in embryologists due to its far-reaching migratory ability and developmental plasticity (Hall, 2000). In fact, identification of NC cells provides an important concept that establishment of progenitor fields during body part formation could include contributions from cells incoming from distant locations (Simões-Costa and Bronner, 2015).

Transplantation experiments in over the past century, first in amphibian embryos (Horstadius, 1950) and later in birds using the classic quail-chick chimeras pioneered by Le Douarin (Le Douarin, 1973), have illustrated the pathways followed by NC cells and extensive array of derivatives to which they contribute (Fig. 9F).

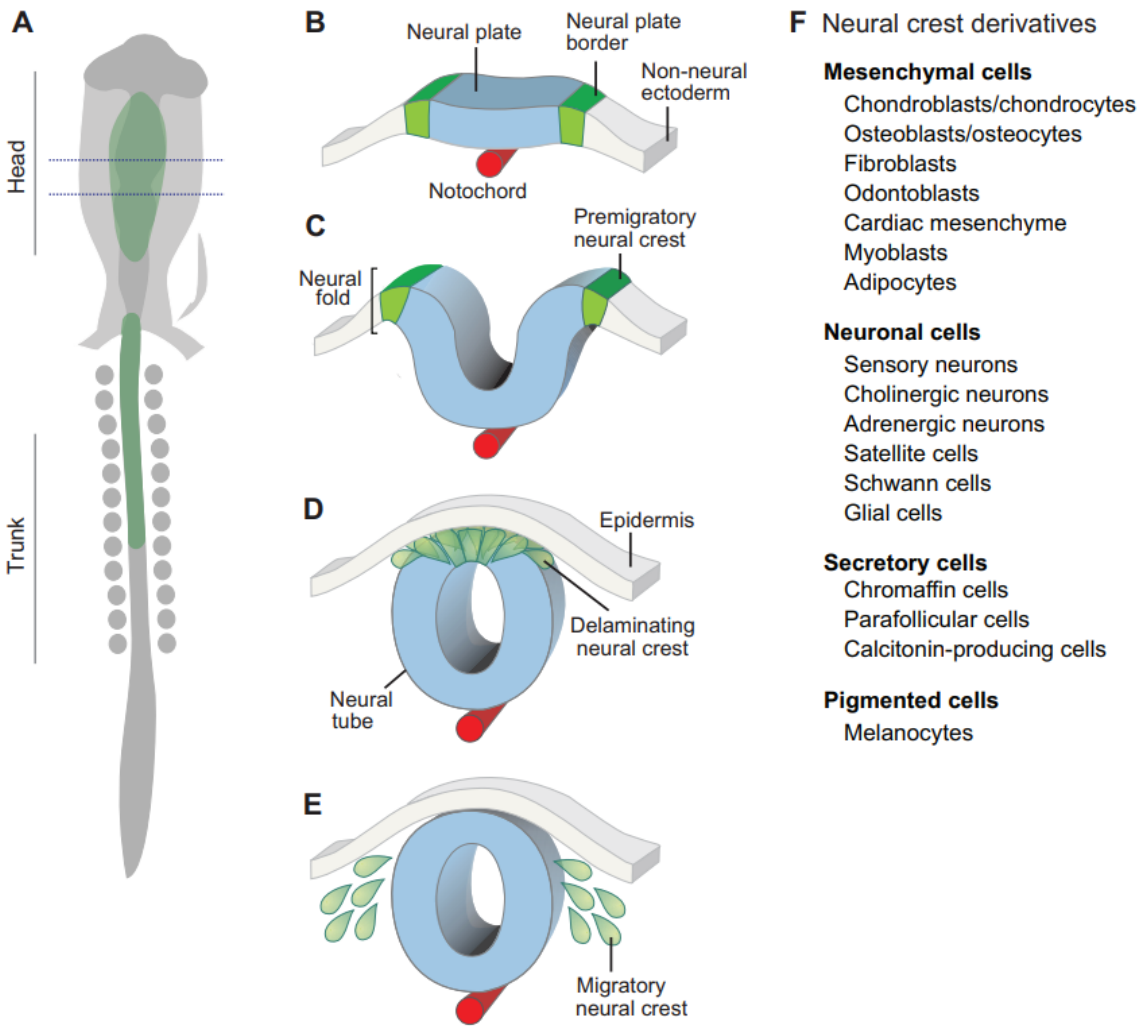


**Fig. 9. The neural crest is a multipotent cell population.** (A) Schematic dorsal view of a ten-somite stage chicken embryo, showing the neural crest in the vicinity of the midline. The dotted lines delimit the embryonic region represented in cross-section (B-E). (B) Development of the neural crest begins at the gastrula stage, with the specification of the neural plate border at the edges of the neural plate. (C) As the neural plate closes to form the neural tube, the neural crest progenitors are specified in the dorsal part of the neural folds. (D) After specification, the neural crest cells undergo EMT and delaminate from the neural tube. (E) Migratory neural crest cells follow stereotypical pathways to diverse destinations, where they will give rise to distinct derivatives. (F) The neural crest cells are multipotent and has the capacity to give rise to diverse cell types, including cells of mesenchymal, neuronal, secretory and pigmented identity (Simões-Costa and Bronner, 2015).

## A brief overview of neural crest development

Ectodermal germ layer induces NC production during gastrulation, consequently resulting in NC territory which initially resides in the neural plate border (NPB) at the lateral edges of the neural plate (Fig. 9B). Upon neural plate folding and closure during neurulation, these two borders territories elevate and come into close contact (Fig. 9C,D), and consequently, nascent NC cells are specified within the dorsal aspect of the neural fold by expression of genes, such as *Foxd3* and *Sox10* (Labosky and Kaestner, 1998; Southard-Smith *et al.*, 1998). After neural tube closure, NC cells subsequently leave the neural tube through epithelial-mesenchymal transition (EMT) (Fig. 9D), transforming into a migratory and multipotent progenitor cell population (Fig. 9E). NC cells move over long distances along highly stereotypic migratory pathways, and represent some of the most far-reaching migrations of any embryonic cell type (Duband, 2006).

Following migration, NC cells under environmental influences encountered during their journey progressively differentiate into distinct cell types (Bronner and Ledouarin, 2012). Ultimately, they generate various cell types to contribute to different tissues in a region-specific manner, including sensory and autonomic ganglia of the peripheral nervous system, melanocytes, the adrenal medulla, smooth muscle cells, cranio-facial cartilages and bones, as well as connective, and endocrine cell subtypes (Fig. 9F) (Le Douarin, 1982). Subpopulations of NC cells originate from four major segments of the neural tube through body axis from anterior to posterior to form cranial (or cephalic), vagal, trunk and sacral NC cells, producing distinct derivatives and following specific migratory pathways. For example, cranial NC cells form the facial skeleton, including upper and lower jaw and bones of the neck, as well as the glia and some neurons of cranial sensory ganglia (Couly *et al.*, 1998). Vagal NC cells contribute to formation of outflow tract of heart and enteric ganglia of the gut (Creazzo *et al.*, 1998). Trunk NC cells populate dorsal root ganglia and sympathetic ganglia of the peripheral nervous system (Le Douarin and Smith, 1988). Furthermore, a stereotypic pattern of NC progenitor migration varies through specific axial levels and animal species. For example, at trunk region of dorsal NT in birds, EMT and cell delamination occur gradually, which lasts about two consecutive days. In contrast, at cranial level NC cells leave the neural tube rapidly and massively as a cohesive group of progenitors

(Duband *et al.*, 1995; Duband *et al.*, 2015). The different EMT mechanisms are illustrated in Fig. 10.

By single cell analysis of mouse embryos, distinct axial positions share similarities in transcriptional profiles over time, while important axial-specific biases are sustained such as mesenchymal fate for cranial NC cells and sensory plus autonomic neuronal fate for trunk NC cells. These biases emerged with high level of Twist1 expression in cranial NC cells during delamination (Soldatov *et al.*, 2019; Rocha *et al.*, 2020). The two sub-populations of NC cells exhibit distinct transcriptional profiles across mouse, chick and *Xenopus* embryos at different times. As such, cranial program is established during delamination in mouse and chick embryos, while in *Xenopus* embryos it happens during early stages of NC specification and Twist1 loss during delamination (Simões-Costa and Bronner, 2015; Rocha *et al.*, 2020)

The high potential of NC cells to contribute to both neural/neuronal and mesenchymal derivatives has been questioned to know how they acquire cellular plasticity (Hu and Sauka-Spengler, 2022). The single-cell sequencing of NC progenitors in mouse embryos revealed the temporal expression of pluripotency-associated genes like Oct4+ that is essential for NC specification and formation of ectomesenchyme, suggesting the reactivation of pluripotency during NC development. In addition, the expression of Oct4+ combined with Nanog (another pluripotency marker) progresses along anterior posterior axis in the cephalic NC progenitors (Zalc *et al.*, 2021; Hu and Sauka-Spengler, 2022).

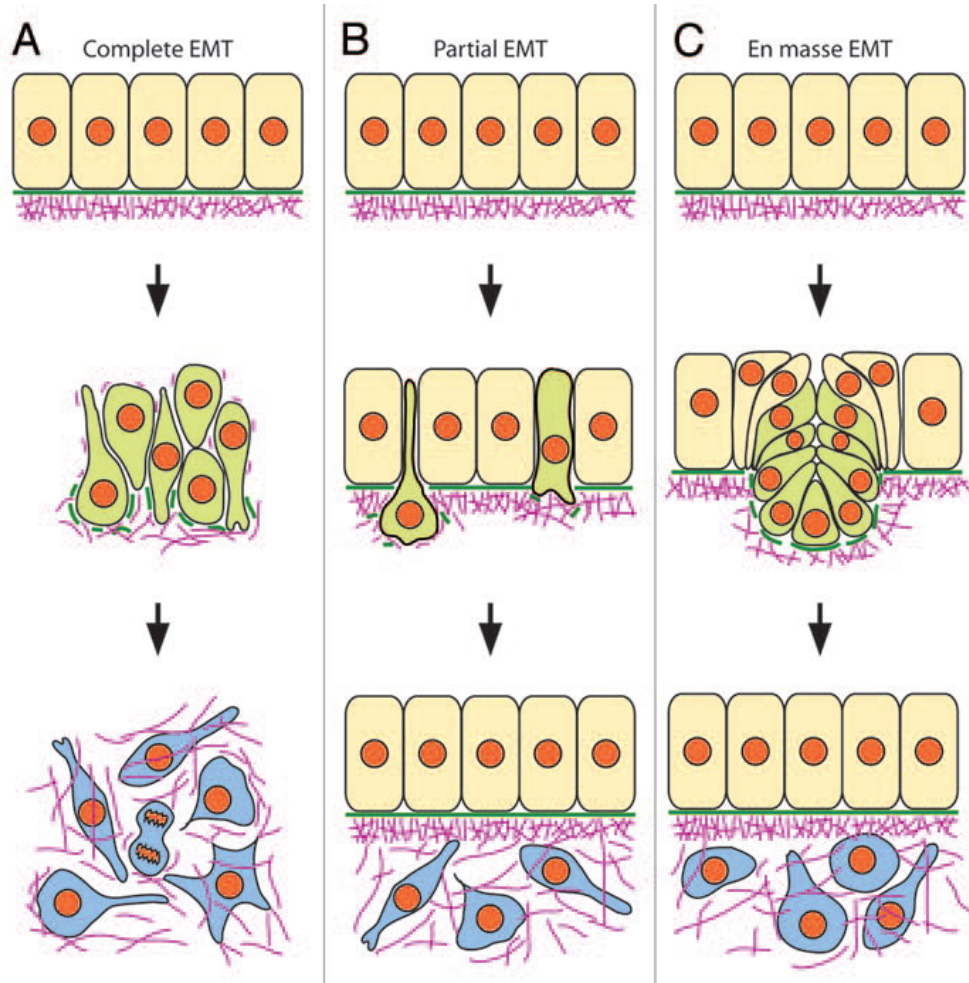


**Fig. 10. Molecular players involved in EMT.** Studies on epithelial cell lines established in vitro and on cancer cells showed that transition between epithelial to mesenchymal cells is promoted by a great variety of growth factors and morphogens, e.g., TGF $\beta$ , BMPs, HGF/SF, FGF, wnt and Notch which all impinge via a few families of transcription factors (Snail, Zeb, Twist and Fox) on the expression of a variety of cellular components involved in the maintenance of the epithelial structure: cell adhesion molecules of the junctional complexes, such as E-cadherin, desmoplakins, occludins and claudins, cell polarity molecules, such as Par and Crumb, cytoskeletal components, such as cytokeratins, and basement membrane components, e.g., laminins. Conversely, mesenchymal cells express a new repertoire of adhesion, cytoskeletal and matrix components that enables them to populate their environment. Epithelial cells are depicted in beige, cells undergoing EMT in green, and mesenchymal cells are in blue. Green solid bars, basement membrane; purple lines, fibrillar extracellular matrix (Duband, 2010).

As evidenced by chromatin immunoprecipitation and sequencing, Foxd3 binding in both wild type and mutant zebrafish was denoted as a pioneer factor to prime distal enhancer of NC specification that, in turn, switches to a repressor to modulate differentiation (Lukoseviciute, Martyna *et al.*, 2018; Hu and Sauka-Spengler, 2022). These results broaden our concept about pluripotency of NC progenitors during specification and dual functions of Foxd3 in transition from specification to migration.

#### **4.1) The Neural Crest Gene Regulatory Network**

The different steps of NC development, including induction, specification, migration, and differentiation, are tightly governed by a large gene regulatory network (GRN). The regulatory information obtained from different vertebrates has established the pattern of GRN composed of a large number of genetic interactions between signaling systems, transcription factors and epigenomic regulators (Meulemans and Bronner-Fraser, 2002; Simões-Costa and Bronner, 2015). Therefore, the combined actions of distinct signaling pathways contribute to first establish the neural plate border (NPB) where aborning NC cells settle, and presumptive NC cells set apart from other ectodermal domains (Fig. 9B). This process known as NC specification is crowned with expression of NC markers such as Foxd3, Snail1/ 2, and Sox8/9/10. Once NC cells are specified, they undergo EMT and initiate migratory behavior under radical changes in the set of genes (Duband *et al.*, 2015; Simões-Costa and Bronner, 2015). How GRN governs distinct developmental steps of NC has been a great interest in research that we need to appreciate.

***Induction and formation of the neural plate border (NPB):*** As we found out above, NC development initiates during gastrulation upon establishment of NPB, which is a broad territory between neural and non-neural ectoderm. Indeed, a multi progenitor cell population resides in this territory that empower NPB to give rise to NC cells, ectodermal placodes, epidermal cells, roof plate cells and sensory neurons of the central nervous system. The intersection of distinct transcription factors shapes different cell identities in time and space (Duband, 2010; Groves and Labonne, 2014; Simões-Costa and Bronner, 2015). There are some differences between species in the details of the NC induction process. But a general pattern has emerged from observations of frog, chick and zebrafish that appears to hold true across vertebrates (Simões-Costa and Bronner, 2015).

The generation of distinct cell identities during embryonic development involves several steps along dorsoventral axis of neural tube. During neural induction, first, signaling pathways drive the expression of NPB specific genes under a balance between concentrations of antagonistic signals. For example, bone morphogenetic protein (BNP) and Wnt signals secreted from lateral regions of embryo, while inhibitors of these pathways originate in middle region such as neural plate domain. Therefore, a mediolateral gradient of Wnt and BMP activity is generated that leads to establishment of NPB in this zone (Fig. 11). In addition, FGF signal works in concert with inhibitors of both Wnt and BNP to facilitate the balance of signals. Subsequently, NPB cells induce expression of a distinct new set of transcription factors known as NPB specifier, like *Tfap2*, *Msx1*, *Zic1*, *Gbx2*, *Pax3/7*, *Dlx5/6*, *Gata2/3*, *Foxi1/2*. Consequently, a series of positive regulatory interactions occurs, comprising the overlapping expression of NPB's specifier genes. For example, *Tfap2* and *Msx1* positively activate not only each other, but also *Pax 3/7* and *Zic1*. Consequently, a sharp boundary appears between neural plate and NPB mediated by inhibitory interactions between neural and non-neural transcription factors (Fig. 11)(Simões-Costa and Bronner, 2015).

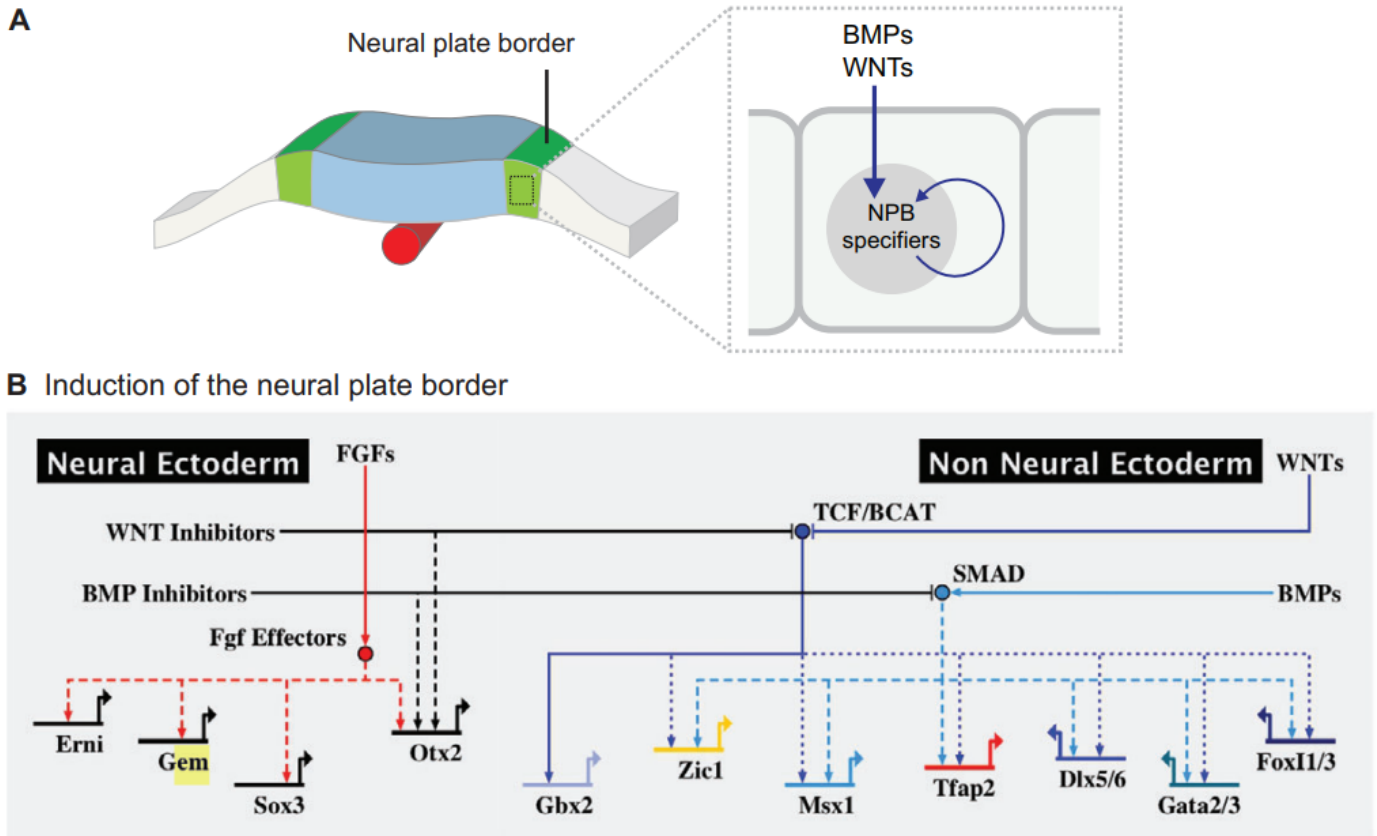


**Fig. 11. GRN module controlling the formation of the neural plate border.** (A) The action of signaling systems such the BMP and WNT signaling pathways results in activation of the neural plate border (NPB) genes in the margins of the neural plate. (B) In the neural ectoderm, FGF signaling drives neural induction by activating proneural genes. In an intermediary territory located between the neural and non-neural ectoderm, WNTs and BMPs activate a number of transcription factors dubbed neural plate border specifiers. Activity of WNTs and BMPs is hampered in the neural ectoderm by a number of inhibitory molecules produced by these cells (Simões-Costa and Bronner, 2015).

**Establishing neural crest identity:** The concerted action of more medial NPB specifiers and signaling pathways leads to emergence of NC cells from NPB via the enhanced expression of NC specifiers. The core NC specifiers present pivotal functions, which involve not only activation of EMT effector program to enable NC cells to delaminate and become migratory, but also maintenance of a number of specifier genes in delaminating and migratory NC cells via their regulatory function. Therefore, the plasticity and developed potential of NC cells is encoded in gene regulatory circuits such that the combination of transcription factors maintains NC cells in an undifferentiated state. In chick, the first NC specifiers expressed in aborning NC cells are Snail 1/2, FoxD3 and Ets1 (Fig. 12). Ets1 is specific for cranial NC cells and not for trunk types in chick and zebrafish embryos (Rocha *et al.*, 2020). The upstream regulation of these genes is mediated by some NPB specifiers like Pax3/7 and Msx1, which directly bind to two cis-regulatory regions leading to differential expression in cranial and trunk NC of chick (Duband, 2006; Duband *et al.*, 2015; Simoes-Costa and Bronner, 2016). As said above, regulatory pattern of NC development is different through the species. For example, in amphibian embryos Zic1 and Pax3/7 upregulate Snail1/2 expression whereas in chick their target gene is FoxD3. Beside Pax7 and Msx1, other genes expressions like Myb and Myc are necessary in NC specification.

Signaling input is also thought to regulate NC specifiers. For instance, in chick, inhibition of Wnt signaling after NPB specification precludes Snail2 and FoxD3 expression, while in frog Wnt signaling works in concert with Zic1 and Pax3 to drive NC specification (García-Castro *et al.*, 2002; Simões-Costa and Bronner, 2015). Owing to the direct activation of Snail2 expression via TCF/LEF and  $\beta$ -catenin downstream of the canonical Wnt signaling, it has been postulated that Wnt works as permissive factor in NC specification. However, direct activation of other NC specifier expression via Wnt signaling has not been observed (Simões-Costa and Bronner, 2015).

Consequently, the NC specifier genes positively cross-regulate each other, much like the NPB specifier genes (Fig. 10). In frog, Snail1/2 positively regulate Twist, FoxdD3 and Sox9, while in mouse FoxD3 promotes Sox10 expression. Finally, the process of NC specification results in emergence of pre-migratory NC cells settled between neural plate and ectoderm regions, which express full suite of NC specifier genes like FoxD3, Snail2, Ets1, Sox8/9/10 and Pax3/7. Subsequently, these cells undergo changes at cellular level lead to delamination from neural tube via EMT (Fig. 12)(Simões-Costa and Bronner, 2013; Duband *et al.*, 2015; Simões-Costa and

Bronner, 2015). To know what fate NC cells suffer needs to gain more information about their aborning features during their accommodation at dorsal region of neural tube.

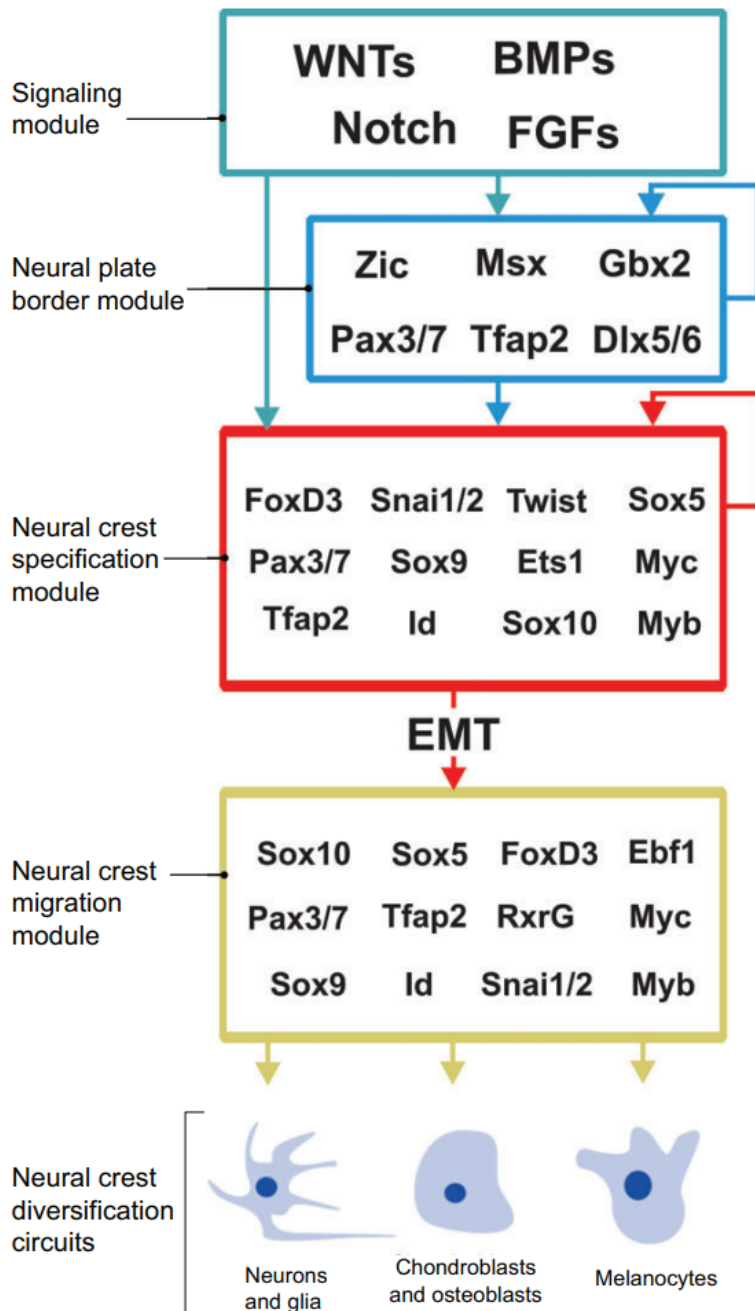


**Fig. 12. A GRN controls neural crest formation.** Outline of the GRN controlling neural crest development. Different inductive signals pattern the embryonic ectoderm and induce the expression of neural plate border specifier genes, which define the neural plate border territory. These genes engage in mutual positive regulation and also drive neural crest specification by activating the neural crest specifier genes. The neural crest specification program results in the activation of the EMT machinery that allows the neural crest cells to become migratory. The migratory neural crest cells express a set of regulators that endow them with motility and the ability to initiate different differentiation programs (Simões-Costa and Bronner, 2015).

**Neural crest pre-migratory behavior and cell emigration:** Upon NC specification during neurulation, the dorsal region of the neural tube contains pre-migratory NC cells. Indeed, this region is a transient epithelial state that progenitor cells either delaminate progressively or fully dissociate as migratory mesenchymal cells. As described above, in avian neural tube at trunk level, NC progenitors leave neural tube through a gradual event and individually. During this time, although dorsal neural tube lacks N-cadherin protein expression prior to the delamination, its epithelial structure is still preserved (Duband *et al.*, 2015). Cranial NC cells, in contrast, under a partial EMT escape from neural tube as a cohesive group of progenitors and rapidly split into distinct streams of cells.

The pre-migratory domain at trunk level is considered as reservoir of proliferative stem cells that upon cell division, exit from the neural tube in an ordered model via non-stem cell mechanism. It was shown that they leave their birthplace without leaving residual progeny in neural tube that is apart from the asymmetric model of stem-cells emigration (Rekler and Kalcheim, 2021). Therefore, upon initiation and progression of NC exit, a ventral to dorsal relocation of pre-migratory neuroepithelial progenitors is observed, until exhaustion of NC pool (Krispin *et al.*, 2010). Thus, dorsal region of neural tube is a dynamic region and acts as a transition zone for gradual departure of cells.

Owing to transition region of dorsal neural tube where induction and emigration of NC cells continuously occur, there is a molecular heterogeneity of NC population, either at the spatial or temporal level. Indeed, at trunk level, after NC specification, early pre-migratory progenitors are detected via Snail2, Sox9 and Foxd3 expression, while later progenitors lose them. In addition, at cranial level, five distinguishable NC clusters have been recognized such that a central portion expressed a combination of NC, pluripotency and differentiation markers, whereas a more lateral subdomain exhibits only NC genes. These data resulted from transcriptional signature at both global and single cell level deciphers the molecular heterogeneity at cranial level (Lignell *et al.*, 2017; Rekler and Kalcheim, 2021).

**Molecular control of the neural crest EMT program:** EMT is the critical step in NC development in which pre-migratory cells acquire the capacity to leave the neuroepithelium followed by cell

delamination and generation of mesenchymal/migratory NC cells. As such, the emigration of NC cells from neural tube is contingent on first, presence of an appropriate substratum for migration, second, loss of intercellular adhesion, and third the acquisition of migratory ability (Ji *et al.*, 2019). In response to the suitable microenvironment for NC cell migration, canonical Wnt signaling (Wnt/ B-catenin) induces G1/S transition and prepares NC cells for EMT at trunk level in chick embryos, causing that individual NC cells escape from the neural tube during the S-phase of cell cycle. Indeed, at trunk level, both EMT and delamination rely on cell cycle. The cranial NC cells, in contrast, are irrespective to cell cycle for delamination from neural tube in chick embryos. In addition, the canonical Wnt signaling participates in EMT induction through transcriptional and post-transcriptional regulation of Snail1/2 (Burstyn-Cohen and Kalcheim, 2002; Simões-Costa and Bronner, 2015; Ji *et al.*, 2019; Rekler and Kalcheim, 2021). What is interesting in this step is that the same genes driving NC identity have role in turning EMT on, indicating the connection between NC specification and EMT (Fig. 12) (Simões-Costa and Bronner, 2015). Further information about participation of Wnt and other signaling pathways during delamination of NC cells are depicted on Figure 13.

Furthermore, upon EMT, the changing of cell surface interactions necessitates remodeling of structure to dissolve adherent junctions, allowing pre-migratory NC cell to gain mesenchymal feature. Therefore, transcriptional regulation of cadherin can be considered as the key step in this process. In cranial level, the switch between type 1 cadherins (Ecad and cadherin2 (Ncad) and type 2 (Cad7 and Cad11) is required to facilitate NC delamination. The type 1 cadherins provide the strong cell-cell interactions to stabilize epithelial structure. Thus, NC cells need to lose this strong interaction with their neighbors in neural tube to exit and emigrate. Across species, EMT mechanism can change in terms of cadherins. For example, N cadherin is required for cranial NC delamination and migration (Kashef *et al.*, 2009; Simões-Costa and Bronner, 2015). Align with the tie between NC specification genes and EMT, overexpression of FoxD3 contributes also to downregulation of Ncad and upregulation of Cad7 in chick embryos; and subsequently Sox10 promotes Ncad repression in migratory cells (Cheung *et al.*, 2005; Simões-Costa and Bronner, 2015). Moreover, Snail1/2, considered as one of the important NC specifier transcription factor, influences EMT through repression of type 1 cadherins during

EMT. Snail1/ 2 also induce Cad6b repression, which is a classical type 2 cadherin required to be downregulated for NC delamination (Coles *et al.*, 2007).

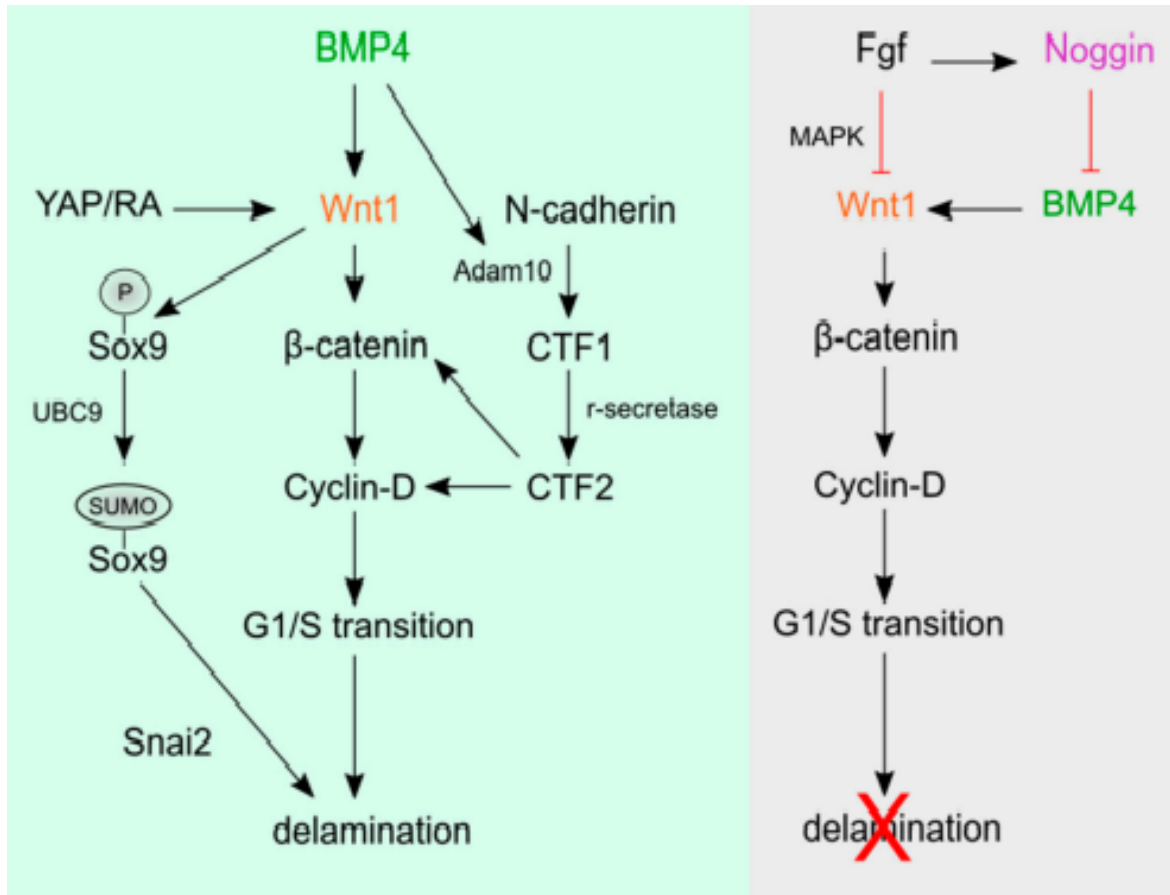


**Figure 13. Bmp/Wnt signaling regulates trunk neural crest cell delamination.** Undefined factors from somites inhibit Noggin (purple) expression anteriorly, creating a gradient of Bmp activity with a high level in anterior and low level in posterior part of the dorsal neural tube. Bmp4, Yap, and RA signaling induce canonical Wnt1 expression, leading to Cyclin D1 transcription and G1/S transition to promote NC cell emigration. However, at the segmental plate mesoderm at the posterior region, Fgf signaling maintains high levels of Noggin that inhibits Bmp activity. Low Bmp activity blocks Wnt signaling, which prevent NC delamination from caudal neural tube (Ji *et al.*, 2019).

Another interesting aspect of EMT in NC cells is that we have two uncouple steps of EMT including delamination and cell dispersion in NC development. For example, in *X. leavis*, NC cells detach as a group from neural tube and at later stages, they become individual cells as mesenchymal (Theveneau *et al.*, 2010). It seems that Twist and its regulator, Hif-1, have a role in dissociation of NC cells via downregulation of Ecad (Barriga *et al.*, 2013). In chick, detachment of NC from neural tube necessitates repressing cad6B, while cell-cell adhesion mediated by Ecad is downregulated by Zeb2 (Duband, 2006; Duband *et al.*, 2015). Altogether, the two steps of EMT comprise delamination of NC cells from the neural tube and subsequently acquisition of mesenchymal properties. Repression of Cad6B by Snail2 drives the delamination step leading to NC escape from neural tube. In the next step Twist or Zeb2 represses Ecad to allow NC cells to acquire migratory property (Simões-Costa and Bronner, 2015).

#### **4.2) Migratory Neural Crest Cells**

After delamination, a novel regulatory state is required for migratory NC cells, which expresses genes important for cell migration and differentiation program. Of these, some NC specifier genes sustain in migratory cells, like FoxD3 and Sox10. However, these genes render different regulatory input mediated by two different cis-regulatory. For example, in pre-migratory cranial NC cells FoxD3 expression is regulated by early enhancer (NC1), while maintenance of its expression in migratory NC cells is under another enhancer (NC2). Therefore, even though pre-migratory and migratory NC cells have common transcriptional factors, the regulatory expression can vary greatly as a function of time (Simões-Costa and Bronner, 2015).

Since migratory NC cells are exposed to different environmental signals and are also initiating to differentiation into diverse derivatives, these cells present a complex form of regulatory viewpoints. Intermixing of migratory NC cells with other cell types makes them difficult to isolate and characterize as a pure cell population. Thus, only a few transcriptional regulators are identified within migratory NC cells. Of these, Sox10 is a hallmark of migratory NC cells in chick. There is little information about how signaling molecules and receptors are controlled by GRN of migratory NC. Nevertheless, Sox10 plays a critical role in these cells (Simões-Costa and Bronner, 2015).

As NC cells migrate and colonize different places of the embryo, they transition from mesenchymal/ migratory to aggregates of cells within complex structures, called mesenchymal-to-epithelial transition (MET) as the reciprocal feature of EMT. Subsequently, they contribute to neurons and glia of peripheral ganglia, cartilage and many organs. A gene regulatory program again involves in this process. For instance, differentiation of NC cells to melanocytes relies on regulatory function of Pax3/7 and Sox10 along with a permissive signaling pathway (Wnt), causing the activation of transcription factor Mitf as a specific marker of the melanocytic lineage. Then, Mitf in turn initiates another positive cascade leading to activation of several enzymes responsible for melanin synthesis in pigmented cells. In addition, BMP signaling governs differentiation of NC cells to sympathetic neurons through activation of Ascl1 and Phox2b, which in turn drive other genes like tyrosine hydroxylase (Th) and dopamine  $\beta$ -hydroxylase (Dbh). Generally, NC differentiation depends upon the interplay of the cell-intrinsic transcriptional machinery and its interpretation of environmental cues conveyed by distinct signaling pathways (Simões-Costa and Bronner, 2015).

Regarding the dynamic region of the dorsal neural tube, it is logical that upon EMT, the metabolism is pivotal to meeting the energy demands of the cytoskeleton remodeling of NC cells to change their surface through the removal of either their interaction with neighbors or substratum. There are few studies which investigated the tie between metabolism and cranial NC cells at the initial steps of their development. We briefly take a look at these studies below.

### 4.3) Metabolic Regulation of NC Development

Bhattacharya and her colleagues recently demonstrated the connection between Warburg effect and cranial NC development in both delamination and migration steps. To address this key question, they cultured several neural folds at different stages during delamination, i.e. at HH9+ and HH7+; in medium containing 10 mM glucose, 2 mM glutamine and 1 mM pyruvate. The authors of this study narrated that the increased expression of glycolytic enzymes was the metabolic response to NC cells transition from delamination to migration. They reinforced the parallel between metabolic shift in NC cells development and metastatic behavior and motile cells in cancers. In addition, the pharmacological inhibition of aerobic glycolysis inhibited EMT and migration of NC cells, indicating the metabolic transition required for proper cell movement. Moreover, the increased glycolytic flux induced connection between YAP and TEAD1 protein and led to activation of Yap/Tead signaling pathway. Indeed, Yap signaling drove EMT and migration of NC cells through direct binding to tissue-specific enhancer (Bhattacharya, Debadrita *et al.*, 2020).

Moreover, delaminating and migratory NC in neural tube explant of amphibian embryos were found to rely on low oxygen uptake, and oxygen consumption increased align to beginning of differentiation (Flickinger Jr, 1949). Likewise, the activity of cytochrome C oxidase as the critical OXPHOS enzymes was low in undifferentiated migratory quail NC cells, while it was increased in differentiated cells (Liu *et al.*, 1990). In addition, in *Xenopus leavis*, glycolysis is upregulated during and after neurulation mediated by overexpression of *pfkfb4* (6-phosphofructo-2-kinase/fructose-2,6-bisphosphatase 4) via GRN of NC cells. Indeed, PFKFB4 is essential not only for NC specification but also for pre-migratory NC cells to emigrate from neural tube. Moreover, AKT signaling induce PFKFB4 function in NC late specification; and then both AKT signaling plus glycolysis regulate NC migration (Figueiredo *et al.*, 2017).

## Objectives

Owing to tightly regulation of NC development via GRN, the combination of transcription factors in response to environmental cues leads to forming the signaling pathways to regulate plasticity and potential of NC development. On the other hand, the sensitivity of metabolic enzymes to their substrate availability represents an intimate link between metabolism and environment, which governs cellular decisions due to their dual functions including epigenetically regulatory and canonical functions (anabolic and bioenergetic function). Accordingly, regarding to PSC potential for proliferation and differentiation, the integration of metabolism and GRN is pivotal to regulate normal NC development. As we saw above, although all subpopulations of NC cells are defined as highly migratory stem cells, they exhibit distinct mechanisms of GRN, EMT, migration, and cellular fate. Thus, the intriguing possibility of the metabolic influence over NC development across axial level can be a fascinating issue in research. Therefore, in my thesis, I sought to further our understanding of trunk NC cells at this scope in avian embryos.

To understand how metabolic pathways drive NC development, we need to explore metabolic enzymes contributing to GRN to establish NC development, which has been unknown. But this aim requires first to appreciate the NC development in response to nutrient availability. So, we follow two aims in this study:

- 1) impact of nutrient availability and metabolic stress on all steps of NC development including proliferation, delamination, migration and differentiation.
- 2) intrinsic metabolic pathway driving both EMT and delamination of NC cells, as the crucial step of their development.

## **II. Results**

# *Part A*

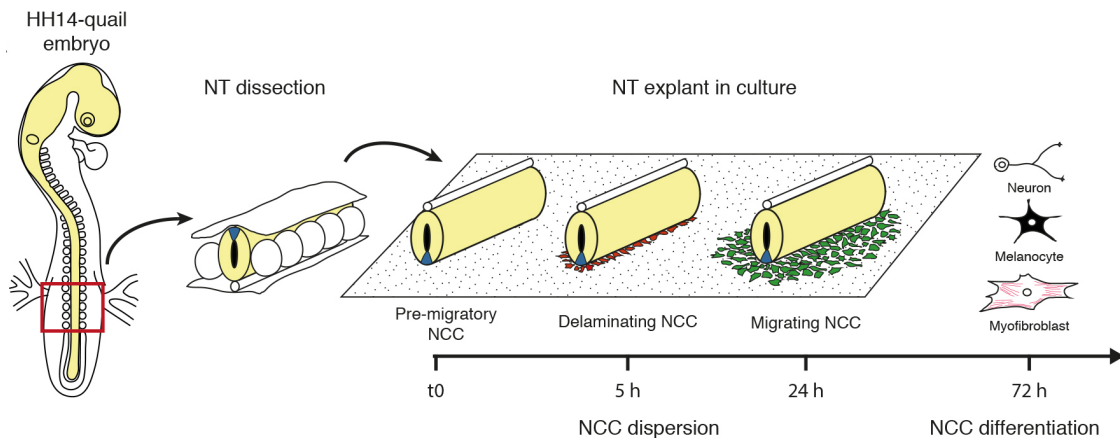
## *Neural Crest Development Relies on Glucose Oxidation*

My PhD work started in the Team 6 “Morphogenesis and molecular genetics” headed by Sylvie Dufour in our institute. This study was conducted in collaboration with two other members of Team 6, Redouane Fodil and Sophie Féréol, and with Roberto Motterlini and Roberta Foresti of Team 12 “Drug Discovery and Cell Therapy in Cardiovascular Diseases” headed by R. Motterlini (now, they have joined the Ghaleh’s team in our institute). Since January 2020, our team has joined the Team BNMS “Biology of the neuromuscular system” headed by Frederic Relaix and my PhD work has continued in this team.

### **Objective**

Since investigating NC cells metabolic features and their impact on their developmental program cannot be performed directly in intact living embryos, we developed an alternative strategy based on *ex vivo* culture in defined conditions recapitulating the delamination, migration, and differentiation steps of NC development, as well as their main features (timing and kinetics of cellular events, rate of proliferation, cellular interactions) (Duband, J. L. *et al.*, 2020). We characterized the metabolic traits of avian trunk NC cells under standard conditions, and we modified the activity of some of the key metabolic enzymes or the nutrient supplies to decipher the role of carbon metabolism in NC dispersion and differentiation.

For this purpose, a neural tube (NT) portion collected at the level of last five somites was dissected and plated in a defined medium to produce the primary culture of trunk NC cells, as shown in below:



Schematic representation of the procedure to culture NT explants from quail embryos indicating the timing of main steps of NCC dispersion (i.e. delamination and migration) and differentiation.



Phase contrast images showing of the overall aspect of NT explants and surrounding NCC population, and the morphology of individual NCC after 5 h, 24 h, and 72 h in control culture condition. Bars = 100  $\mu$ m

As shown in the panels above, this culture medium was suitable for the complete development (from delamination to differentiation) of avian trunk NCC in primary culture and referred as the control medium, which is supplemented by DMEM containing glucose (5 mM), pyruvate (2 mM), and glutamine (1 mM) as bioenergetic and biosynthetic nutrients and supplied with 1% serum to minimize the contribution of exogenous growth factors and fatty acids. Such a medium was able to elicit NC dispersion from NT explants, and NC differentiation (Rovasio *et al.*, 1983; Santiago and Erickson, 2002; Dupin, Elisabeth *et al.*, 2018).

## 1. Multiple Metabolic Pathways are Mobilized during Trunk NC Dispersion

We first investigated whether NC cell dispersion (i.e. their ability to delaminate and migrate away from NT explants) relies on specific metabolic pathways, using inhibitors of glycolysis, OXPHOS, and PPP (Fig. 1A). The inhibitors were applied at onset of culture (except in video microscopy analyses, where they were applied just before recording to reveal real-time effects, Fig. 1C), and the behavior of the NC population over 24 h was compared to that of explants in control medium, focusing on outgrowth area at 5 and 24 h (Fig. 1B); outward progression of the migration front over time (Fig. 1C); and outgrowth aspect (Fig. 1D). In the presence of 2-deoxyglucose (2-DG), a potent inhibitor of upper glycolysis, NC segregated normally from the NT and their progression during the first 5 h was close to that of controls, but cells became rapidly less spread, less compact, with a spindle shape. After 5 h, expansion of the population almost completely stalled, and NC cells started to round up. At 24 h they displayed poor survival and formed a sparse population occupying a limited area around the NT, compared with the large outgrowth with numerous well-spread and dense cells seen in controls. Oligomycin, an inhibitor of mitochondrial ATP synthase, marginally affected NC progression during the first 5 h, but cells were densely packed, causing a reduction of the outgrowth area. NC expansion decreased subsequently with a progressive reduction in cell spreading, resulting in a reduced outgrowth of sparse, round cells at 24 h. A similar effect was obtained with rotenone combined with antimycin-A (Rot-AA), blockers of complex I and III of the mitochondrial electron transport chain, except that reduction in dispersion was immediate and massive, producing after 5 h a population of spread cells limited to the NT rim. 6-aminonicotinamide (6-AN) which blocks PPP at the level of the 6-phosphogluconate dehydrogenase showed no apparent effect on the initial dispersion of NC cells; however, the progression of cells slowed down after 5-8 h, and a strongly reduced outgrowth with many round cells was observed at 24 h.

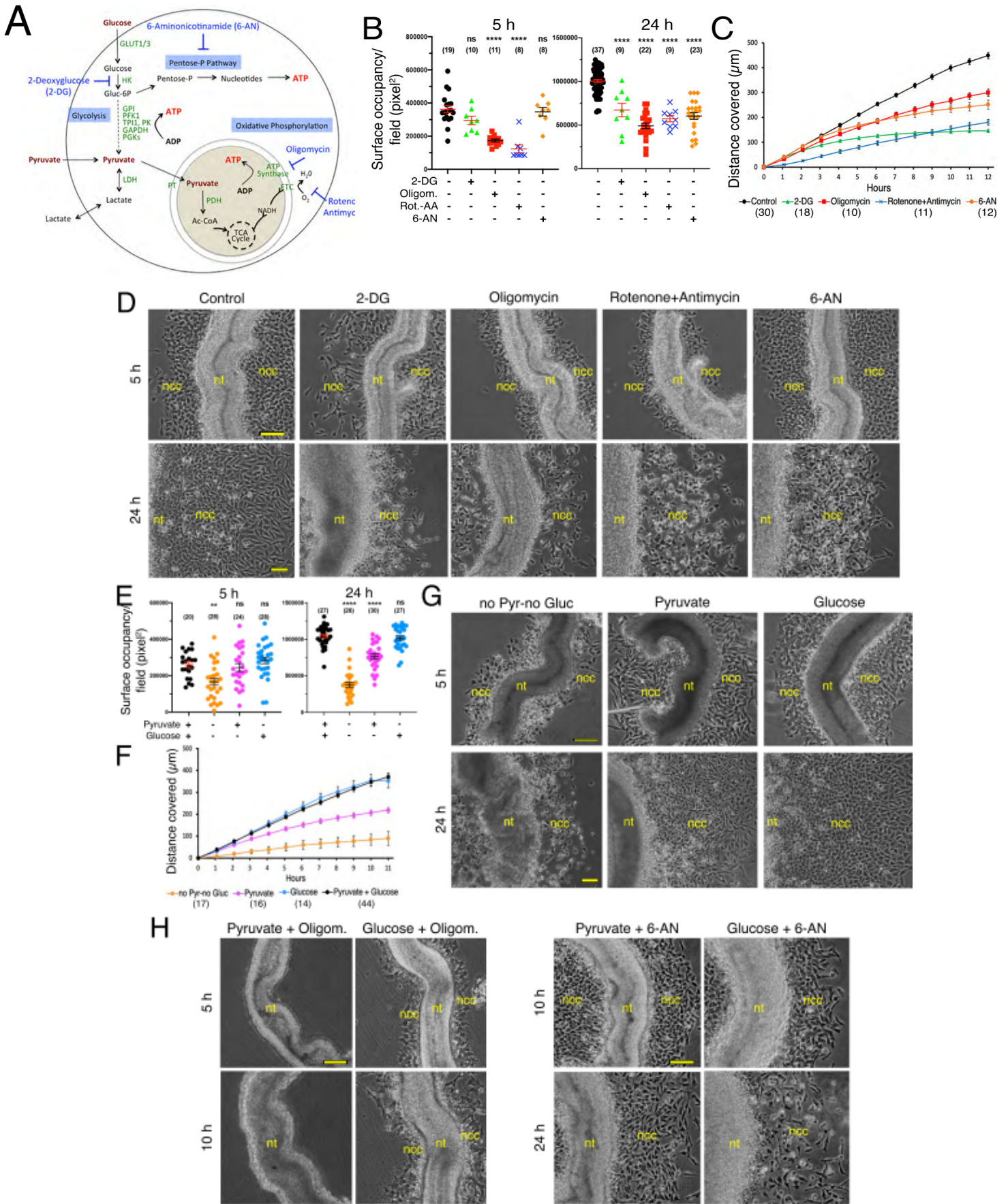


**Fig. 1. Multiple metabolic pathways are mobilized during trunk NCC dispersion.** (A) Schematic representation of the main pathways of glucose and pyruvate metabolism indicating the specific targets of the respective inhibitors of glycolysis (2-DG, ATP synthase (oligomycin), complex I and III of the electron transport chain (Rot-AA), and PPP (6-AN). (B-G) Effect of inhibitors of glucose metabolism and of nutrients on NCC dispersion: (B, E) NCC outgrowth area; (C, F) Progression of the migratory front of the NCC population over time; (D, G) Overall aspect of NT explants. (H) Overall aspect of NT explants in culture in pyruvate or glucose and in the presence of oligomycin or 6-AN. Bars in D, G, and H = 100  $\mu$ m. Error bars = S.E.M.

Because 2-DG inhibits all metabolic pathways downstream of glucose uptake, we also tested the effect of Na-iodoacetate, an inhibitor of glyceraldehyde-3-phosphate dehydrogenase, an enzyme of lower glycolysis (Fig. S1A). This chemical reduced significantly NC dispersion after 24 h but less dramatically than 2-DG (Fig. S1B). Unlike 2-DG, Na-iodoacetate did not alter cell survival but produced sparse outgrowths containing NC cells with round to elongated morphologies. Thus, all inhibitors of glucose metabolism and modulators of the mitochondrial respiratory chain affected NC dispersion (even if with specific kinetic and morphological effects), suggesting that all metabolic pathways downstream of glycolytic pathway are mobilized in a cooperative manner in NC cells.

## 2. Nutrient Availability Affects Trunk NC Dispersion

To investigate whether NC development is influenced by nutrient availability and to document the specific roles of glucose and pyruvate metabolism in NC dispersion, we cultured NT explants in conditions in which, beside glutamine, only pyruvate, glucose, or neither were provided (Fig. 1E-G). In the absence of pyruvate and glucose, although NC cells initiated migration from the NT, they failed to follow the normal progression and dispersion by the time, leading to considerable death after 24 h. In the presence of pyruvate, NC dispersion occurred almost normally at culture onset but stopped after 5-8 h, with cells exhibiting elongated spindle shaped morphologies, thus mimicking strikingly the behavior and morphology of NC cells treated with 2-DG. However, and in contrast to 2-DG effect, NC cells did not undergo cell death in the long term. In the presence of glucose, progression of NC outgrowths and cell morphologies were virtually indistinguishable from those observed in controls.

We then examined the effect of ATP synthesis inhibition and PPP blockade on NC cells cultured in the presence of pyruvate or glucose (Fig. 1H). Oligomycin exerted a much more immediate and stronger effect on NC cells cultured in pyruvate than in glucose, with a complete abrogation of cell dispersion. Conversely, 6-AN greatly affected dispersion in glucose-containing medium but had little effect on NC cells in the presence of pyruvate even after 24 h. We also analyzed the effect of the UK-5099 compound, a potent inhibitor of the mitochondrial pyruvate carrier (Fig. S1A)(Schell, John C *et al.*, 2017). UK-5099 reduced NC dispersion and affected their spreading, severely in medium containing pyruvate and more moderately in the presence of glucose or under control conditions (Fig. S1C-E).

Finally, we analyzed whether nutrient concentration affects NC dispersion. We found 1 mM pyruvate and 5 mM glucose present in the control medium as the most optimal condition for NC dispersion (Fig. S2A), while either lower or higher concentrations of these nutrients were unable to provide large outgrowth of NC cells (Fig. S2A). In addition, pyruvate at low concentration did not support NC cell spreading while at high concentration it induced extensive cell flattening in the long term (Fig. S2B). Glucose, in contrast, favored NC cell spreading at all concentrations used (Fig. S2B).

All together, these results suggest that NC dispersion relies strongly on the amount of nutrient inputs and downstream metabolic pathways. The significant impact of UK-5099 on NC dispersion in control or glucose condition proposed glucose oxidation as the dominant metabolic profile for dispersion.

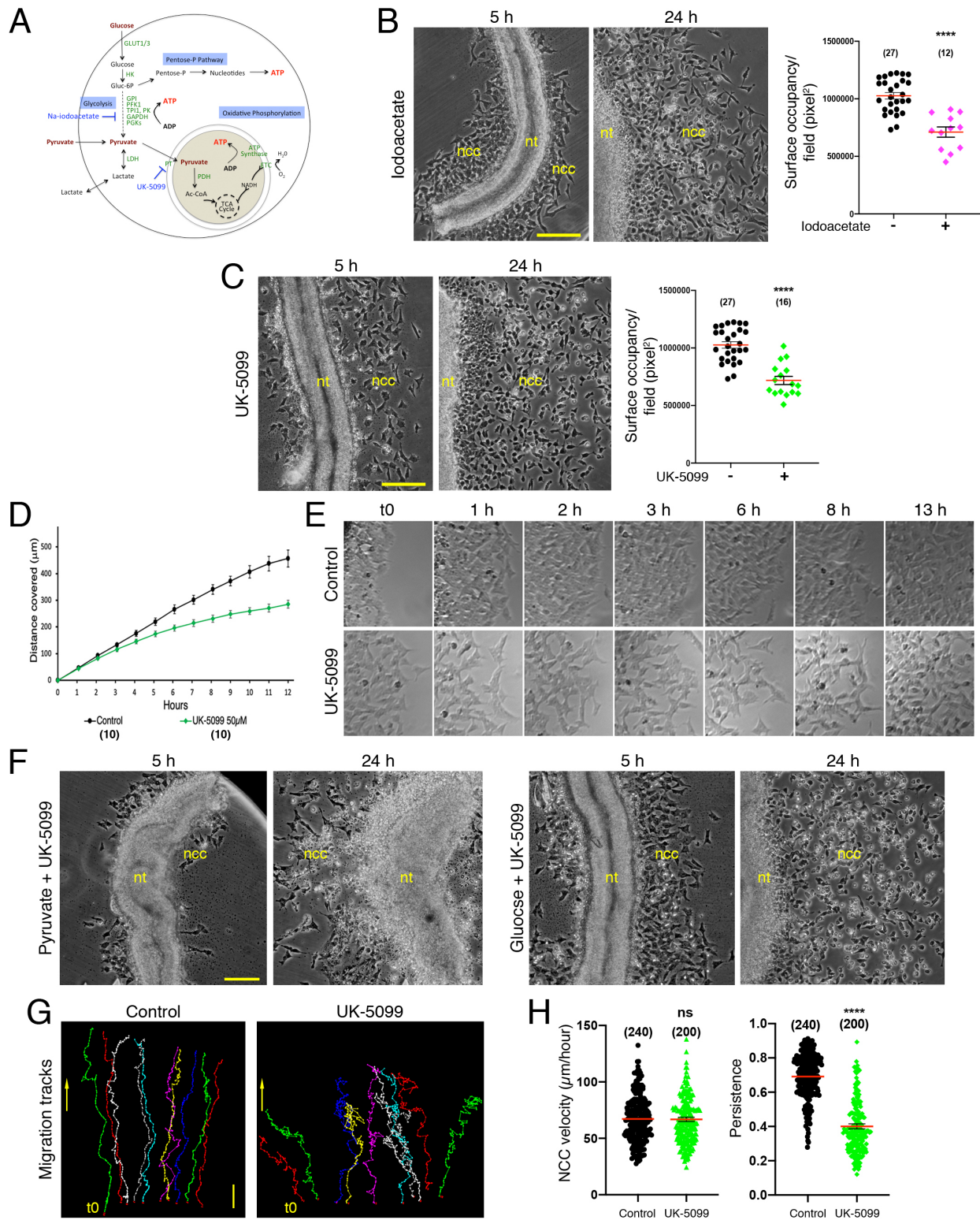


**Fig. S1. Effect of the metabolic inhibitors Na-iodoacetate and UK-5099 compound on NCC dispersion, morphology, and locomotory capacity.** (A) Schematic representation of the main pathways of glucose and pyruvate metabolism (glycolysis, PPP and OXPHOS) indicating their major steps, the main metabolite transporters and enzymes involved, and the specific targets of Na-iodoacetate and UK-5099, namely glyceraldehyde-3-phosphate dehydrogenase and mitochondrial pyruvate transporter, respectively. (B, C) Overall aspect of NT explants after 5 and 24 h in the presence of Na-iodoacetate (B) and UK-5099 (C), each added at the time of NT culture, and quantitation of the NCC outgrowth area after 24 h, compared with controls. (D, E) Progression and morphological aspect of NCC at the migratory front over time in culture in the presence or not of UK-5099 (see legend of Fig. S2, for details). (F) Overall aspect of NT explants after 5 and 24 h in pyruvate or glucose and in the presence of UK-5099. (G) Representative migration tracks of NCC

(in controls and in the presence of UK-5099 over 18 h. The position of the NT is to the bottom of the image and the periphery of the outgrowth to the top. the initial position of cells at beginning of recording is shown at t0, and the arrow gives the orientation of cell progression over time. (H) NCC velocity and persistence over the complete timing of recording in UK-5099. Bars in B, C, F, and G = 100  $\mu\text{m}$ . Error bars = S.E.M.

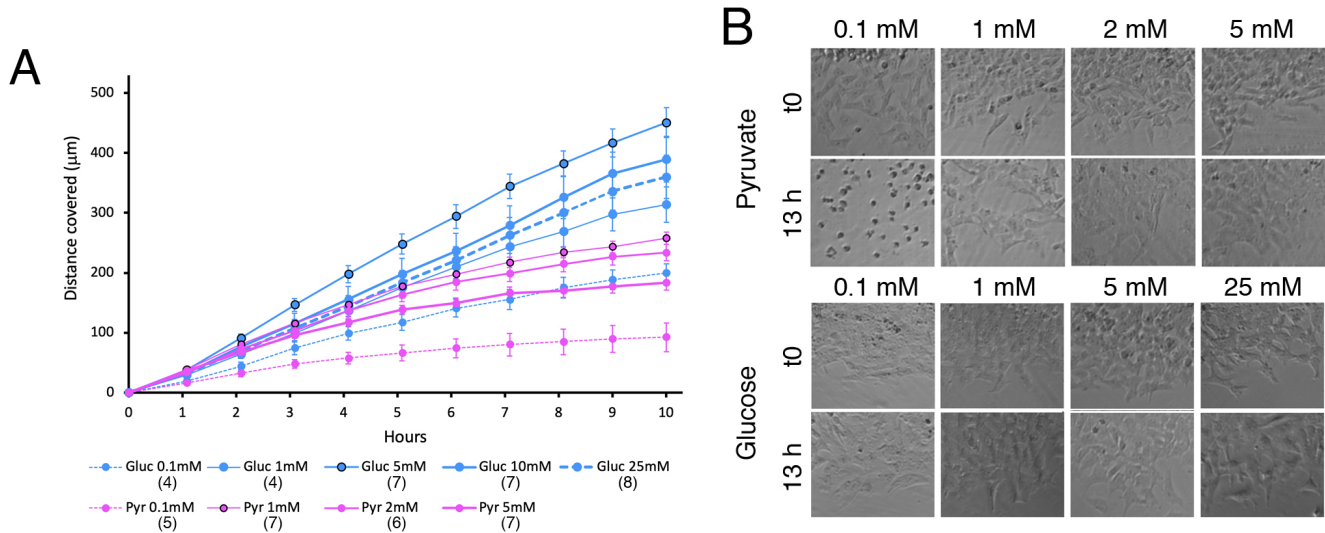


**Fig. S2. Characterization of NCC locomotory capacity with pyruvate and glucose at various concentrations.** (A) Progression of the migratory front of the NCC population over time in culture in pyruvate (pink curves) and in glucose (blue curves). (B) Morphological aspect of NCC at the migratory front at t0 and after 13 h in pyruvate (upper panels) or in glucose (lower panels).

### 3. Metabolic Profiling of NC Cells Reveals a Typical OXPHOS Signature during Migration

To probe the OXPHOS based glucose as the dominant metabolic profile of NT explant, we assessed cellular bioenergetics in NT explants and measured mitochondrial respiration and glycolysis using a Seahorse XF analyzer. For greater accuracy, measurements of the oxygen consumption rate (OCR) and extracellular acidification rate (ECAR) were performed on individual NT explants. Analyses of the bioenergetic profiles of more than 300 samples combined with MitoStress assays revealed that a great majority of the explants displayed a strong OXPHOS signature characterized by high OCR and low ECAR (Fig. 2A, B). Measurements performed on explants after 5 and 24 h did not reveal notable changes in OCR and ECAR (Fig.

2B), suggesting that the metabolic activity was constant throughout migration. We then investigated the impact of metabolic inhibitors on OCR and ECAR (Fig. 2C-E) as well as on production of ATP (Fig. 2F). 2-DG or oligomycin caused a sharp drop in OCR with no significant alteration in ECAR, and they strongly reduced ATP production. Reciprocally, the extracellular lactate level was irresponsive to these inhibitors (Fig. 2G). In contrast, 6-AN had no effect on OCR and ATP levels (Fig 2-C-F). These results demonstrate that, in explants cultured with control medium, most of the ATP production relies primarily on glucose oxidation through OXPHOS and suggest that OXPHOS inhibition does not cause metabolic rewiring to aerobic glycolysis with increased lactate production. We next characterized the bioenergetic features of explants cultured in pyruvate or glucose. Similar to the control condition, NT explants exposed to glucose or pyruvate condition were quite sensitive to mito-stress (Fig. 2H). The lower OCR and ECAR values combined with ATP production in pyruvate condition (Fig. 2H-K), revealed a higher yield in energy production for glycolysis coupled to OXPHOS than for extracellular pyruvate-evoked OXPHOS. To lend further support, the impact of 2-DG or oligomycin were examined in these conditions, which indicated that 2-DG and oligomycin similarly decreased OCR levels (Fig. 2I, J) and sharply reduced ATP production (Fig. 2K) but did not affect lactate production (Fig. 2L).

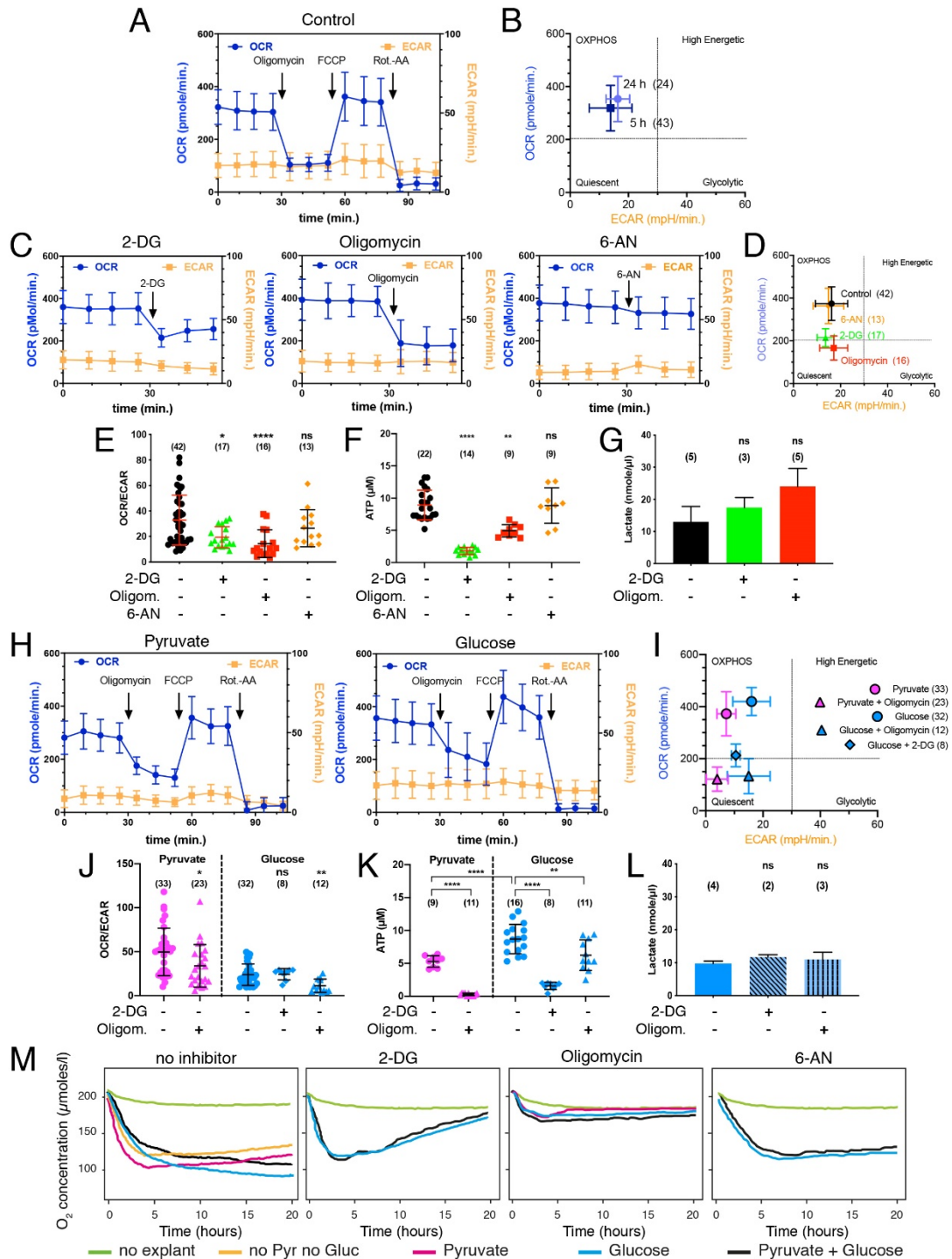


**Fig. 2. Metabolic profiling of NCC reveals a typical OXPHOS signature during migration.** (A-L) Quantitation analyses of O<sub>2</sub> consumption rate (OCR) and extracellular acidification rate (ECAR) using a Seahorse analyzer, and ATP and lactate productions in individual NT explants cultured for 5 h (and 24 h in B) in control medium after treatment with inhibitors of glucose metabolism, and in different nutrients: (A, H) MitoStress assays; (B, D, I) Energetic maps deduced from OCR and ECAR measurements; (C) OCR and ECAR profiles over time in explants cultured in control medium in the presence of metabolic inhibitors; (E, J) Values of OCR/ECAR ratio; (F, K) Intracellular ATP measurement; (G, L) Extracellular lactate measurement. (M) Representative profiles of O<sub>2</sub> concentration curves over time in NCC primary cultures using the Presens technology. Error bars = S.D.

Because the Seahorse technology is not suitable for prolonged exposures to drugs to evaluate long-term effects in cell cultures, we used the Presens technology. Although less sensitive (measurements cannot be performed on single explants), this technology allows an accurate measurement of O<sub>2</sub> levels at the vicinity of NT explants throughout the course of NC migration (Fig. 2M). O<sub>2</sub> levels obtained in the presence of explants showed an immediate decrease over time compared to those measured with medium alone, indicating that the explants actively consume O<sub>2</sub> in a measurable manner. Strikingly, the profiles of the curves differed with the nutrients. In absence of nutrients, O<sub>2</sub> concentration decreased rapidly within the first 4 h but after reaching a minimal value, it increased gradually, signaling a decrease in cellular respiration. This was also observed for explants in pyruvate, except that O<sub>2</sub> consumption during the first 4 h was significantly higher than with no nutrient. Intriguingly, the inflection points in the curves corresponded to the time when expansion of the NC population ceased (see Fig. 1C). In glucose or in control medium, in contrast, O<sub>2</sub> concentration decreased less abruptly than in pyruvate during the first 4 h, but continued to decrease, consistent with the expansion of the population. Addition of 2-DG had no immediate effect on O<sub>2</sub> consumption, but after 5 h, it caused an increase in O<sub>2</sub> levels, reflecting most likely poor cell survival. 6-AN showed a minimal effect on cellular respiration with only a gradual slowing down with time. In contrast, addition of oligomycin rapidly and totally blocked mitochondrial respiration. These data therefore provide a causal relationship between O<sub>2</sub> consumption and long-term NC dispersion and survival.

Finally, we analyzed the topical features of mitochondria network in NC cells using MitoTracker Red labeling (Fig. S3). While in NC cells cultured in glucose or in control medium, mitochondria had a large globular structure and were organized as rings homogeneously distributed throughout the cell body, in pyruvate, they were smaller, elongated and often organized as chains extending into the cell processes (Fig. S3A). As expected, mitochondria were small and poorly organized in the absence of nutrients (Fig. S3B) as observed in presence of oligomycin or UK-5099 (Fig. S3B), further illustrating the critical role of mitochondria in NC cells.

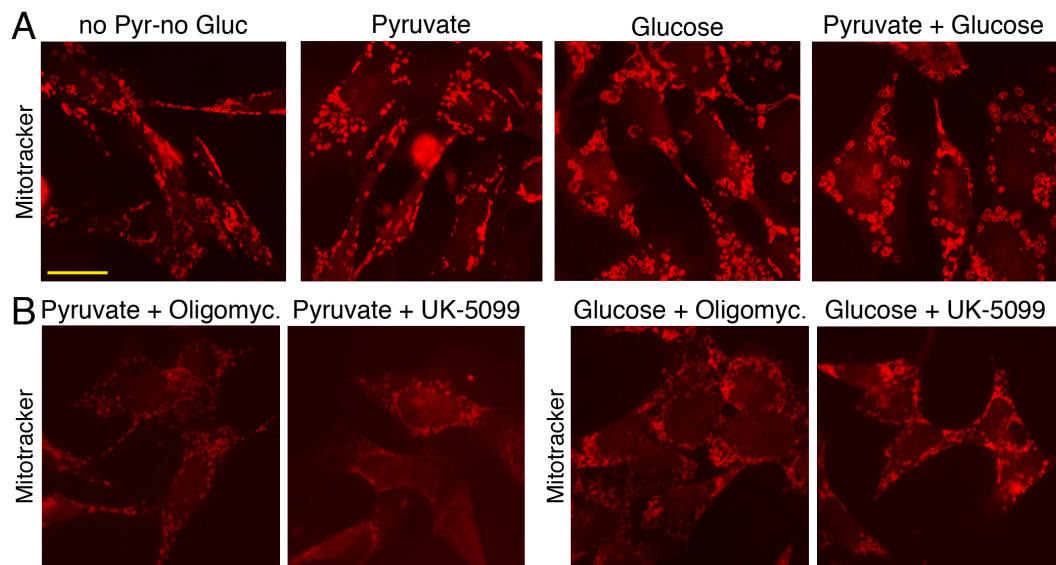


**Fig. S3. Morphological features of mitochondria networks in NCC cultured in different nutrient conditions and in the presence of metabolism inhibitors.** Images of MitoTracker red labeling of NCC cultured for 24 h with no nutrient, in pyruvate, glucose, or in control medium (A) and in NCC cultured for 5 h in pyruvate or glucose in the presence of oligomycin or UK-5099. Bar = 10  $\mu$ m.

#### 4. Expressions of Glucose Transporter and Glycolysis Enzymes are Regulated at the Time of Migration

Because glucose appeared to be the most important nutrient for NC dispersion, we analyzed the expression of key players of glycolysis in NC cells. The glucose transporter *Glut-1* was expressed equally on the surface of NC cells in pyruvate and glucose (Fig. 3A). To probe the link between nutrient availability and metabolic genes expression, we compared the expression of several metabolic genes in glucose and pyruvate conditions. *Glut-1* mRNA as well as those for phosphofructokinase *PFK*, a major rate-limiting enzyme of upper glycolysis (Feng *et al.*, 2020), were clearly expressed in the NT but were not in NC cells. In addition, they were both up regulated in the presence of glucose compared to pyruvate (Fig. 3B, C), indicating that their expression largely relied on nutrient availability. In contrast, phosphoglycerate kinase-1 (*PGK-1*), an enzyme of lower glycolysis, was expressed in both the NT and migrating NC cells and did not show much differential expression with nutrients (Fig. 3B). We then analyzed the expression of *Glut-1*, *PFK*, and *PGK-1* in the trunk region of whole embryos at stages of initiation of NC migration (Fig. 3D). In agreement with previous studies (Oginuma, Masayuki *et al.*, 2017), we found that *Glut-1* and *PFK* genes are poorly expressed in the caudal part of the embryo except in the NT in which they are strongly but transiently up regulated at the time of NC delamination. Again, *PGK-1* was conspicuously expressed in all tissues, but was also increased in the NT during delamination. These data indicate that while lower glycolysis is constantly active in migrating NC cells, upper glycolysis is subjected to spatial and temporal regulation at onset of migration. Therefore, these results raised the intriguing possibilities that, in migrating NC cells, (i) lower glycolysis may be fed by exogenous metabolic intermediates possibly provided by the NT; and (ii) localized activation of glycolytic enzymes in tissues may be due to differential distribution of nutrients and metabolites in the embryo.

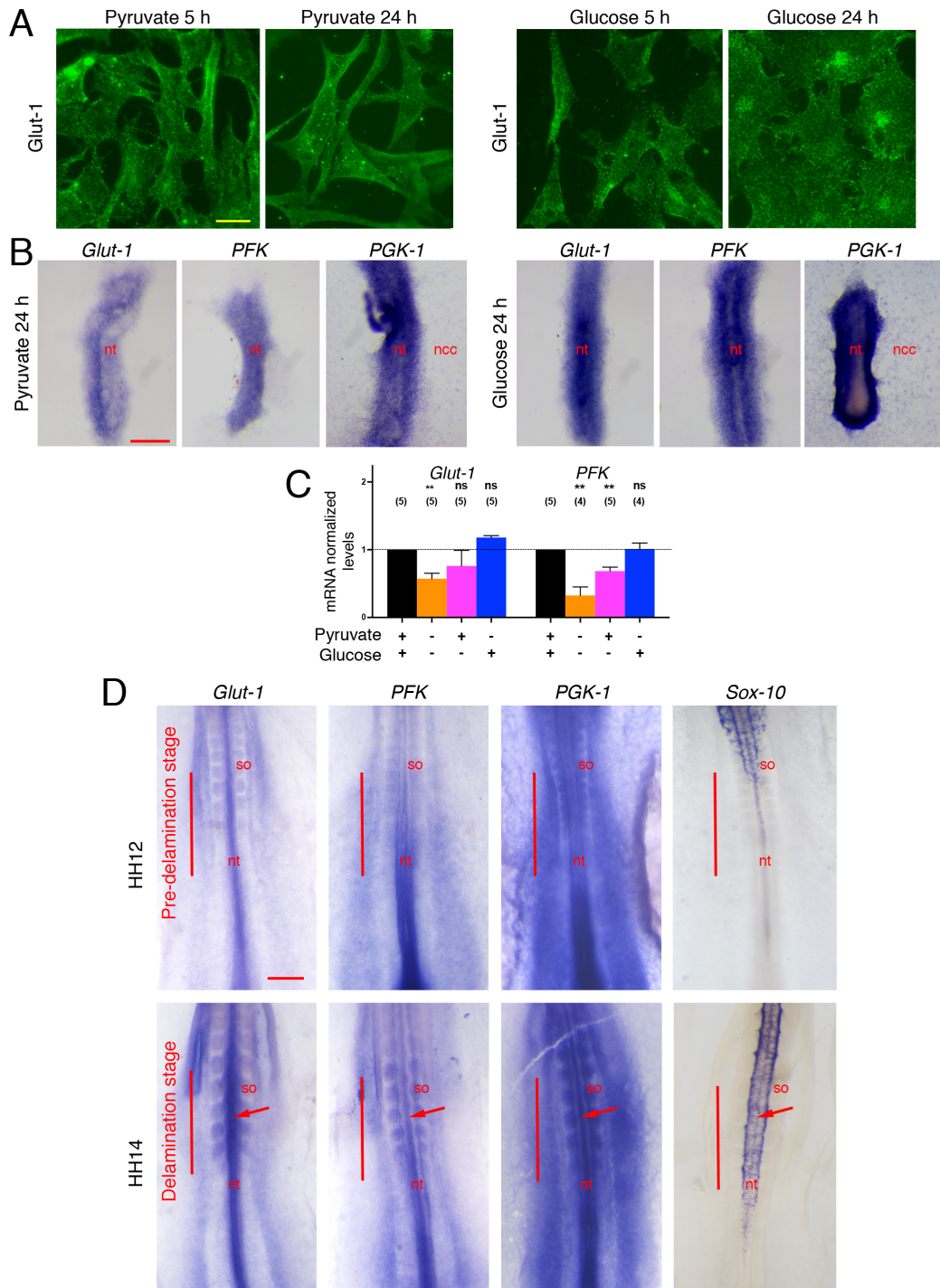


**Fig. 3. Expressions of glucose transporter and glycolytic enzymes are regulated at the time of NCC migration.** Immunostaining (A), in situ hybridization (B), and qPCR (C) analyses of the expression of the glucose transporter Glut-1 and of glycolytic enzymes PFK and PGK-1 in NCC and NT explants. (D) Whole mount in situ hybridization for Glut-1, PFK, and PGK-1 and for the migratory NCC marker Sox-10 in avian embryos at stage HH12 and 14 (i.e. 17 and 22 somites, respectively), showing the caudal part of the embryo at the level of the last formed somites (so) and of the unsegmented mesoderm. The bars indicate the axial levels at which NCC are in the pre-delamination stage at HH12 and in the delamination stage at HH14. Arrows point at the strong staining for Glut-1, PFK, and PGK-1 in the NT at levels of delaminating NCC, contrasting with the fainter NT staining in regions of pre-delaminating NCC. Bars in A = 10  $\mu$ m, in B = 100  $\mu$ m, and in D = 200  $\mu$ m. Error bars = S.E.M.

## 5. Glucose Metabolism Regulates Expression of EMT Genes during Delamination

The high expression of metabolic enzymes upon NC emergence indicated the link between NC dispersion and metabolism. NC dispersion results from multiple cellular processes acting in synergy and in concerted manner: EMT during delamination, changes of substratum and cell adhesion, activation of the locomotory machinery, and proliferation. We therefore studied the role of metabolic pathways in these different phases.

Thus, we developed an assay suitable for discriminating delaminated from migrating NC cells after 5 hours NT explants culture (Fig. 4A). Interestingly, the number of delaminated cells was halved by addition of 2-DG, oligomycin, or Rot-AA, as well as in pyruvate medium (Fig. 4B). Delamination in the presence of 6-AN was similar to control. Then, we investigated the expression pattern of the transcription factor Snail2, a major EMT player involved in NC delamination (Nieto, 2002; Duband, 2010); Fig. 4C). In the presence of glucose, Snail2 staining was high in delaminated NC cells while it declined gradually as cells dispersed away from the NT. Likewise, NC cells conserved the pattern of Snail2 staining under PPP inhibitor (6-AN) consistent with an unchanged delamination rate in response to 6-AN (Fig 4B). In contrast, in the presence of 2-DG or in pyruvate condition, Snail2 was strongly diminished in both NC compartments. Intriguingly, with OXPHOS inhibitors and particularly with Rot-AA, Snail2 completely disappeared in delaminated NC cells but remained highly expressed in migrating cells, proposing the pivotal role of OXPHOS on NC delamination. Expression of *Snail2* messengers in NT explants (Fig. 4D) was almost totally abrogated by 2-DG and strongly diminished by oligomycin, and was low in pyruvate and no nutrient, consistent with the reduction of Snail2 protein.

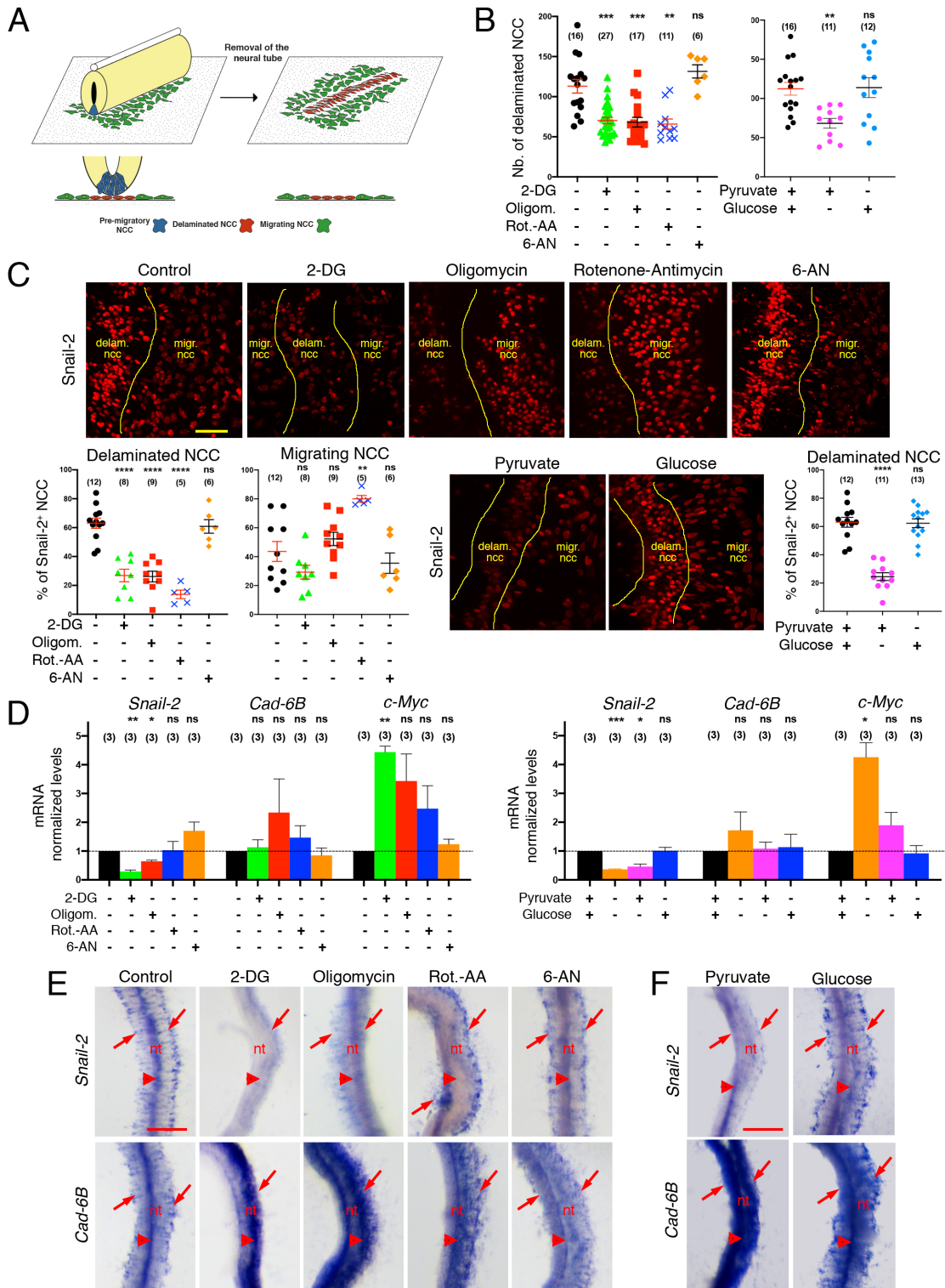


**Fig. 4. Glucose Metabolism Regulates Expression of EMT Genes during NCC Delamination.** (A) Schematic representation of the delamination assay. (B, C) Number of delaminated cells per explant (B) and expression of the *Snail-2* transcription factor (C) in delaminated vs. migrating NCC. (D, E) qPCR (D) and in situ hybridization (E) analyses of expression of *Snail-2*, *Cad-6B*, and *cMyc* in NT explants. In control medium, in the presence of 6-AN or with glucose, *Snail-2* and *Cad-6B* messages show overlapping distribution patterns in premigratory NCC in the dorsal NT (arrowheads) as well as in the delaminated NCC visible in either sides of the NT (arrows). In the presence of 2-DG, oligomycin, and pyruvate, *Snail-2* is much decreased in both premigratory and migratory NCC while in the presence of Rot-AA, it drops only in premigratory cells. Conversely, *Cad-6B* is strongly enhanced in the whole NT, particularly in the presence of 2-DG, oligomycin, and pyruvate. Bars in C = 50  $\mu$ m and E and F = 100  $\mu$ m. Error bars = S.E.M.

Conversely, *Snail2* expression was not much altered by Rot-AA, probably as a result of its increase in the migrating pool (Fig. 4D). We also analyzed in NC primary cultures the expression of other EMT-related genes (Fig. 4D, E), including *Cad6B*, a member of the cadherin family of adhesion receptors downregulated by Snail-2 at delamination and *cMyc*, a proto-oncogene involved in the maintenance of the NCC pool before delamination (Kerosuo and Bronner, 2016; Dady and Duband, 2017). While *Cad6B* expression remained unchanged under metabolic inhibitors, *cMyc* expression elevated in response to 2-DG and OXPHOS harness in agreement with the regulatory function of *cMyc* in metabolism (Pérez-Escuredo *et al.*, 2016). Similarly, pyruvate and no nutrient conditions caused a strong inhibition of NC delamination (Fig. 4D). Despite being normally restricted to pre-delaminating NC cells and a few NT cells in the floor plate, *Cad6B* was surprisingly increased in all NT cells in the presence of metabolic inhibitors or in pyruvate (Fig. 4E, F). All together, these data indicate that glucose metabolism is required for NC cell delamination by regulating the coordinated expressions of EMT-related genes and that OXPHOS resulting from pyruvate condition is necessary but not sufficient for this process.

## 6. Glucose Metabolism is Crucial for Locomotion

Avian trunk NC cells display a locomotory behavior different from the ones described for cranial or enteric NC populations (Rovasio *et al.*, 1983; Li *et al.*, 2019). Movement of individual cells involves substrate adhesion and intense protrusive activity, while outward directionality is driven by transient cell adhesion and mechanical forces resulting from high cell density. To understand the contribution of glucose metabolism to NC locomotion, we analyzed by video microscopy the effect of metabolic inhibitors applied after initiation of NC migration to avoid any bias due to the delamination process (Figs. 5A-E, S2 C, D). We plotted the migration tracks

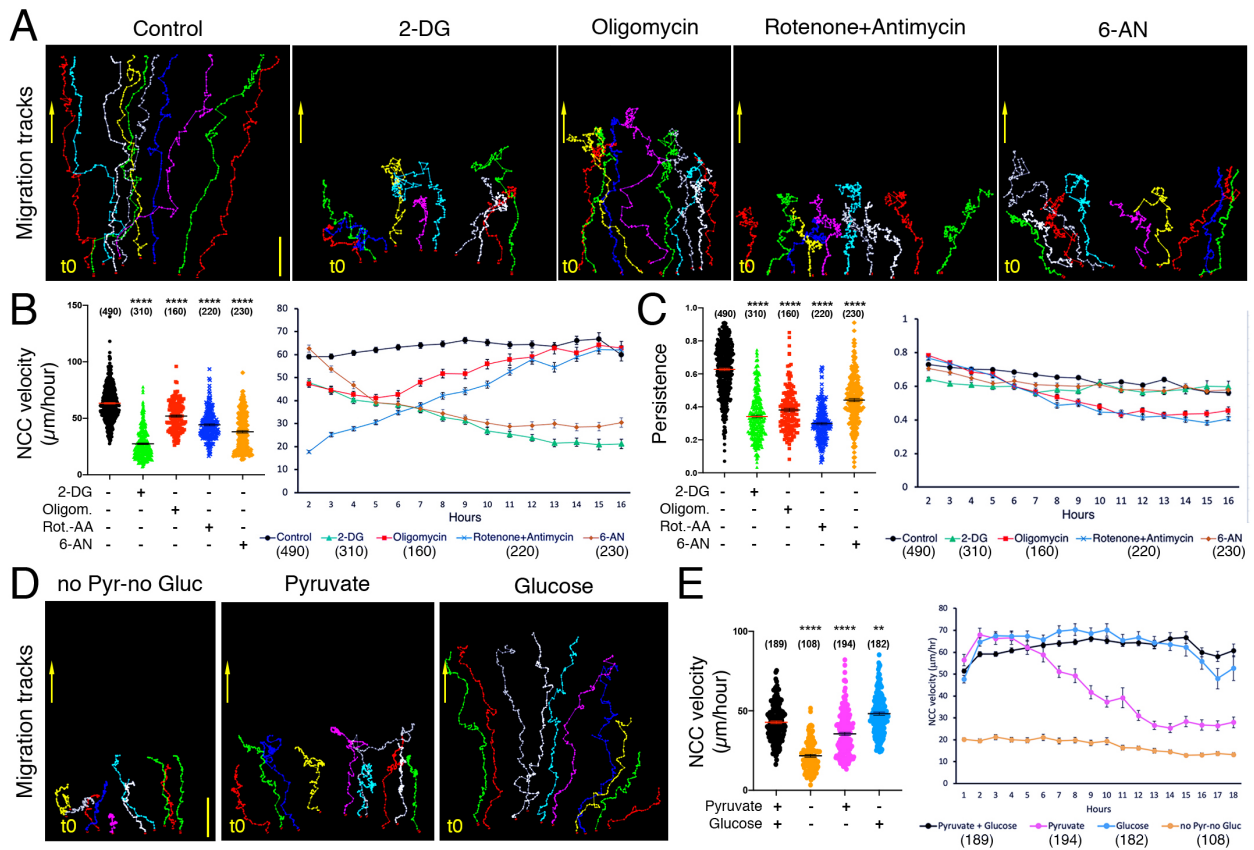


**Fig. 5. Glucose Metabolism is crucial for NCC locomotion and coordinates substrate and cell adhesions.**

(A-E) Effect of inhibitors of glucose metabolism and of different nutrients on NCC locomotion. (A, D) Migration tracks of several cells from a representative NT explant. The initial position of the cells is indicated at  $t_0$  and the direction of migration is given by the arrow. (B, E) Velocity of individual NCC throughout the duration of the video microscopy recording and variation of NCC velocity over time in culture. (C) Persistence of migration of individual NCC throughout the duration of the video microscopy recording and variation of the persistence over time in culture. Bars in A and D = 100  $\mu\text{m}$  and in F, G, and H = 20  $\mu\text{m}$ . Error bars = S.E.M.

of single NC cells situated at the migration front (Fig. 5A, D) and deduced NC cell velocity and persistence of movement over time (Fig. 5B, C, E). In control, NC cells generally exhibited persistent and directional migration oriented perpendicular to the NT leading to relatively linear trajectories. Both the velocity and persistence of cells were constant over the 18 h measurements, due to maintenance of high cell density. With 2-DG, cells trajectories were at first relatively linear but became more random with time. The most striking effect of 2-DG, however, was a rapid and continuous decrease of velocity over time and a progressive rounding up, resulting in the almost complete immobilization of cells. Unlike 2-DG effect on NC cell locomotion, cell trajectories were generally not much affected by oligomycin, while velocity was decreased during the first 6 h. Then, with time, cell migration became extremely random with a

significant decrease in persistence associated with increased velocity, gradual rounding up of the cells, and lack of cell-cell contacts. A very similar response was observed with UK-5099 (Fig. S 2G, H). Interestingly, Rot-AA showed a much stronger effect than oligomycin. Trajectories were very short because velocity was almost knocked-out after 2 h and remained weak during 8 h. However, as with oligomycin, velocity increased with time and persistence decreased coincident with cell rounding up. Lastly, 6-AN affected velocity strongly and gradually during the first 8 h before stabilizing, and cell trajectories became less linear.

We also analyzed NC cell locomotion in the different nutrient conditions (Figs. 5D, E, S2D). In glucose, trajectories, velocity, and persistence over time were very similar to those observed in control. In contrast, trajectories in the presence of pyruvate exhibited a profile similar to those seen with 2-DG, with a gradually decreasing velocity and reduced persistence, proposing the effective role of upstream glycolytic reaction in NC cell locomotion. Under no nutrient condition, velocity was consistently low combined very short migration tracks. For further supporting the glucose function in NC cell locomotion, we analyzed different concentration of pyruvate and glucose. In agreement with the dispersion curves (Fig. S2A in above), velocity peaked for pyruvate concentrations of 1 and 2 mM and plateaued at glucose concentrations  $\geq 5$  mM (Fig. S2C). Persistence, in contrast, was greater at pyruvate concentrations  $\geq 2$  mM and constant at glucose concentrations higher than 1 mM, possibly reflecting the differences in cell spreading observed (Fig. S2B). These results therefore illustrate the critical contribution of glucose metabolism to NC cell locomotion and also reveal that this process relies on other metabolic processes, notably PPP as well as mitochondrial activities involving TCA metabolites and byproducts.

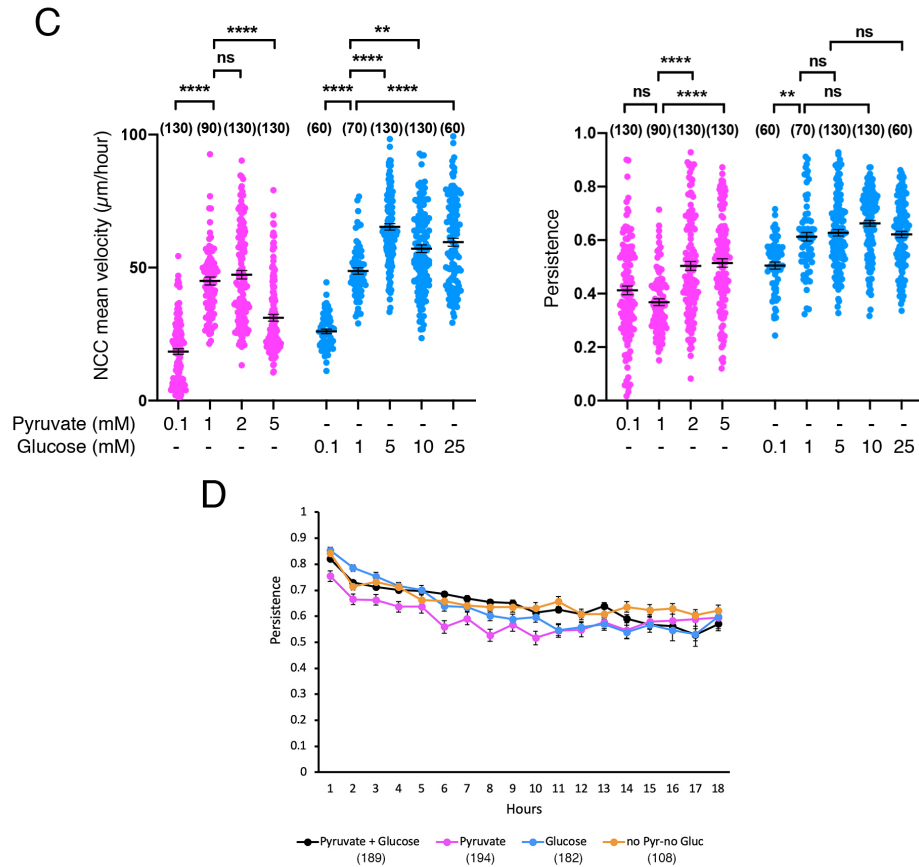


**Fig. S2.** (C) NCC velocity and persistence over the complete timing of recording in pyruvate (pink dots) and glucose (blue dots). (D) Variation of persistence of NCC displacement over time in culture, no nutrient (yellow curve), pyruvate (pink curve), glucose (blue curve), and control medium (black curve).

## 7. Glucose Metabolism Coordinates Substrate and Cell Adhesions

To gain insight into the impact of metabolism on cell adhesions, two pivotal aspects of NC delamination and migration, we examined the cellular localization of paxillin and B-catenin, two cytoplasmic partners of integrins- and cadherins-adhesion complexes, respectively (Fig. 5F-I). Compared to controls, we found that after 5 h, the number of substrate adhesions per NC cells was significantly reduced with 2-DG and increased with oligomycin, consistent with changes in cell spreading (Fig. 5F). Likewise, oligomycin increased substantially cell adhesions during the first 5 h (Fig. 5G). Finally, we observed that the number of substrate and cell-cell adhesions differed considerably with the nutrients (Fig. 5H, I). In control medium, NC cells exhibited large substrate adhesions with a four-fold increase in their number with time, while with no nutrient

they developed substrate adhesions at 5 h but did not increase their number with time. In pyruvate, NC cells displayed more elongated substrate adhesions, which did not increase in number with time. In contrast, in glucose NC cells exhibited substrate adhesions similar to those of control with a two-fold increase in their number with time (Fig. 5H). Quantification of intercellular adhesions in NC cells revealed that in control as well as in glucose, NC cells are always engaged in transient contact with 1-3 neighbors while in pyruvate, they remain as individuals (Fig. 5I). These data indicate that glucose metabolism regulates the balance between substrate and cell-cell adhesion in NC cells, thereby favoring optimal conditions for delamination and migration.

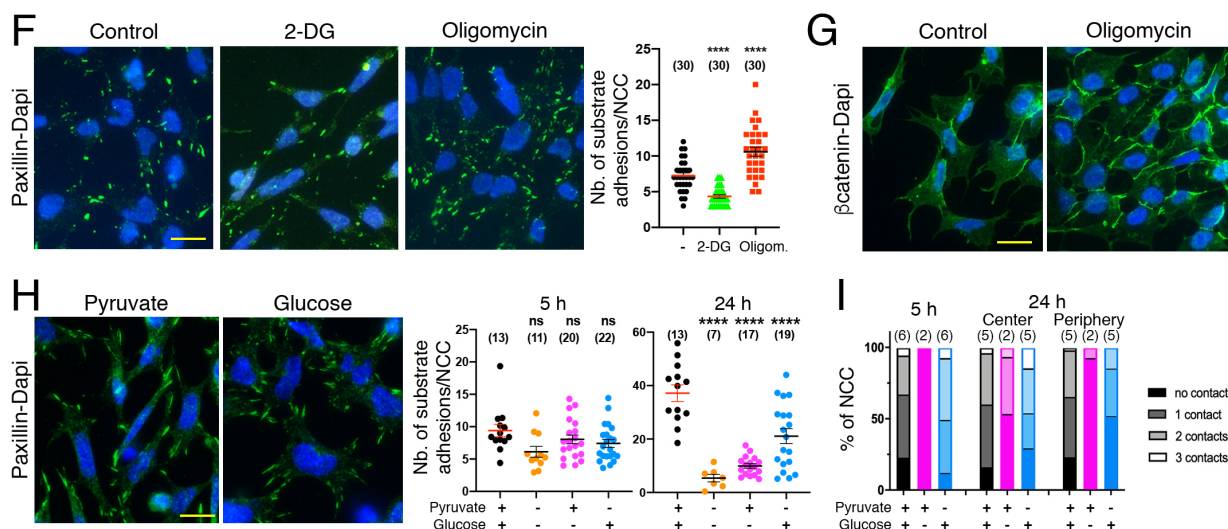


**Fig. 5. Glucose Metabolism is crucial for NCC locomotion and coordinates substrate and cell adhesions.**

(F-I) Effect of inhibitors of glucose metabolism and of nutrients on NCC substrate and cell-cell adhesions. (F, H) Visualization of paxillin and Dapi (blue) expression and quantification of the number of substrate adhesions in migrating NCC. (G, I) Visualization of B-catenin (Duband *et al.*) and Dapi (blue) expression and quantification of the number of cell-cell adhesions in migrating NCC. Bars in A and D = 100 μm and in F, G, and H = 20 μm. Error bars = S.E.M.

The convergence of mechanical and metabolic impacts on NC migration has been investigated in parallel by Redouane Fodil, Sophie Féreol and Sylvie Dufour. The data showed that trunk NC cells are mechano-responsive, and their response is determined by specific metabolic activities. In glucose, owing to their capacity to accommodate their stiffness and energy production to their environment, NC cells are endowed with the ability to migrate in a great diversity of biophysical constraints. In pyruvate, NC cells are less prone to modulate their stiffness and negatively respond to modifications in the rigidity of their environment by decreasing their adhesive and migratory response. These results are detailed in submitted version of the manuscript presenting the Part A study, added in the annex part.

## **8. Glucose Metabolism is Required for Sustained Proliferation**

Contrary to many motile cells, NC cells maintain active cell division throughout migration, and although this process by itself is not the driving force of migration, it is required for delamination (Burstyn-Cohen and Kalcheim, 2002) and contributes strongly to expansion of the population (Ridenour *et al.*, 2014). Using short pulse EdU incorporation, we studied NC cell proliferation from delamination to late migration steps. While numerous delaminating EdU<sup>+</sup> NC cells could be identified along the NT apical side in control medium, only few proliferative cells were observed in the presence of glycolysis or OXPHOS inhibitors (Fig. 6A). These results indicate the contribution of glycolytic and mitochondrial intermediates in NC cell proliferation and subsequently delamination. Similarly, during migration, all inhibitors decreased both the proportion of EdU<sup>+</sup> NCC and the EdU-staining intensity (Fig. 6B). Interestingly, unlike other compounds, the impact of 6-AN on proliferation decreased by the time, possibly reflecting the contribution of other metabolic pathways to the adaptation and compensation of 6-phosphogluconate dehydrogenase harness in PPP. With no nutrient, proliferation was strongly decreased at 5 h and was almost abolished after 24 h. Interestingly, consistent with the kinetics of their dispersion (see Fig. 1G), NC proliferation observed in glucose was similar to that of control whereas it was dramatically reduced after 24 h in pyruvate (Fig. 6C). These data reveal

that NC cell proliferation is pivotal in maintenance of developmental steps since all metabolic pathways are implicated in a cooperative manner in the control of proliferation.

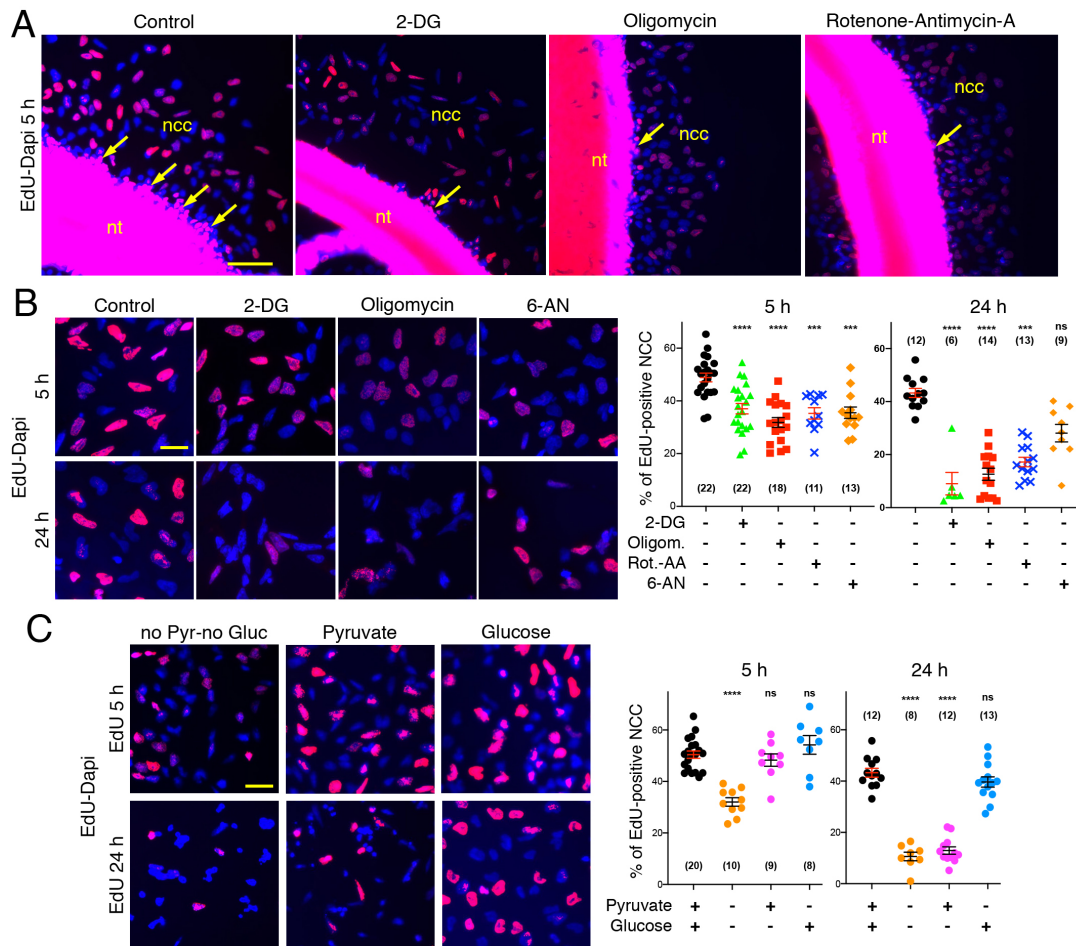


**Fig. 6. Glucose metabolism is required for NCC sustained proliferation.** Visualization and quantification of EdU staining in NT explants in the presence of metabolic inhibitors and in medium with individual nutrients. (A) Cells delaminating out of the neural tube (arrows). (B, C) Migrating NCC after 5 and 24 h cultures. Nuclei are visualized with Dapi. Bar in A = 50  $\mu$ m and in B, C = 10  $\mu$ m. Error bars = S.E.M.

## 9. Fate Decision is Dictated by Exogenous Nutrient Inputs

Finally, we investigated whether metabolic activity affects NC stem cell capacity and influence their fate. First, we analyzed the expression patterns of the transcription factors Sox10 and Foxd3, two essential regulators of NCC pluripotency (Simões-Costa *et al.*, 2012; Lukoseviciute, M. *et al.*, 2018; Schock, E. N. and Labonne, C., 2020). At 5 h in control medium, the vast majority of migrating NC cells as well as some delaminating cells exhibited Sox10<sup>+</sup> nuclei, a pattern that mirrors that of Snail2 (Fig. 8A, compare with Fig. 4C). Addition of 2-DG resulted in a strong diminution of the number of Sox10<sup>+</sup> cells with a few remaining strongly expressing cells while oligomycin and Rot-AA caused an overall reduction of staining intensity in all NC cells (Fig. 7A). Likewise, *Sox10* and *Foxd3* mRNA levels dropped strongly with 2-DG and more moderately with oligomycin and Rot-AA (Fig. 7B). In addition, *Foxd3* expression was selectively repressed by 2-DG, oligomycin or Rot-AA in pre-migratory NC cells but less so in delaminating and migrating cells (Fig. 7C).

Levels of *Sox10* and *Foxd3* messages and proteins were also much reduced in delaminating and migrating NC cells cultured in pyruvate or with no nutrient compared with glucose (Fig. 7A-C). At 24 h (Fig. 7D, E), repression of *Sox10* and *Foxd3* expression was even more pronounced in the presence of metabolic inhibitors or in absence of glucose. Interestingly, both markers were also decreased with 6-AN. These results indicate that sustained glucose metabolism is required for maintenance of high levels of pluripotency markers during NC migration.

Then, to determine whether NC fate may be instructed by metabolism, we searched for the appearance of differentiated cells in culture over time and analyzed the kinetics of expression of markers of NCC differentiation into the neural, melanocytic, and myofibroblastic/mesenchymal lineages. Because of the long-term deleterious effects of the metabolic inhibitors and in the absence of nutrient on NC cells, we only examined cells cultured in pyruvate, glucose or both (Fig. 8, S1C).

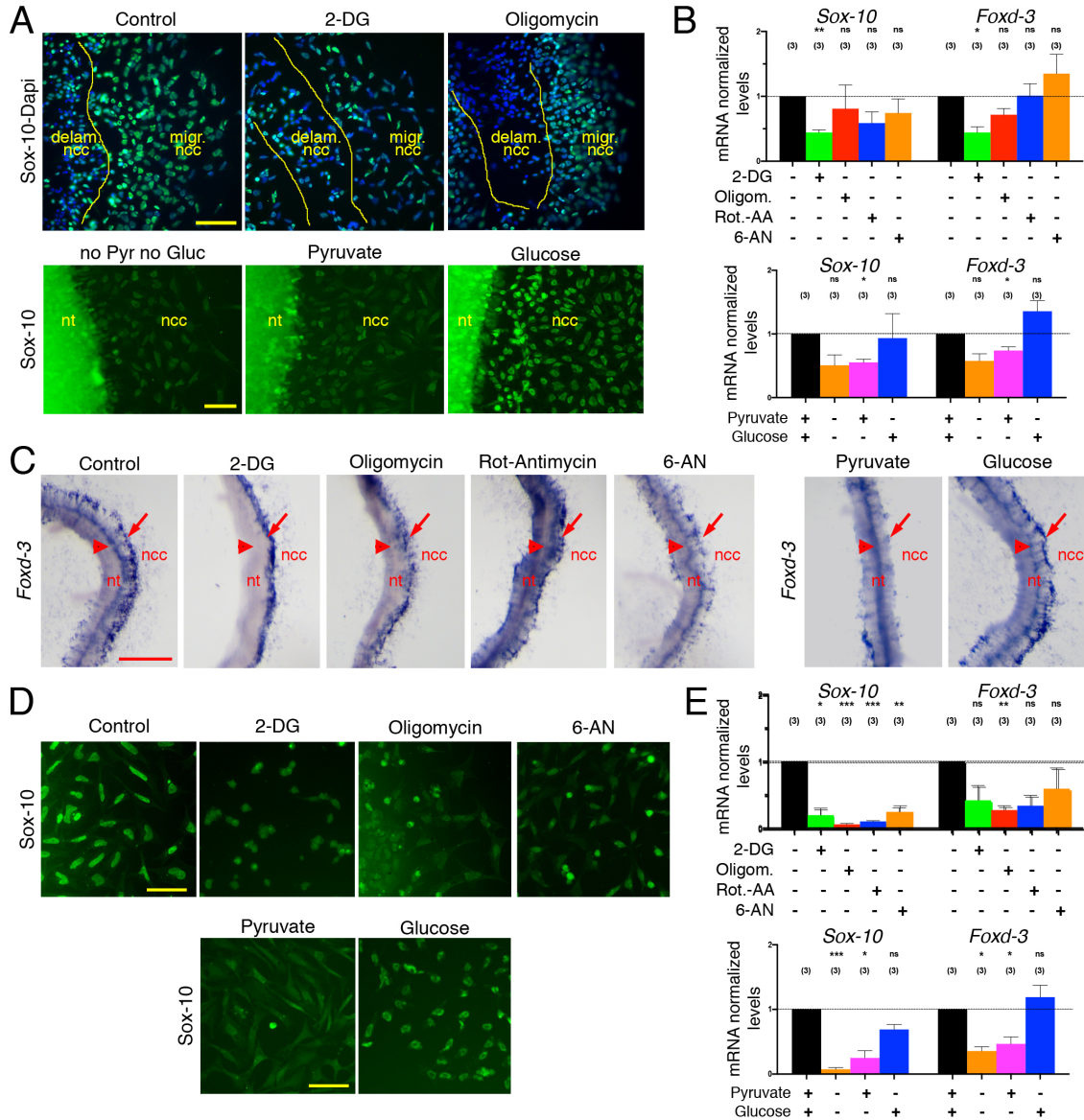


**Fig. 7. Glucose metabolism is required for NCC pluripotency.** Immunostaining for Sox-10 (A, D) and qPCR (B, E), and in situ hybridization (C) analyses of the expression of *Sox-10* and *Foxd-3* transcripts in delaminating and migrating NCC after 5 h (García-Castro *et al.*) and 24 h (D, E). In A and D, nuclei are visualized with Dapi. In control medium and in glucose, *Foxd-3* messages are distributed in premigratory NCC in the dorsal NT (arrowheads) as well as in the delaminated cells visible in either sides of the NT (arrows) similar to that of *Snail-2*. In 2-DG and oligomycin, it is decreased essentially in premigratory cells whereas in pyruvate it is reduced only in delaminating cells. Bars in A, D = 50  $\mu$ m and C = 100  $\mu$ m. Error bars = S.E.M.

In pyruvate, expansion of the NC population stalled during the first day of culture and cell morphologies gradually shifted predominantly to a large, flattened fibroblastic shape after 3 days (Fig. 8A). In glucose in contrast, the NC population steadily expanded, both in the number of cells and in the area occupied, accompanied by the appearance of neurons and other cells presenting a great diversity of morphologies. In addition, the number of cells with a NC cell shape did not decrease as dramatically as in the presence of pyruvate (Fig. 8A). In glucose, the proportion of NC progenitors (Sox10<sup>+</sup> and HNK1<sup>+</sup>) remained high over time (> 75%) while the number of neurons (Tuj1<sup>+</sup>, Sox10<sup>-</sup> and HNK1<sup>+</sup>) and melanoblasts (MITF<sup>+</sup>, Sox10<sup>+</sup> and HNK1<sup>-</sup>) increased up to 20% (Fig. 8B). In pyruvate, the proportion of NC progenitors (Sox-10<sup>+</sup>) dropped to less than 50% at the benefit of myofibroblasts ( $\alpha$ -SMA<sup>+</sup> and Sox10<sup>-</sup>), which peaked to about 40%. Of note, the number of melanoblasts did not increase much in pyruvate while the number of HNK1<sup>+</sup> cells was constantly very low. A likely explanation for this persistent absence of HNK-1 staining is that the HNK1 epitope is a glycoconjugate moiety and needs glucose for its biosynthesis (Tucker *et al.*, 1984). These data therefore show that NC differentiation programs are dependent on nutrient inputs, with glucose favoring neural and melanoblast differentiation, while pyruvate promotes a limited range of phenotypes where myofibroblasts are predominant.

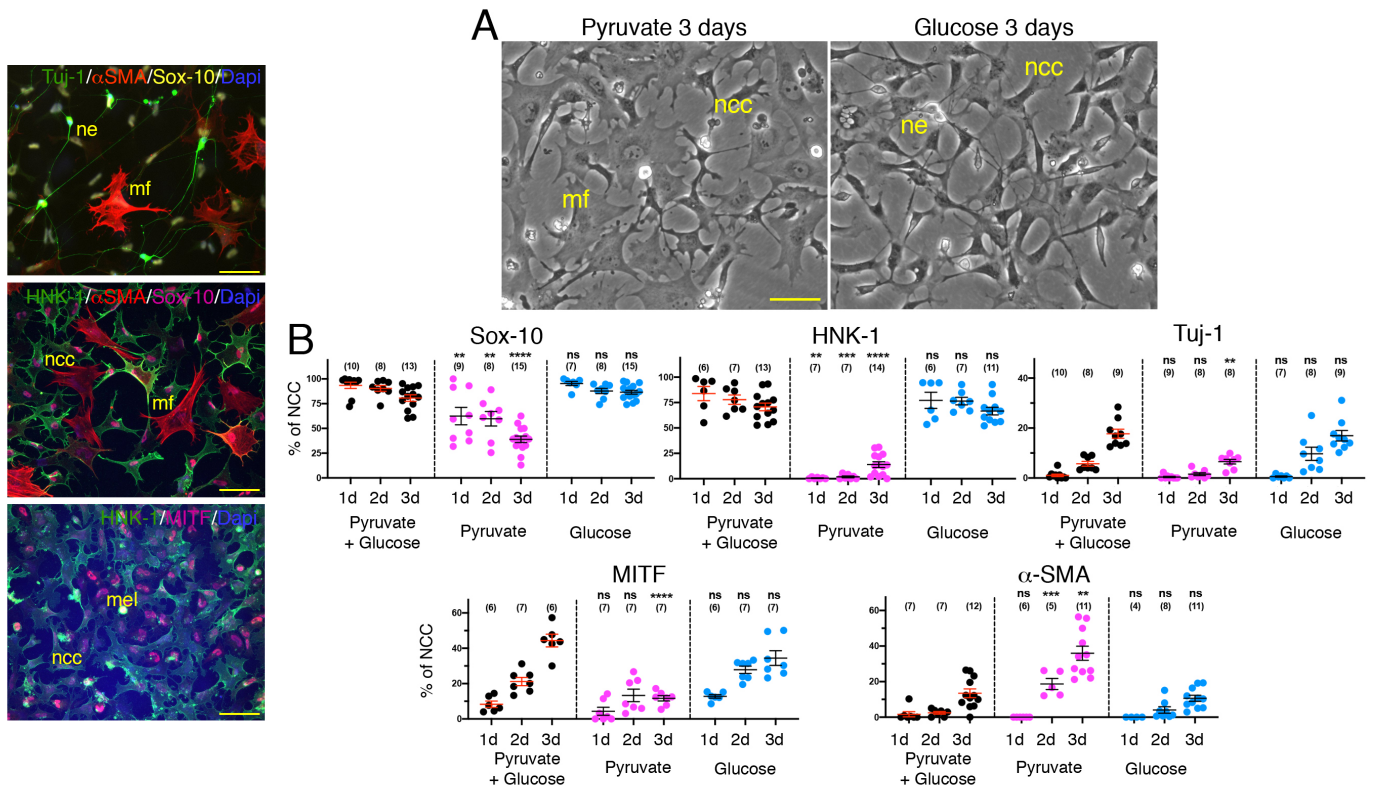


**Fig. 8. NCC fate decision is biased by exogenous nutrient inputs.** (A) Cellular morphologies in 3-day cultures of NT explants showing the presence of numerous large, flattened myofibroblasts (mf) in pyruvate and of neurons (ne) in glucose, coexisting with NCC-like cells characterized by their stellate morphology. (B) Quantification of the proportion of Sox-10<sup>+</sup>, HNK-1<sup>+</sup>, Tuj-1<sup>+</sup>, MITF<sup>+</sup>, and  $\alpha$ -SMA<sup>+</sup> cells in NCC primary cultures over time under different nutrient conditions. Bar in A = 50  $\mu$ m. Error bars = S.E.M..

From this first part of my study, we could acquire a general view of the metabolic impacts on NC development, indicating that NC cells recruit multiple routes of nutrients uptake and catabolism in order to adapt their survival and developmental steps in response to metabolic stress. Interestingly, trunk NC cells were dominantly characterized with glucose-based OXPHOS to maintain their stemness and support their delamination, proliferation and migration. A manuscript Nekooie-Marnany et al is submitted for publication and has been deposited in open access preprint repository bioRxiv (see in the annex).

# *Part B*

## *Nuclear Translocation of Glutaminase (GLS) Aligned with Metabolic Remodeling Steers Neural Crest Delamination*

### **Objective**

In this step I intended to go beyond and sought the intersection of metabolism with developmental NC steps. To know how metabolism can integrate into NC development, we first need to achieve a comprehensive picture of metabolic gene expression, metabolic dynamics and NC stages, providing a metabolic landscape in each step of NC development. Here, I focused on EMT, a crucial step in NC development governed by NC specifier genes, like *Sox9*, *Snail2*, *Foxd3*, *Cadherin-6B*, *cMyc*, *Ets*, *Twist*, incorporating environmental and cellular intrinsic inputs to regulate cell identity (Duband *et al.*, 1995; Duband *et al.*, 2015; Simoes-Costa and Bronner, 2016; Martik and Bronner, 2017; Duband, Jean-Loup *et al.*, 2020; Hovland *et al.*, 2020).

### **Background**

Extensive studies have investigated the crosstalk between metabolism and EMT in cancer cells, indicating the complex connection between cellular identity and diverse metabolic strategies, which triggers wide varieties in cellular and metabolic phenotypes (Schwab *et al.*, 2018; Baksh *et al.*, 2020; Arnold *et al.*, 2022). Indeed, cancer cells at distinct stages of EMT, known as hybrid E/M cells, can be considered as stem cells with common behavior but with different metabolic

profiles (Jia *et al.*, 2021). For instance, the differentiated epithelial cancer cells with OXPHOS metabolic phenotype can increase glycolysis upon undergoing EMT and acquiring stemness and generate hybrid E/M-like cancer stem cells, resulting in “OXPHOS high/glycolysis high” phenotype. These cells, consequently, can either diminish OXPHOS or glycolysis, to adopt mesenchymal-like cancer stem cell phenotype or lose stemness (Zu and Guppy, 2004; Colacino *et al.*, 2018; Jia *et al.*, 2021). Thus, the emergence of distinct metabolic phenotypes in stem cells with a common behavior indicates that there is no simple rule to coordinate different EMT or cellular stages with various metabolic reactions. The systematic investigation of quantitative dynamics necessitate solving EMT-metabolic programming puzzle (Jia *et al.*, 2021; Zhao *et al.*, 2021). Aligning with this view, the link between NC cell identity and metabolism should be critical to empower them to delaminate from NT trough EMT and migrate rapidly over a long distance.

Let us see the second super-interesting part of results.

In this part, we focused on how endogenous metabolic pathways can integrate into the sequence of cellular events driving trunk NC segregation from NT. Due to their transient nature and diversity in cellular states, we examined the metabolic profile of a large number of individual NT explants to obtain metabolic dynamics in trunk NC development.

We explored central carbon metabolism, utilizing the culture of early NT explants in a DMEM-based culture medium containing glucose (5 mM), glutamine (2 mM) and 1% FCS, supporting delamination, migration and proliferation of NC cells (see Results Part A). Similar to the part A of results, experiments were normalized at the primary step by size of NT and stage of embryos. As such, NT at the level of last five somites were dissected from embryos with the same developmental stage (we examined two stages either HH12 or HH14-15 considered as pre-migratory and migratory stages in this part); and cultured for around 5 hours to focus on the segregation and early migration steps of NC development.

### **1. Metabolic Remodeling Incorporates into the Transition from Delamination to Migration Steps of Neural Crest Development**

Just as a brief reminding of what was explained above (Fig. 1A): the trunk NC progenitors after specification, exhibit typical patterns of proliferation and consequently follow EMT and cell delamination individually in a gradual event (Duband, 2006; Rekler and Kalcheim, 2021). NC specification genes induce EMT and the delamination step. As such, progressively increased expression of *Snail2*, *cMyc*, and *Foxd3* contribute to EMT, synchronized with down regulation of type-II cadherin (*Cadherin-6B*) expression (Fig. 1A) (Duband *et al.*, 2015; Simoes-Costa and Bronner, 2016; Dady and Duband, 2017). Thus, early pre-migratory NC progenitors are defined by the elevated expression of *Snail2*, *cMyc* and *Foxd3*, whereas late pre-migratory NC cells (at the end of delaminating step) exhibit an opposing pattern of this gene expression combined

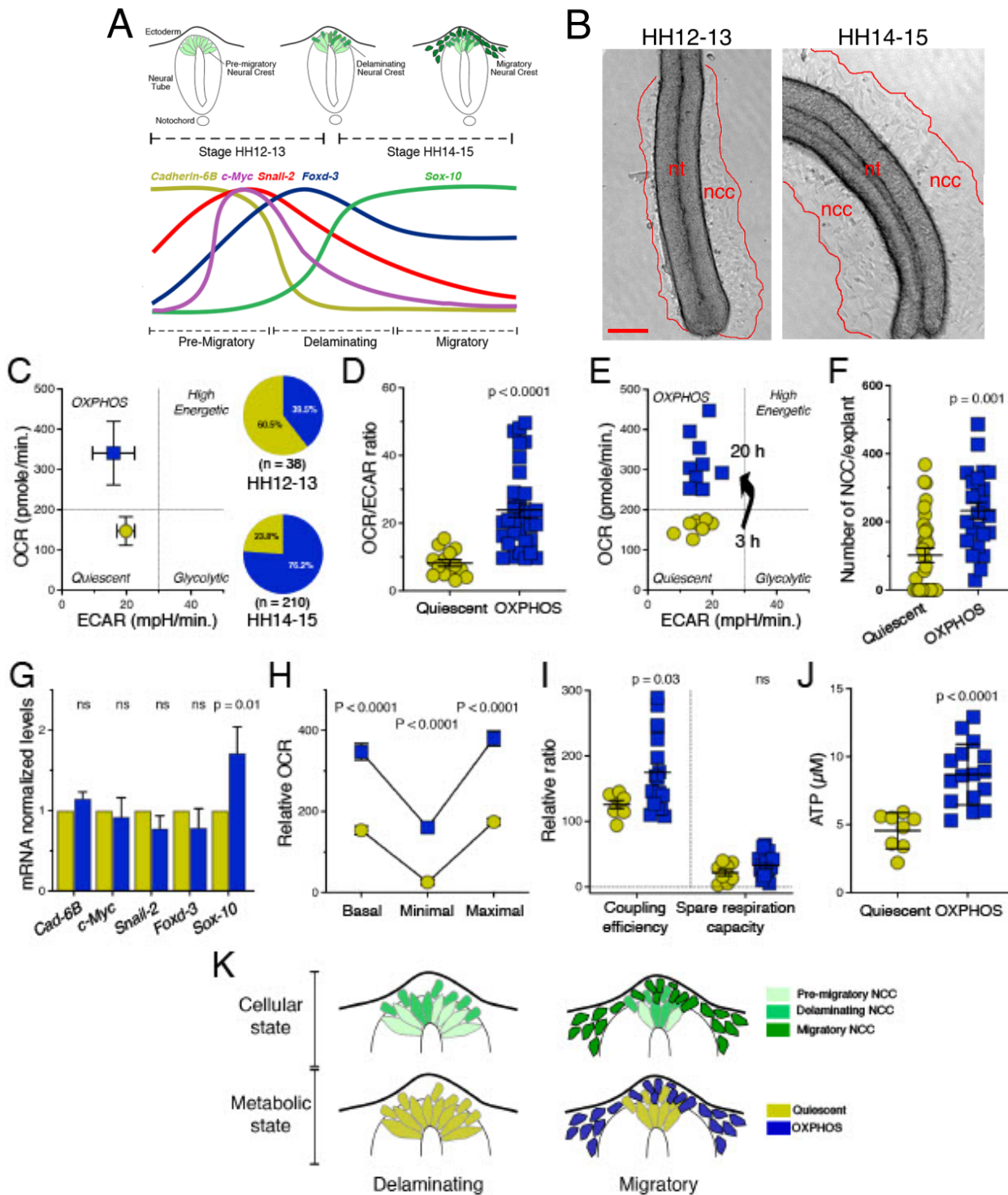


**Fig. 1. Integration of metabolic profiles into NC development:** A) Dynamic pattern of NC development. At top, the diagram depicts the developmental steps of pre-migratory, delamination and migration of NC cells in developmental stages HH12-13 and HH14-15. At bottom, a diagram illustrating the gene regulatory network controlling trunk NC development. B) Phase contrast images of HH12-13 and HH14-15 NT explants after 5 hours of culture in control condition. C) Metabolic profiles of NT explants cultures. At left, the energetic map of NT explants population (n=248, HH12-15 stage) revealed two metabolic profiles: OXPPOS and quiescent. At right, the proportion of OXPPOS (Blue) and quiescent (yellow) metabolic profiles at HH12-13 and HH14-15 stages. D) OCR/ECAR ratio taken at measurement 4 for NT explants presenting quiescent (n=14) and OXPPOS (n=34) metabolic profile. E) Evolution of metabolic profile of NT explants with quiescent profile by the time. The energetic map of the same individual NT explants (n=9) obtained at 3h (yellow circle) and at 20h (blue square) of culture. F) Quantification of NC numbers in quiescent

(n= 27) and OXPPOS (n= 25). NC numbers were counted in outgrowth of NT explants from pictures taken prior Seahorse assay and categorized according to their metabolic profiles. G) qPCR analysis of NC specifier genes in quiescent (yellow bars) and OXPPOS (blue bars) groups. Data were shown by  $\Delta\Delta_{ct}$  normalized by  $\beta$ -actin expression as internal control (n=5 experiments). H) Quantification of basal, minimal and maximal OCRs in quiescent (n=8) and OXPPOS (n=22) groups. I) The relative ratio of coupling efficiency (CE) and spare respiration capacity (SRC) in quiescent (n=8) and OXPPOS (n=22) groups. J) ATP production in NT explants with quiescent (n=8) and OXPPOS (n=16) profiles performed after Seahorse assay. K) Drawing of metabolic profile in link with NC development. The quiescent profile is a marker of delaminating stage and OXPPOS profile marker of migratory stage of NC cells. Data are presented as mean ( $\pm$  SEM) except the energetic map with mean ( $\pm$  SD). ncc: neural crest cells, nt: neural tube.

with an enhanced expression of *Sox10*, considered as the marker of migratory NC cells (Fig. 1A) (Duband *et al.*, 2015; Simoes-Costa and Bronner, 2016; Dady and Duband, 2017). As supported by in-vitro experiment, NC outgrowth in NT explants displayed high numbers of NC cells in the migratory stage (HH 14-15) relative to the pre-migratory stages (HH12-13) (Fig. 1B).

Concerning the heterogeneous nature of NC population mediated by continuous steps of the induction and emigration events, understanding of how metabolic networks integrate in the NC development could provide the key insight into the convergence of extrinsic and intrinsic cues. Therefore, to probe metabolic phenotypes of trunk NC cells and capture their metabolic map in both EMT (delaminating) and migratory steps, we measured the OXPPOS and glycolysis level in individual NT explants at two developmental stages, pre-migratory NC (HH12) and migratory (HH 14-15) via Seahorse XF24. Firstly, we optimized the bioenergetic approach to detect oxygen consumption rate (OCR) and extracellular acidic rate (ECAR) in a single NT explant with low cell numbers (Fig. S1A) (see materials and methods). Of note, despite the same developmental stage and axial level of NT, two different metabolic profiles were observed in 5 hours NT explant cultures: the OXPPOS profile identified with high OCR and low ECAR; and the “metabolically quiescent profile” defined by low level of both OCR and ECAR (Fig. 1 C-left panel, D). Interestingly, albeit the presence of two metabolic profiles, their frequency varied significantly among developmental stages. As such, among the population of NT explants analyzed in pre-migratory stage (HH12), 61% (n=23) of NT explants exhibited the quiescent profile

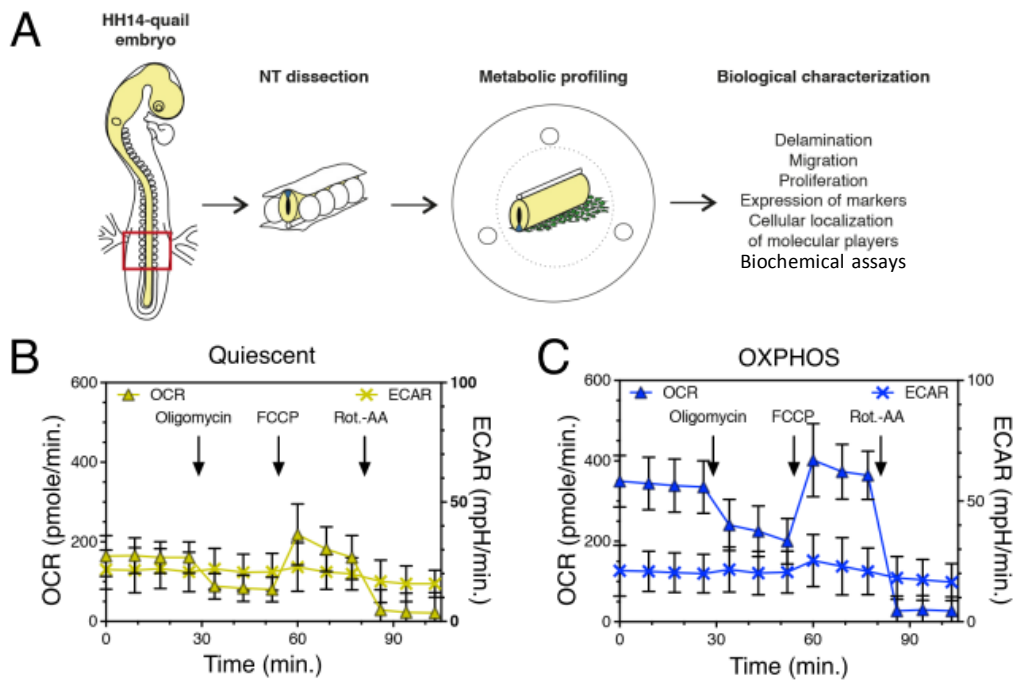


**Fig. 5 1. Metabolic behaviors of NT explants.** A) The drawing figure of NT dissection. NTs at the level of last 5 somites were dissected and lied in central well of Seahorse plate (see the material and methods). After 2 hours of NT culture, the bioenergetic assays were performed to consider all biological characterization. B) the mito-stress of NT explants with the quiescent profile.C) the mito-stress of NT explants with the migratory profile.

and 39% (n=15) the OXPHOS phenotype (Fig. 1 C-right). In contrast, in the migratory stages (HH14-15), this metabolic proportion changed to the reverse; such that the major group presented the OXPHOS profile (76%, n=160) and the minor group a quiescent profile (23%, n=50) (Fig. 1C-right). The pursuit of bioenergetic analysis with time revealed that all NT explants with quiescent phenotype in first 3 hours transitioned to OXPHOS profile at 20 hours (Fig. 1E). However, in agreement with results described in part A, NT explants with OXPHOS profile remained unchanged by the time (data not shown). Moreover, the metabolic shift from quiescent to OXPHOS elucidated the reasons for both the metabolic heterogeneity in the NT explants population and the fluctuation of their frequency among developmental stages.

We next explored the physiological character of these metabolic profiles, showing that the NT explants with OXPHOS profile has a significantly high capacity to produce NC cells in comparison

with those of quiescent group during the first 3 hours (Fig. 1F). Furthermore, to find the link between metabolic profiles and GRN involved in NC development, we compared the gene expression between these metabolic groups. Strikingly, among the analyzed GRN markers, we observed that *Sox10* was expressed two times more in the OXPPOS than in the quiescent group (Fig. 1G) consistent with the yield of NC cells in pre-migratory and migratory stages (Fig. 1B).

Then, we performed the mitochondrial stress assay to evaluate the bioenergetic properties of each metabolic group (Fig. S1B, C). The OXPPOS group depicted significantly higher mitochondrial activity with basal, minimal, and maximal respiration than quiescent group (Fig. 1H). The proportion of the respiratory contribution to the ATP production was identified via the coupling efficiency (CE: Minimal/Basal OCR) (Ferrick *et al.*, 2008)(Fig 1I). The raised CE in OXPPOS group indicated the relevant effect of higher OCR level in energy supplement, proved by higher intracellular ATP production in that group (Fig. 1J). The spare respiratory capacity (SRC: Maximal/Basal OCR) known to reflect the energy production under stress to promote survival (Oburoglu *et al.*, 2014; Winer and Wu, 2014) was found similar in both OXPPOS and quiescent groups (Fig. 1I).

Collectively, these results depict the incorporation of metabolic profiles (extrinsic feature) into intrinsic developmental steps (GRN), suggesting that metabolic transition from quiescent to OXPPOS is essential for developmental shift from EMT / delamination to migration (Fig. 1K). Thus, in the subsequent results, the quiescent and OXPPOS signatures are referred as delaminating and migratory stages, respectively.

## 2. Glucose Metabolism Modulates Metabolic States during Neural Crest Development

Metabolic reprogramming refers to changes in cellular metabolite demands, supporting anabolic and catabolic reactions required for cellular states. In order to explore which metabolic pathways corresponded to developmental steps, we primarily focused on glycolytic pathway and analyzed expression of some genes like *SLC2A1* encoding glucose transporter protein type1 (GLUT1), phosphofructokinase (*PFK*), lactate dehydrogenase (Bertero *et al.*) (Bertero *et al.*) and pyruvate dehydrogenase complex (*PDHX*) (subunit E3 (DLD)) (Fig. 2A). Notably, *SLC2A1*, *PFK* and *PDHX(E3)* were upregulated in the migratory state compared with the delaminating one (Fig. 2B). Nevertheless, *LDH* remained unchanged, reflecting the low level of detected ECAR in both stages. Likewise, HIF-1 $\alpha$ , the well-known transcription factor in hypoxia conditions promoting the glycolytic pathway via the upregulation of Glut1, glycolytic enzymes and lactate secretion (Bertero *et al.*) (Denko, 2008), was not related with the delaminating-migratory transition, which can underly the constant *LDH* expression and subsequently the low ECAR level in both states.

Collectively, the analysis of metabolic genes proposed a possibility that glucose oxidation supplies high-energy demands of the migratory group relative to the delaminating state. To verify this assumption, we pharmacologically assessed the metabolic activity in these two developmental steps by injection of either 2-deoxyglucose (2-DG), a potent inhibitor of hexokinase (HK) or oligomycin (Fig. 2A) via Seahorse assay. The OCR level in the delaminating group was unresponsive to 2-DG, but sharply decreased with oligomycin; and the ECAR level was either slightly affected or unchanged respectively (Fig. 2C-upper and middle panels).

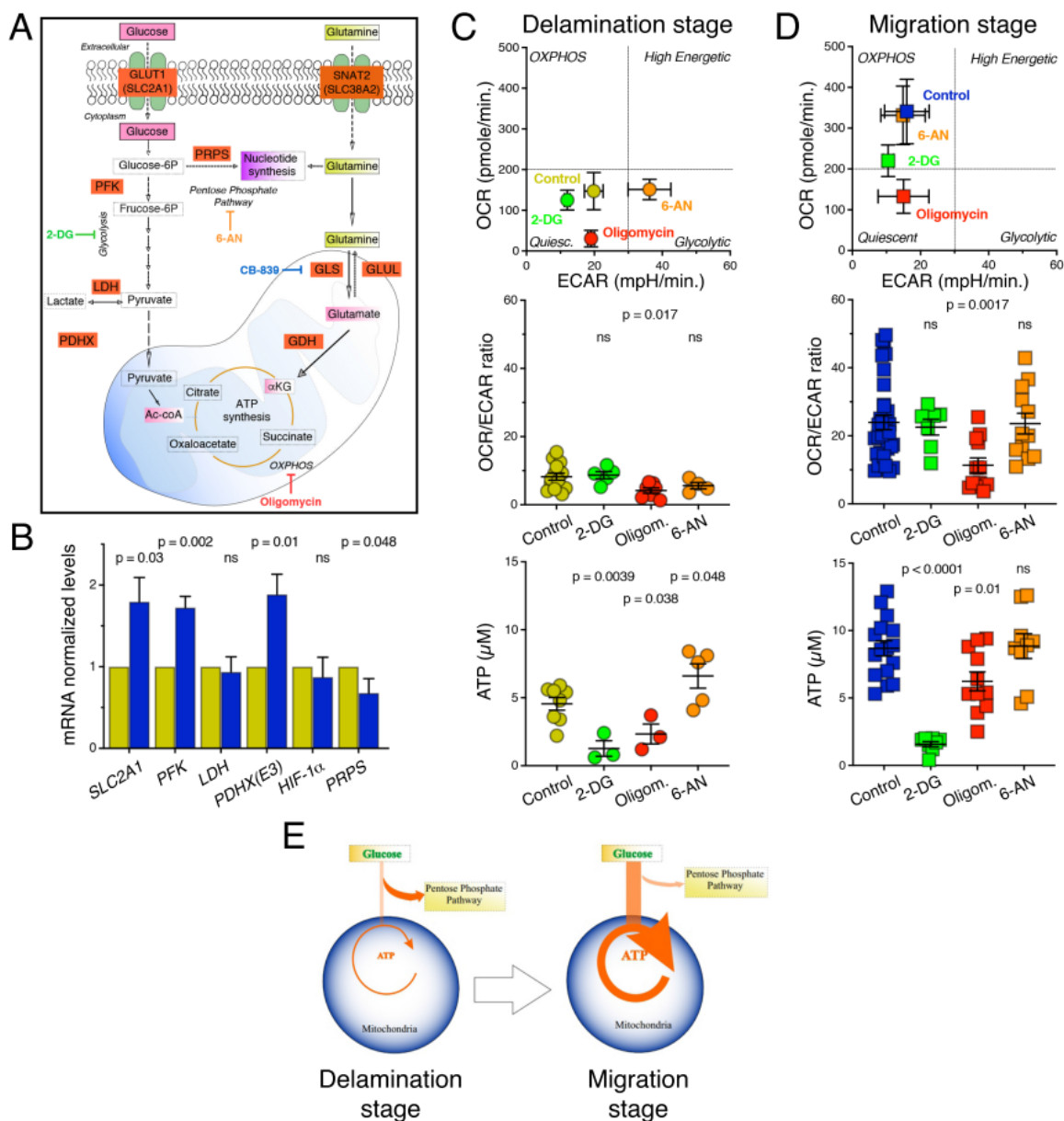
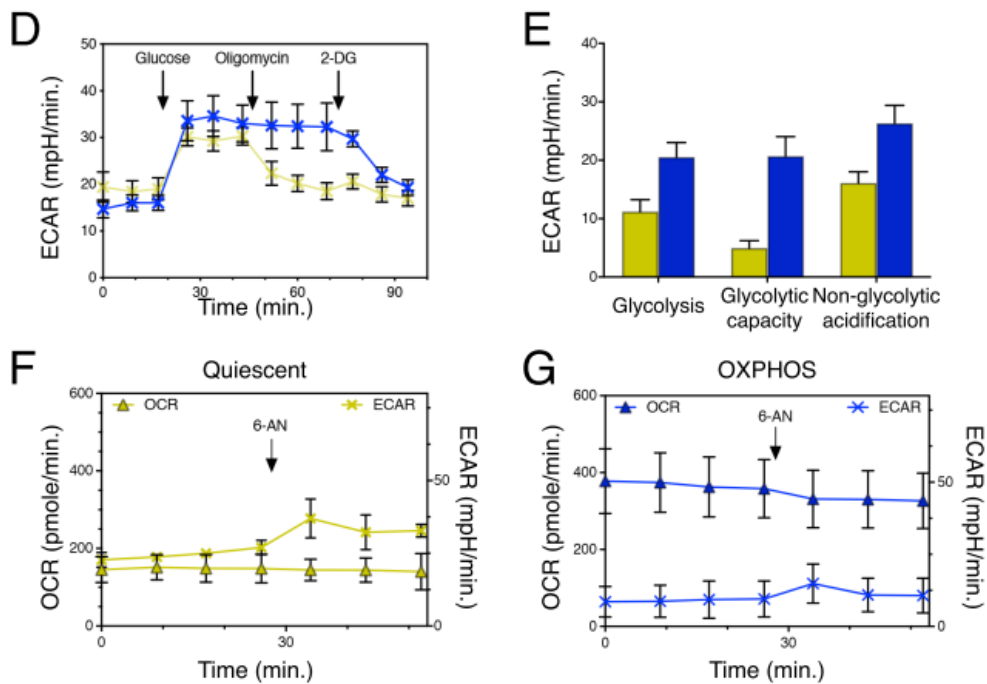


**Fig. 2. Role of glucose metabolism in NC development.** A) Drawing of glycolytic and glutamine metabolisms in the cell. B) qPCR analysis for glycolytic pathway of NT explants at delaminating (yellow bars) and migratory (blue bars) stages. Data were shown by  $\Delta\Delta C_t$  normalized by  $\beta$ -actin expression as internal control (n= 5 experiments). C) At top, the energetic map of the NT explants at delaminating state under 2-DG (10 mM), Oligomycin (1  $\mu$ M), 6-AN (500  $\mu$ M) and control conditions. We first measured basal OCR and ECAR level and then added a target inhibitor (control n=14; Oligomycin n= 7; 2-DG n=4; 6-AN n=5). At middle, the corresponding OCR/ECAR ratio taken at measurement 3. At bottom, the ATP production of NT explants after Seahorse assay ( control n=8; 2-DG and Oligomycin, n= 3; 6-AN n = 5). D) At top, energetic map of the of NT explants at migratory state under 2-DG (10 mM), Oligomycin (1 $\mu$ M), and 6-AN (500  $\mu$ M) performed as for delaminating stage (control n= 34; 2-DG n=7; Oligomycin and 6-AN, n=12). At middle panel, the corresponding OCR/ECAR ratio in the migratory group. At bottom, ATP production in NT explants at migratory stage (control n= 16; Oligomycin n= 11; 2-DG and 6-AN, n= 8). E) Drawing of shift in glucose usage during NC progression from delamination to migration. Data are presented as mean ( $\pm$  SEM) except the energetic map with mean ( $\pm$  SD).

The significant impact of 2-DG on ATP production emphasized the importance of glucose in that group (Fig. 2C-bottom panel), whereas the lack of OCR response to 2-DG (Fig. 2C) suggested the poor activity of downstream glycolytic reaction. On the other hand, the impact of oligomycin on both OCR and ATP levels highlighted the mitochondrial function in this stage, which proposed the possibility of other metabolite contributions to the mitochondrial feeding more than glucose. Therefore, the passive reaction of downstream glycolytic pathway in delaminating stage suggests that glucose might stimulate the pentose phosphate pathway (PPP), a shunt of upper glycolytic pathway (Fig. 2A). Intriguingly, we found that while 6-amminonicotinamide (6-AN), a blocker of PPP at the level of the 6-phosphogluconate dehydrogenase (6-PGDH) (Fig. 2A), has no impact on OCR, it strongly increased ECAR level (Fig. 2C). This result indicated the rewired downstream glycolytic pathway under the PPP harness, resulting in the metabolic shift to the glycolytic profile (Fig. 2C, Sup Fig.1F). This also led to increased ATP production due to promoted glycolytic pathway (Fig. 2 C-bottom panel). In contrast, the migratory stage exhibited a drastically decrease in OCR level and ATP production under 2-DG and oligomycin effect (Fig. 2D). The unchanged ECAR level under oligomycin effect implies that migratory state is unable to rewire glycolytic pathway through the inhibition of mitochondrial respiration, known as glycolytic capacity (Fig. S 1D, E)(Winer and Wu, 2014). Collectively, as observed by both

depleted ATP production and OCR level in response to either 2-DG or oligomycin (Fig. 2 D), glucose oxidation is the main source of energy supplier for the migratory phase. This is further supported by the unchanged metabolic profile and ATP production by 6-AN treatment (Fig. 2D, S 1G). The PPP-derived nucleotide synthesis is promoted in delaminating compared to migratory



state. It was further supported by expression of phosphoribosyl pyrophosphate synthase (PRPS), known as a key enzyme of purines and pyrimidines synthesis in PPP (Fig. 2B). Altogether, the change in glucose function from anabolic to bioenergetic reactions drives transition from delamination to migration steps in NC development (Fig. 2E). These findings reinforce the notion that how metabolite demands can modulate cellular state .

### 3. Glutamine plays a profound role in NC production

Besides the glycolytic pathway, we next probed the role of glutamine in the metabolic profiles and NC development. Thus, we withdrew the extracellular glutamine from the culture medium supplemented with glucose. In contrast to the control condition, NT explants under glutamine deprivation emerged with a homogenous metabolic profile: the OXPHOS phenotype (Fig. 3A). In comparison to the OXPHOS profile in the control condition (defined as corresponding to “migratory group”), the mito-stress assay indicated that mitochondria functions were unresponsive to the glutamine stress (Fig. 3B, C). In addition, the unchanged levels of CE (Fig. 3D) and ATP production (Fig. 3E) suggested that the glucose proportion in the energy production was more weighted against glutamine. Conversely, NT explants in glucose-free medium with glutamine were unable to maintain not only mitochondrial activity ( Fig. S 2D,E), but also their own survival due to the drastic low level of SRC (Fig. S 2F-G), caused to exclude this condition from our further study. Moreover, although mitochondria activities and ATP production remained unaffected under glutamine deprivation, the qPCR analysis revealed that expression of NC specifiers was halted versus the migratory group (Fig. 3 F). Unlike most NC specifiers, the expression of *cMyc* was elevated which might be correlated with its role in regulation of glutamine metabolism (Pérez-Escuredo *et al.*, 2016). Further supporting the role of *cMyc* in glutamine metabolism, the gene expression of glutamine pathway (Fig. 2A) depicted increased expression of *GLUL* (glutamine synthetase) and unchanged *GLS* (Glutaminase) expression under glutamine-stress (Fig. 3G).

In the next step, regardless of their metabolic profile, we explored the NC production in the NT explants cultured in the control condition or without glutamine for 5 hours. The glutamine deprivation strongly impacted on NC generation consistent with downregulated NC markers (Fig 3 H,I).

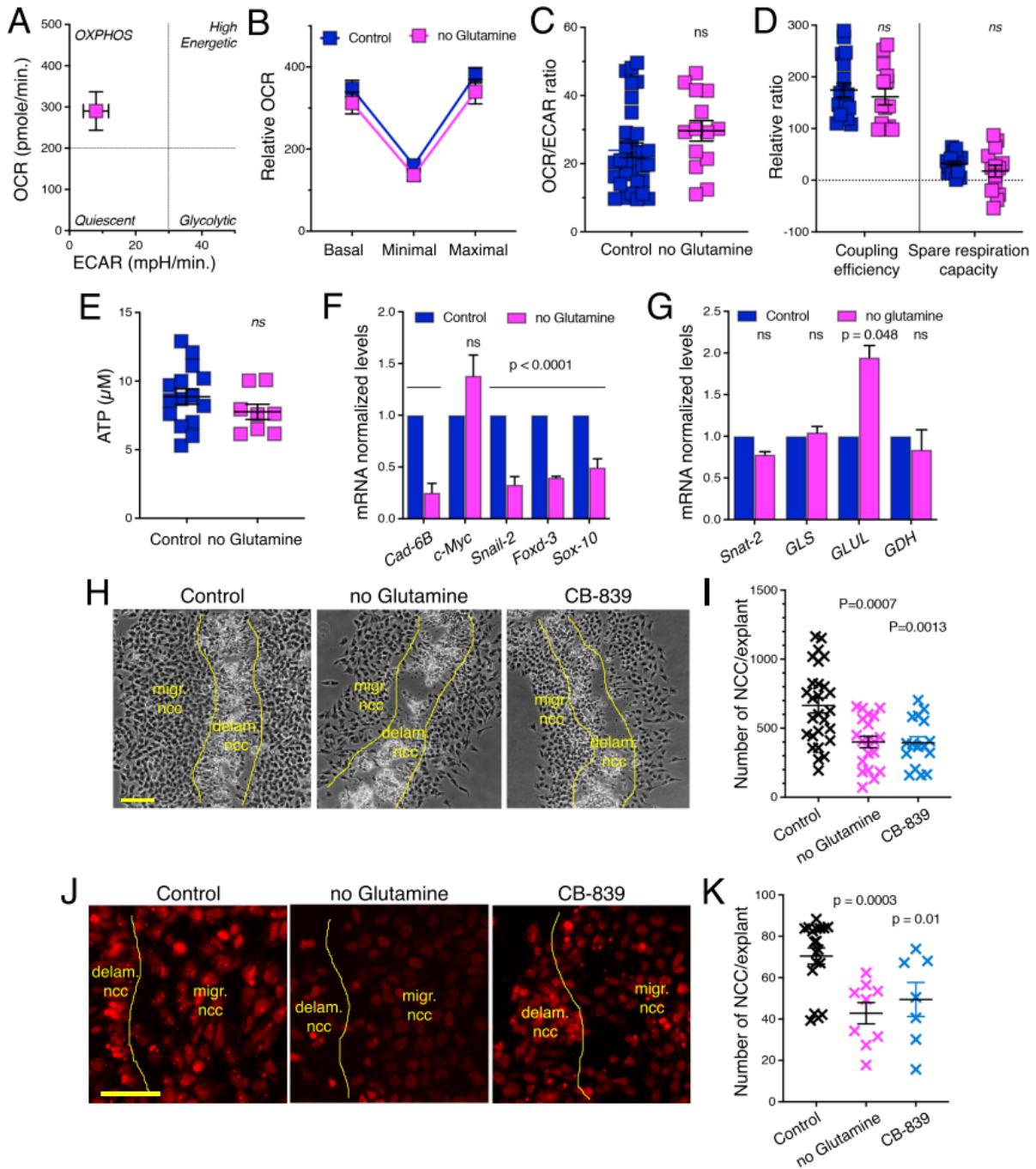


**Fig. 3. Pivotal role of glutamine in NC delamination.** A) Energetic map of NT explants in the glutamine deprivation (n=66). B) Quantification of basal, minimal, and maximal OCRs in no-glutamine condition (n=15) and control condition (OXPHOS group, n=22). C) OCR/ECAR ratio in no-glutamine (n=15) and control (OXPHOS group, n= 34). D) The relative ratio of CE and SRC in no-glutamine group (n=15) and control (OXPHOS group, n=22). E) ATP production in no-glutamine (n=8) and control (OXPHOS group, n=16). F) qPCR analysis for the expression of NC specific genes in the no-glutamine versus the control OXPHOS group. G) qPCR analysis of glutamine metabolism in the no-glutamine versus the control OXPHOS group. qPCR data were shown by  $\Delta\Delta C_t$  and normalized by  $\beta$ -actin expression as the internal control (n= 5 experiments). H) Phase contrast images of NT prints after 5h of culture in control (n=27), no-glutamine (n=20) or control with CB-839 (n=16) conditions. I) Quantification of total delaminating and migratory NC cell numbers in NT prints in control, no-glutamine or CB-839 conditions. J) Visualization of Snail2 in NT prints in the control (n=34), no-glutamine (n=10) and CB-839 (n=14) conditions. K) Quantification of NC cells positive for Snail2 expression in NT prints in the control (n=20), no-glutamine (n=9) and CB-839 (n=7) conditions. Data are presented as mean ( $\pm$  SEM), except energetic map ( $\pm$ SD). migr. ncc: migrating neural crest cells. delam. ncc: delaminating neural crest cells.

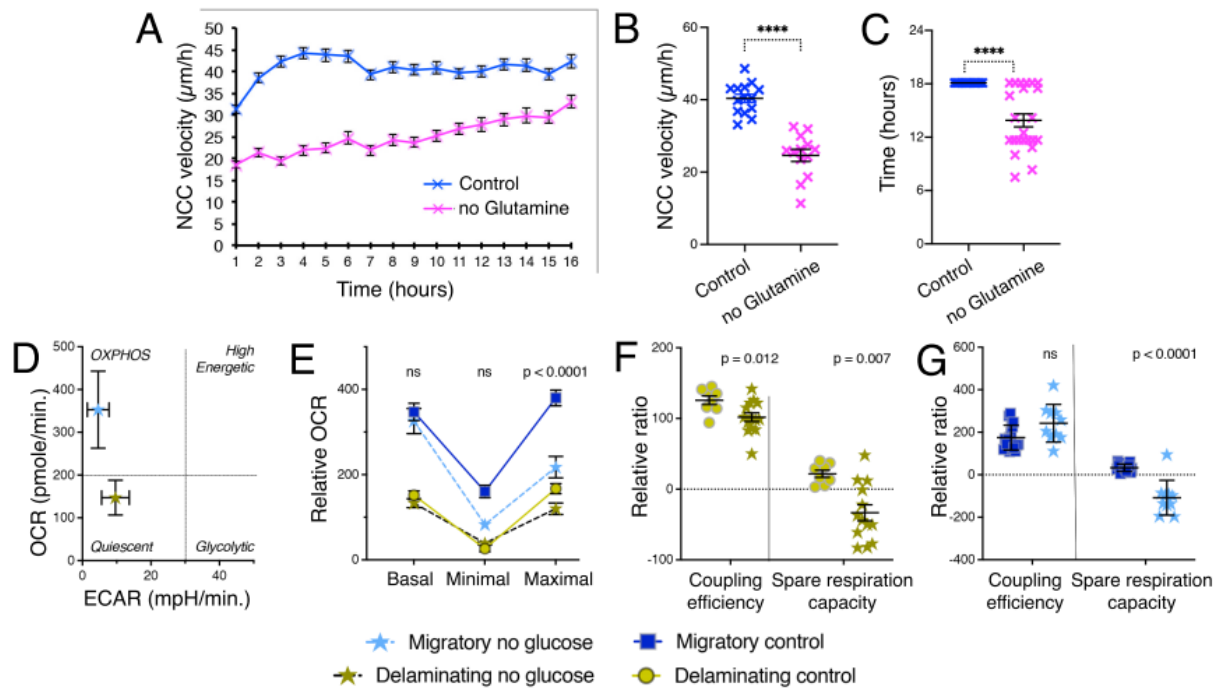


**Fig. S 2. The impact of the glutamine deprivation.** A) The speed evolution through NC migration with time in no-glutamine versus control condition. B) The mean speed of NC velocity in non-glutamine versus control condition. Each dot corresponds to the mean value of 20 NC cells/ NT (n=?). C) Duration of NC production from NT in non-glutamine and control conditions. D) The energetic map in glucose-free medium supplied with glutamine versus the control condition. NT explants emerged with two metabolic profiles in the non-glucose condition. The OCR and ECAR levels in this condition were unfit with the delaminating and migratory groups in the control condition. E) the quantitative basal, minimal and maximal respiration in no-glucose condition. in comparison with control groups, NT explants did not respond well to the inhibitors of mit-stress (n=17 quiescent, n=10 OXPHOS group). F) The relative ratio of CE and SRC of the quiescent group in no-glucose condition and control (the delaminating group). The significant decreased SRC level of non-glucose condition pointed to the low capacity of NT explants in their own survival. G) The relative ratio of CE and SRC of the quiescent group in no-glucose condition and control (the migratory group).

Reciprocally, the faint immunostaining of Snail2 in NT explants verified the low capacity of glucose alone to support NC delamination (Fig. 3J, K). Moreover, even though glucose alone supplied the energy demands of the system (Fig. 3E), the glutamine absence was prone to disrupt NC migration (Fig. S 2A, B), and NC production from NT over the time (Fig. S 2C). Collectively, these results infer that glutamine is essential for NC specifiers and delamination at early stage of NC development wherein glucose was unable to compensate lack of glutamine; and largely affected the cell identity.

Concerning the proliferation of trunk NC progenitors upon EMT, the strong impact of glutamine stress on NC delamination postulates the contribution of glutamine to nucleotide synthesis. To examine this assumption, we cultured NT explants in the control condition plus the CB-839 compound to perturb the bioenergetic reaction of glutamine pathway by GLS inhibition (Fig. 2A). Surprisingly, CB-839 negatively influenced NC delamination, as evidenced by both reduced NC generation (Fig. 3H, I) and protein expression of Snail2 (Fig. 3 J, K). In the next step, to decipher how glutamine metabolism governs NC delamination, we first determined the NC-developmental states in NT explants by bioenergetic assay. Then, expressions of key enzymes in the glutamine pathway (Fig. 2A), such as cellular membrane of glutamine transporter (*SLC 38A2 (Snat2)*), *GLS*, glutamate dehydrogenase (*GDH*) and *GLUL*, were compared between delaminating and migratory states (Fig. 4A). Interestingly, in the migratory group the *GDH* expression is remarkably increased consistent with promoted glucose-oxidation in that stage. The moderate change in *Snat2* and *GLUL* expressions suggested a decline of glutamine preference during developmental transition. Thus, we measured intracellular glutamine and glutamate concentrations in NT explants of the delaminating and migratory groups (Fig. 4B). Strikingly, the glutamine concentration was lower in delaminating versus migratory group indicating that glutamine consumption was higher in delaminating versus migratory group; and the glutamate level was unfit for the rate of glutamine consumption, which suggests the poor GLS activity in the delaminating stage. The glutamine preference in that stage can be contingent on the convergence of glutamine and glucose in nucleotide synthesis. However, the EdU assay indicated the same percentage of S-phase and mitotic cells among delaminating and migratory stages (data not shown). Altogether, these results suggested a possibility of the non-enzymatic role for GLS in NC development.

#### 4. GLS has a non-enzymatic function to support NC production

For further analysis of the GLS function in the developmental NC states, we injected either CB-839 or medium (for control group) after the measurement of the basal respiration in NT explants, allowing us to identify the developmental NC stages before injections (Fig. 4C-left panel). Then, after 2 hours of treatment, total RNA of each NT explant was extracted, and the lysates were pooled according to their metabolic group prior to qPCR analyses (Fig. 4 C-middle and right panels). Interestingly, at the delaminating stage, GLS inhibition had no significant effect on the OCR level, while considerably reduced the expression of NC specifiers versus the control. This result supported our above assumption that GLS has the non-enzymatic function in delaminating state (Fig. 4 C-middle panel).

Moreover, the gene expression of glutamine metabolism can provide a view of cellular sensitivity to metabolites requirements upon GLS inhibition (Fig. 4C-right panel). For instance, given the low GLS activity in the delaminating stage, downregulated *GLUL* expression under CB-839 suggested that delaminating NC cells require low amount of glutamate, leading to eluding the more synthesis of GLS substrate. Conversely, in the migratory group, CB-839 had a notable impact on OCR level but failed to change the expression of NC specifiers versus the control (Fig. 4D left and middle panels). In addition, the migratory group displayed an opposing response with keeping unchanged *GLUL* expression and increased glutamine uptake via enhanced *Snat2* expression (Fig. 4D-right panel). Counting of NC cell numbers after 2 hours of CB-839 treatment indicated that GLS harness significantly reduced NC delamination but has not affect at migratory stage (Fig. 4E). Then, we assessed the enzymatic GLS function by measuring ATP (Fig. 4F) and glutamate (Fig 4G) concentrations in the presence of CB-839.

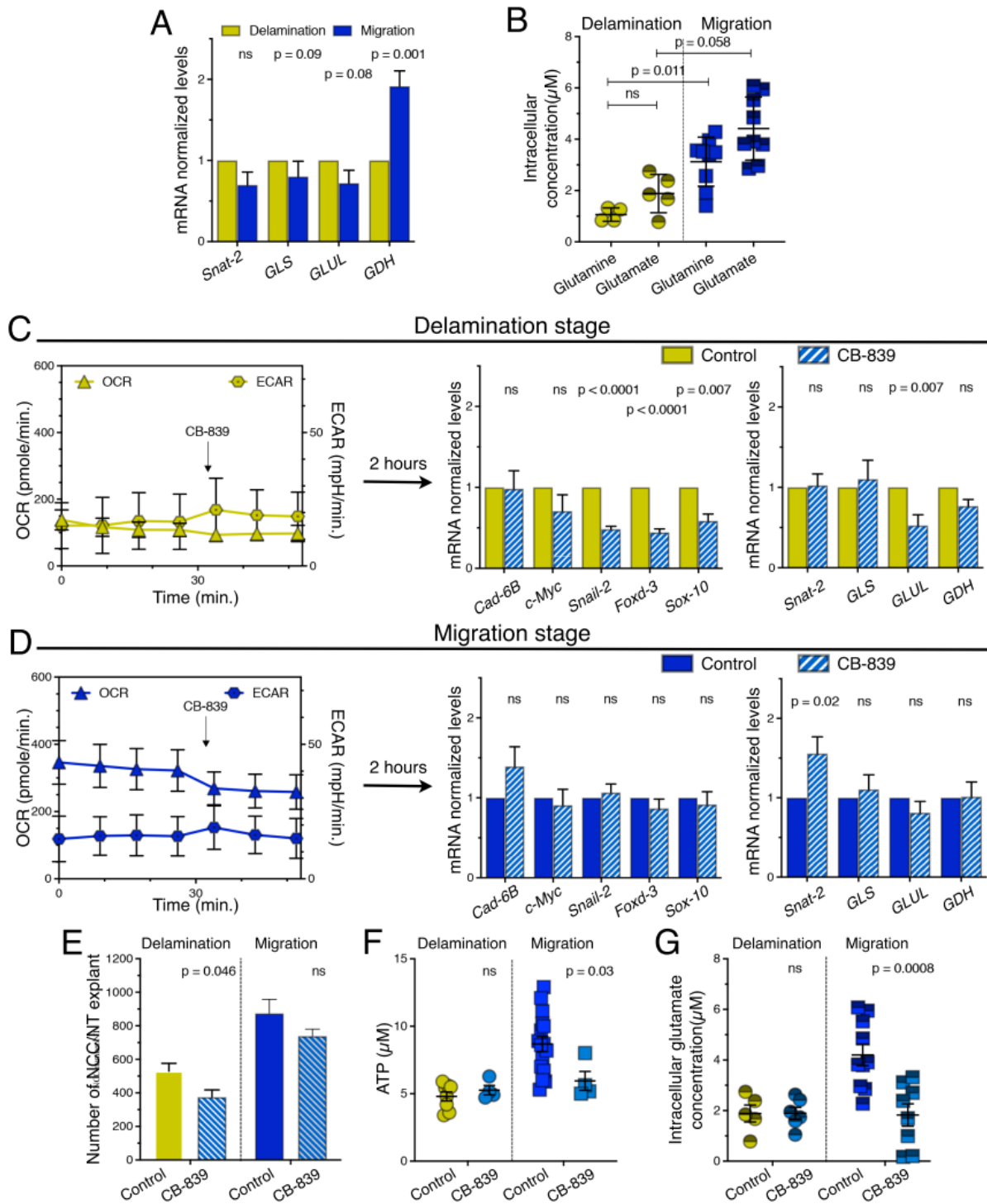


**Fig. 4. Putative non-enzymatic role of GLS in NC delamination.** A) qPCR analysis for genes expression of glutamine metabolism in control condition for delaminating and migratory groups. Data were shown by  $\Delta\Delta C_t$  and normalized by  $\beta$ -actin expression as the internal control (n= 5 experiments). B) Quantification of both intracellular glutamine and glutamate in delaminating (n=5) and migratory (n=10) groups. C) Effect of CB-839 on OCR level (representative graph, left panel) and genes expression of NC specifiers (middle panel) and glutamine metabolism (right panel) in delaminating group. Firstly, the basal respiration in NT explants was measured to determine the developmental NC stages and then CB-839 was injected to wells via seahorse machine. The control group in that case is defined by NT explants that instead of CB-839 received medium. After Seahorse assay, the NT explants were remained with treatment for 2 hours. And then, total RNA was extracted from NT explants for qPCR analysis (n=5 experiments). D) Effect of CB-839 on OCR level (representative graph; left panel) and genes expression of NC specifiers (middle panel) and glutamine metabolism (right panel) in the migratory group (n=6 experiments). E) Quantification of NC cell numbers after 2 hours

effect of CB-839 in the delaminating (n= 7) and migratory (n= 14) groups. NC numbers were counted in outgrowth of NT explants from pictures taken at the end of Seahorse assay and 2 hours treatment with either CB-839 or medium. F) ATP production under CB-839 effect in the delaminating (n=4) and migratory groups (n= 4). G) Impact of CB-839 on the intracellular glutamate concentration in delaminating (n=6) and migratory groups (n=8).

In contrast to the migratory state, the GLS inhibition had no effect on both glutamate and ATP production in delaminating stage. Altogether, these results supported the non-enzymatic role of GLS in delamination and enzymatic role in the migratory stage.

To find out whether the non-enzymatic function of GLS in NC delamination is related to glutamine-derived  $\alpha$ -ketoglutarate ( $\alpha$ -KG) activity, we supplied medium with glucose plus glutamate (10  $\mu$ M) and withdrew glutamine. As evidenced by quantifications of NC production and Snail2 expression in NT explant cultures (Fig. S 3 A-D), exogenously added glutamate was unable to rescue the negative impact of glutamine deprivation on NC delamination. Nevertheless, the NT explants population under the glutamate condition displayed two metabolic profiles: the OXPHOS (83%, n=40), and quiescent (16%, n=8) profiles (Fig. S 3E), similar to metabolic profiles distribution in control condition (Fig. S 3F, G). The downregulated expression of NC markers in metabolic groups under glutamate condition compared with controls (Fig. S 3H, I left panels) indicates an uncoupling of metabolic profiles with developmental NC stages under glutamine deprivation. In addition, regarding the negative influence of glutamate on NC specifiers, the upregulated expression of *GDH* at both stages suggests an enzymatic function for GDH in NC development (Fig. S 3 H, I right panels). Of note, the decline of GLS expression mediated by feedback regulation might negatively impact on the expression of NC markers. Altogether, our findings demonstrated that GLS has non-enzymatic functions in NC development, raising the intriguing possibility that GLS has a gene-regulatory function in NC development, besides its enzymatic role.

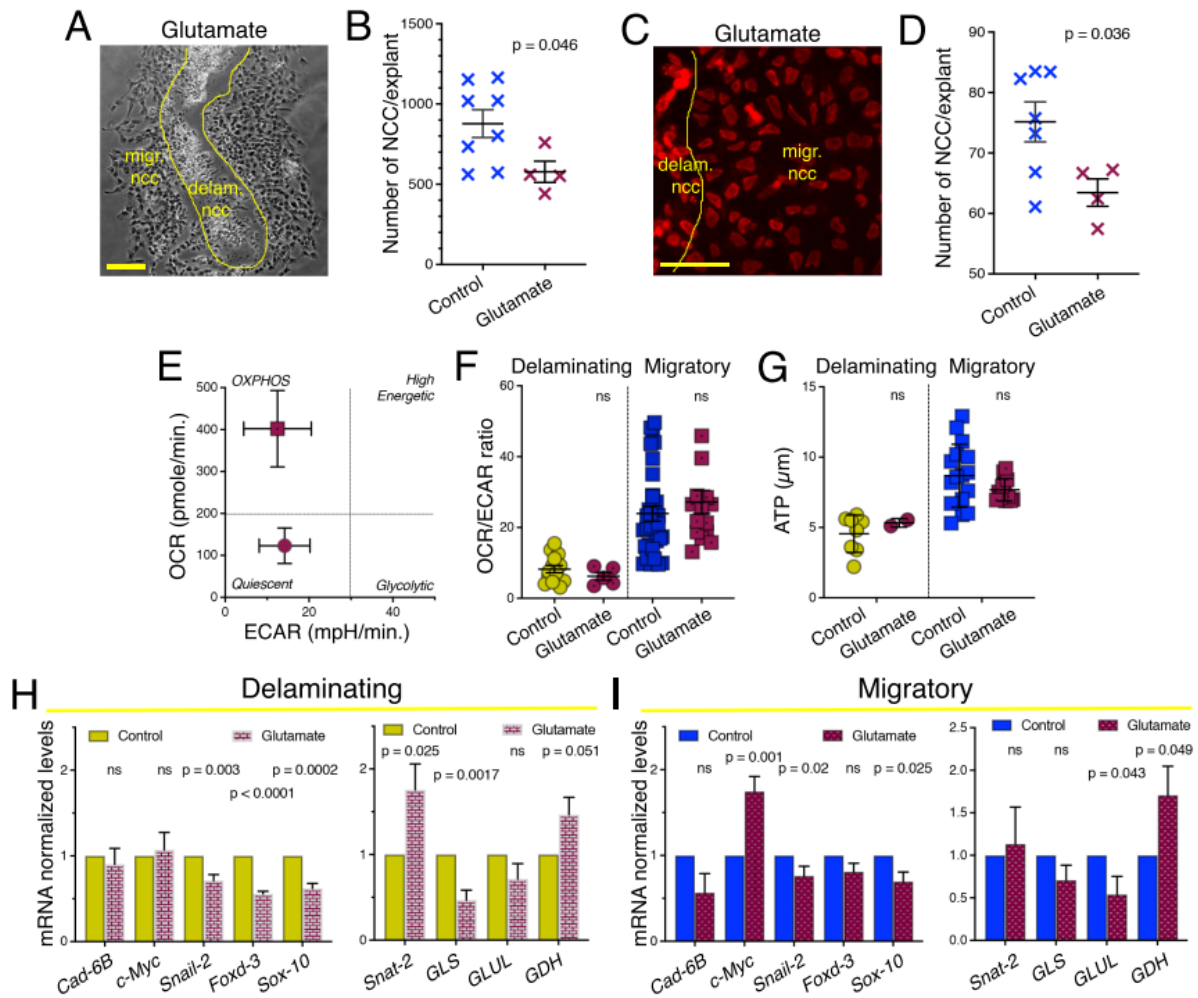


**Fig. 3. Glutamate impacts.** A) Morphology of NT print in the glutamate condition. B) Quantification of total delaminating and migratory NC cell numbers in control (n=8) and glutamate condition (n=4). C) Immunostaining for Snail2 in the glutamate condition. D) Quantification of NC cells positive with Snail2 expression in the control (n= 7), glutamate (n= 4). E) Energetic map of NT explants in the glutamate condition. F) The OCR/ECAR ratio in two metabolic profiles of the glutamate condition (n=) versus delaminating and migratory groups in control condition (n=). G) Intracellular ATP production in 2 groups of glutamate condition compared with control ones. H) QPCR analysis of NC markers (left panel) and glutamine metabolism (right panel) in quiescent group pf glutamate (n=4 experiments) versus the delaminating group in control. I) QPCR analysis of NC markers (left panel) and glutamine metabolism (right panel) in OXPHOS group pf glutamate (n=4 experiments) versus the migratory group in control. Data are presented as mean ( $\pm$  SEM), except energetic map ( $\pm$ SD).

## 5. Nuclear expression of GLS in NC cells

Being a gene regulator necessitates entering to the nucleus prompted us to analyze the localizations of GLS protein in two developmental groups. We removed NT from NT explants at the end of 5h culture wherein we could have access to delaminating and migratory NC cells and compared the localizations of GLS protein in the two NC cell categories (Fig. 5A). Intriguingly, we found that beside of cytoplasmic localization, GLS was more notably located in nucleus of delaminating NC cells versus migratory ones (Fig. 5 B, C). We next explored the expression of *GLS* in trunk region of whole embryos at the stage of initiation of NC migration (Fig. 5D). Indeed, *GLS* expression resembled the pattern of *Foxd3* expression with enriched expression of *GLS* in the pre-migratory region that was progressively decreased anteriorly until be poorly expressed in regions where migratory NC cells largely appeared. Therefore, *GLS* and *Sox10* expressions displayed opposing patterns along NT. In contrast, *GDH* displayed a homogenous expression along the neural tube (Fig. 5D). As evidenced by the immunostaining on whole embryo, the GLS protein was also observed with nuclear localization in NT (Fig. 5E). Indeed, in pre-migratory region where delaminating markers are at highest level and NC migratory marker was poorly expressed, we could find GLS protein located in nucleus (Fig. 5E). CB-839-driven inhibition of GLS activity in NT explant cultures withdrew GLS from nucleus in delaminating NC cells but had no effect on migratory ones (Fig. 5F), which was in agreement with our findings that the GLS harness leads to deficient expression of NC markers in the delaminating stage (Fig. 4C). In addition, GLS was infrequently located in nucleus under glutamine-free conditions with or without glutamate (Fig. 5G), suggesting the essential role of glutamine as a signal for GLS localization.

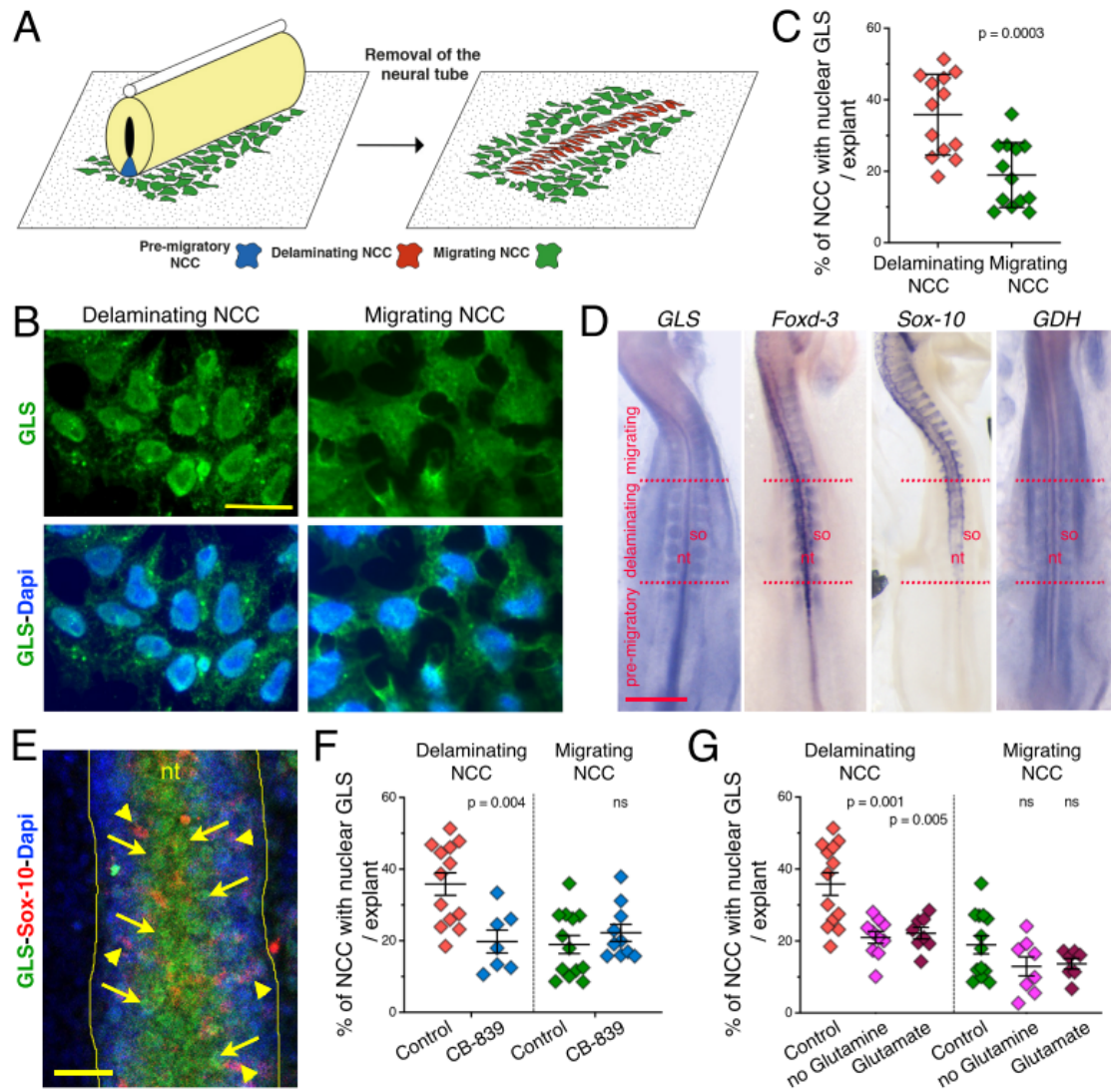
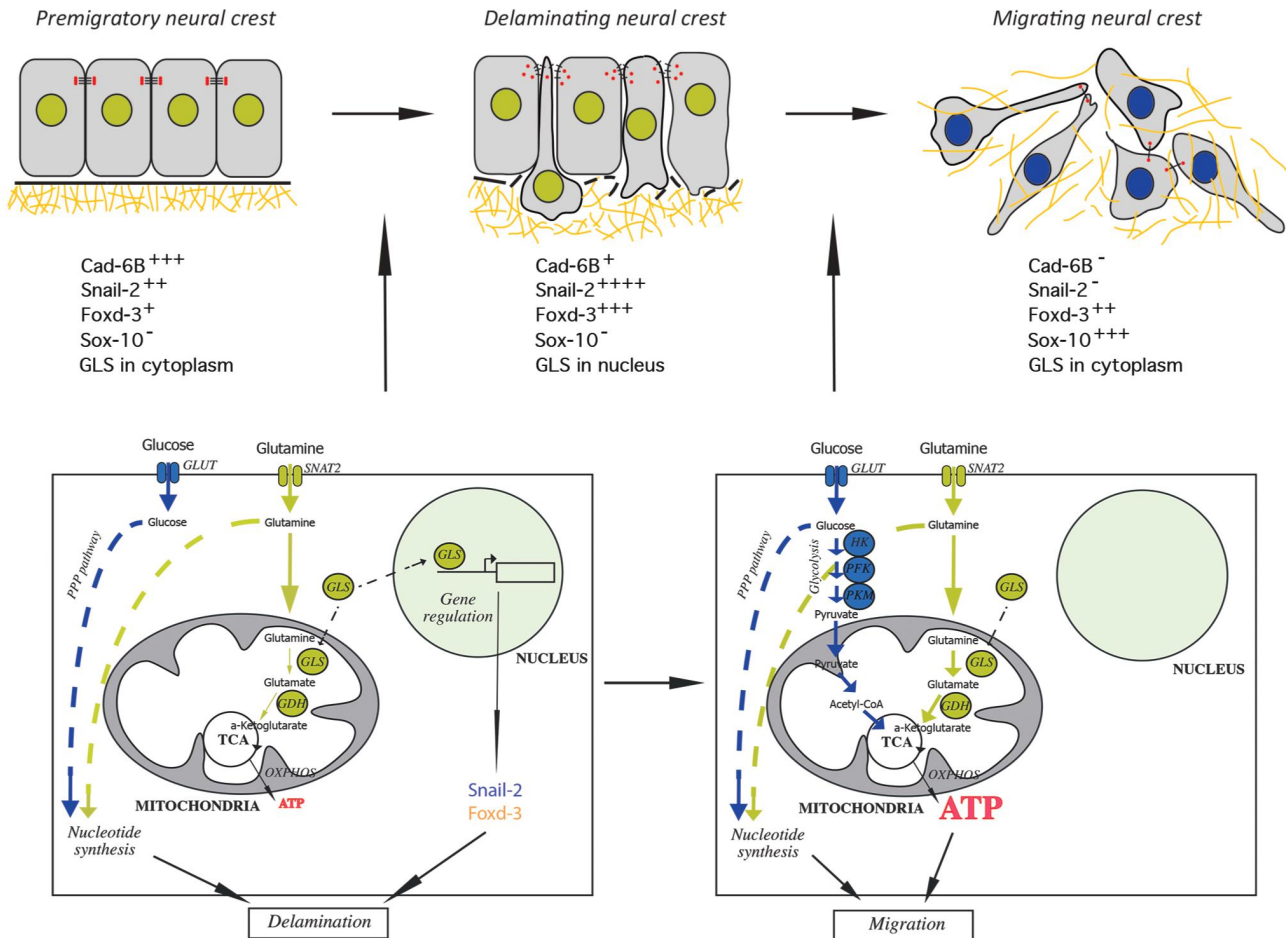


**Fig. 5. Nuclear localization of GLS in delaminating NC cells.** A) Schematic representation of the procedure to produce NT prints from NT explant after 5 hours culture giving access to both delaminating and migratory NC cells. B) Visualization of GLS and nuclei in delaminating and migratory NC cells. C) Quantification of nuclear GLS expression in delaminating versus migratory NC cells (n=13). D) Whole mount in situ hybridization for *GLS*, *FOXD3*, *SOX10* and *GDH* in whole embryo. E) Whole mount immunostaining for GLS and SOX10 at the delaminating region of NT. F) Quantification of NC cells with nuclear GLS localization in control (n=13) and CB-839 (n=8) conditions. G) Quantification of NC cells with nuclear GLS localization in control (n=13), no-glutamine (n= 10) and in glutamate (n=8) conditions. Data are presented as mean ( $\pm$  SEM). The bars in B: 20  $\mu$ m, D: 500  $\mu$ m, and E: 50  $\mu$ m. NCC = neural crest cells.

Collectively, these results indicate a regulatory function of GLS in NC development. Therefore, upon developmental transition from pre-migratory to delamination step, GLS moves to nucleus where it might contribute to expression of other NC specifiers and displays low enzymatic activities. Reciprocally, glucose and glutamine integrate in anabolic reactions with low energy demands which ultimately emerges in metabolic quiescent profile. Then, upon metabolic remodeling from quiescent to OXPHOS, GLS is mostly found in mitochondria and displays its



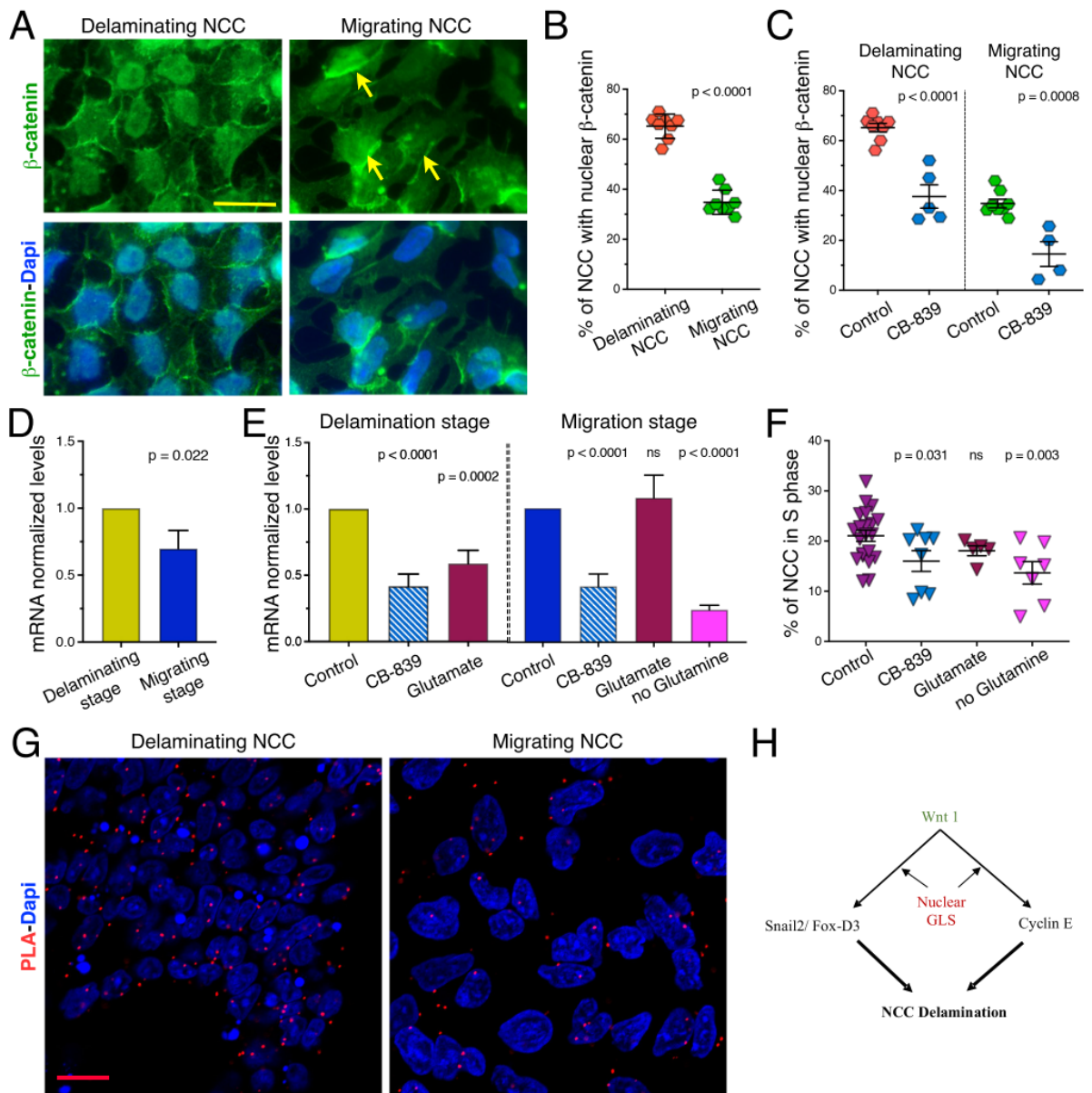
canonical function to contribute into glucose oxidation via feeding TCA cycle (Fig. 6).

**Fig. 6. Model for intersection of metabolism and NC development.** NC progenitors upon EMT exhibited nuclear GLS combined with increased *Snail2*, *Foxd-3* expression and precluded *Cad-6B* expression. Nucleotide synthesis is promoted by glucose and glutamine at this this step. Delaminating- migratory transition is accompanied by promoted glucose and glutamine oxidation and increased *Sox10* expression. GLS at this step shows canonical function.

## 6. Contribution of GLS to Wnt signaling

The canonical Wnt signaling regulates delamination of trunk NC cells. This pathway is activated in subsequent steps: 1) binding of Wnt proteins to their cell surface receptors and recruitment of scaffold protein Axin, leading to degradation of B-catenin inhibitors, 2) accumulation and translocation of B-catenin to the nucleus, and finally, regulation of cyclin-D1 causing G1/S transition and delamination of NC cells (Burstyn-Cohen and Kalcheim, 2002; De Melker *et al.*, 2004). Analyses of B-catenin localization in delaminating and migratory NC cells revealed similarities to the pattern of nuclear GLS expression in those cells (Fig. 7A, B), suggesting a possible tie between Wnt signaling and non-canonical function of GLS. Indeed, we had more cells with nuclear B-catenin localization relative to cell-cell contacts in delaminating NC cells, whereas migratory NC cells had a reverse distribution. Importantly, we observed that the nuclear GLS depletion by CB-839 negatively influenced B-catenin localization in the nucleus in both delaminating and migratory NC cells (Fig. 7C).

To lend further support, we compared the expression of *cyclin-E*, a potent cyclin-dependent kinase (CDK) of G1/S transition, by qPCR in delaminating and migratory stages defined by metabolic characterization of NT explants. We chose to analyze *cyclin-E* because, unlike *cyclin D1*, its expression sharply increases at G1/S transition of cell cycle (Yang *et al.*, 2006; Caldon and Musgrove, 2010). Our results demonstrated that at the migratory stage *cyclin-E* expression was downregulated compared with delaminating stage (Fig. 7D). It was consistent with *PRPS* expression (Fig. 2B), further supporting the nucleotide synthesis in PPP and G1/S transition. Subsequently, CB-839 negatively affected *cyclin-E* expression in both delaminating and migratory stages while glutamate decreased *cyclin-E* expression only in the delaminating group (Fig. 7E). Thus, *cyclin-E* expression in migratory stage seems likely to rely on the downstream part of glutamate metabolism, such as epigenetic remodeling by  $\alpha$ -KG. Conversely, the glutamine deprivation strongly decreased *cyclin-E* expression in migrating group (Fig. 7E). We then investigated S-phase cell cycle through short EdU incorporation to probe the metabolic impact on the cell cycle. Similarly, CB-839 and the glutamine starvation impacted significantly on proliferation rate of NC cells, while the glutamate condition did not (Fig. 7F).



Altogether, these findings raised an intriguing possibility about binding between B-catenin and GLS. To answer this question, we utilized immunofluorescence and proximity ligation assay (PLA) to enquire the interaction between these proteins. As a preliminary result, one PLA analysis revealed the physical interaction between GLS and B-catenin in both delaminating and migratory NC cells (Fig 7G). Additional experiments and quantifications are planned. Altogether, these findings suggest a non-canonical role for GLS governing both canonical Wnt signaling and genes expression in NC development (Fig 7 H).

After covering the PLA experiments, the results of the part B study will be submitted for publication. Thus, a second manuscript (Nekooie-Marnany et al.) is under writing process.

### **III. Discussion and perspective**

# *Part A*

## *Neural Crest Development relies on Glucose Oxidation*

In this part, we could acquire a general view of the metabolic impacts on NC development. Although OXPHOS was the predominant metabolic signature in trunk NC cells, they recruited several metabolic pathways to overcome nutrient or metabolic stress. Thus, NC cells utilize glucose, pyruvate and glutamine rewiring coincidentally anabolic and bioenergetic pathways to cover their G1/S transition, intermediates and energy demands required for EMT and progression. However, the convergence of all these metabolic profiles emerges as glucose-based OXPHOS. As such, our data established that, though necessary for trunk NC development, OXPHOS alone is not sufficient to support all the cellular events involved in this process. In addition, a PPP inhibitor strongly affected NC progression despite a minimal effect on mitochondrial respiration and ATP production. Finally, only glucose could elicit the complete cellular response of NC cells, i.e. delamination, adhesion, migration, proliferation, maintenance of stemness, and widespread differentiation.

Contrary to the general assertion that OXPHOS has a bioenergetic role in differentiated cells and that aerobic glycolysis has a biosynthetic role in proliferating non-differentiated stem cells (Shyh-Chang, Ng *et al.*, 2013; Ito, Keisuke and Suda, Toshio, 2014), NC development relies on the concerted and sustained mobilization of all metabolic pathways dependent on glucose metabolism, i.e. glycolysis, OXPHOS, and PPP, cooperating together. These findings illustrate the necessity for the NC population to make the most of the potential of the carbon metabolism route, so that they are endowed with the capacity to meet the high metabolic demands suitable for the coordinated execution of diverse cellular events, in a minimum of time and in a rapidly evolving environment. How NC cells maintain balanced activities of the different metabolic pathways is currently unknown. This may be achieved through regulated levels of metabolic enzymes and products of each pathway, under the control of intrinsic genetic programs as well as extrinsic factors, including nutrient availability and demand (Lempradl *et al.*, 2015). This view

is supported by our observations as well as a previous report (Oginuma, M. *et al.*, 2017) that glycolytic enzymes are not uniformly expressed in the embryo at the time of NCC dispersion.

Indeed, the lack of RNA expression of upper-glycolytic enzymes like glucose transporter (GLUT1) and phosphofructokinase (PFK) in migratory NC cells compared with NT is against the general concept of ubiquitous expression of metabolic enzymes in cells. The varying metabolic enzyme expressions among cell types raise an intriguing possibility of NC cells reliance on neighbors, particularly NT, that is coincident with vesicles appearance at the margin of the NT at onset of NC segregation. This is further supported by our experience that NC cells fail to survive without NT during first hours of culture. These observations reinforce the pivotal communication between NT and NC cells. Furthermore, the high rate of proliferation in NC cells combined with the poor expression of *GLUT1* and *PFK* in these cells increase this hypothesis that conceivably, NC progenitors evoke upper glycolysis pathway and PPP in their cell neighbors (NT) upon EMT event. Consequently, this type of cross talk between two cell types possibly leads to NT-derived vesicles to meet proliferative demands of NC cells. Therefore, identification of metabolic genes regulation during onset of NCC segregation can foster our general comprehension about how NT can conceive NC cells requirements and imbues them with vesicles.

In our study, we found no evidence for a significant contribution of a Warburg effect to trunk NC development. Indeed, assessment of ECAR using the Seahorse technology and measurement of lactate in the extracellular medium both revealed low lactate production in NT explants, demonstrating that glucose is not used for ATP production through lactate production, but serves to fuel OXPHOS, PPP, and possibly amino acid pathways for biosynthetic purposes. Moreover, the fact that oligomycin did not increase lactate levels indicate that glucose metabolism cannot be rewired from OXPHOS to aerobic glycolysis in NT explants. Our conclusion contrasts with a recent report, which proposed that, similarly to cancer cells, cranial NC cells display a Warburg effect (Bhattacharya, D. *et al.*, 2020). The difference in metabolic activity between cranial and trunk NC cells is likely to reside in the local O<sub>2</sub> concentration in their environment, besides other different biochemical cues. As for cancer cells in which hypoxia is known to promote metastatic spread (Semenza, 2012), cranial NC cells reside in a hypoxic milieu, which favors prolonged NC cells production from the NT through maintenance of EMT gene expression. Indeed, exposure to high O<sub>2</sub> levels or knockdown of the hypoxia-

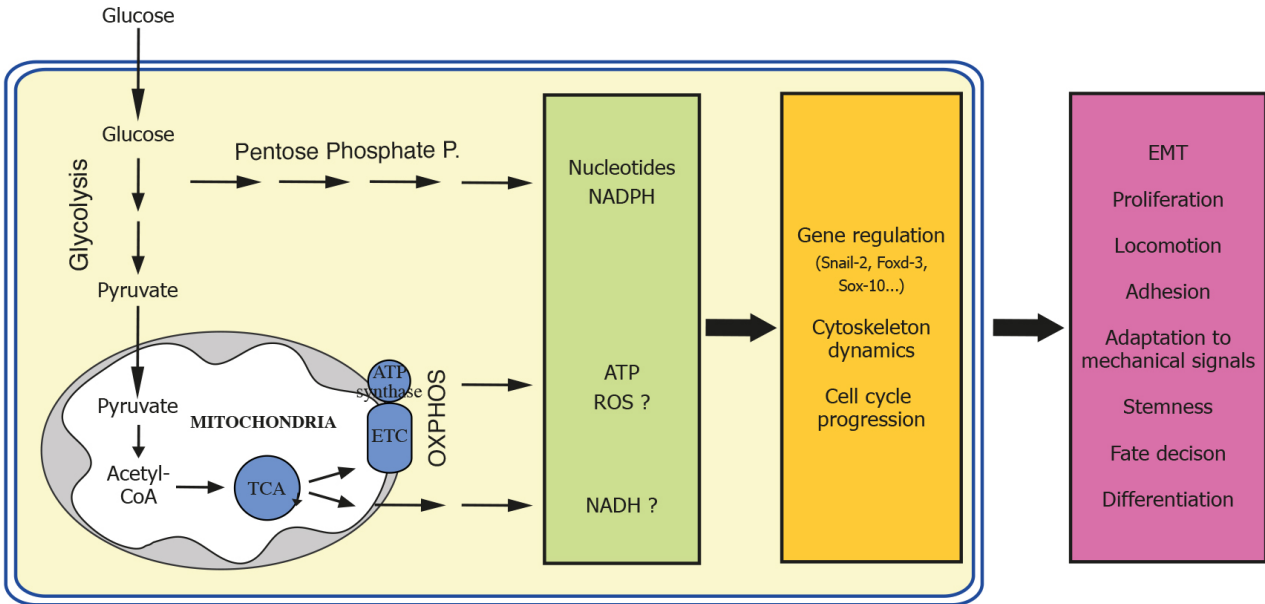
inducible factor HIF-1 cause strong reduction of *Snail2* expression and attenuation of NC production (Scully *et al.*, 2016). Trunk NC cells dispersion in contrast is intimately associated with blood vasculature (Thiery *et al.*, 1982; Schwarz *et al.*, 2009), and it is not affected by high O<sub>2</sub> levels or by deletion of the HIF-1 gene (Morriss and New, 1979; Iyer *et al.*, 1998).

Scrutinizing NC cellular responses to individual nutrients and to metabolic inhibitors revealed interesting features behind the overall classical scheme. In particular, we could not attribute to any metabolic pathway a specific role in the basic cellular processes, adhesion, locomotion and division. For example, despite PPP having a well-recognized role in nucleotide synthesis and maintenance of cellular redox balance (Patra and Hay, 2014), this pathway was not recruited solely for NC proliferation but significantly contributed to cell velocity and persistence of movement as well. Likewise, OXPHOS and ATP production in mitochondria were not exclusively aimed at supporting active migration, but also played a key role in EMT and proliferation. A likely explanation is that these processes are extremely demanding in both bioenergetic and biosynthetic supplies. Cell locomotion is known to consume much energy for actomyosin contraction necessary for cellular deformation but also needs continuous renewal of integrin and cadherin-mediated adhesions (Zanotelli *et al.*, 2021). Likewise, cell division needs high production of nucleotides for DNA replication as well as energy for mitotic spindle assembly and cytokinesis (Salazar-Roa and Malumbres, 2017). Another reason is that metabolic pathways, enzymes, metabolites and byproducts are known to influence cellular programs independently of their canonical bioenergetics and biosynthetic roles (Miyazawa, H. and Aulehla, A., 2018). NADH produced through TCA protects cells from oxidative stress (Bigarella *et al.*, 2014; Khacho *et al.*, 2016). This is illustrated by our observation that Rot-AA exhibits a stronger effect on NC cells than oligomycin. Likewise, similarly to neurons (Herrero-Mendez, A. *et al.*, 2009), the use of the PPP for metabolizing glucose may ensure NADPH production for the maintenance of a cellular redox balance. TCA cycle intermediates, in particular acetyl-CoA and  $\alpha$ -ketoglutarate, are involved in epigenetic regulation through histone acetylation and methylation (Kaelin and Mcknight, 2013). Regulation of gene expression during NC formation is under tight epigenetic control, involving DNA methylation, histone modifications, and ATP-dependent chromatin remodelers (Hu *et al.*, 2014).

An intriguing finding in our study is related to the effect of pyruvate on NC differentiation and fate decision. Consistent with previous studies showing that mitochondrial pyruvate metabolism represses stem cell state and proliferation (Schell, J. C. *et al.*, 2017), we found that providing pyruvate to NC cells in absence of glucose caused cell cycle arrest and loss of stem cell markers. But contrary to what has been reported for many other embryonic and stem cells (Shyh-Chang, N. *et al.*, 2013; Ito, K. and Suda, T., 2014; Khacho *et al.*, 2016; Khacho and Slack, 2017), it biased differentiation to a limited range of cell types where myofibroblasts predominate. In the embryo, myofibroblasts do not normally derive from trunk NC cells but are only provided by cranial NC. However, in *ex vivo* cultures in the presence of various hormones and growth factors (Dupin, E. *et al.*, 2018), myofibroblasts have been recurrently recorded in avian and mammalian trunk NC progeny, together with skeletogenic and adipogenic cells. These data have been interpreted as a dormant capacity of trunk NC cells to differentiate into non-neural derivatives normally obtained with cranial NC cells relieved by exogenous factors. Our observation that myofibroblastic differentiation occurs essentially in pyruvate conditions in the complete absence of additives suggests that this dormant capacity can be uncovered by culture conditions, thereby illustrating the key role of nutrient supplies and metabolism in instructing NC fate.

In conclusion, our data reveal that, contrary to pluripotent stem cells and cancer cells, NC in the embryonic trunk region rely primarily on glucose oxidation through glycolysis and mitochondrial respiration for energy production and mobilize a large range of metabolic pathways to meet their important bioenergetics and biosynthetic needs as well as to instruct their gene circuits driving their behavior and fate (see the schematic below).

How these metabolic pathways are regulated to accommodate the different steps of NC cells formation both temporally and spatially remains to be investigated. To obtain a comprehensive view of the metabolic landscape of NC cells during EMT and migration, a large-scale characterisation of intracellular metabolites in primary cultures can be conducted via NMR. In that case, after evaluation if NC primary cultures can give rise to enough cell numbers for analysis, it could be possible to identify metabolites produced by proton-based High-Resolution Magic Angle Spinning (HR-MAS) at different NC developmental steps. Then, High-Resolution Liquid NMR on cell extracts or culture medium can provide higher resolved signals.



In addition to the metabolome analysis, the transcriptome asset is required to broaden our understanding of NC EMT and migration steps. Since NC primary cultures are heterogeneous cell population consisting of a mixed population of NT cells together with NC cells at the pre-migratory, EMT, and migration stages, unambiguously establishing the list of the molecular targets of metabolic pathways involved in each step of NC development requires analyses at the single cell level. An unbiased transcriptomics analysis using scRNA-seq technology can be performed on avian trunk NC primary cultures whose metabolic profiles have been characterised by Seahorse machine. After cell sorting using flow cytometry, single-cell cDNA libraries will be constructed, tagged, and processed for sequencing using a modified Smart-seq2 protocol. Importantly, this protocol allows a much deeper interrogation of the spatio-temporality of cell identities and complexity. A number of specific markers such as Sox2, Sox9, Snail2, and Sox10, can be used to discriminate NT cells and each of the various NC cell populations in the data processing and bioinformatics analyses.

# *Part B*

## *Nuclear Translocation of glutaminase (GLS) aligned with Metabolic Remodeling Steers Neural Crest Delamination*

In this part, we identified the metabolic properties of trunk NC cells in two critical steps of their development. When induced to do EMT, trunk NC progenitors rewire PPP to supply anabolic requirements. Indeed, the contribution of glutamine and glucose to nucleotide synthesis underpins cellular building blocks whereby it reduces energy requirements. Unlike the delaminating step, NC cells at the migratory stage exploits the glucose and glutamine oxidation for high-energy demands. Thus, NC cells adapt their nutrient preference corresponding to bioenergetic demands through their developmental steps.

As evidenced by results part A, glucose is a fundamental substrate to support all aspects of NC development in NT explants cultures. But the contribution of glutamine present in the culture medium to the NC development was neglected. Here, we showed that extracellular glutamine endows NC progenitors with pluripotent potential. As such, glucose in glutamine-free medium was unable to maintain not only Foxd3 expression, a critical marker of NC pluripotency (Lukoseviciute, Martyna *et al.*, 2018; Schock, Elizabeth N and Labonne, Carole, 2020; Hu and Sauka-Spengler, 2022), but also the NC lineage marker, Sox10. In contrast to NC progenitors, embryonic stem cells (ESC) reduce cellular reliance on exogenous glutamine upon pluripotent cells-reprogramming to maintain their pluripotency and self-renewal (Vardhana *et al.*, 2019); and subsequently, primed PSC elevate glutamine anaplerosis and glycolysis mediated by core transcription factors of pluripotency like Oct4, Sox2, cMyc etc (Kim *et al.*, 2015b; Tsogtbaatar *et al.*, 2020). Therefore, the fluctuation between metabolic preference among different pluripotent phases, such as naïve, formative and primed PSC (Smith, 2017), reflects precarious states in both metabolic features and gene expressions of PSC before constituting lineage competence. Here, we indicated the intersection of metabolism and NC reprogramming from pluripotent to commitment, defined respectively by the high Foxd3, low Sox10 expressions plus metabolic quiescent profile and the low Foxd3, high Sox10 expression with OXPHOS phenotype.

There is growing evidence supporting the correlation between GLS and EMT in different cancer types. Two types of glutaminase serve for glutamate conversion from glutamine in mammals, comprising GLS and GLS2 with different patterns of expression, regulation, and localization. GLS is regulated by oncogenes such as KRAS and Myc, it localizes ubiquitously and encodes two alternatively spliced forms like GAC and KGA. But GLS2 is mostly found in organs like liver, pancreas and brain (Cai *et al.*, 2018; Ramirez-Peña *et al.*, 2019). In chicken, only the GLS type without alternative spliced form is found (NCBI data base). Overexpression of GLS In colorectal cancers increases invasion of cancer cells and patient mortality. Indeed, upregulated HIF-1 $\alpha$  expression in hypoxia conditions sets GLS as a target, underlying elevated GLS expression and sequentially increased invasion in colorectal cancer cells (Xiang *et al.*, 2019). GLS also has critical role in development of prostate cancer and loss of GLS resulted in cell cycle arrest and apoptosis (Zhang, J. *et al.*, 2019). Therefore, although the link between EMT and GLS is well documented in cancer, the mechanism of how GLS integrates into the cell invasion process remained elusive and it was commonly attributed to its bioenergetic role. Our study uncovers for the first time the translocation of GLS to the nucleus of NC progenitors, which subsequently pertains to the gene expression of NC specifiers. It is indeed likely that the induction of delaminating step and NC commitment to migratory phenotype are contingent on the convergence of the nuclear localization of GLS and pluripotency in NC precursors. Therefore, metabolism is not only the consequence of cellular behavior but also has the potential to determine cellular identity through the non-canonical functions of metabolic enzymes.

The mechanism of settling GLS in the nucleus besides mitochondria is still unknown. In this study, the impaired nuclear localization of GLS in glutamine-free culture reveals that glutamine serves as an intrinsic cue for GLS localization. To lend further support, Cai and colleagues recently demonstrated that GLS specifically and directly senses glutamine availability to induce mitochondria fusion under glutamine stress (Cai *et al.*, 2018). These data raise the hypothesis that high glutamine consumption at the delaminating stage of NC cells may correlate to GLS localization to the nucleus, conferring a high glutamine dependency. Furthermore, overexpression of *cMyc* or unchanged *GLS* expression under glutamine deprivation raises a possibility that the amount of *GLS* and *Myc* expression is uncoupled with the nuclear GLS localization, suggesting that a regulatory mechanism at protein structure level of GLS may

control its localization. Reciprocally, appreciating why GLS is intended to enter the nucleus instead of mitochondria is an interesting question. Since glutamine plays as a signaling cue for GLS, it can be hypothesized that a higher concentration of glutamine in the nucleus triggers nuclear translocation of GLS. A possible assay to check this hypothesis could be to measure glutamine concentration in the nucleus of sorted Foxd3<sup>+</sup>, Snail2<sup>+</sup> NC cells combined to the analysis of nuclear GLS expression.

We also observed a direct interaction between GLS and B-catenin and their nuclear accumulation in delaminating stage of NC cells. Our study provides some arguments about how B-catenin enters to nucleus in absence of nuclear localization signal (NLS) in the molecule (Fagotto et al., 1998; Anthony et al., 2020). However, it remains unclear whether GLS acts as B-catenin carrier to drag it into the nucleus using its own NLS sequence. Zhang and colleagues suggested a non-canonical function for GLS in prostate cancer, evidenced by harness of canonical Wnt pathway via suppressed GLS expression (Zhang, J. et al., 2019). These findings point out the critical role of GLS in early stage of embryonic development where canonical Wnt signaling controls NC induction, lineage commitment and differentiation. Collectively, our study reinforces the notion of GLS being a master gene regulator through nuclear localization and Wnt signaling. Complementary experiments with PLA assay under glutamine deprivation or CB-839 and the quantification of positive interactions of GLS and B-catenin in delaminating and migratory NC cells can provide an insight into whether GLS has a carrier role for B-catenin in the nucleus. In addition, Chromatin immunoprecipitation (ChIP) assay could be of the great interest for a better understanding of the role of nuclear GLS localization, especially to determine whether it is involved in gene expression through DNA binding in association with B-catenin or with other proteins. The need to switch to another cellular system, such as Crestospheres, neuroepithelial cells obtained from NT prior to NC emigrate that enables NC cells self-renewal and maintain multipotency (Tang and Bronner, 2020), can be inevitable. It can help to obtain more delaminating cells expressing EMT markers for ChIP or other techniques requiring higher cell numbers than our NCC primary cultures. But its utilization as a model is contingent to the observation of nuclear expression of GLS in crestosphere-derived delaminating cells combined with expression of EMT markers.

Here, although limitation in obtaining sufficient cell numbers hampered to carry out precise metabolomic analyses, we give a key insight of anabolic and catabolic metabolism in two critical steps of NC development. Conceivably, our understanding of the intersection of metabolic patterns and the cellular reprogramming promises an intriguing possibility to promote or hinder NC development by metabolic manipulation for therapeutic purpose of neurocristopathy. Proposing the non-canonical function for GLS as a gene regulatory function in EMT and delamination stage of NC development broadens the concept of metabolism from the metabolite-derived epigenetic regulation to the metabolic enzymes with genetic regulatory function.

## *Postface:*

During this journey in energy consumption across distinct cellular populations, we found out how different cells of metazoans intelligently cooperate to share their constant energy-carrier, like what we saw in the communication between neurons and astrocytes or between NT and NC cells. Regarding energy consumption across the countries, most energy sources are biased towards rich countries. Therefore, at this time that we are experiencing the truly global energy crisis, we need to reshape our pattern of energy consumption to overcome this crisis. Since all of us belong to one community, the human community in one planet with constant resources, it is really promising if we imitate the intimate communication of different cells in metazoans for energy sources. As such, since rich countries took advantages of the most amount of primary energy sources for higher socio- development, these countries, regardless of political or polarized views, can share either another type of energy, product or their technology with other countries, which not only contributes to socio-development of other countries but also maximizes the energy efficiency. It can be promising to have a clean and happy earth!!!

## **IV. Material and Methods**

## Reagents

Bovine plasma fibronectin (1mg/ml stock) was from Sigma (cat. no. F1141). Dispase II at 5 U/ml stock solution in Hanks' balanced saline was from Stemcell Technologies (cat. no. 07913). We utilized two types of DMEM from Gibco without glucose and pyruvate supplemented either with glutamine (cat.no. 11966-025) or without glutamine (cat.no. A1443001). The following chemicals were prepared and used according to the manufacturers' guidelines: 2-deoxy-D-glucose (2-DG, Sigma, cat. no. D8375), Na-iodoacetate (Sigma, cat. no. I2512), oligomycin-A (Sigma, cat. no. 75351), rotenone (Sigma, cat. no. R8875), antimycin-A (Sigma, cat. no. A8674), FCCP (Sigma, cat. no. C2920), 6-aminonicotinamide (6-AN, Cayman Chemicals, cat. no. 10009315), UK-5099 (Tocris Biosciences, cat. no. 4186), glutamate (Sigma, cat.no. G8415) and CB-839 (Sigma, cat. no. 5337170001). 2-DG was prepared as a 1 M stock solution in glucose-, pyruvate- and glutamine-free DMEM and used at 5-10 mM; Na-iodoacetate was prepared as a 15 mM stock solution in H<sub>2</sub>O and used at 15 μM; oligomycin, rotenone, antimycin-A, and FCCP were prepared in DMSO as 100 μM stock solutions and used at 1 μM; 6-AN was prepared as 100 mM solution in DMSO and used at 100 μM, except in Seahorse analyses where it was used at 500 μM. UK-5099 was prepared as 100 mM solution in DMSO and used at 100 μM. CB-839 was prepared in DMSO as 34 mM stock solution and used at 20 μM.

## Cell Culture

**Generation of NCC primary cultures:** NCC cultures were produced from NT explants obtained from quail embryos (*Coturnix coturnix japonica*) as described below and in Duband et al 2020. Fertilized eggs purchased from a local farm (La Caille de Chanteloup, Corps Nuds, France) were incubated at 37-38°C for the number of hours required to obtain embryos of stages corresponding to the chick stages 12-15 of Hamburger and Hamilton (Peng *et al.*) (1951), i.e. comprising 16-25 somite pairs. The eggshell was opened with curved dissecting scissors and the yolk transferred into phosphate-buffered saline (PBS). The embryo was cut off from the yolk and transferred into PBS in an elastomer-containing dish. An embryo portion of about 750-μm long was excised at the level of the last 5 somites with a scalpel under a stereomicroscope and subjected to mild enzymatic digestion by treatment with dispase II at 2.5 U/ml for 5-10 minutes

at room temperature. The NT was dissected out manually using fine dissection pins under a stereomicroscope, freed from the surrounding tissues, and transferred for 30-60 minutes in DMEM medium (no glucose, no pyruvate, Gibco, cat. no. 11966025) supplemented with 0.5% fetal bovine serum for recovery from enzyme treatment. NT were explanted onto culture dishes or coverglasses previously coated with fibronectin at 10 µg/ml in PBS (i.e. about 5 µg/cm<sup>2</sup>) for a minimum of 1 h at 37°C. To ensure rapid initiation of NCC migration, NT were positioned with their dorsal side oriented down toward the substratum. Explants were cultured at 37°C under normoxic conditions in a humidified 5%-CO<sub>2</sub> incubator in DMEM containing 1% serum, 100 U/ml penicillin, 100 µg/ml streptomycin, and 2 mM glutamine, and supplemented or not with 5 mM glucose and 1 mM pyruvate. In the glutamate condition, we utilized DMEM without glutamine supplemented with glucose (5mM) and 10 µM glutamate instead of glutamine. For glutamine condition again DMEM without glutamine supplemented with glucose (5mM) was utilized. The NT explants were considered during the first 5 hours of culture. Throughout each experiment, the morphology of the NT explant, area and progression of the NCC outgrowth, as well as individual cell shape and viability were evaluated, imaged, and assessed regularly under an inverted phase contrast Nikon microscope equipped with 6.3X, 10X, and 20X objectives. The choices of the culture dish, culture medium, and duration of the culture were determined according to the purpose of the experiment and the method of analysis used (see below). Throughout each experiment, the morphology of the NT explant, area and progression of the NCC outgrowth, as well as individual cell shape and viability were evaluated, imaged, and assessed regularly under an inverted phase contrast Nikon microscope equipped with 6.3X, 10X, and 20X objectives.

**Delamination assay:** NT explants were cultured for 5 h, a time sufficient to allow NCC segregating from the dorsal NT to adhere to the substrate. NT was then removed manually from the dish using fine dissection pins under a stereomicroscope or by gentle flushing of culture medium with a pipet tip, to uncover delaminated cells.

## Cellular Bioenergetic Analyses

**Seahorse analyses:** Bioenergetic profiles of NCC primary cultures were determined using a Seahorse Bioscience XF24 Analyzer. A single NT was deposited precisely at the center (Sup Fig 1A in part B of results) of each well of 24-well Seahorse plate previously coated with fibronectin and containing 100  $\mu$ l culture medium according to the purpose of the experiment, and NCC were allowed to undergo migration for 2 hours. Before preparation of the plate for Seahorse analysis, picture of NT explants were taken under phase contrast microscope and the areas of the NT explants were measured. Cultures were subsequently rinsed in Seahorse XF medium (Agilent, cat. no 103575-100) without serum and incubated for 30 minutes at 37°C in 500  $\mu$ l assay medium supplemented with the same metabolites prior the rinsing step, except FCS. The, the Seahorse assay was run according to the manufacturer's instructions. Oxygen consumption rate (OCR) and extracellular acidification rate (ECAR) values, as readouts of basal mitochondrial respiration and lactate production, were assessed regularly every cycle (mix, wait and measurement during 3 minutes), the basal measurement consisting of 4 cycles and drug injections, 3 cycles during 30 minutes. The impacts of all inhibitors were investigated from measurement 5 to 7. All drugs solutions were prepared to the final concentration by dilution of the stock in assay medium supplied with glucose and glutamine. The key parameters of mitochondrial respiration (ATP-linked respiration, maximal respiratory capacity and proton leak) were measured by means of a Mitostress test after sequential additions of oligomycin at 1  $\mu$ M, FCCP at 0.75  $\mu$ M, and Rot-AA at 1  $\mu$ M through 3 cycles of measurements in 30 minutes. We evaluate the bioenergetic profiles of each metabolic subgroup as follows: 1) ATP synthase inhibition with Oligomycin to evaluate ATP production, 2) assess the maximal mitochondrial activity independently of ATP synthesis by FCCP (Carbonyl cyanide-4-(trifluoromethoxy)phenylhydrazone) uncoupling ATP synthesis from ETC to disperse the mitochondrial membrane potential, and 3) non-mitochondrial oxygen consumption by Antimycin and Rotenone to block residual mitochondrial activity.

When appropriate, after metabolic profiling by Seahorse analysis, NCC primary cultures were processed for immunolabeling, RNA extraction for qPCR analysis, or cell lysate preparation for measurements of intracellular ATP, glutamine and glutamate as well as lactate levels. For

evolution of metabolic profile during the time, we performed two times Seahorse assays / plate on the same NT explants, such that after detection of metabolic profiles of NT explants at the first 3 hours of culture, the plate was removed from the analyzer, the assay medium was changed for 100 µl of culture medium (control condition) and the plate incubated for overnight in 37°C under normoxic conditions in a 5%-CO<sub>2</sub> prior to proceed for the second seahorse assay. All experiments were normalized via both length of neural tube and stage of embryos in primary step of experiments. The OCR and ECAR value were not normalized.

**Presens analyses:** The SDR Sensor Dish reader (Presens, Regensburg, Germany) was used for long-term measurements of O<sub>2</sub> levels in medium of NCC primary cultures. 6-7 NT were displayed at the center of each well of OxoDish OD24 plates (Presens) in culture medium. The plate was installed on the reader within a humidified 5%-CO<sub>2</sub> incubator for 24 h at 37°C. The O<sub>2</sub> concentration was measured every 5 minutes. When necessary, the plate was removed from the sensor for NT culture imaging at defined time points (4 and 8 h) and then returned to the incubator. After 24 h, the cultures were fixed and imaged.

**Intracellular ATP and lactate measurements:** Intracellular ATP and extracellular lactate levels were measured for each NCC primary cultures after Seahorse analysis using an ATPlite Bioluminescence assay kit from PerkinElmer (cat. no. 6016943) and the Lactate Fluorometric Assay kit from BioVision (cat. no. K607), respectively, according to the manufacturers' instructions.

**Glutamine and glutamate measurement:** Intracellular glutamine and glutamate levels for each NCC primary cultures after Seahorse analysis using a Glutamine/glutamate-Go assay (J8021) assay kit from Promega (cat. no. J8021).

## Fluorescence Labeling of NCC Cultures

For immunolabeling, the following primary antibodies were used: Rabbit monoclonal antibody (mAb) to Snail-2 (clone C19G7, Cell Signaling, 1/300), mouse mAb to Sox-10 (Clone A2, Santa Cruz, 1/200), mouse mAb to b-catenin (clone 14, BD-Transduction Laboratories, 1/200), Rabbit polyclonal antibody to GLS (PA535365, Life technologies SAS, 1/50) mouse mAb to paxillin (Clone 165, BD-Transduction Laboratories, 1/100), mouse mAb to  $\alpha$ -SMA conjugated to Cy3 (Clone 1A4, Sigma, 1/300), mouse mAb to  $\beta$ -tubulin conjugated to Alexa488 (Clone Tuj-1, R&D Systems, 1/500), mouse mAb to HNK-1 described previously ((Tucker *et al.*, 1984), undiluted culture supernatant), mouse mAb to MITF (clone C5, Abcam, 1/200), and mouse mAb to Glut-1 (Ab14683, Abcam, 1/50). Filamentous actin was detected using Texas Red<sup>TM</sup>-X Phalloidin (Molecular probe, cat. no. T7471).

NCC primary cultures were performed in 4-well plates or in 8-well Chambered Coverglass (Nunc, cat. no. 154511) coated with fibronectin, and fixed in 4% paraformaldehyde (PFA) in PBS for 15 minutes at room temperature for detection of all antigens, except for Snail-2 (5 minutes in 4% PFA), b-catenin (45 minutes in 1.5% PFA), and Glut-1 (see below). After permeabilization with 0.5% Triton X-100 in PBS for 15 minutes, cultures were blocked in PBS-3% BSA and subjected to immunofluorescence labeling using primary antibodies followed by incubation with appropriate secondary Ab conjugated to Alexa-fluor 488, Cy-3 or Cy-5 (Jackson ImmunoResearch Laboratories), and processed for DAPI or Hoechst staining to visualize cells' nuclei before mounting in ImmuMount medium (Shandon). For Glut-1 immunolabeling, unfixed NCC cultures were incubated with the Glut-1 antibody diluted in DMEM for 15 minutes at 15°C to avoid antibody internalization and immediately fixed in 100% ethanol at -20°C before rinsing in PBS and secondary antibody treatment. For labeling of mitochondria, MitoTracker Red (Invitrogen, cat. no. M7512) was added at 1  $\mu$ M to unfixed cultures and incubated for 20-30 minutes at 37°C. After washes with 37°C pre-warmed PBS, cells were briefly fixed with 4% PFA and mounted. Preparations were observed with a Zeiss AxioImager M2 epifluorescence microscope equipped with 10X-63X fluorescence objectives (Acroplan 10X/0.25, 20X/0.45, Plan-Neofluar 40X/0.75 and 63X/1.25 oil) or with a Zeiss LSM 900 confocal microscope equipped with 10X-40X fluorescence objectives (Plan-Apochrome 40X/1.30 oil). Data were collected using the Zen or

Airyscan2 software and processed using ImageJ software. For each series of experiments, images were acquired using equal exposure times and settings.

### **In Situ Hybridizations for mRNA Detection on NCC Primary Cultures and Whole Mount Embryos**

PCR technique was utilized for generation of in situ hybridization probe of GLS and GDH : primers of our target genes were designed from coding sequence of mRNA information available from NCBI data bases for 400-500 bp product. After obtaining the primer sequences, the sequence of RNA polymerase T7 binding site plus 5'-GAG-3' was added to the reverse primer: T7: 5'-TAATACGACTCACTATAGGG-3'.

The primer of GLS was: 5'-GAGTAATACGACTCACTATAGGGTGCTCCAGCATTACCATAGG-3' and GDH: 5'- GAGTAATACGACTCACTATAGGGCAGTACGCATGATTTGTCGAGC. Then PCR was performed to generate probes. We utilized Platinum Taq DNA polymerase (Invitrogen, Ca. no. 10966018), 2.5 µL 10X PCR buffer, 0.75 µL mgCL<sub>2</sub> (50mM), 0.5 µl dNTP, 0.5 µL forward primer (10 µM stock), 0.5 µL reverse primer (10µM stock), 1µM cDNA template, water to reach a final 25 µl total for each reaction. PCR program was utilized with lid temperature 105 °C, in this sequence: 95°C for 2s, 95°C for 15s, 60 °C for 30s, 72°C for 1min for each cycle, 35 cycles, 72°C for 1min. PCR product was check by run on gel to confirm successful amplification and purify the whole PCR product was purified by Qiaquick PCR cleanup protocol. The following plasmids for mRNA probe synthesis were used: *Snail-2* from A. Nieto, *Cadherin-6B* from M. Takeichi, *Foxd-3* from C. Erickson, *Sox-10* from P. Scotting, *Glut-1*, *PFK*, *PGK-1* and *PKM* from O. Pourquié. Linearized plasmid DNA was used to synthesize digoxigenin-UTP (Roche) labeled antisense probes with RNA polymerases from Promega and RNA probes were purified with Illustra ProbeQuant G-50 microcolumns (GE Healthcare).

In situ hybridizations were performed either on NCC primary cultures produced in fibronectin-coated plastic dishes or on whole mount intact embryos collected at the appropriate developmental stages, using essentially the same procedure. Samples of embryos and cultures were fixed in 4% PFA in PBS for 2 h at room temperature or overnight at 4°C. They were hybridized overnight at 65°C with the digoxigenin-UTP-labeled RNA probes in 50% formamide,

10% dextran sulfate and Denhart's buffer (0.5 µg probe/ml hybridization buffer) and washed twice in 50% formamide, 1x SSC and 0.1% Tween-20 at 65°C, then 4 times at room temperature in 100 mM maleic acid, 150 mM NaCl pH 7.5 and 0.1% Tween-20 (MABT buffer). After a 1-h pre-incubation in MABT buffer containing 10% blocking reagent (Roche) and 10% heat-inactivated lamb serum, samples were incubated overnight at room temperature with the anti-digoxygenin antibody (Roche). After extensive rinsing with MABT buffer, they were preincubated in 100 mM NaCl, 50 mM MgCl<sub>2</sub>, 1% Tween-20, and 25 mM Tris-HCl, pH 9.5, and stained with NBT-BCIP (Roche) following manufacturer's guidelines. Preparations were observed and imaged with a Nikon stereomicroscope and data analyzed with ImageJ software.

### RNA Quantification by Quantitative RT-PCR Analyses

Total RNA of Part A result were extracted from cultures of 5-8 NT explants using the Ambion PureLink RNA Mini Kit (Invitrogen, cat. no. 12183018A) following the manufacturer's guidelines. After quantification of RNA concentration, double-strand cDNA was synthesized from RNA using SuperScript IV reverse transcriptase (Invitrogen, cat. no. 18090050). In part B, after characterization of metabolic profile in NT explants plated 1NT/ well in Seahorse cell culture XF24, the total RNA was isolated from NT explants with same metabolic profile using Trizol (Invitrogen) according to manufacturer instructions. 500 ng RNA was used for cDNA synthesis using SuperScript IV reverse transcriptase (Invitrogen, cat. no. 18090050). Quantitative real time PCR were performed using the Power Syber Green Master Mix (Applied Biosystems, cat. no. 4368708) in a StepOne Plus RT-PCR apparatus (Applied Biosystems). Gene expression was assessed by the comparative CT ( $\Delta\Delta_{Ct}$ ) method with  $\beta$ -actin as the reference gene. The following primers were used are presented in the table below:

<i>Snail2fwd</i>	GATGCGCTCGCAGTGATAGT
<i>Snail2rev</i>	AGCTTTCATACAGGTATGGGGATA
<i>Cad6Bfwd</i>	ACCGTGAAAACAGGGAGCAA
<i>Cad6Brev</i>	TGAATTGGTAGGTGCTCTGGG
<i>cMycfwd</i>	GCAGCGACTCGGAAGAAGAACAAGAA;
<i>cMycrev</i>	GGTGGGGCTTACAGTGCTCC

<i>Sox10fwd</i>	CGGAGCACTCTTCAGGTCAG
<i>Sox10rev</i>	CCCTTCTCGCTTGGAGTCAG
<i>Foxd3fwd</i>	TCTGCGAGTTCATCAGCAAC
<i>Foxd3rev</i>	TTCACGAAGCAGTCGTTGAG
<i>Glut1fwd</i>	AAGATGACAGCTCGCCTGATG
<i>Glut1rev</i>	AGTCTTCAATCACCTTCTGCGG
<i>PFKfwd</i>	TTGGAATTGTCAGCTGCCCG
<i>PFKrev</i>	TGCAGACAACCTTTCATAGGCATCAG
<i>LDH fwd</i>	GAGCGGAGTGAATGTTGCTG
<i>LDH rev</i>	ACCTCATAGGCACTGTCCAC
<i>PDHX fwd</i>	CTGCTGCTGACTGTGACATTG
<i>PDHXrev</i>	TCACATCTGGCATTGCTTCA
<i>HIF-1<math>\alpha</math>fwd</i>	TCAGGCAGTTGGAATTGG-GTC
<i>HIF-1arev</i>	CGTAACTCGTGAGTTGGGGT
<i>PRPSfwd</i>	GCATCTCAGATTCAGGGCTTT
<i>PRPSrev</i>	GTCACTCTCTTGGCTCCACC
<i>GLSfwd</i>	GTCGCCTCCTTTGGACAAGA
<i>GLSrev</i>	GCACAGAGAAACCAGATCATGACA
<i>GDHfwd</i>	GGAGATGTCCTGGATCGCTG
<i>GDHrev</i>	CCCACGTTACCAAATCCCTGA
<i>GLULfwd</i>	TGGAGGTCTCAAGCACATCG
<i>GLULrev</i>	AGCCTTTCTTCTCATGGCCC
<i>Snat2 fwd</i>	AGCAACGACTTCAGTACCC
<i>Snat2 rev</i>	GGAAGTGGTACCCGGATGATAC
<i>Cyclin-E fwd</i>	GCTCCTGAAGACTTGACAAT
<i>Cyclin-E rev</i>	TTTGCTTGAGCTTTGTCCAGC
<i><math>\beta</math>Actinfwd</i>	CTGTGCCCATCTATGAAGGCTA
<i><math>\beta</math>Actinrev</i>	ATTTCTCTCTCGGCTGTGGTG

### **Whole mount immunolabeling**

The selected embryos were fixed with PFA 4% for 2 hours at 4 C°. Then the flat and fixed embryos were washed 2 times with PBS + 0.1% triton in 5 minutes. Before immunolabeling, all non-embryonic tissues were cut with scalpel and incubated with blocking solution (PBS +0.1% triton + BSA 1% and glycine 0.15 %) for 2 days at 4 C° with shaking. After removing the blocking solution, the primary antibodies for GLS (1:50) and SOX10 (1:200) diluted in blocking solution were added and samples were incubated for one night at 4 C° with gentle shaking. In the following day, samples were washed with blocking solution 3 times for 20 minutes ; then secondary antibodies coupled to Cy3 and Alexa- fluor 488 (1:300) in blocking solution were added to the samples for another night at the same conditions of primary antibody. In the last step, samples were washed with blocking solution 3 times for 20 minutes and then we transferred embryos on a Coverwell imaging chamber (Grace bio lab Ca. no 635041) to have dorsal axial at bottom of coverslip and removed all liquid to keep them flat, added few droplets of mounting medium on coverslip and gently put slid on the coverslip, kept for 24 hours at room temperature before imaging with confocal microscope 20X fluorescence objectives.

### **Cell Proliferation Assay**

Cell proliferation in culture was monitored using the Plus EdU Cell proliferation kit for imaging from Life Technologies (cat. no. C10638). Briefly, NCC primary cultures were generated on fibronectin-coated coverglasses as for immunolabelings and were incubated with EdU at 20  $\mu$ M in culture medium for 1 h at varying times of NCC development. Immediately after EdU incorporation, cultures were fixed in 4% PFA in PBS for 15 minutes at room temperature, permeabilized in 0.5 Triton-X100 for 15 minutes and treated for EdU detection using Alexa-555 Fluor azide in accordance with the manufacturer's guidelines. After DNA staining with Hoechst, cultures were optionally processed for immunostaining and analyzed as described for immunolabelings.

## **Cell Locomotion Assays**

NCC primary cultures were performed in 8-well Chambered Coverglass coated with fibronectin. Up to 4 NT explants were distributed separately into each well, and were maintained at 37°C in a humidified 5%-CO<sub>2</sub> incubator for about 2 h until the NT adhered firmly to the dish and NCC initiated migration on the substratum; then the cultures were transferred into a heated chamber (Ibidi) with a humid atmosphere containing 5% CO<sub>2</sub>/95% air placed on the motorized stage of a Leica DMIRE2 microscope equipped with a CoolSNAP HQ camera (Roper Scientific). Time-lapse video microscopy was performed with a 10x objective and phase contrast images were captured every 5 minutes during 16-24 h using the Micromanager software. Trajectories and positions of individual NCC in several explants recorded in parallel were tracked using Metamorph 7 software. The velocity of each cell was calculated as the ratio between the total length of its trajectory and the duration of the acquisition time and the persistence of movement as the ratio between the linear distance from the cell's initial to final positions and the total distance covered by the cell. Evolution of speed and persistence every hour were determined. The progression of the migratory front of the NCC population every hour was measured using a custom GUI written in Matlab<sup>®</sup> (MathWorks<sup>®</sup>, Natick, Massachusetts, USA).

## **Proximity Ligations Assay (PLA)**

After 5 hours of NT explant cultures, the NTs were removed and cultures were fixed with 4% PFA for 15 mins and, followed by permeabilization with 0.5% Triton X-100 in PBS for 5 minutes, cultures were blocked in PBS-3% BSA and subjected to immunofluorescence labeling using primary antibodies. We utilized primary antibodies prepared in blocking solution in following dilution: B-catenin (clone 14, BD-Transduction Laboratories, 1/200), Rabbit polyclonal antibody to GLS (PA535365, Life technologies SAS, 1/50). Following primary antibody incubation, the NT prints were washed 3X times in PBS for 5 mins and then diluted Plus and Minus PLA probes (1:5) were added and followed by Duolink-in situ orange starter kit Mouse/Rabbit kit ( Ca. no. DUO92102).

## Statistical Methods

Statistical analyses were performed using Prism 7 (GraphPad). Multiple comparisons were done respective to the control in the same experimental conditions. For statistical analysis of data in part A, we used One-way ANOVA parametric test after the validation of normality and equality of variances using Shapiro-Wilk and Brown-Forsythe methods, respectively. Otherwise, non-parametric Kruskal-Wallis test was used. And for part B, we utilized t-test for all analysis of data. For comparison between two conditions, we use unpaired t-test two-tailed test after the validation of normality and equality of using Shapiro-Wilk and equality of variances. Otherwise, non-parametric Mann-Whitney test was used. For statistical analysis of qPCR results, the data obtained for each drug or nutrient condition were compared to that of the control medium using unpaired t-test two-tailed test. Unless specified, at least three independent experiments were carried out for each procedure. Each NT explants was considered as an individual sample. The n of samples analyzed is indicated in each graph. Data are expressed as mean values  $\pm$  S.D. or S.E.M and the P values are \*  $p < 0.05$ , \*\*  $p < 0.01$ ; \*\*\*  $p < 0.001$ ; \*\*\*\*  $p < 0.0001$ . Results are considered statistically significantly different when  $p < 0.05$ .

## References

- ALTSHULER, A. et al. RAS regulates the transition from naive to primed pluripotent stem cells. **Stem cell reports**, v. 10, n. 3, p. 1088-1101, 2018. ISSN 2213-6711.
- ANASTASIOU, D. et al. Pyruvate kinase M2 activators promote tetramer formation and suppress tumorigenesis. **Nature chemical biology**, v. 8, n. 10, p. 839-847, 2012. ISSN 1552-4469.
- ANTHONY, C. C. et al. Nuclear regulation of Wnt/ $\beta$ -catenin signaling: it's a complex situation. **Genes**, v. 11, n. 8, p. 886, 2020.
- ARNOLD, P. K. et al. A non-canonical tricarboxylic acid cycle underlies cellular identity. **Nature**, v. 603, n. 7901, p. 477-481, 2022. ISSN 1476-4687.
- BAKSH, S. C.; FINLEY, L. W. Metabolic coordination of cell fate by  $\alpha$ -ketoglutarate-dependent dioxygenases. **Trends in cell biology**, v. 31, n. 1, p. 24-36, 2021. ISSN 0962-8924.
- BAKSH, S. C. et al. Extracellular serine controls epidermal stem cell fate and tumour initiation. **Nature cell biology**, v. 22, n. 7, p. 779-790, 2020. ISSN 1476-4679.
- BARRIGA, E. H. et al. The hypoxia factor Hif-1 $\alpha$  controls neural crest chemotaxis and epithelial to mesenchymal transition. **Journal of Cell Biology**, v. 201, n. 5, p. 759-776, 2013. ISSN 1540-8140.
- BERGER, S. L. The complex language of chromatin regulation during transcription. **Nature**, v. 447, n. 7143, p. 407-412, 2007. ISSN 1476-4687.
- BERTERO, T. et al. Tumor-stroma mechanics coordinate amino acid availability to sustain tumor growth and malignancy. **Cell metabolism**, v. 29, n. 1, p. 124-140. e10, 2019. ISSN 1550-4131.
- BHATTACHARYA, D.; AZAMBUJA, A. P.; SIMOES-COSTA, M. Metabolic reprogramming promotes neural crest migration via yap/tead signaling. **Developmental cell**, v. 53, n. 2, p. 199-211. e6, 2020. ISSN 1534-5807.
- BHATTACHARYA, D.; AZAMBUJA, A. P.; SIMOES-COSTA, M. Metabolic reprogramming promotes neural crest migration via Yap/Tead signaling. **Dev Cell**, v. 53, n. 2, p. 199-211.e6, Apr 20 2020. ISSN 1534-5807 (Print) 1534-5807.
- BIGARELLA, C. L.; LIANG, R.; GHAFARI, S. Stem cells and the impact of ROS signaling. **Development**, v. 141, n. 22, p. 4206-18, Nov 2014. ISSN 0950-1991 (Print) 0950-1991.
- BLACKSTONE, N. W. Charles Manning Child (1869–1954): the past, present, and future of metabolic signaling. **Journal of Experimental Zoology Part B: Molecular and Developmental Evolution**, v. 306, n. 1, p. 1-7, 2006. ISSN 1552-5007.
- BOND, M. R.; HANOVER, J. A. A little sugar goes a long way: the cell biology of O-GlcNAc. **Journal of Cell Biology**, v. 208, n. 7, p. 869-880, 2015. ISSN 1540-8140.
- BONINI, S. A. et al. Potential role of microtubule stabilizing agents in neurodevelopmental disorders. **International journal of molecular sciences**, v. 18, n. 8, p. 1627, 2017. ISSN 1422-0067.
- BOROUGHES, L. K.; DEBERARDINIS, R. J. Metabolic pathways promoting cancer cell survival and growth. **Nature cell biology**, v. 17, n. 4, p. 351-359, 2015. ISSN 1476-4679.
- BOUKOURIS, A. E.; ZERVOPOULOS, S. D.; MICHELAKIS, E. D. Metabolic enzymes

- moonlighting in the nucleus: metabolic regulation of gene transcription. **Trends in biochemical sciences**, v. 41, n. 8, p. 712-730, 2016. ISSN 0968-0004.
- BRONNER, M. E.; LEDOUARIN, N. M. Development and evolution of the neural crest: an overview. **Developmental biology**, v. 366, n. 1, p. 2-9, 2012. ISSN 0012-1606.
- BULUSU, V. et al. Spatiotemporal analysis of a glycolytic activity gradient linked to mouse embryo mesoderm development. **Developmental cell**, v. 40, n. 4, p. 331-341. e4, 2017. ISSN 1534-5807.
- BULUSU, V. et al. Acetate recapturing by nuclear acetyl-CoA synthetase 2 prevents loss of histone acetylation during oxygen and serum limitation. **Cell reports**, v. 18, n. 3, p. 647-658, 2017. ISSN 2211-1247.
- BURSTYN-COHEN, T.; KALCHEIM, C. Association between the cell cycle and neural crest delamination through specific regulation of G1/S transition. **Developmental cell**, v. 3, n. 3, p. 383-395, 2002. ISSN 1534-5807.
- CABLE, J. et al. Metabolic decisions in development and disease—a Keystone Symposia report. **Annals of the New York Academy of Sciences**, v. 1506, n. 1, p. 55-73, 2021. ISSN 0077-8923.
- CAI, L. et al. Acetyl-CoA induces cell growth and proliferation by promoting the acetylation of histones at growth genes. **Molecular cell**, v. 42, n. 4, p. 426-437, 2011. ISSN 1097-2765.
- CAI, W.-F. et al. Glutaminase GLS1 senses glutamine availability in a non-enzymatic manner triggering mitochondrial fusion. **Cell research**, v. 28, n. 8, p. 865-867, 2018. ISSN 1748-7838.
- CALDON, C. E.; MUSGROVE, E. A. Distinct and redundant functions of cyclin E1 and cyclin E2 in development and cancer. **Cell division**, v. 5, n. 1, p. 1-13, 2010. ISSN 1747-1028.
- CAO, Y. et al. miR-290/371-Mbd2-Myc circuit regulates glycolytic metabolism to promote pluripotency. **The EMBO journal**, v. 34, n. 5, p. 609-623, 2015. ISSN 0261-4189.
- CAREY, B. W. et al. Intracellular  $\alpha$ -ketoglutarate maintains the pluripotency of embryonic stem cells. **Nature**, v. 518, n. 7539, p. 413-416, 2015. ISSN 1476-4687.
- CHA, Y. et al. Metabolic control of primed human pluripotent stem cell fate and function by the miR-200c–SIRT2 axis. **Nature cell biology**, v. 19, n. 5, p. 445-456, 2017. ISSN 1476-4679.
- CHANG, C.-H. et al. Posttranscriptional control of T cell effector function by aerobic glycolysis. **Cell**, v. 153, n. 6, p. 1239-1251, 2013. ISSN 0092-8674.
- CHAZAUD, C.; YAMANAKA, Y. Lineage specification in the mouse preimplantation embryo. **Development**, v. 143, n. 7, p. 1063-1074, 2016. ISSN 1477-9129.
- CHEUNG, M. et al. The transcriptional control of trunk neural crest induction, survival, and delamination. **Developmental cell**, v. 8, n. 2, p. 179-192, 2005. ISSN 1534-5807.
- CHILD, C. M. Patterns and problems of development. 1941.
- CHU, S. The world's energy problem and what we can do about it. **Bulletin of the American Academy Winter**, p. 53, 2008.
- CLIFF, T. S. et al. MYC controls human pluripotent stem cell fate decisions through regulation of metabolic flux. **Cell stem cell**, v. 21, n. 4, p. 502-516. e9, 2017. ISSN 1934-5909.

- COLACINO, J. A. et al. Heterogeneity of human breast stem and progenitor cells as revealed by transcriptional profiling. **Stem Cell Reports**, v. 10, n. 5, p. 1596-1609, 2018. ISSN 2213-6711.
- COLES, E.; TANEYHILL, L.; BRONNER-FRASER, M. A critical role for Cadherin6B in regulating avian neural crest emigration. **Developmental biology**, v. 312, n. 2, p. 533-544, 2007. ISSN 0012-1606.
- COMERFORD, S. A. et al. Acetate dependence of tumors. **Cell**, v. 159, n. 7, p. 1591-1602, 2014. ISSN 0092-8674.
- COULY, G. et al. Determination of the identity of the derivatives of the cephalic neural crest: incompatibility between Hox gene expression and lower jaw development. **Development**, v. 125, n. 17, p. 3445-3459, 1998. ISSN 1477-9129.
- CREAZZO, T. L. et al. Role of cardiac neural crest cells in cardiovascular development. **Annual review of physiology**, v. 60, p. 267, 1998. ISSN 0066-4278.
- DADY, A.; DUBAND, J. L. Cadherin interplay during neural crest segregation from the non-neural ectoderm and neural tube in the early chick embryo. **Developmental Dynamics**, v. 246, n. 7, p. 550-565, 2017. ISSN 1058-8388.
- DAI, X. et al. Histone lactylation: Epigenetic mark of glycolytic switch. **Trends in Genetics**, 2021. ISSN 0168-9525.
- DANN, S. G. et al. Reciprocal regulation of amino acid import and epigenetic state through Lat1 and EZH 2. **The EMBO journal**, v. 34, n. 13, p. 1773-1785, 2015. ISSN 0261-4189.
- DE MELKER, A. A.; DESBAN, N.; DUBAND, J. L. Cellular localization and signaling activity of  $\beta$ -catenin in migrating neural crest cells. **Developmental dynamics: an official publication of the American Association of Anatomists**, v. 230, n. 4, p. 708-726, 2004. ISSN 1058-8388.
- DE PALMA, S. et al. Changes in muscle cell metabolism and mechanotransduction are associated with myopathic phenotype in a mouse model of collagen VI deficiency. **PLoS one**, v. 8, n. 2, p. e56716, 2013. ISSN 1932-6203.
- DE QUEIROZ, R. M. et al. Hexosamine biosynthetic pathway and glycosylation regulate cell migration in melanoma cells. **Frontiers in Oncology**, v. 9, p. 116, 2019. ISSN 2234-943X.
- DEBERARDINIS, R. J.; CHANDEL, N. S. Fundamentals of cancer metabolism. **Science advances**, v. 2, n. 5, p. e1600200, 2016. ISSN 2375-2548.
- DENICOLA, G. M. et al. NRF2 regulates serine biosynthesis in non-small cell lung cancer. **Nature genetics**, v. 47, n. 12, p. 1475-1481, 2015. ISSN 1546-1718.
- DENKO, N. C. Hypoxia, HIF1 and glucose metabolism in the solid tumour. **Nature Reviews Cancer**, v. 8, n. 9, p. 705-713, 2008. ISSN 1474-1768.
- DUBAND, J.-L. Neural crest delamination and migration. **Neural Crest Induction and Differentiation**, p. 45-77, 2006.
- \_\_\_\_\_. Diversity in the molecular and cellular strategies of epithelium-to-mesenchyme transitions: Insights from the neural crest. **Cell adhesion & migration**, v. 4, n. 3, p. 458-482, 2010. ISSN 1933-6918.
- DUBAND, J.-L.; DADY, A.; FLEURY, V. Resolving time and space constraints during neural crest formation and delamination. **Current topics in developmental biology**, v. 111, p. 27-67, 2015. ISSN 0070-2153.

DUBAND, J. L. et al. Epithelium-mesenchyme transition during neural crest development. **Acta Anat (Basel)**, v. 154, n. 1, p. 63-78, 1995. ISSN 0001-5180 (Print)

0001-5180 (Linking). Available at: < <https://www.ncbi.nlm.nih.gov/pubmed/8714290> >.

DUBAND, J. L.; NEKOOIE-MARNANY, N.; DUFOUR, S. Establishing primary cultures of trunk neural crest cells. **Curr Protoc Cell Biol**, v. 88, n. 1, p. e109, Sep 2020. ISSN 1934-2616.

DUBAND, J. L.; NEKOOIE-MARNANY, N.; DUFOUR, S. Establishing Primary Cultures of Trunk Neural Crest Cells. **Current Protocols in Cell Biology**, v. 88, n. 1, p. e109, 2020. ISSN 1934-2500.

DUPIN, E. et al. The issue of the multipotency of the neural crest cells. **Dev Biol**, v. 444 Suppl 1, p. S47-S59, Dec 1 2018. ISSN 1095-564X (Electronic)

0012-1606 (Linking). Available at: < <https://www.ncbi.nlm.nih.gov/pubmed/29614271> >.

DUPIN, E. et al. The issue of the multipotency of the neural crest cells. **Developmental Biology**, v. 444, p. S47-S59, 2018. ISSN 0012-1606.

EVERS, T. M. et al. Reciprocal regulation of cellular mechanics and metabolism. **Nature metabolism**, v. 3, n. 4, p. 456-468, 2021. ISSN 2522-5812.

FAGOTTO, F.; GLÜCK, U.; GUMBINER, B. M. Nuclear localization signal-independent and importin/karyopherin-independent nuclear import of  $\beta$ -catenin. **Current Biology**, v. 8, n. 4, p. 181-190, 1998. ISSN 0960-9822.

FAN, J. et al. Glutamine-driven oxidative phosphorylation is a major ATP source in transformed mammalian cells in both normoxia and hypoxia. **Molecular systems biology**, v. 9, n. 1, p. 712, 2013. ISSN 1744-4292.

FENG, J. et al. Emerging roles and the regulation of aerobic glycolysis in hepatocellular carcinoma. **Journal of Experimental & Clinical Cancer Research**, v. 39, n. 1, p. 1-19, 2020. ISSN 1756-9966.

FERRICK, D. A.; NEILSON, A.; BEESON, C. Advances in measuring cellular bioenergetics using extracellular flux. **Drug discovery today**, v. 13, n. 5-6, p. 268-274, 2008. ISSN 1359-6446.

FIGUEIREDO, A. L. et al. PFKFB4 control of AKT signaling is essential for premigratory and migratory neural crest formation. **Development**, v. 144, n. 22, p. 4183-4194, 2017. ISSN 1477-9129.

FLICKINGER JR, R. A. A study of the metabolism of amphibian neural crest cells during their migration and pigmentation in vitro. **Journal of Experimental Zoology**, v. 112, n. 3, p. 465-484, 1949. ISSN 0022-104X.

GANS, C.; NORTHCUTT, R. G. Neural crest and the origin of vertebrates: a new head. **Science**, v. 220, n. 4594, p. 268-273, 1983. ISSN 0036-8075.

GARCÍA-CASTRO, M. N. I.; MARCELLE, C.; BRONNER-FRASER, M. Ectodermal Wnt function as a neural crest inducer. **Science**, v. 297, n. 5582, p. 848-851, 2002. ISSN 1095-9203.

GIOVANNUCCI, D. et al. Sustainable Development in the 21st Century (SD21). **Food and Agriculture: The Future of Sustainability**, 2012.

GROVES, A. K.; LABONNE, C. Setting appropriate boundaries: fate, patterning and competence at the neural plate border. **Developmental biology**, v. 389, n. 1, p. 2-12, 2014. ISSN 0012-1606.

GU, W. et al. Glycolytic metabolism plays a functional role in regulating human pluripotent stem cell state. **Cell stem cell**, v. 19, n. 4, p. 476-490, 2016. ISSN 1934-5909.

- HALL, B. K. The evolution of the neural crest in vertebrates. **Regulatory Processes in Development**, v. 76, p. 101-113, 2000.
- HERRERO-MENDEZ, A. et al. The bioenergetic and antioxidant status of neurons is controlled by continuous degradation of a key glycolytic enzyme by APC/C-Cdh1. **Nat Cell Biol**, v. 11, n. 6, p. 747-52, Jun 2009. ISSN 1465-7392.
- HERRERO-MENDEZ, A. et al. The bioenergetic and antioxidant status of neurons is controlled by continuous degradation of a key glycolytic enzyme by APC/C-Cdh1. **Nature cell biology**, v. 11, n. 6, p. 747-752, 2009. ISSN 1476-4679.
- HIS, W. **Untersuchungen über die erste Anlage des Wirbelthierleibes: die erste Entwicklung des Hühnchens im Ei**. FCW Vogel, 1868.
- HORSTADIUS, S. **The neural crest**. Geoffrey Cumberlege Oxford University Press, London, 1950.
- HOSIOS, A. M. et al. Amino acids rather than glucose account for the majority of cell mass in proliferating mammalian cells. **Developmental cell**, v. 36, n. 5, p. 540-549, 2016. ISSN 1534-5807.
- HOVLAND, A. S.; ROTHSTEIN, M.; SIMOES-COSTA, M. Network architecture and regulatory logic in neural crest development. **Wiley Interdisciplinary Reviews: Systems Biology and Medicine**, v. 12, n. 2, p. e1468, 2020. ISSN 1939-5094.
- HU, N.; STROBL-MAZZULLA, P. H.; BRONNER, M. E. Epigenetic regulation in neural crest development. **Dev Biol**, v. 396, n. 2, p. 159-68, Dec 15 2014. ISSN 0012-1606 (Print)  
0012-1606.
- HU, Z.; SAUKA-SPENGLER, T. Cellular plasticity in the neural crest and cancer. **Current Opinion in Genetics & Development**, v. 75, p. 101928, 2022. ISSN 0959-437X.
- HUBAUD, A.; POURQUIÉ, O. Signalling dynamics in vertebrate segmentation. **Nature reviews Molecular cell biology**, v. 15, n. 11, p. 709-721, 2014. ISSN 1471-0080.
- INTLEKOFER, A. M. et al. Hypoxia induces production of L-2-hydroxyglutarate. **Cell metabolism**, v. 22, n. 2, p. 304-311, 2015. ISSN 1550-4131.
- INTLEKOFER, A. M.; FINLEY, L. W. Metabolic signatures of cancer cells and stem cells. **Nature metabolism**, v. 1, n. 2, p. 177-188, 2019. ISSN 2522-5812.
- INTLEKOFER, A. M.; FINLEY, L. W. S. Metabolic signatures of cancer cells and stem cells. **Nat Metab**, v. 1, n. 2, p. 177-188, Feb 2019. ISSN 2522-5812 (Electronic)  
2522-5812 (Linking). Available at: <  
<https://www.ncbi.nlm.nih.gov/pubmed/31245788>  
>.
- ITO, K.; SUDA, T. Metabolic requirements for the maintenance of self-renewing stem cells. **Nat Rev Mol Cell Biol**, v. 15, n. 4, p. 243-56, Apr 2014. ISSN 1471-0080 (Electronic)  
1471-0072 (Linking). Available at: <  
<http://www.ncbi.nlm.nih.gov/pubmed/24651542>  
>.
- ITO, K.; SUDA, T. Metabolic requirements for the maintenance of self-renewing stem cells. **Nature reviews Molecular cell biology**, v. 15, n. 4, p. 243-256, 2014. ISSN 1471-0080.
- IYER, N. V. et al. Cellular and developmental control of O<sub>2</sub> homeostasis by hypoxia-inducible factor 1 alpha. **Genes Dev**, v. 12, n. 2, p. 149-62, Jan 15 1998. ISSN 0890-9369 (Print)  
0890-9369.

- Ji, Y. et al. Wnt signaling in neural crest ontogenesis and oncogenesis. **Cells**, v. 8, n. 10, p. 1173, 2019.
- JIA, D. et al. Towards decoding the coupled decision-making of metabolism and epithelial-to-mesenchymal transition in cancer. **British Journal of Cancer**, v. 124, n. 12, p. 1902-1911, 2021. ISSN 1532-1827.
- KAELIN, W. G., JR.; MCKNIGHT, S. L. Influence of metabolism on epigenetics and disease. **Cell**, v. 153, n. 1, p. 56-69, Mar 28 2013. ISSN 0092-8674 (Print)  
0092-8674.
- KASHEF, J. et al. Cadherin-11 regulates protrusive activity in *Xenopus* cranial neural crest cells upstream of Trio and the small GTPases. **Genes & Development**, v. 23, n. 12, p. 1393-1398, 2009. ISSN 0890-9369.
- KEROSUO, L.; BRONNER, M. E. cMyc regulates the size of the premigratory neural crest stem cell pool. **Cell reports**, v. 17, n. 10, p. 2648-2659, 2016. ISSN 2211-1247.
- KHACHO, M. et al. Mitochondrial dynamics impacts stem cell identity and fate decisions by regulating a nuclear transcriptional program. **Cell Stem Cell**, v. 19, n. 2, p. 232-247, Aug 4 2016. ISSN 1875-9777.
- KHACHO, M.; SLACK, R. S. Mitochondrial activity in the regulation of stem cell self-renewal and differentiation. **Curr Opin Cell Biol**, v. 49, p. 1-8, Dec 2017. ISSN 0955-0674.
- KIM, H. et al. Core pluripotency factors directly regulate metabolism in embryonic stem cell to maintain pluripotency. **Stem cells**, v. 33, n. 9, p. 2699-2711, 2015a. ISSN 1066-5099.
- KIM, H. et al. Core pluripotency factors directly regulate metabolism in embryonic stem cell to maintain pluripotency. **Stem cells**, v. 33, n. 9, p. 2699-2711, 2015b. ISSN 1066-5099.
- KOTTAKIS, F. et al. LKB1 loss links serine metabolism to DNA methylation and tumorigenesis. **Nature**, v. 539, n. 7629, p. 390-395, 2016. ISSN 1476-4687.
- KRISPIN, S. et al. Evidence for a dynamic spatiotemporal fate map and early fate restrictions of premigratory avian neural crest. **Development**, v. 137, n. 4, p. 585-595, 2010. ISSN 1477-9129.
- LABOSKY, P. A.; KAESTNER, K. H. The winged helix transcription factor Hfh2 is expressed in neural crest and spinal cord during mouse development. **Mechanisms of development**, v. 76, n. 1-2, p. 185-190, 1998. ISSN 0925-4773.
- LACROIX, A. S.; ROTHENBERG, K. E.; HOFFMAN, B. D. Molecular-scale tools for studying mechanotransduction. **Annual review of biomedical engineering**, v. 17, p. 287-316, 2015. ISSN 1523-9829.
- LE DOUARIN, N. A biological cell labeling technique and its use in experimental embryology. **Developmental biology**, v. 30, n. 1, p. 217-222, 1973. ISSN 0012-1606.
- LE DOUARIN, N. The neural crest, source of mesenchymal cells. **The neural crest**, p. 54-86, 1982.
- LE DOUARIN, N. M.; SMITH, J. Development of the peripheral nervous system from the neural crest. **Annual review of cell biology**, v. 4, p. 375-404, 1988. ISSN 0743-4634.
- LEMPRADL, A.; POSPISILIK, J. A.; PENNINGER, J. M. Exploring the emerging complexity in transcriptional regulation of energy homeostasis.

**Nature Reviews Genetics**, v. 16, n. 11, p. 665-681, 2015. ISSN 1471-0064.

LI, S. et al. Serine and SAM responsive complex SESAME regulates histone modification crosstalk by sensing cellular metabolism. **Molecular cell**, v. 60, n. 3, p. 408-421, 2015. ISSN 1097-2765.

LI, Y. et al. In Vivo Quantitative Imaging Provides Insights into Trunk Neural Crest Migration. **Cell Rep**, v. 26, n. 6, p. 1489-1500 e3, Feb 5 2019. ISSN 2211-1247 (Electronic). Available at: < <https://www.ncbi.nlm.nih.gov/pubmed/30726733> >.

LIGNELL, A. et al. Identification of a neural crest stem cell niche by Spatial Genomic Analysis. **Nature communications**, v. 8, n. 1, p. 1-11, 2017. ISSN 2041-1723.

LIU, S. et al. Developing neural crest cells in culture: correlation of cytochrome oxidase activity with SSEA-1 and dopamine- $\beta$ -hydroxylase immunoreactivity. **Brain research**, v. 535, n. 2, p. 271-280, 1990. ISSN 0006-8993.

LOSMAN, J.-A.; KAELIN, W. G. What a difference a hydroxyl makes: mutant IDH,(R)-2-hydroxyglutarate, and cancer. **Genes & development**, v. 27, n. 8, p. 836-852, 2013. ISSN 0890-9369.

LOSMAN, J.-A. et al. (R)-2-hydroxyglutarate is sufficient to promote leukemogenesis and its effects are reversible. **Science**, v. 339, n. 6127, p. 1621-1625, 2013. ISSN 0036-8075.

LU, C. et al. IDH mutation impairs histone demethylation and results in a block to cell differentiation. **Nature**, v. 483, n. 7390, p. 474-478, 2012. ISSN 1476-4687.

LU, V.; ROY, I. J.; TEITELL, M. A. Nutrients in the fate of pluripotent stem cells. **Cell Metabolism**, v. 33, n. 11, p. 2108-2121, 2021. ISSN 1550-4131.

LUKOSEVICIUTE, M. et al. From pioneer to repressor: bimodal foxd3 activity dynamically remodels neural crest regulatory landscape in vivo. **Developmental cell**, v. 47, n. 5, p. 608-628. e6, 2018. ISSN 1534-5807.

LUKOSEVICIUTE, M. et al. From pioneer to repressor: bimodal Foxd3 activity dynamically remodels neural crest regulatory landscape in vivo. **Dev Cell**, v. 47, n. 5, p. 608-628.e6, Dec 3 2018. ISSN 1534-5807 (Print) 1534-5807.

LUNT, S. Y.; VANDER HEIDEN, M. G. Aerobic glycolysis: meeting the metabolic requirements of cell proliferation. 2011. ISSN 1081-0706.

MÄCHLER, P. et al. In vivo evidence for a lactate gradient from astrocytes to neurons. **Cell metabolism**, v. 23, n. 1, p. 94-102, 2016. ISSN 1550-4131.

MARTELLO, G.; SMITH, A. The nature of embryonic stem cells. **Annual review of cell and developmental biology**, v. 30, p. 647-675, 2014. ISSN 1081-0706.

MARTIK, M. L.; BRONNER, M. E. Regulatory logic underlying diversification of the neural crest. **Trends in Genetics**, v. 33, n. 10, p. 715-727, 2017. ISSN 0168-9525.

MATHIEU, J.; RUOHOLA-BAKER, H. Metabolic remodeling during the loss and acquisition of pluripotency. **Development**, v. 144, n. 4, p. 541-551, 2017. ISSN 1477-9129.

MEULEMANS, D.; BRONNER-FRASER, M. Amphioxus and lamprey AP-2 genes: implications for neural crest evolution and migration patterns. 2002. ISSN 1477-9129.

- MIYAZAWA, H.; AULEHLA, A. Revisiting the role of metabolism during development. **Development**, v. 145, n. 19, Oct 1 2018. ISSN 1477-9129 (Electronic) 1534-5807 (Linking). Available at: < <https://www.ncbi.nlm.nih.gov/pubmed/28245921> >.
- 0950-1991 (Linking). Available at: < <http://www.ncbi.nlm.nih.gov/pubmed/30275240> >.
- MIYAZAWA, H.; AULEHLA, A. Revisiting the role of metabolism during development. **Development**, v. 145, n. 19, p. dev131110, 2018. ISSN 1477-9129.
- MIYAZAWA, H. et al. Rewiring of embryonic glucose metabolism via suppression of PFK-1 and aldolase during mouse chorioallantoic branching. **Development**, v. 144, n. 1, p. 63-73, 2017. ISSN 0950-1991.
- MORRISS, G. M.; NEW, D. A. Effect of oxygen concentration on morphogenesis of cranial neural folds and neural crest in cultured rat embryos. **J Embryol Exp Morphol**, v. 54, p. 17-35, Dec 1979. ISSN 0022-0752 (Print) 0968-0004.
- 0022-0752.
- MOUSSAIEFF, A. et al. Glycolysis-mediated changes in acetyl-CoA and histone acetylation control the early differentiation of embryonic stem cells. **Cell metabolism**, v. 21, n. 3, p. 392-402, 2015. ISSN 1550-4131.
- NIETO, M. A. The snail superfamily of zinc-finger transcription factors. **Nature reviews Molecular cell biology**, v. 3, n. 3, p. 155-166, 2002. ISSN 1471-0080.
- OBUROGLU, L. et al. Glucose and glutamine metabolism regulate human hematopoietic stem cell lineage specification. **Cell stem cell**, v. 15, n. 2, p. 169-184, 2014. ISSN 1934-5909.
- OGINUMA, M. et al. A gradient of glycolytic activity coordinates FGF and Wnt signaling during elongation of the body axis in amniote embryos. **Dev Cell**, v. 40, n. 4, p. 342-353 e10, Feb 27 2017. ISSN 1878-1551 (Electronic) 1534-5807 (Linking). Available at: < <https://www.ncbi.nlm.nih.gov/pubmed/28245921> >.
- OGINUMA, M. et al. A gradient of glycolytic activity coordinates FGF and Wnt signaling during elongation of the body axis in amniote embryos. **Developmental cell**, v. 40, n. 4, p. 342-353. e10, 2017. ISSN 1534-5807.
- PANOPOULOS, A. D. et al. The metabolome of induced pluripotent stem cells reveals metabolic changes occurring in somatic cell reprogramming. **Cell research**, v. 22, n. 1, p. 168-177, 2012. ISSN 1748-7838.
- PATRA, K. C.; HAY, N. The pentose phosphate pathway and cancer. **Trends Biochem Sci**, v. 39, n. 8, p. 347-54, Aug 2014. ISSN 0968-0004 (Print) 0968-0004.
- PENG, M. et al. Aerobic glycolysis promotes T helper 1 cell differentiation through an epigenetic mechanism. **Science**, v. 354, n. 6311, p. 481-484, 2016. ISSN 0036-8075.
- PEREIRA, S. L. et al. From gametogenesis and stem cells to cancer: common metabolic themes. **Human Reproduction Update**, v. 20, n. 6, p. 924-943, 2014. ISSN 1355-4786. Available at: < <https://doi.org/10.1093/humupd/dmu034> >. Accessed on: 6/13/2022.
- PERESTRELO, T. et al. Metabolic and mechanical cues regulating pluripotent stem cell fate. **Trends in cell biology**, v. 28, n. 12, p. 1014-1029, 2018. ISSN 0962-8924.
- PÉREZ-ESCUREDO, J. et al. Lactate promotes glutamine uptake and metabolism in oxidative cancer cells. **Cell cycle**, v. 15, n. 1, p. 72-83, 2016. ISSN 1538-4101.
- PLOSS, C. et al. Mutations in regulators of the epigenome and their connections to global

- chromatin patterns in cancer. **Nature reviews genetics**, v. 14, n. 11, p. 765-780, 2013. ISSN 1471-0064.
- PRIGIONE, A. et al. The senescence-related mitochondrial/oxidative stress pathway is repressed in human induced pluripotent stem cells. **Stem cells**, v. 28, n. 4, p. 721-733, 2010. ISSN 1066-5099.
- RAFFEL, S. et al. BCAT1 restricts  $\alpha$ KG levels in AML stem cells leading to IDHmut-like DNA hypermethylation. **Nature**, v. 551, n. 7680, p. 384-388, 2017. ISSN 1476-4687.
- RAMIREZ-PEÑA, E. et al. The epithelial to mesenchymal transition promotes glutamine independence by suppressing GLS2 expression. **Cancers**, v. 11, n. 10, p. 1610, 2019.
- REKLER, D.; KALCHEIM, C. From Neural Crest to Definitive Roof Plate: The Dynamic Behavior of the Dorsal Neural Tube. **International Journal of Molecular Sciences**, v. 22, n. 8, p. 3911, 2021.
- RIDENOUR, D. A. et al. The neural crest cell cycle is related to phases of migration in the head. **Development**, v. 141, n. 5, p. 1095-103, Mar 2014. ISSN 1477-9129 (Electronic)
- 0950-1991 (Linking). Available at: < <https://www.ncbi.nlm.nih.gov/pubmed/24550117> >.
- ROCHA, M. et al. From head to tail: regionalization of the neural crest. **Development**, v. 147, n. 20, p. dev193888, 2020. ISSN 1477-9129.
- ROMANI, P. et al. Crosstalk between mechanotransduction and metabolism. **Nature Reviews Molecular Cell Biology**, v. 22, n. 1, p. 22-38, 2021. ISSN 1471-0080.
- ROVASIO, R. A. et al. Neural crest cell migration: requirements for exogenous fibronectin and high cell density. **The Journal of cell biology**, v. 96, n. 2, p. 462-473, 1983. ISSN 0021-9525.
- SALAZAR-ROA, M.; MALUMBRES, M. Fueling the cell division cycle. **Trends Cell Biol**, v. 27, n. 1, p. 69-81, Jan 2017. ISSN 0962-8924.
- SANTIAGO, A.; ERICKSON, C. A. Ephrin-B ligands play a dual role in the control of neural crest cell migration. 2002. ISSN 1477-9129.
- SHELL, J. C. et al. Control of intestinal stem cell function and proliferation by mitochondrial pyruvate metabolism. **Nature cell biology**, v. 19, n. 9, p. 1027-1036, 2017. ISSN 1476-4679.
- SHELL, J. C. et al. Control of intestinal stem cell function and proliferation by mitochondrial pyruvate metabolism. **Nat Cell Biol**, v. 19, n. 9, p. 1027-1036, Sep 2017. ISSN 1465-7392 (Print) 1465-7392.
- SCHOCK, E. N.; LABONNE, C. Sorting Sox: Diverse roles for Sox transcription factors during neural crest and craniofacial development. **Front Physiol**, v. 11, p. 606889, 2020. ISSN 1664-042X (Print) 1664-042x.
- SCHOCK, E. N.; LABONNE, C. Sorting sox: diverse roles for sox transcription factors during neural crest and craniofacial development. **Frontiers in physiology**, v. 11, p. 1564, 2020. ISSN 1664-042X.
- SCHUG, Z. et al. Acetyl-coA synthetase 2 promotes acetate utilization and maintains cell growth under metabolic stress. **Cancer & Metabolism**, v. 2, n. 1, p. 1-1, 2014. ISSN 2049-3002.
- SCHWAB, A. et al. Polyol pathway links glucose metabolism to the aggressiveness of cancer cells. **Cancer research**, v. 78, n. 7, p. 1604-1618, 2018. ISSN 0008-5472.

SCHWARZ, Q. et al. Neuropilin 1 signaling guides neural crest cells to coordinate pathway choice with cell specification. **Proc Natl Acad Sci U S A**, v. 106, n. 15, p. 6164-9, Apr 14 2009. ISSN 0027-8424 (Print)

0027-8424.

SCULLY, D. et al. Hypoxia promotes production of neural crest cells in the embryonic head. **Development**, v. 143, n. 10, p. 1742-52, May 15 2016. ISSN 1477-9129 (Electronic)

0950-1991 (Linking). Available at: < <https://www.ncbi.nlm.nih.gov/pubmed/27190038> >.

SEMENZA, G. L. Molecular mechanisms mediating metastasis of hypoxic breast cancer cells. **Trends Mol Med**, v. 18, n. 9, p. 534-43, Sep 2012. ISSN 1471-4914 (Print)

1471-4914.

SETOGUCHI, K. et al. P53 regulates rapid apoptosis in human pluripotent stem cells. **Journal of molecular biology**, v. 428, n. 7, p. 1465-1475, 2016. ISSN 0022-2836.

SHEEHY, S. P.; PARKER, K. K. The role of mechanical forces in guiding tissue differentiation. In: (Ed.). **Tissue engineering in regenerative medicine**: Springer, 2011. p.77-97.

SHYH-CHANG, N.; DALEY, G. Q.; CANTLEY, L. C. Stem cell metabolism in tissue development and aging. **Development**, v. 140, n. 12, p. 2535-2547, 2013. ISSN 1477-9129.

SHYH-CHANG, N.; DALEY, G. Q.; CANTLEY, L. C. Stem cell metabolism in tissue development and aging. **Development**, v. 140, n. 12, p. 2535-47, Jun 2013. ISSN 1477-9129 (Electronic)

0950-1991 (Linking). Available at: < <http://www.ncbi.nlm.nih.gov/pubmed/23715547> >.

SIMOES-COSTA, M.; BRONNER, M. E. Reprogramming of avian neural crest axial identity and cell fate. **Science**, v. 352, n. 6293, p. 1570-1573, 2016. ISSN 0036-8075.

SIMÕES-COSTA, M.; BRONNER, M. E. Insights into neural crest development and evolution from genomic analysis. **Genome research**, v. 23, n. 7, p. 1069-1080, 2013. ISSN 1088-9051.

\_\_\_\_\_. Establishing neural crest identity: a gene regulatory recipe. **Development**, v. 142, n. 2, p. 242-257, 2015. ISSN 0950-1991.

SIMÕES-COSTA, M. S. et al. Dynamic and differential regulation of stem cell factor FoxD3 in the neural crest is Encrypted in the genome. **PLoS Genet**, v. 8, n. 12, p. e1003142, 2012. ISSN 1553-7390 (Print)

1553-7390.

SIVANAND, S.; VINEY, I.; WELLEN, K. E. Spatiotemporal control of acetyl-CoA metabolism in chromatin regulation. **Trends in biochemical sciences**, v. 43, n. 1, p. 61-74, 2018. ISSN 0968-0004.

SMITH, A. Formative pluripotency: the executive phase in a developmental continuum. **Development**, v. 144, n. 3, p. 365-373, 2017. ISSN 1477-9129.

SOLDATOV, R. et al. Spatiotemporal structure of cell fate decisions in murine neural crest. **Science**, v. 364, n. 6444, p. eaas9536, 2019. ISSN 0036-8075.

SOLMONSON, A. et al. Compartmentalized metabolism supports midgestation mammalian development. **Nature**, v. 604, n. 7905, p. 349-353, 2022. ISSN 1476-4687.

SOUTHARD-SMITH, E. M.; KOS, L.; PAVAN, W. J. Sox10 mutation disrupts neural crest development

- in Dom Hirschsprung mouse model. **Nature genetics**, v. 18, n. 1, p. 60-64, 1998. ISSN 1546-1718.
- SPRATT JR, N. T. Nutritional requirements of the early chick embryo. III. The metabolic basis of morphogenesis and differentiation as revealed by the use of inhibitors. **The Biological Bulletin**, v. 99, n. 1, p. 120-135, 1950. ISSN 0006-3185.
- STINE, Z. E. et al. MYC, metabolism, and cancer. **Cancer discovery**, v. 5, n. 10, p. 1024-1039, 2015. ISSN 2159-8274.
- SU, R. et al. R-2HG exhibits anti-tumor activity by targeting FTO/m6A/MYC/CEBPA signaling. **Cell**, v. 172, n. 1-2, p. 90-105. e23, 2018. ISSN 0092-8674.
- SU, X.; WELLEN, K. E.; RABINOWITZ, J. D. Metabolic control of methylation and acetylation. **Current opinion in chemical biology**, v. 30, p. 52-60, 2016. ISSN 1367-5931.
- SUMMERS, M. C.; BIGGERS, J. D. Chemically defined media and the culture of mammalian preimplantation embryos: historical perspective and current issues. **Human reproduction update**, v. 9, n. 6, p. 557-582, 2003. ISSN 1460-2369.
- TANG, W.; BRONNER, M. E. Neural crest lineage analysis: from past to future trajectory. **Development**, v. 147, n. 20, p. dev193193, 2020. ISSN 1477-9129.
- TESSARZ, P.; KOUZARIDES, T. Histone core modifications regulating nucleosome structure and dynamics. **Nature reviews Molecular cell biology**, v. 15, n. 11, p. 703-708, 2014. ISSN 1471-0080.
- THEUNISSEN, T. W. et al. Systematic identification of culture conditions for induction and maintenance of naive human pluripotency. **Cell stem cell**, v. 15, n. 4, p. 471-487, 2014. ISSN 1934-5909.
- THEVENEAU, E. et al. Collective chemotaxis requires contact-dependent cell polarity. **Developmental cell**, v. 19, n. 1, p. 39-53, 2010. ISSN 1534-5807.
- THIERY, J. P.; DUBAND, J.-L.; DELOUVÉE, A. Pathways and mechanism of avian trunk neural crest cell migration and localization. **Develop. Biol.**, v. 93, p. 324-343, 1982.
- TOHYAMA, S. et al. Glutamine oxidation is indispensable for survival of human pluripotent stem cells. **Cell metabolism**, v. 23, n. 4, p. 663-674, 2016. ISSN 1550-4131.
- TSOGTBAATAR, E. et al. Energy metabolism regulates stem cell pluripotency. **Frontiers in cell and developmental biology**, v. 8, p. 87, 2020. ISSN 2296-634X.
- TUCKER, G. C. et al. Identical reactivity of monoclonal antibodies HNK-1 and NC-1: Conservation in vertebrates on cells derived from the neural primordium and on some leukocytes. **Cell Diff.**, v. 14, p. 223-230, 1984.
- TURNBULL, T. Energy, history, and the humanities: against a new determinism. **History and Technology**, v. 37, n. 2, p. 247-292, 2021. ISSN 0734-1512.
- VANDER HEIDEN, M. G.; CANTLEY, L. C.; THOMPSON, C. B. Understanding the Warburg effect: the metabolic requirements of cell proliferation. **science**, v. 324, n. 5930, p. 1029-1033, 2009. ISSN 0036-8075.
- VANDER HEIDEN, M. G.; DEBERARDINIS, R. J. Understanding the intersections between metabolism and cancer biology. **Cell**, v. 168, n. 4, p. 657-669, 2017. ISSN 0092-8674.
- VARDHANA, S. A. et al. Glutamine independence is a selectable feature of pluripotent stem cells.

- Nature metabolism**, v. 1, n. 7, p. 676-687, 2019. ISSN 2522-5812.
- WANG, R. et al. The transcription factor Myc controls metabolic reprogramming upon T lymphocyte activation. **Immunity**, v. 35, n. 6, p. 871-882, 2011. ISSN 1074-7613.
- WARD, P. S. et al. The common feature of leukemia-associated IDH1 and IDH2 mutations is a neomorphic enzyme activity converting  $\alpha$ -ketoglutarate to 2-hydroxyglutarate. **Cancer cell**, v. 17, n. 3, p. 225-234, 2010. ISSN 1535-6108.
- WEINBERGER, L. et al. Dynamic stem cell states: naive to primed pluripotency in rodents and humans. **Nature reviews Molecular cell biology**, v. 17, n. 3, p. 155-169, 2016. ISSN 1471-0080.
- WELLEN, K. E. et al. ATP-citrate lyase links cellular metabolism to histone acetylation. **Science**, v. 324, n. 5930, p. 1076-1080, 2009. ISSN 0036-8075.
- WINER, L. S. P.; WU, M. J. P. O. Rapid analysis of glycolytic and oxidative substrate flux of cancer cells in a microplate. v. 9, n. 10, p. e109916, 2014. ISSN 1932-6203.
- XIANG, L. et al. Glutaminase 1 expression in colorectal cancer cells is induced by hypoxia and required for tumor growth, invasion, and metastatic colonization. **Cell death & disease**, v. 10, n. 2, p. 1-15, 2019. ISSN 2041-4889.
- YANG, K.; HITOMI, M.; STACEY, D. W. Variations in cyclin D1 levels through the cell cycle determine the proliferative fate of a cell. **Cell division**, v. 1, n. 1, p. 1-8, 2006. ISSN 1747-1028.
- YANG, W. et al. ERK1/2-dependent phosphorylation and nuclear translocation of PKM2 promotes the Warburg effect. **Nature cell biology**, v. 14, n. 12, p. 1295-1304, 2012. ISSN 1476-4679.
- YU, L. et al. Core pluripotency factors promote glycolysis of human embryonic stem cells by activating GLUT1 enhancer. **Protein & cell**, v. 10, n. 9, p. 668-680, 2019. ISSN 1674-8018.
- ZALC, A. et al. Reactivation of the pluripotency program precedes formation of the cranial neural crest. **Science**, v. 371, n. 6529, p. eabb4776, 2021. ISSN 0036-8075.
- ZANOTELLI, M. R.; ZHANG, J.; REINHART-KING, C. A. Mechanoresponsive metabolism in cancer cell migration and metastasis. **Cell Metab**, v. 33, n. 7, p. 1307-1321, Jul 6 2021. ISSN 1550-4131 (Print) 1550-4131.
- ZHANG, D. et al. Metabolic regulation of gene expression by histone lactylation. **Nature**, v. 574, n. 7779, p. 575-580, 2019. ISSN 1476-4687.
- ZHANG, H. et al. Distinct metabolic states can support self-renewal and lipogenesis in human pluripotent stem cells under different culture conditions. **Cell reports**, v. 16, n. 6, p. 1536-1547, 2016. ISSN 2211-1247.
- ZHANG, J. et al. UCP2 regulates energy metabolism and differentiation potential of human pluripotent stem cells. **The EMBO journal**, v. 30, n. 24, p. 4860-4873, 2011. ISSN 0261-4189.
- ZHANG, J. et al. Inhibition of GLS suppresses proliferation and promotes apoptosis in prostate cancer. **Bioscience reports**, v. 39, n. 6, 2019. ISSN 0144-8463.
- ZHANG, J. et al. Metabolism in pluripotent stem cells and early mammalian development. **Cell metabolism**, v. 27, n. 2, p. 332-338, 2018. ISSN 1550-4131.
- ZHAO, J. et al. Metabolic remodelling during early mouse embryo development. **Nature Metabolism**, v. 3, n. 10, p. 1372-1384, 2021. ISSN 2522-5812.

- ZHENG, L.; ROEDER, R. G.; LUO, Y. S phase activation of the histone H2B promoter by OCA-S, a coactivator complex that contains GAPDH as a key component. **Cell**, v. 114, n. 2, p. 255-266, 2003. ISSN 0092-8674.
- ZHOU, W. et al. HIF1 $\alpha$  induced switch from bivalent to exclusively glycolytic metabolism during ESC-to-EpiSC/hESC transition. **The EMBO journal**, v. 31, n. 9, p. 2103-2116, 2012. ISSN 0261-4189.
- ZU, X. L.; GUPPY, M. Cancer metabolism: facts, fantasy, and fiction. **Biochemical and biophysical research communications**, v. 313, n. 3, p. 459-465, 2004. ISSN 0006-291X.

## **V. Annex**



# Establishing Primary Cultures of Trunk Neural Crest Cells

Jean-Loup Duband,<sup>1,2</sup> Nioosha Nekooie-Marnany,<sup>1</sup> and Sylvie Dufour<sup>1</sup>

<sup>1</sup>Institut Mondor de Recherches Biomédicales, INSERM U955, Université Paris-Est Créteil, Créteil, France

<sup>2</sup>Corresponding author: [jean-loup.duband@inserm.fr](mailto:jean-loup.duband@inserm.fr)

Neural crest cells constitute a unique population of progenitor cells with extensive stem cell capacities able to navigate throughout various environments in the embryo and are a source of multiple cell types, including neurons, glia, melanocytes, smooth muscles, endocrine cells, cardiac cells, and also skeletal and supportive tissues in the head. Neural crest cells are not restricted to the embryo but persist as well in adult tissues where they provide a reservoir of stem cells with great therapeutic promise. Many fundamental questions in cell, developmental, and stem cell biology can be addressed using this system. During the last decades there has been an increased availability of elaborated techniques, animal models, and molecular tools to tackle neural crest cell development. However, these approaches are often very challenging and difficult to establish and they are not adapted for rapid functional investigations of mechanisms driving cell migration and differentiation. In addition, they are not adequate for collecting pure populations of neural crest cells usable in large scale analyses and for stem cell studies. Transferring and adapting the neural crest system in tissue culture may then represent an attractive alternative, opening up numerous prospects. Here we describe a simple method for establishing primary cultures of neural crest cells derived from trunk neural tubes using the avian embryo as a source of cells. This protocol is suited for producing pure populations of neural crest cells that can be processed for cytological, cellular, and functional approaches aimed at characterizing their phenotype, behavior, and potential. © 2020 Wiley Periodicals LLC.

**Basic Protocol:** Primary cultures of avian trunk neural crest cells

**Support Protocol:** Adaptations for immunofluorescence labeling and videomicroscopy

Keywords: avian embryo • cell culture • cell lineage • cell migration • neural crest • phenotyping • stem cells

## How to cite this article:

Duband, J.-L., Nekooie-Marnany, N., & Dufour, S. (2020). Establishing primary cultures of trunk neural crest cells. *Current Protocols in Cell Biology*, 88, e109. doi: 10.1002/cpcb.109

## INTRODUCTION

Because neural crest cells constitute a population of stem cells of the vertebrate embryo able to colonize numerous tissues and provide a large array of cell types (Le Douarin & Kalcheim, 1999; Trainor, 2013), they represent an attractive model for cell and developmental biologists to investigate how the basic cellular processes, such as proliferation, survival, adhesion, migration, and differentiation, are coordinated in time and space to generate highly organized and specialized cellular assemblies in the organism. In brief, the neural crest develops all along the embryonic anteroposterior (or rostrocaudal) axis,

Duband et al.

1 of 25



*Current Protocols in Cell Biology* e109, Volume 88  
Published in Wiley Online Library ([wileyonlinelibrary.com](http://wileyonlinelibrary.com)).  
doi: 10.1002/cpcb.109  
© 2020 Wiley Periodicals LLC

at the junction between the ectoderm, i.e., the future epidermis, and the neural plate, i.e., the primordium of the central nervous system. After specification early during development, progenitors of the neural crest situated initially at the periphery of the blastoderm become gradually positioned at the apex of the neural tube along the embryonic midline. Later on, by a mechanism related to epithelium-mesenchyme transition, they delaminate from the neural tube and disperse through defined, spatially restricted pathways to colonize many different territories throughout the embryo. Ultimately, they differentiate into a large collection of cell types, ranging from neurons, glia, or melanocytes, to endocrine and cardiac cells, as well as most skeletal and supportive tissues of the head. Interestingly, neural crest cells provide large contingents of stem cells in adult tissues, such as in the nervous system, heart, skin, gut, teeth, and bones (Liu & Cheung, 2016), and a recent and growing literature highlighted that a population of neural crest cells persists in adulthood, which are able to give rise to derivatives in several body sites just as their embryonic counterparts (Furlan & Adameyko, 2018). As a consequence, any shortcomings in neural crest cell development may lead to dramatic congenital craniofacial, cardiac, or enteric disorders and may be as well associated with the occurrence of various pathologies later after birth and in the adult, notably pediatric cancers like neuroblastoma, neurofibromatosis, and melanoma. Therefore, neural crest cells represent a challenging and promising cellular population with a formidable potential in tissue repair and replacement therapies both during embryogenesis and in the adult.

Neural crest cells are partitioned spatially into distinct populations (cranial, cardiac, vagal, trunk, and sacral) differing by their cellular properties and fate all along the rostrocaudal axis of the embryo and this is instrumental for elucidating how intrinsic and extrinsic influences integrate over time to direct their spatially appropriate differentiation. Strikingly, unlike many other embryonic populations, neural crest cells execute their main developmental steps (specification, dispersion, expansion, and differentiation) sequentially and in separate locations of the embryo (Duband, Dady, & Fleury, 2015), making this system highly suitable for analyzing each step individually and for understanding how they are temporally coordinated.

The last few decades witnessed the emergence of a variety of elaborated techniques, animal models and molecular tools to investigate neural crest cell development *in vivo* (Baggiolini et al., 2015; Betancur, Bronner-Fraser, & Sauka-Spengler, 2010; Hockman et al., 2019; Li et al., 2019; Soldatov et al., 2019; Williams et al., 2019). These studies are at the origin of considerable progress in our understanding of this cell population. However, these approaches are often very challenging and out of reach for most cell biology laboratories. Because many of them require a combination of different specific skills in developmental biology, they are difficult, take a long time to establish, and may be costly. In addition, they either cannot be easily tailored to current cell biology techniques, notably high-resolution imaging, or would require very sophisticated devices. Hence, they do not allow rapid and easy analyses to address specific questions on defined cellular events. Therefore, transferring the neural crest system in culture may represent a very attractive alternative opening numerous perspectives.

Unlike many other embryonic cells, neural crest cells cannot be conveniently collected for culture in large quantities and free of contaminants directly from the embryo. Indeed, during migration, they are scattered among the neighboring embryonic tissues and they cannot be easily discriminated from other cells for extirpation. In addition, often soon after initiation of migration, neural crest cells engage precociously into differentiation and may then lose some of their initial properties. Conversely, at early developmental stages, neural crest progenitors fail to develop further in culture and to acquire all neural crest cell features, in particular their migration capacity and differentiation potential. Nevertheless, neural crest cells can be successfully cultured *in vitro* if they are derived

from the neural tube precisely at the time when they are about to initiate migration. At this stage, the neural tube is a well-delineated tissue that can be easily excised out of the embryo and, upon explantation in culture, it releases swiftly its neural crest cell contingent which then adheres to the dish, migrates, and proliferates, forming ultimately after 24 hr a large cell outgrowth surrounding the neural tube. Moreover, neural crest cells can be cultured for relatively prolonged time periods, up to 1 or 2 weeks, and under appropriate conditions, they can undergo differentiation into various cell types (Dupin & Coelho-Aguiar, 2013; Dupin, Calloni, Coelho-Aguiar, & Le Douarin, 2018). Thus, using this method, each of the different steps that accompany neural crest cell development as well as their main features (rate of cell proliferation, cellular interactions within the population, and timing and kinetics of the cellular events) can be recapitulated in vitro and analyzed individually. Practically, this method relies on the fact that neural crest ontogeny proceeds along a rostrocaudal gradient. During the third day of embryonic development, only the portion of the neural tube situated along the last-formed somites is able to produce immediately large quantities of migrating neural crest cells when explanted in culture, and neither more anterior nor more posterior neural tubes can produce significant populations of cells with a complete neural crest phenotype (Duband, Blavet, Jarov, & Fournier-Thibault, 2009).

Neural crest cell development has been explored in a variety of vertebrate species ranging from lower vertebrates (lamprey), fish, and frogs (zebrafish and *Xenopus*) to amniotes (chick, quail, mouse, rat, and now human). Although cultures of neural crest cells can be theoretically generated from most of these species, the use of the avian model is recommended for beginners for a variety of reasons. First, it can be easily and rapidly set up with no special reagents and skills. A little practice is generally sufficient. In addition, it is affordable and may even be used for experiments requiring relatively large quantities of biological material because embryos can be collected in larger amounts than with mouse and synchronized to the same developmental stage. Finally, most neural crest cell derivatives can be successfully obtained in culture with avian embryos and the evolutionary proximity between birds and mammals make it convenient for the use of all sorts of molecular tools for functional studies. Here we describe the basic method to isolate neural tube explants from trunk segments of quail embryos and produce pure populations of neural crest cells, and we present tools necessary for their phenotypic characterization.

*NOTE:* It should be stressed that the method described below requires neither specific technical skill nor long practice and expertise in experimental developmental biology. Calm, meticulousness, and patience generally help to overcome all the issues, and there are no particularly difficult and stressful steps that have to be conducted in a very limited time. Train first with a few eggs, e.g., a dozen, to get practice and appreciate the difficulties and pitfalls of the method and to know your limits, and follow the basic rules and recommendations that are explained below. A few days of training are generally sufficient to undertake a full-scale experiment in a completely autonomous fashion. Failing with a few eggs at the beginning is no big deal (they are cheap) and should not discourage you to persevere. The only important recommendation concerns the tools used for dissection as they are key for your success. Don't hesitate to customize them to your hand (particularly left versus right) and avoid sharing them with others.

*NOTE:* There is no specific requirement for primary cultures of avian embryonic tissues (they are grown essentially as mammalian cells in standard culture medium, at 37°C and under a humidified CO<sub>2</sub> atmosphere), but use of proper aseptic technique is recommended as well as appropriate biosafety practices to protect the experimenter and avoid contamination of the culture. In addition, all solutions and equipment, such

---

Duband et al.

3 of 25

as microsurgery tools and dishware, coming into contact with tissues and cells must be sterile. However, because most neural crest cultures are usually not maintained for long, it is not necessary to work in a dedicated culture room and under a sterile tissue culture hood. A clean bench in a quiet lab room with minimal passage generally suffices.

**BASIC  
PROTOCOL**

**PRIMARY CULTURES OF AVIAN TRUNK NEURAL CREST CELLS**

**Materials**

- Fertilized quail (*Coturnix coturnix japonica*) or hen (*Gallus Gallus*, White or Brown Leghorn strains) eggs (e.g., from local commercial source)
- PBS without  $\text{Ca}^{2+}$  and  $\text{Mg}^{2+}$  (prepare from sterile 10× stock solutions available from numerous suppliers, e.g., MilliporeSigma, cat. no. P5493; Dulbecco's PBS, i.e., phosphate buffer supplemented with glucose, sodium pyruvate, and antibiotics, is an option but is not required)
- Fibronectin from bovine plasma, 1 mg/ml (e.g., MilliporeSigma, cat. no. F1141; fibronectin is inactivated when frozen; store at 4°C as recommended by the manufacturer, for up to 12 months)
- Dispase II in Hanks' balanced salt solution, 5 U/ml (e.g., Stemcell Technologies, cat. no. 07913; aliquot and store at −20°C)
- DMEM with low glucose (1 g/L) and sodium pyruvate (1 mM), supplemented with glutamine (2 mM) and penicillin and streptomycin (each at 100 units/ml)
- FBS (heat inactivated at 56°C for 30 min)
  
- 37°C incubator (for eggs)
- Stereomicroscope, zoom range: ~0.8-5× (corresponding to an 8-50 fold magnification) and semi-rigid swan-neck fiber optic illumination (for dissection)
- Tissue culture humidified, 5%  $\text{CO}_2$  incubator
- Inverted microscope with 10× and 20× phase contrast objectives, equipped with camera connected to a computer for analyses (heated chamber adapted to the microscope will help maintain cultures under optimal conditions; required for videomicroscopy)
- Specific glassware (Fig. 1A): Widened bowl, ~15-cm diameter; glass Petri dish, ~7-cm diameter containing a layer of silicone rubber (cast from commercially available liquid silicone colored in black and solidified with a catalyst)
- Microsurgery tools (Fig. 1B; e.g., Fine Science Tools or Euronexia):
  - Curved scissors with sharp ends
  - Moria perforated spoon
  - Pair of straight forceps with thin tips (0.1 mm, e.g., Drumont no. 4)
  - Straight scissors with sharp ends
  - Pair of pin holders with screw
  - Rigid stainless steel insect pins (rod diameter: 0.25-0.3 mm)
  - Stainless steel minuten pins (rod diameter: 0.1-0.2 mm)
  - Scalpel with disposable no. 15 blade
  - Arkansas stone (for tool sharpening)
- Plastic culture dishes and plates (various sizes)
- Culture wells, e.g.:
  - Cloning cylinders, 6- to 10-mm diameter in borosilicate (Bellco, cat. no. 2090-00808) or stiff polystyrene (easily manipulated, sterilized, and reused; Belart, cat. no. H37847-0000)
  - Silicone culture-inserts with 2, 3, or 4 wells (ibidi, cat. no. 80209, 80309, 80409; appropriate alternative because they are specifically designed for migration assays)
  - Custom-made culture wells from Falcon 3912 MicroTest III flexible 96-well assay plate (Becton Dickinson; inexpensive and easy to use)

Duband et al.

4 of 25

Current Protocols in Cell Biology

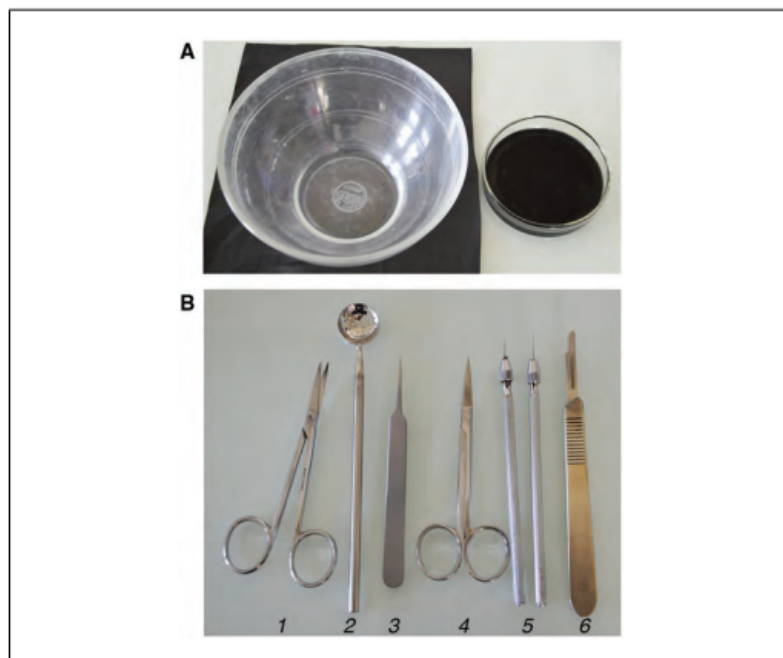


**Figure 1** Specific glassware and microsurgery tools used for neural crest cell culture. **(A)** A widened bowl to collect yolks from the eggs (left) and a glass Petri dish containing silicone rubber to collect and dissect embryos. **(B)** Microsurgery tools used throughout the protocol: 1. curved scissors with sharp ends; 2. Moria perforated spoon; 3. straight forceps with very thin tips (Dumont no. 4); 4. straight scissors with sharp ends; 5. a pair of minutien pins mounted on pin holders with screw for microdissections; 6. scalpel with disposable no. 15 blade.

#### **Collect embryos from eggs**

1. Preparing eggs for incubation: Store freshly laid eggs, purchased from local farms, in a fresh room at 15°-20°C up to 1 week upon receipt. Place eggs in the incubator with their blunt end at the top and set incubator timer for a 54-58 hr incubation to obtain embryos at the ideal stage for trunk neural crest cell cultures.

*Avoid storing eggs at 4°C or for >1 week as this will result in a significant proportion of embryos presenting severe developmental abnormalities. Optimal temperature of incubation is 37°-38°C; not higher as this does not speed up the embryo development, rather it causes frequent neural tube defects and may ruin your experiment. Caution, when using quail eggs, handle them with care as their shells are generally more prone to crushing than hens' eggs.*

2. At the completion of the incubation period, take eggs out of the incubator.

*Incubated eggs can be stored at room temperature for up to 2-3 hr before manipulation with no adverse effects and minimal developmental progression.*

Before starting, maintain PBS and DMEM solutions at room temperature to minimize thermal shock.

3. Collect yolk from egg (Fig. 2A): Hold eggs with their blunt end down and remove the sharp end of the shell first by making a small slit in the shell, then with a circular movement all around it, using curved dissecting scissors. Eliminate excess of albumin and gently transfer yolk into a bowl half-filled with PBS. Collect ~10-15 yolks at a time in the bowl.

Duband et al.

5 of 25

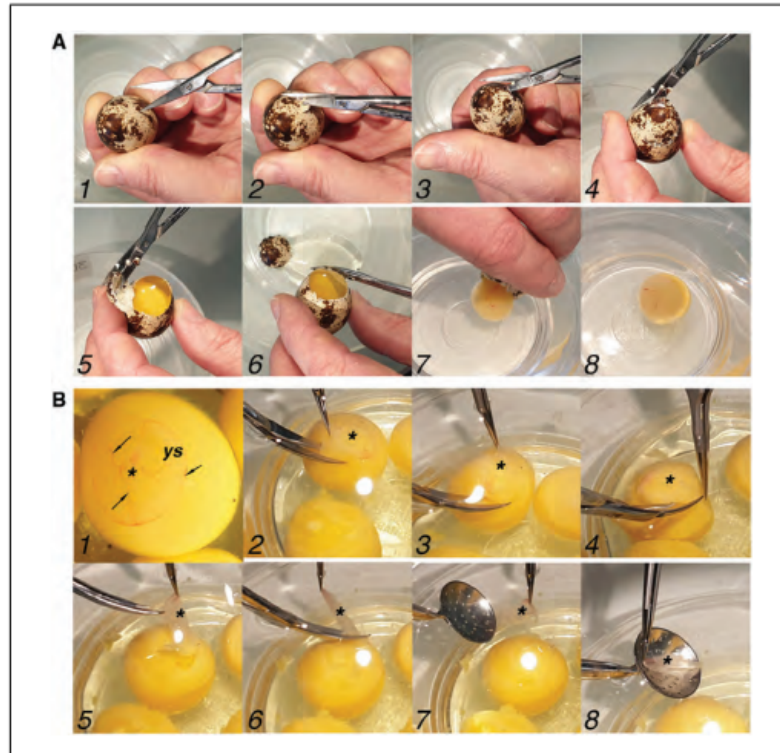


**Figure 2** Collecting embryo from the egg. **(A)** Collecting the yolk out of the shell. Panels 1-8 depict the method for opening the egg with curved-end scissors and transferring the yolk into a bowl half-filled with PBS. **(B)** Separating embryo from the yolk. Panel 1 shows a detailed view of an intact embryo surrounded by its yolk sac (ys) prior to extirpation from the yolk. Arrows point to the blood vessel network and blood islands in the yolk sac. Panels 2-8 depict the different steps of the method for trimming the embryo and its surrounding tissues with forceps and curved-end scissors and grabbing with a perforated spoon. The position of the embryo is indicated by the asterisk.

*The location of the opening in the egg optimally should be in its upper third, such that the yolk is not pierced while cutting the shell and such that it can pass freely through the opening while being transferred into the bowl. It is recommended that a wide bowl with no steep edges be used for easy manipulation during the following step. Once it is deposited in PBS, the yolk will automatically rotate such that the embryo is presented always on the top of the yolk.*

4. Collect embryo from the yolk (Fig. 2B): The embryo can now be easily visualized with its surrounding vitelline membrane (or yolk sac). Normally at this developmental stage, the part of the vitelline membrane adjacent to the embryo proper is being vascularized with formation of many blood islands, delimiting a well-defined area. Cut vitelline membrane around the vascularized area with curved scissors while holding it with forceps. Then, gently shake embryo in PBS to remove excess yolk and the covering, opalescent chorionic membrane, and transfer it to a PBS-containing dish using a perforated spoon.

*The use of a perforated spoon is dispensable and may be replaced by forceps, as at this developmental stage the vitelline membrane is resistant enough to be manipulated with them without damaging the embryo.*

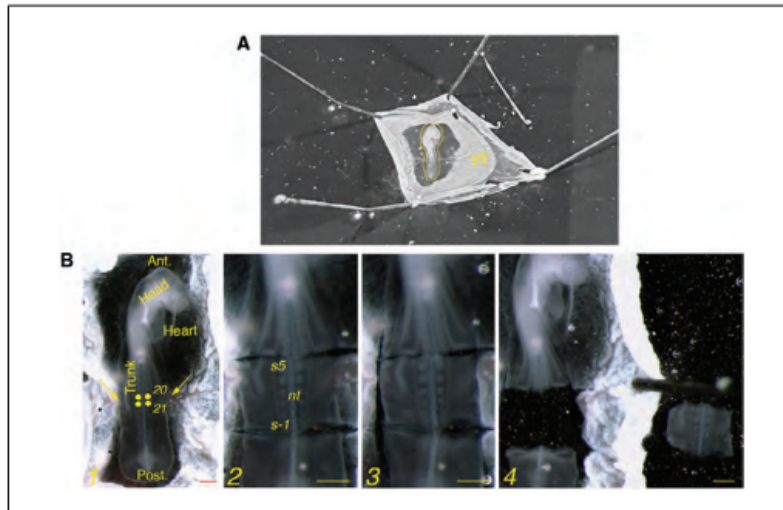


**Figure 3** Isolating trunk segments. **(A)** Overview of an embryo at stage 14-15 with 25 somite pairs which has been removed from the yolk and pinned down onto silicone in a glass dish filled with PBS. The vitelline membrane is stretched out with 4 insect pins placed away from the embryo out of the vascularized area of the yolk sac (ys). The embryo proper is surrounded by a yellow line. **(B)** Panel 1 is a detailed view of the embryo shown in A before dissecting the trunk segment out. The embryo is oriented with its anterior (ant.) side at the top and the posterior (post.) one at the bottom. Note that while the head of the embryo is turned such that it presents its right side to the observer (the heart can be seen on the right), the trunk remains straight and is oriented with its dorsal side up. Arrows point to the large extraembryonic blood vessels entering the embryo at the level of the twentieth and twenty-first somites indicated by yellow dots. Panels 2-4 show the different steps of trimming the trunk segment situated between the fifth somite pair above the last formed one and the first nascent pair in the anterior part of the unsegmented mesoderm, noted s5 and s-1 respectively. The neural tube (nt) is the solid cord situated in the midline and flanked by the two rows of ball-shaped somites. Bars in B1-B4 = 500  $\mu$ m.

#### Isolate trunk segments

5. Display embryos for trunk segment isolation (Fig. 3A): Once all embryos are collected, transfer them into a silicone-containing glass Petri dish filled with PBS. With forceps, spread out the vitelline membrane in the dish with the embryo dorsal side up, pin it down to the silicone layer with four insect pins, and examine embryo carefully under the stereomicroscope at zoom range 2 $\times$  to detect any abnormalities and calculate its developmental stage.

*There are several ways to locate the dorsal side of the trunk region in an embryo. The simplest one is to orientate the embryo such that its anterior half presents its right side to the observer as shown in Figure 3A. Indeed, during the third day of development, most embryos (but not all of them) have their head turned and present their right side up. Meanwhile, the trunk region has not yet rotated and still lies with its ventral side oriented to the yolk and its dorsal side up. An additional indication particularly useful for the outliers is that the embryo's head protrudes above the vitelline membrane toward the dorsal side. Lastly, another way though less easy, is to look at the entry points of the large extraembryonic blood vessels into the embryo. The dorsal side is where they are the least discernable.*

*Staging can be done according to the Hamburger and Hamilton (HH) chart (Hamburger & Hamilton, 1951) or, for greater precision, by counting the total number of somite pairs, knowing that in 36- to 72-hr embryos, a pair of somites is formed approximately every 60-90 min. Note that in embryos older than 22 somites, it is not necessary to count all somites but simply to count those situated caudally to the twentieth to twenty-first somite pairs.*

Duband et al.

7 of 25

Both somites are situated on either side of the entry point of the large extraembryonic blood vessels into the embryo. Embryos should be in the range of 18-28 somite pairs or at HH13-15.

Finally, with practice, pinning down the embryos can be dispensable, allowing you to reduce manipulations and save time.

6. Dissect trunk segments (Fig. 3B): With a scalpel, trim a rectangular section of tissues surrounding the neural tube and the flanking somites and covering the last five to six somite pairs as well as the nascent pair in the anterior most part of the unsegmented paraxial mesoderm. Transfer trunk segments into DMEM in a 35-mm dish using forceps. Collect all trunk portions before the following step.

*Take great care at the axial level where the explant is taken out. Trimming should be done away from the somites in the lateral mesoderm to leave a trunk segment large enough for easy handling with forceps for transfer.*

7. Prepare culture dishes: On the back of the 35- or 60-mm dish or 4-well plates, draw circles of ~1-cm diameter with a marker pen to delineate the areas of the dish to be coated with extracellular matrix proteins; fibronectin is routinely used as a coating protein. Deposit inside of each circle a 50-100  $\mu$ l drop of fibronectin at concentrations ranging from 1-100  $\mu$ g/ml (optimal coating concentration in plastic dishes: 10  $\mu$ g/ml). Coating of dishes should last at least 45 min at 37°C.

*Although neural crest cell cultures can in theory be performed on uncoated cell culture-treated dishes, it is important to coat the dish with extracellular matrix proteins to speed up neural tube anchorage and neural crest cell outgrowth.*

*In order to favor a rapid conditioning of their culture medium optimal for their development and survival, neural tubes and neural crest cells explanted in vitro should be maintained in limited amounts of medium (ideally 10-50  $\mu$ l per neural tube explant). Therefore, we recommend that restricted spots are delineated within the dish for receiving the culture wells into which the neural tube explants will be deposited.*

#### **Dissect neural tubes**

8. Prepare dispase solution: Deposit a 500- $\mu$ l drop of a freshly prepared 2.5 U/ml dispase solution in DMEM in the lid of a 35-mm dish placed under the dissecting microscope.

*Dispase II is a bacterial neutral protease that offers a decisive advantage over trypsin in that it is stable and active at room temperature and does not require serum to be inactivated.*

9. Aspirate trunk explants in a 1,000- $\mu$ l pipet tip that has been cut at its end with straight scissors, enough (~1-2 mm from the end) to allow easy passage of the explants, and transfer them into the dispase solution.

*Because the explants tend to stick to the plastic of the tip during aspiration and if so cannot be easily retrieved, we strongly recommend coating the inside of the tip with 0.5% FBS in DMEM by repeated pipetting. Take care not to dilute the dispase solution too much by adding excessive amounts of DMEM (<100  $\mu$ l) together with the explants.*

10. Incubate trunk explants in dispase ~5 min at room temperature. Remove the bulk of dispase solution with a 200- $\mu$ l pipet tip (but do not aspirate all of it), replace with fresh DMEM, and regularly monitor the explants' aspects. When the neural tube becomes slightly wavy (generally within 5 min after rinsing), start the dissection.

*Important notice: The duration of explant incubation in dispase should not exceed 10 min as prolonged exposure ultimately affects the viability of tissues. However, we recommend not aspirating all dispase solution; leave ~50-100  $\mu$ l (out of the initial 500  $\mu$ l) before rinsing with DMEM, to maintain minimal activity, thereby facilitating the manual dissection of the neural tube.*

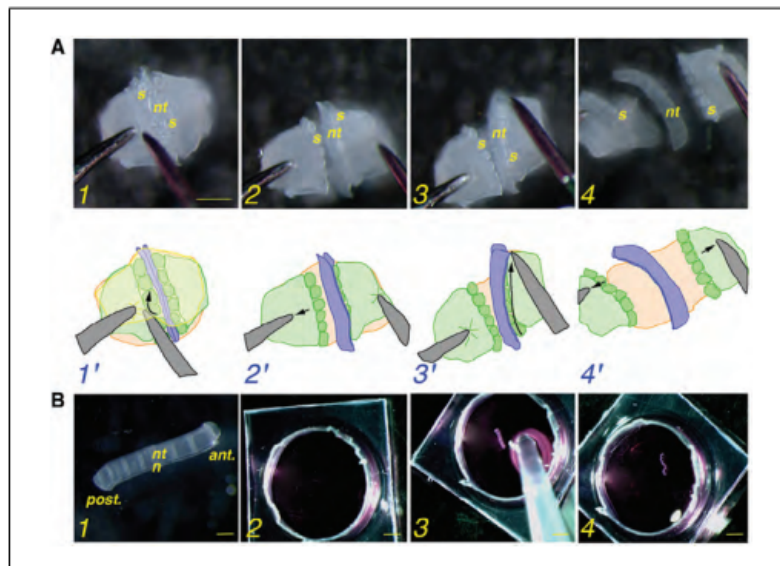


**Figure 4** Dissecting and transferring the neural tubes to culture dish. **(A)** Panels 1-4 show the main steps of neural tube dissection with dissection pins: Removal of the overlying ectoderm, separation of the left row of somites (s) from the neural tube (nt), separation of the right row, and complete isolation of the neural tube. Panels 1'-4' are schematic representations of the trunk segment shown in panels 1-4 to illustrate the different tissues for an easier orientation: Ectoderm in yellow, neural tube in blue, somites and lateral mesoderm in dark and light green, and endoderm in red. The arrows indicate the movements of the dissection pins. Bar = 500  $\mu$ m. **(B)** Panel 1 shows the dissected neural tube (nt) free of neighboring tissues except the notochord (n) attached to its ventral side. Bar = 100  $\mu$ m. Panel 2 shows a culture well made from flexible 96-well Falcon plates deposited in a 35-mm dish and filled with DMEM before transferring the dissected neural tube. Panels 3-4 show the neural tube transfer into the culture well with a 200- $\mu$ l pipet tip and its positioning and orientation into the well. Bars in 2-4 = 1 mm.

11. Dissect neural tubes (Fig. 4A): Under the dissecting microscope at 3 $\times$  zoom range, first place trunk segments dorsal side up. Then, while holding explant in place with one of the minutien pins mounted on a pin holder with a screw (thereafter referred to as dissection pins), introduce the other pin under the ectoderm and along the neural tube and gently peel ectoderm off. Then, separate neural tube from the somites on either side and discard ectoderm, somites, and endoderm. Finally, if required, once all neural tubes have been dissected out, detach notochord from each of them, starting from one extremity.

*At this step, identifying the dorsal side of the explant is less easy than before on the whole embryo. By manipulating the explant, it is possible to define the dorsal side as the one where the neural tube is protruding externally and the ventral side as the one where the notochord is aligned with the neural tube.*

*In most experiments, removing the notochord from the explants before transferring to the culture dish is optional. Indeed, as explained below, the notochord remains attached to the neural tube during most of the culture and does not hamper neural crest cell outgrowth. Moreover, it helps orient the neural tube during deposition into the culture wells.*

*Important recommendations concerning the dissection procedure: First, the principle of dissection relies primarily on the enzymatic action of dispase and secondarily on the manual separation of the tissues. If tissues cannot be dissociated apart easily with the dissecting pins, it means that the enzymatic digestion is not complete and should*

Duband et al.

9 of 25

*be allowed to last longer. It is then better to leave the explants still and wait for a moment (~5 min) prior to resuming dissection, rather than risking severe neural tube damage. Second, do not hesitate to customize the dissecting tools to your hands, e.g., a rigid, straight needle for holding the explant and a more flexible, bent-end needle for trimming the tissues apart. Third, if you don't feel comfortable with the procedure shown on Figure 4A, do not hesitate to make your own, provided you succeed in isolating the neural tube with no damage and free of adjacent tissues. Important: Avoid opening the neural tube on its dorsal side as a book, as it will result in a poor neural crest cell outgrowth.*

12. Aspirate neural tubes with a 200- $\mu$ l pipet tip previously coated with 0.5% FBS and transfer them into 0.5% FBS in DMEM in a 35-mm dish for a 15-30 min recovery period at room temperature.

*Once dissected, avoid leaving the isolated neural tubes in the dispase solution for long. We suggest dissecting out about five to ten neural tubes at once (depending on your experience, speed, and skill), collect them, and transfer immediately into the 0.5% FBS in DMEM-containing dish.*

#### **Transfer neural tube explants to culture dish**

13. During the recovery period, rinse each fibronectin-coated spot in the culture dishes with DMEM and, if necessary, prepare custom-made culture wells into which neural tube explants will be maintained in culture.

*Wells made from flexible assay plates with 96 flat-bottom wells (Falcon 3912 MicroTest III flexible assay plate from Becton Dickinson) are easy to make, convenient, and cheap. They should be discarded at the end of the experiment. Cut each well out of the plate with straight sharp-end scissors, remove its bottom but keep its edges intact so it can stably hold onto the dish (see Fig. 4B). Wash wells briefly in PBS followed by rinsing with DMEM before using.*

14. After removing DMEM, place wells over each fibronectin-coated spot in the culture dishes and fill them with 100  $\mu$ l culture medium. For basic experiments, use DMEM supplemented with 2 mM glutamine, 1% penicillin-streptomycin, and 1% FBS. Transfer neural tubes with a 200- $\mu$ l pipet tip into each well, up to five neural tubes/well, taking care not to dilute culture medium too much in the well. Under the dissecting microscope, arrange neural tubes within the wells with the mounted dissection pins in order to separate them and avoid overlap of neural crest cell outgrowths (Fig. 4B). Place dish in a humidified 37°C, 5% CO<sub>2</sub> incubator.

*In addition to maintaining neural tubes in a low amount of medium, culture wells have the advantage of minimizing turbulence that might displace the explants during transfer to the incubator.*

*Whenever possible, orientate neural tubes with their ventral (i.e., lining the notochord) side up and their dorsal side in contact with the dish. This position is highly favorable for almost immediate dispersion of neural crest cells (see Understanding Results).*

*High serum concentrations are not required for obtaining maximal neural crest migration and survival; concentrations of 1%-5% generally suffice. If serum must be omitted from the culture medium, it is possible to culture neural crest cells in medium consisting of DMEM supplemented with 0.1% ovalbumin (w/v), 10  $\mu$ g/ml transferrin, and 10  $\mu$ g/ml insulin, instead of FBS.*

15. The following day, remove culture wells gently to avoid detachment of the neural tubes and fill the dish with fresh prewarmed medium before examination under an inverted microscope. If necessary, remove neural tube from the culture dish either by gentle lifting its end using mounted dissection pins (taking care to not make scratches in the plastic) or by flushing medium with pipet tips.

*Neural crest cells can be maintained in culture for several days without change of medium.*

## ADAPTATIONS FOR IMMUNOFLUORESCENCE LABELING AND VIDEOMICROSCOPY

SUPPORT  
PROTOCOL

The Basic Protocol is designed to generate a typical outgrowth of neural crest cells suitable for a large variety of studies: Immunolabeling and imaging analyses, in situ hybridization (ISH), videomicroscopy, biochemical approaches, and functional assays. However, adaptations to this protocol are required for the type of culture dish to be utilized in the cases of immunofluorescence and videomicroscopy investigations.

### *Immunofluorescence labeling of cells*

Because of the poor optic qualities of most plastic dishes, neural crest cell cultures should be performed on glass coverslips for immunofluorescence analyses. Utilization of 18- × 18-mm square coverslips or round coverslips of 10- or 12-mm diameter is particularly suitable because their area and size fit well in multiwell plates and can accommodate all types of culture wells.

Clean coverslips with ethanol to remove any grease residues, rinse in PBS, and coat with fibronectin at 20 µg/ml instead of 10 µg/ml, because the yield of fibronectin adsorption on glass is lower than on plastic. Place glass coverslips into 35- or 60-mm dishes or in multiwell plates and proceed to the culture as described in the Basic Protocol. Use preferably multiwell plates with one coverslip per well to exclude any possible overlapping between coverslips. In addition, these plates can be used for blocking and rinsing steps of the immunolabeling procedure. An alternative is to use 4- or 8-well plates with glass bottoms specifically designed for immunofluorescence studies (µ-slide chambers from ibidi, cat. no. 80427 and 80827, or Lab-Tek chambers from Nunc, cat. no. 154526 and 154534).

### *Videomicroscopy*

Due to their size and shape, culture wells do not permit optimal phase-contrast microscopic observations of neural crest cells and therefore cannot be used for videomicroscopy. Several options are possible anyway.

If analyses have to be performed on the initial steps of neural crest cell migration (i.e., during the first 10-12 hr), we strongly recommend Terasaki 60-well plates, available from many different commercial sources. Their flat-bottom wells are adapted to inverted microscopy and they are suited for culturing individual neural tube explants in a limited amount of medium (15 µl). Coat each well with 15 µl fibronectin at 10 µg/ml in PBS and after rinsing with DMEM, add 20 µl culture medium to make a dome at the surface of the well. Avoid medium leaking out of the wells, otherwise the subsequent steps are compromised. Deposit gently one neural tube per well, orientate it appropriately in the well, add a glass coverslip very gently over the culture medium, being very careful to avoid trapping air bubbles between the glass and the medium in the well, and cover the plate with its lid. The glass coverslip ensures excellent phase contrast optics and prevents rapid evaporation of the medium. Under these conditions, the neural tube culture can be visualized by videomicroscopy and maintained for a prolonged time period (up to 12 hr) at 37°C in a humidified atmosphere. However, Terasaki plates cannot be used for long-term cultures of neural crest cells for two main reasons. First, because the medium is limited in amount in each well, it may become rapidly exhausted by highly proliferating cells. Second, actively migrating neural crest cells rapidly cover the entire bottom of the well and reach its edges.

If long-term migration (up to 24 hr) has to be investigated, several companies have developed many devices and designed a large variety of dishes optimized for videomicroscopy analyses. We recommend using the µ-Slide Angiogenesis from ibidi (cat. no. 81506), a plate with fifteen wells particularly adapted for neural tube explants. Each well contains up to 50 µl culture medium and is designed to eliminate meniscus formation, thereby

Duband et al.

11 of 25

favoring phase contrast visualization.  $\mu$ -Slide 8 Well also from ibidi (cat. no. 80826) is a good alternative, offering the possibility to track several explants in each well. Finally, it is possible to use the 4- or 8-well plates with glass bottoms designed for immunofluorescence studies mentioned above and also for videomicroscopic analyses. Interestingly, these slides are fitted for live imaging using high resolution objectives and may be combined with immunofluorescence microscopy.

An important issue when doing videomicroscopy is to provide optimal conditions for maintaining cell survival throughout the course of the recording. Survival in culture is affected by inadequate temperatures (both too high and too low), pH (acidic or alkaline), or osmolarity due to the absence of a thermostat, inappropriate CO<sub>2</sub> concentrations, or medium evaporation. Having access to a high-resolution phase-contrast microscope with a motorized stage and equipped with a heated chamber connected to temperature and gas controlling system is therefore required. Otherwise, a few simple adjustments may help to compensate for the lack of this device but only for relatively short-term recordings, for example, adding HEPES at 25 mM may temporarily maintain the pH at acceptable levels and adding mineral oil over the culture medium may prevent too rapid evaporation.

## COMMENTARY

### Background Information

The protocol for culturing avian trunk neural crest cells presented here derives from the method initially devised by Cohen and Konigsberg and later by Sieber-Blum and Cohen (Cohen & Konigsberg, 1975; Sieber-Blum & Cohen, 1980) to generate neural crest cell clones and study their differentiation potential. Since then, this technique has been applied to trunk neural crest cells from other species, notably mouse, rat, and human (Etchevers, 2011; Ito & Sieber-Blum, 1993; Stemple & Anderson, 1992; Thomas et al., 2008). In parallel, other methods based sometimes on different approaches have been developed to produce *in vitro* cultures of neural crest cells from other axial levels. Thus, cranial neural crest cells can be retrieved from embryos at stage HH9 (six to eight somites) using either whole neural tubes dissected at midbrain and anterior hindbrain levels or after extirpation of the neural folds only (Calloni, Glavieux-Pardanaud, Le Douarin, & Dupin, 2007). Another strategy is to dissect out cranial neural crest cells during the course of their lateral migration under the ectoderm in embryos at stage 10 to 11 (ten to twelve somites; Ziller, Dupin, Brazeau, Paulin, & Le Douarin, 1983). Using the same principle of extirpation, cranial neural crest cells from the *Xenopus* embryo have also been the matter of intense *in vitro* studies (Cousin & Alfandari, 2018; Scarpa et al., 2015).

These techniques all produce neural crest cells with migration and differentiation capacities but it should be stressed that they are generally more challenging and less accessible to beginners due to some inherent technical con-

straints and hurdles. For example, mouse neural tubes can be dissected only with difficulty because of the reduced size of the embryo as well as its curved, compact shape. In addition, collecting many neural tubes at the same developmental stage in mouse is costly and necessitates many pregnant mice because embryos in the same litter often grow at different speeds. Neural crest cells at cranial levels are also difficult to collect even in birds for similar reasons: Embryos at stage 9 or 11 are comparatively much smaller and more fragile than at stages 13 to 15, and the neural tube or the neural folds cannot be easily dissected out free of the ectoderm because at these stages, both tissues are not yet segregated. In addition, contrary to trunk neural tubes, which can be obtained from embryos at several embryonic stages, the time window to collect cranial neural tubes is very narrow. Finally, unlike avian neural crest cells which can be grown in minimal medium with as little as 1% serum or even in serum-free medium, culture medium for mammalian neural crest cells requires several additives, such as fibroblast growth factor or leukemia inhibitory factor, for optimal cell survival (Etchevers, 2011). For all these reasons, we recommend starting with avian trunk neural crest cells and, once all the technical difficulties have been solved, to switch to another neural crest cell population or to another animal model when relevant.

Neural crest cells derived from other animal species or from other axial levels often differ from avian trunk neural crest cells by several features. In mouse for example, neural crest cells are produced in lesser numbers

and more slowly, and their migration behavior can be examined only after 24 hr in culture (Gonzalez Malagon et al., 2019). *Xenopus* cranial neural crest cells do not migrate individually and randomly, instead they form highly cohesive structures migrating collectively by a mechanism driven by contact-inhibition of movement as well as co-attraction (Carmona-Fontaine et al., 2008; Carmona-Fontaine et al., 2011). Finally, at variance to most other species, human neural crest cells show the unique ability to persist and self-renew in culture as progenitors for prolonged periods and can be replated many times as established cell lines (Thomas et al., 2008).

With the spectacular development of the stem cell field, the last decade witnessed the establishment of several procedures to produce neural crest stem cells from embryonic, fetal, and adult tissues. Thus, the use of embryonic stem cells, induced pluripotent stem cells, neuroepithelial “crestospheres” that self-renew and retain multipotency for weeks, or reprogrammed cells from adult teeth, skin, or nerves proved to be extremely potent, in particular for generating large amounts of cells usable for comprehensive large scale analyses, such as epigenomic and transcriptome profiling (Bajpai et al., 2017; Kerosuo, Nie, Bajpai, & Bronner, 2015; Liu & Cheung, 2016; Mohlin et al., 2019; Prescott et al., 2015). Mastering primary cultures of neural crest cells certainly provides the fundamentals and the knowledge for developing these sophisticated approaches.

### Critical Parameters and Troubleshooting

If quail eggs are not available, hens’ (*Gallus gallus*, White or Brown Leghorn strains) eggs can be used instead although the quality of the cultures (number and viability of neural crest cells) obtained from them is generally lower than with quail. Also keep in mind that melanocytes issued from White Leghorn chick embryo neural crest cells are not pigmented.

No need to use specialized egg incubators for poultry breeding with oscillating plates and controlled humidified atmosphere as eggs are incubated for <3 days. A basic incubator, e.g., for microbiology, generally suffices. However, the use of incubators equipped with timers is recommended to set the timing of incubation at will.

Use only fiber optic epi-illumination and stereomicroscopes with thin stands, not diascopic stands as they are too high and not comfortable for prolonged dissections. Also be careful that the working distance between the

objective and the stand is not too short for good access to the samples and easy manipulation.

The elastic properties of silicone rubber make it extremely convenient to pin embryos down for trimming of tissue explants and its opacity allows visualization of the detailed structure of the animal. In addition, it can be sterilized and reused many times.

Tungsten minuten pins are an interesting option because of their hardness and stiffness but they are not easy to sharpen.

Neural crest cells can be cultured equally well on any kind of support (cell culture-treated or non-treated plastic or glass), provided it is coated with appropriate extracellular matrix proteins, routinely fibronectin. The choice of the dishes depends primarily on the final goal of the culture (see Support Protocol). For basic cultures, use preferably 35- or 60-mm dishes or 4- to 24-well plates. We do not recommend 96-well culture dishes because the wells are too deep and their edges are too steep to allow easy handling of the neural tube explant inside of the well.

In order to favor a rapid conditioning of their culture medium optimal for their development and survival, neural tubes and neural crest cells explanted in vitro should be maintained in limited amounts of medium (ideally 10-50  $\mu$ l per neural tube explant). It is therefore preferable to place them in culture wells at least for the first day in culture, even in multiwell plates.

### Understanding Results

#### *Phenotypic characterization of neural crest cells during the first 24 hr in culture*

##### *Collective behavior and morphological features of neural crest cells in culture*

At variance to many other embryonic tissues which spread out gradually on the dish to form large uniform monolayers, neural tubes evolve in culture in a strikingly different way, characterized by very rapid kinetics of cell dispersion, due primarily to the very active migratory potential of neural crest cells combined with a high proliferation rate. Several scenarios must, however, be considered depending on the initial conformation of the neural tube onto the dish.

When the neural tube lies dorsally on the substratum (Fig. 5A), a row of protruding neural crest cells appears on either side of the explant, first in its anterior most portion, almost immediately after its initial anchorage to the dish (i.e., within an hour or so after

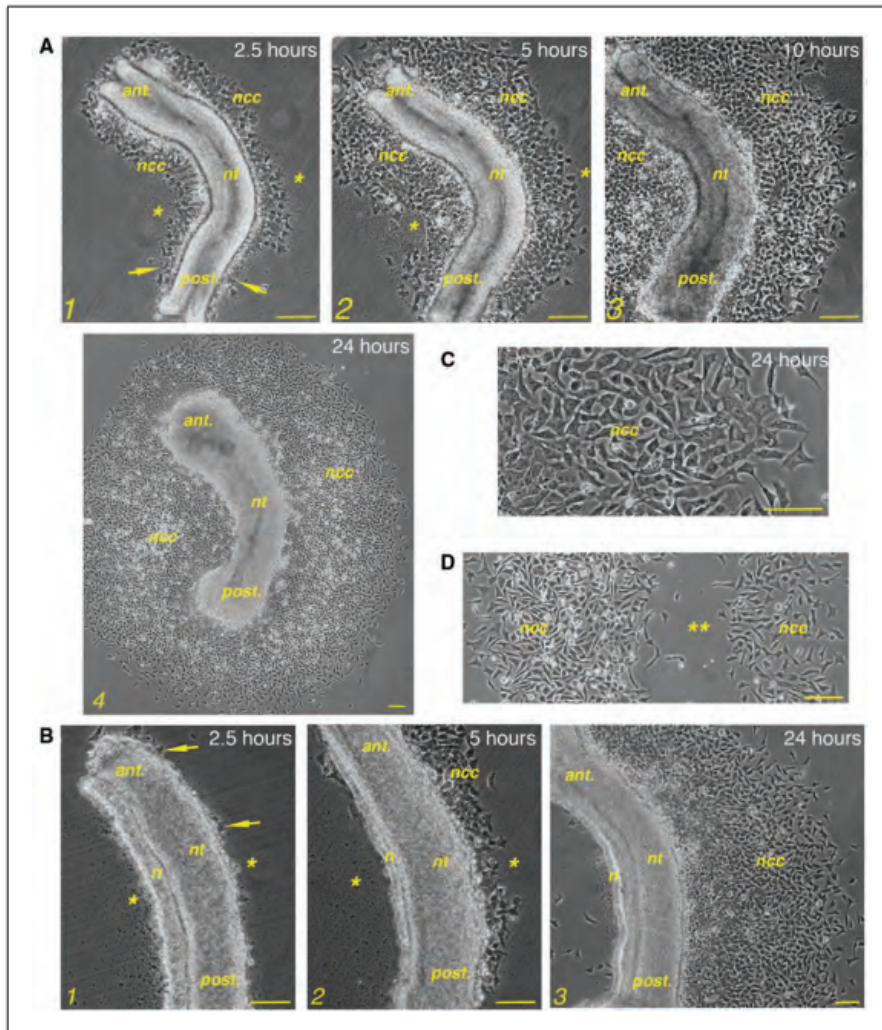


**Figure 5** Morphological and population features of neural crest cells in 24 hr-cultures. Comprehensive phase contrast views over time of a neural tube initially deposited on the dish either dorsally (**A**) or laterally (**B**) and cultured in DMEM medium supplemented with 1% serum. The midline of the neural tube in **A** appears as a darker zone along its entire length. Delaminating neural crest cells initiating spreading onto the substratum are indicated by arrows. Note the presence of numerous vesicles released by the neural tube on the dish during the early steps of the culture (asterisks, \*). These vesicles are in no way contaminants or cell debris due to massive cell death. They are taken up by migrating neural crest cells and disappear with time. (**C**) Detailed phase contrast views of a neural tube explant showing the morphology of migrating neural crest cells. Individual neural crest cell contours can be easily distinguished even in the middle of the outgrowth where cell density is high. (**D**) Phase contrast view of a neural crest outgrowth in which the neural tube explant has been removed manually after 24 hr in culture, leaving its print (double asterisk, \*\*) surrounded by intact neural crest cells. Bars = 100 μm. ncc, neural crest cell; nt, neural tube; ant., anterior; post., posterior; n, notochord.

the beginning of the culture). After 2 to 3 hr, both sides of the neural tube are entirely lined throughout the rostrocaudal axis by several rows of spread and cohesive neural crest cells (Fig. 5A1). During the subsequent 10 to 12 hr, the neural crest population expands rapidly and steadily away from the neural tube, forming after 24 hr a large halo, 1 to 2 mm wide, composed of ~1,000 to 2,000 cells distributed evenly around the neural tube (Fig. 5A 2-A4). If the neural tube interacts initially with the substratum through one of its lateral sides (Fig. 5B), neural crest cells are seen dispersing onto the dish only after a 2- to 4-hr delay. The first delaminating cells are arranged as clumps of round cells attached to the dorsal border of the neural tube and it is only progressively that they spread out on the substratum and form several rows of cells migrating away (Fig. 5B1-B2). In the opposite ventral side of the neural tube, in contrast, virtually no neural crest cells can be detected along the notochord. After 24 hr, the entire neural crest cell population is contiguous to the dorsal side of the neural tube where they form a large outgrowth of spread out cells essentially as in the previous configuration, whereas the other side is almost entirely free of any dispersing cells (Fig. 5B3). It should be noted, however, that in most situations, the neural tube explant is neither strictly oriented dorsoventrally on the dish nor lying precisely on its lateral side. As a result, neural crest cells emerge on either sides of the neural tube but in different amounts and at slightly different times, forming after 24 hr a cell population asymmetrically distributed around the neural tube.

At the cellular level, neural crest cells display morphological traits strikingly different from those of other embryonic cells cultured on two-dimensional substrates. Although they exhibit a great diversity of cell shapes related to their dynamics of locomotion, they can be easily discriminated from other embryonic cells, e.g., from contaminating mesodermal cells that remained attached to the neural tube after dissection. On fibronectin substrates, they rarely show a bipolar aspect characteristic of sparse motile fibroblasts, with a broad lamellipodium at the leading edge and a thin trailing edge. Instead, they present alternatively round, elongated, or stellate shapes with restricted intercellular contacts, despite a high cell density (Fig. 5C).

Quite remarkably, the neural tube itself does not spread onto the substratum during the first 24 hr of culture. Instead, it retains its compact hollow tube shape whose lumen is visi-

ble by transparency along the explant length (a striking example is shown in Fig. 6A1). In addition, the explant presents sharp limits and is surrounded with no transition by the neural crest outgrowth. Only in its rostral and caudal extremities do some neural tube cells become organized as monolayers of densely packed epitheloid cells, as a result of a wound-healing response provoked during explant trimming. Therefore, neural tube explants comprise two strictly segregated cell populations: Dispersing neural crest cells at the periphery and the intact neural tube in the center. Because of this particularity, the neural tube can be easily removed manually from the dish leaving behind a pure intact population of neural crest cells (Fig. 5D).

#### *Characterizing neural crest cell phenotype in culture using cell lineage markers*

Neural crest cell identity in culture can be ascertained using a number of cell lineage markers which can be conveniently detected by immunofluorescence staining and by *in situ* hybridization (Table 1). To date, Sox-10 constitutes the most universal marker for neural crest cells at the time of their outward migration from the neural tube. Sox-10 is a member of the SoxE subclass of high-mobility-group domain-containing Sox transcription factors, which plays a critical role in the maintenance of the progenitor/stem cell state of neural crest cells (Hong & Saint-Jeannet, 2005; Weider & Wegner, 2017). It exists in all vertebrates examined so far, from lamprey to human, and it is expressed at all axial levels by neural crest cells at the time of their segregation from the neural tube and during their subsequent migration to their target sites (Hockman et al., 2019; Williams et al., 2019). In culture, Sox-10 shows essentially the same expression pattern in neural crest cells as in the embryo. Both its transcripts and proteins are expressed by virtually all neural crest cells immediately at the time when they segregate from the neural tube (Fig. 6A1, B2). Interestingly, Sox-2, another member of the Sox family of transcription factors, also involved in cell stemness but for neural epithelial cells, shows the converse expression pattern to Sox-10. It is expressed in neural tube cells but not in neural crest cells, whether they are delaminating or migrating (Fig. 6A2, B3).

Snail-2 is an interesting marker that complements Sox-10 and Sox-2 for tracing and characterizing neural crest cells in culture. Snail-2 is a member of the Snail family of Zn-finger transcription factors, which operates as

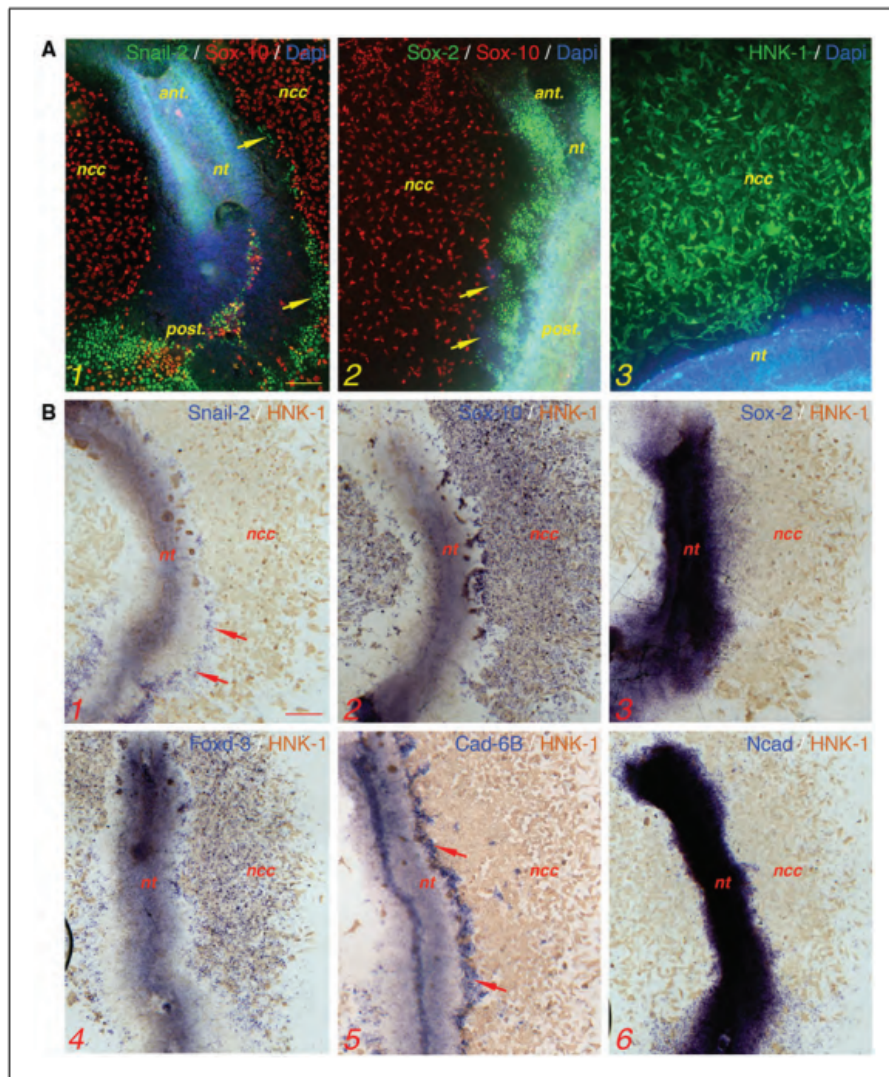


**Figure 6** Phenotypic characterization of neural crest cell cultures after 24 hr with cell lineage markers. **(A)** Immunofluorescence labeling of neural tube explants with antibodies to Sox-10, Snail-2, Sox-2, and HNK-1 revealed by secondary antibodies conjugated to Alexa-488 (green) or Cy-3 (red). Cells' nuclei are visualized with Hoechst staining (blue). **(B)** In situ hybridizations (blue colors) for Snail-2, Sox-10, Sox-2, Foxd-3, cadherin-6B, and N-cadherin, combined with immunoperoxidase stainings for HNK-1 (brown color). After 24 hr in culture, Sox-10 and HNK-1 show widespread expression in almost the entire population of undifferentiated, migrating neural crest cells, while Snail-2 and cadherin-6B identify only a subset of neural crest cells situated along the neural tube explant and corresponding to premigratory and early delaminating neural crest cells (arrows in A1, A2, B1, and B5). Note that Snail-2-positive and cadherin-6B-positive cells are essentially discernable in the posterior half of the neural tube and not in its anterior part, reflecting the temporal progression of neural crest cell emigration along the anteroposterior axis. Finally, Sox-2 and N-cadherin are restricted to neural epithelial cells in the neural tube. Bars = 100  $\mu$ m. ncc, neural crest cell; nt, neural tube; ant., anterior; post., posterior.

**Table 1** Markers for Undifferentiated Neural Crest Cells and Their Derivatives Used in Immunostaining (IS) and In Situ Hybridization (ISH) Techniques

Marker	Cell-type specificity	Detection method	Antibody (antibody source)	Reference for ISH
Sox-10	Undifferentiated, migrating neural crest cells	IS	Mouse mAb clone A2 (Santa Cruz, cat. no. sc-365692) <sup>a</sup>	Cheung et al., 2005
	Schwann cells, melanoblasts	ISH		
Sox-2	Neural epithelial cells	IS	Rabbit polyclonal Ab (Abcam, cat. no. 97959)	Uchikawa, Ishida, Takemoto, Kamachi, & Kondoh, 2003
	Neurons of the peripheral nervous system (PNS)	ISH		
Snail-2	Premigratory and early migrating neural crest cells	IS	Rabbit mAb clone C19G7 (Cell Signaling, cat. no. 9585)	Nieto, Sargent, Wilkinson, & Cooke, 1994
		ISH		
HNK-1	Migrating neural crest cells	IS	Mouse mAb clones 1C10, 3H5, zn-12 (Developmental Studies Hybridoma Bank, RRID: AB_10570406, AB_2314644, AB_531908) <sup>b</sup>	
	Neurons			
Foxd-3	Migrating neural crest cells not melanoblasts	ISH		Thomas & Erickson, 2009
Cadherin-6B	Premigratory neural crest cells	ISH		Dady & Duband, 2017; Nakagawa & Takeichi, 1995
N-cadherin	Neural epithelial cells	IS	Mouse mAb clone GC-4 (MilliporeSigma, cat. no. C3865)	Dady & Duband, 2017
		ISH		
$\alpha$ -SMA	Myofibroblasts	IS	Mouse mAb clone 1A4 (MilliporeSigma, cat. no. A2547)	
$\beta$ III-tubulin	Neurons	IS	Mouse mAb clone TUJ-1 (R&D Systems, cat. no. MAB1195)	
MITF	Melanoblasts	IS	Mouse mAb clone C5 (Abcam, cat. no. ab12039)	
BLBP	Glia	IS	Rabbit polyclonal Ab (MilliporeSigma, cat. no. ABN14)	
GFAP	Glia	IS	Chicken polyclonal Ab (Abcam, cat. no. ab4674)	

<sup>a</sup>Although there are many antibodies to Sox-10 available from many sources, not all of them can be applied for immunolabeling of neural crest cells in avians.

<sup>b</sup>The original HNK-1 hybridoma cell line producing an IgM is available from the ATCC. However, several mouse monoclonal antibodies (mAbs), clones 1C10, 3H5, zn-12, recognizing the HNK-1 epitope can now be purchased from the Developmental Studies Hybridoma Bank (DSHB).

<sup>c</sup>The mAb to cadherin-6B available from DSHB (clone CCD6B) has been successfully used by several groups (Park & Gumbiner, 2012; Taneyhill, Coles, & Bronner-Fraser, 2007). However, for unknown reasons, none of the different batches of this antibody that we tested gave significant reliable staining in our hands.

a master gene for initiation of the epithelium-to-mesenchyme transition process both during embryogenesis and adulthood (Nieto, 2002). During neural crest cell development, Snail-2 drives very precociously the specification of neural crest progenitors and controls their subsequent delamination from the neural tube but it plays no known role during migration (Duband et al., 2015). Unlike Sox-10, which is expressed continuously in migrating neural crest cells at all steps of their dispersion, the Snail-2 expression pattern varies with time in culture. In neural tube explants cultured for <6 hr, when neural crest cell emigration culminates, it is expressed both in premigratory neural crest cells located in the neural tube and, at slightly lower levels, in most migrating cells, together with Sox-10. In contrast, in explants cultured for 24 hr, when neural crest cell delamination is almost terminated, Snail-2 is restricted to a few neural crest cells that are still in the process of delamination in the posterior portion of the neural tube and it is notably absent from the vast majority of migrating neural crest cells (Fig. 6A1, B1). Intriguingly, the Snail-2-positive contingent of premigratory neural crest cells that have not yet undergone complete segregation from the neural tube is devoid of both Sox-10 and Sox-2 (Fig. 6A2). Thus, Snail-2 and Sox-10 define several subpopulations of neural crest cells at different steps of their development during the first day in culture: The Snail-2<sup>+</sup>, Sox-10<sup>-</sup> premigratory cells, the Snail-2<sup>+</sup>, Sox-10<sup>+</sup> delaminating and early migrating cells, and the Snail-2<sup>-</sup>, Sox-10<sup>+</sup> late migrating cells.

The human natural killer-1 (HNK-1) epitope represents another interesting neural crest cell marker that has been widely used in avian species. HNK-1 is historically the first marker for migrating neural crest cells to be identified (Vincent & Thiery, 1984). It consists of a glucidic moiety harbored by various cell surface components, including lipids and cell-adhesion molecules of the Ig superfamily (Tucker, Aoyama, Lipinski, Tursz, & Thiery, 1984). In culture of avian trunk neural tube explants, the HNK-1 epitope is expressed by migrating neural crest cells but not in premigratory cells. It decorates the entire cell surface, making it a very convenient tool for a rapid survey and characterization of cultured neural crest cells (Fig. 6A3). However, caution is needed in interpreting HNK-1 immunostaining for several reasons. First, HNK-1 is barely detectable on neural crest cells during the first 4 to 6 hr after initiation of migration. Sec-

ond, despite a widespread expression in 24-hr cultures, not all neural crest cells (~10% to 20%) express high levels of HNK-1, making it an adequate tool to characterize neural crest cells at the population level but not at the single cell level. Third, although it is conspicuous in migrating neural crest cells, HNK-1 may be detected on the surface of other cells at the same developmental stage (Newgreen, Powell, & Moser, 1990; Vincent & Thiery, 1984). Notably, the extracellular matrix surrounding the notochord, but not notochordal cells themselves, display strong HNK-1 staining both in vivo and in culture. Finally, HNK-1 is not suitable for neural crest cell studies in all vertebrates. Besides chick and quail, it can be used successfully to label migrating neural crest cells in dog, pig, and human but it is not present on migrating neural crest cells in amphibians or mice and is found only transiently on neural crest cells of rats (Tucker, Delarue, Zada, Boucaut, & Thiery, 1988). Therefore, it is important to consider carefully the tissue and species of interest and the timing of development before concluding on the neural crest origin of cells based on the HNK-1 staining. Using additional neural crest markers may prove to be necessary.

Other less commonly used markers may help refine the characterization of neural crest cells in culture. These include Foxd-3, a member of the forkhead family of transcription factors, involved like Sox-10 in the stem cell renewal and pluripotency of neural crest cells (Liu & Labosky, 2008). In vivo as well as in culture, as judged by in situ hybridization analyses, Foxd-3 exhibits grossly the same expression pattern as Sox-10 in delaminating and early migrating neural crest cells. However, in 24-hr cultures, a significant proportion of the neural crest cell population is negative for Foxd-3 (Fig. 6B4), reflecting their engagement in the melanocytic lineage, known to require combined maintenance of Sox-10 expression and Foxd-3 repression (Thomas & Erickson, 2009).

Finally, besides cell lineage markers, cell-adhesion molecules are also instrumental in analyzing neural crest cell development in culture. Cadherin-6B and N-cadherin, two members of the cadherin family of cell-cell adhesion molecules, can in particular discriminate premigratory neural crest cells from both neural epithelial cells and migrating neural crest cells, constituting useful alternatives to Snail-2, Sox-10, and Sox-2 (Fig. 6B5, B6; Dady & Duband, 2017).

Numerous other possible markers for neural crest cells have been reportedly used *in vivo* or *in vitro*, such as the p75 low affinity nerve growth factor receptor (p75-NGFR), nestin, Msx-1, Twist-1, Pax-3, AP-2 $\alpha$ , cMyc, Id-1, or Ets-1, to name a few (Dupin & Sommer, 2012; Soldatov et al., 2019; Williams et al., 2019). Notwithstanding their interest and potential, these markers have been less frequently used or simply cannot be used to characterize avian trunk neural crest cells in culture. Some of them are not found in trunk neural crest cells but rather are specific to cranial neural crest (e.g., Id-1 and Ets-1), some are not found in avians but in mouse (p75-NGFR) or in *Xenopus* (Twist-1), some are expressed in restricted neural crest cell subsets (Msx-1) or conversely are found in other cell types (Pax-3, AP-2 $\alpha$ , cMyc), while others are not expressed in neural crest cells but are used mostly for stem cell analyses (nestin). We therefore recommend using them for specific studies.

#### *Tracking neural crest cell migration in culture using videomicroscopy*

The spontaneous migratory behavior of neural crest cells is certainly one of the most challenging and fascinating issues of their ontogeny which attracted strong interest from both cell and developmental biologists. Strikingly, unlike many other cell migration systems developed *in vitro*, neural crest cell migration can be recapitulated in culture without any experimental artifact and without the assistance of migration-stimulating factors in the culture medium. In addition, it is one of the few systems in which the contribution of both collective behavior and individual cell locomotion can be tackled simultaneously for a comprehensive understanding of population cell displacement. Thus, even though culturing neural crest cells on two-dimensional substrates does not mimic entirely their native embryonic environment in its biochemical, physical, and temporal complexity, considerable information has been gathered using this system regarding how interactions between extracellular matrix components and their cell surface integrin receptors, and the organization of the cytoskeletal locomotory machinery drive cell migration (Duband, Rocher, Chen, Yamada, & Thiery, 1986; Newgreen, Gibbins, Sauter, Wallenfels, & Wütz, 1982; Rovasio, Delouvé, Yamada, Timpl, & Thiery, 1983). In addition, information gleaned from this system led to new interesting concepts on how cell-cell contacts and maintenance of a high cell

density may maximize cell migration (Rovasio et al., 1983; Thomas & Yamada, 1992). Quite remarkably, it is only recently that these data and models were confirmed in *in vivo* imaging studies at high resolution (Li et al., 2019), thereby validating the *in vitro* approach and emphasizing its interest and prospects.

Avian trunk neural crest cell migration in culture can be quantified by simple measurements either of the linear distance between the edge of the neural tube and the rim of the neural crest outgrowth (preferably at the midportion of the neural tube explant) or of the area of the outgrowth. Both parameters provide an accurate estimate of the extension of the neural crest cell population over time but it should be stressed that they do not provide details on individual cell adhesion and locomotion, on cellular interactions among the population as well as on other cellular events such as cell proliferation which all have a strong impact on the final outcome. This is particularly critical in functional studies resulting either in a population of densely packed cells occupying a limited area along the neural tube or in a large outgrowth composed of sparse clusters of round cells distributed away from the neural tube. In both cases, although values for distance and area are at odds, the migration of the whole population is largely compromised, but due to different cellular events affected. The distance and area parameters should then be used as a first approximation and should be completed with more systematic videomicroscopy analyses, giving access to the whole range of individual and collective features.

If long-term migration of the whole neural crest cell population is to be analyzed, time-lapse videomicroscopy should be performed with a 10 $\times$  objective and images captured every 5 min during 12 to 24 hr. For analysis of the dynamics of cellular protrusion in individual cells, it is preferable to use at least 20 $\times$  objectives and images should be recorded every 15 or 20 s during at least 15 min. As mentioned above, the use of a thermostatically controlled chamber coupled with a CO<sub>2</sub> controller mounted on a motorized stage is strongly recommended to avoid any artifact that may alter the quality of the recordings and affect measurements. Figure 7 and Supporting Information Video 1 illustrate an example of an avian trunk neural crest cell outgrowth dispersing under standard conditions for ~16 hr. Image analyses using appropriate software, e.g., MetaMorph (2M's), provide data on the positions of individual cells along the *x* and *y* axes for each image and the

Duband et al.

19 of 25

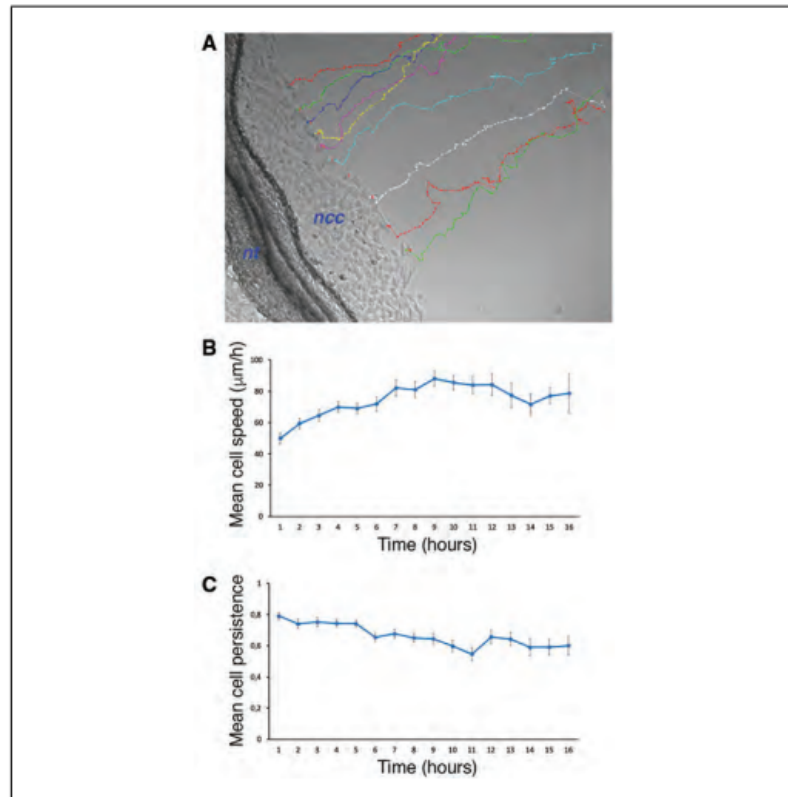


**Figure 7** Tracking avian trunk neural crest cell migration in culture. **(A)** Image of a neural tube explant analyzed by videomicroscopy showing a view of the neural tube taken after 3 hr of culture, at the time of the beginning of recording, and the tracks and positions of several individual cells over time. Time lapse videomicroscopy was performed with a 10 $\times$  objective and images were recorded every 5 min during 16 hr. **(B, C)** Graphs showing the mean values of neural crest cell speed of locomotion in  $\mu\text{m/hr}$  and the directionality of movement every hour, respectively.

distance covered by cells between two consecutive images, two parameters necessary for cell tracking (Fig. 7A). From these data, it is possible to deduce the speed of locomotion of individual cells and the persistence of their movement over time (i.e., the ratio between the linear distance between two positions and the actual distance covered; Fig. 7B and C). Additional parameters can also be appreciated using this technique and analyzed using MetaMorph or ImageJ software: Individual cell shape (area, perimeter, Ferret, compactness, shape index), cell-cell contacts between neighbors (length of intercellular contacts), or cell division (proportion of dividing cells, duration of cell cycle). Results show that avian trunk neural crest cells migrate as individuals and not as a cohesive layer

or as chains as observed for cranial or enteric neural crest cell populations. Movement of individual cells is not uniform as in isolated fibroblasts. Rather it consists of short periods of linear, intense, and fast cell displacement involving a unique large pseudopode followed by stationary phases where the cell exhibits a stellate shape. Movement resumes with retraction of most cell processes and cellular elongation with formation of a single pseudopode. Importantly, both locomotion and directionality are driven essentially by cell-cell contacts and mechanical forces resulting from high cell density. Thus, when an individual cell moves ahead of the rest of the population, either it moves back to rejoin the rest of the population as a result of co-attraction (Carmona-Fontaine et al., 2011) or it stops and will resume

migrating only after being reached and contacted by followers, a process that has been referred to as contact-stimulation of movement (Thomas & Yamada, 1992).

Several attempts have been made over the years to adapt the two-dimensional neural crest cell culture system for investigating the influence of the environment and its physical aspects on neural crest cell migration. For instance, creating alternating stripes consisting of a plastic dish coated or not with extracellular matrix material, or containing attractive or repulsive factors was used to analyze space constraints or guidance mechanisms involved in neural crest cell migration (e.g., see Rovasio et al., 1983; Wang & Anderson, 1997). Likewise, in pioneering studies using Nucleopore filters with pore diameters of varying sizes, Newgreen (1989) could evaluate the ability of neural crest cells to invade restricted cell-free spaces. To date, the emergence of elaborated, controlled technologies to generate two- or three-dimensional micropatterned substrates with defined chemical and physical specificities associated with highly sensitive methods for measuring molecular interactions and physical parameters open new avenues to tackle in a reliable, less empirical way the mechanical properties of neural crest cells during migration (Trichet et al., 2012; Vedula et al., 2012).

#### ***Phenotypic characterization of neural crest cells in long-term culture***

Culturing neural crest cells also proved to be a source of valuable data concerning the issue of the differentiation capacities of individual neural crest cells (Dupin, et al., 2018). Indeed, while neural crest cells display a relatively uniform aspect and collective behavior during the first day in culture, after 24 hr, important changes appear in the overall organization of the population and in individual cell morphologies. The first and most obvious event to occur is a massive neurite outgrowth from the neural tube especially on its ventral side (Fig. 8A). This illustrates the fact that the neural tube is able to pursue its own developmental program into a spinal cord-like structure, in synchrony with that of neural crest cells. These neurites derive most likely from motor neurons, migrate on top of neural crest cells, ultimately covering them entirely. However, contrary to what happens in the embryo, neurites in culture do not organize as bundles as soon as they emerge out of the neural tube explant. Other alterations can be seen both at the periphery of the neural crest

outgrowth and more centrally near the neural tube after the second day of culture (Fig. 8B). Large spread fibroblasts develop at the periphery while small individual neurons appear more centrally. Progressively, other cell types characterized by their own specific morphologies can be detected, often as clones, among the neural crest cell outgrowth. This includes melanoblasts with a small compact cell body and long thin processes, and glial cells with a larger cell body and long thicker cellular extensions, reminiscent of astrocytes. Terminal differentiation occurs generally later after 5 to 7 days in culture, as evidenced for example by the deposition of dark melanin in melanocytes. Therefore, differentiation of neural crest cells can be successfully achieved in culture, yielding the various cell types that are normally derived from trunk neural crest cells *in vivo* (neurons, glia, melanocytes). In addition to them, mesenchymal cells, a derivative normally obtained with cranial neural crest cells only, are also produced in culture, thereby revealing that trunk neural crest cells harbor mesenchymal fibroblastic capacities which can be uncovered *in vitro*. Of note, this diversity of cell types is also observed when the neural tube has been removed from the culture, indicating that these changes are intrinsic to neural crest cells and are not driven primarily under a neural tube influence.

Neural crest cell differentiation can be followed using specific cell lineage markers in classical immunolabeling experiments (Table 1). The  $\alpha$ -smooth muscle actin (SMA) isoform is present in the large fibroblastic cells as an elaborated cytoplasmic meshwork, assessing their myofibroblast identity (Fig. 8C1). Likewise,  $\beta$ III-tubulin, the neuron-specific tubulin isoform recognized by the Tuj-1 antibody, is strongly expressed in individual neurons both in the neurites and in the cell body (Fig. 8C2). Melanocyte inducing transcription factor (MITF), a transcription factor involved in melanocyte determination, is conspicuous in nuclei of melanoblasts (Fig. 8C3) while the glia fibrillary acidic protein (GFAP) and the brain lipid binding protein (BLBP) are both found in the cytoplasm of differentiating glial cells (not shown). Interestingly, expression of the early neural crest cell markers Sox-10 and HNK-1 also evolves during cell lineage diversification. While a substantial number of cells retain their typical stellate morphology associated with strong Sox-10 and HNK-1 labeling—revealing the maintenance of an important pool of neural crest progenitors throughout the culture

Duband et al.

21 of 25

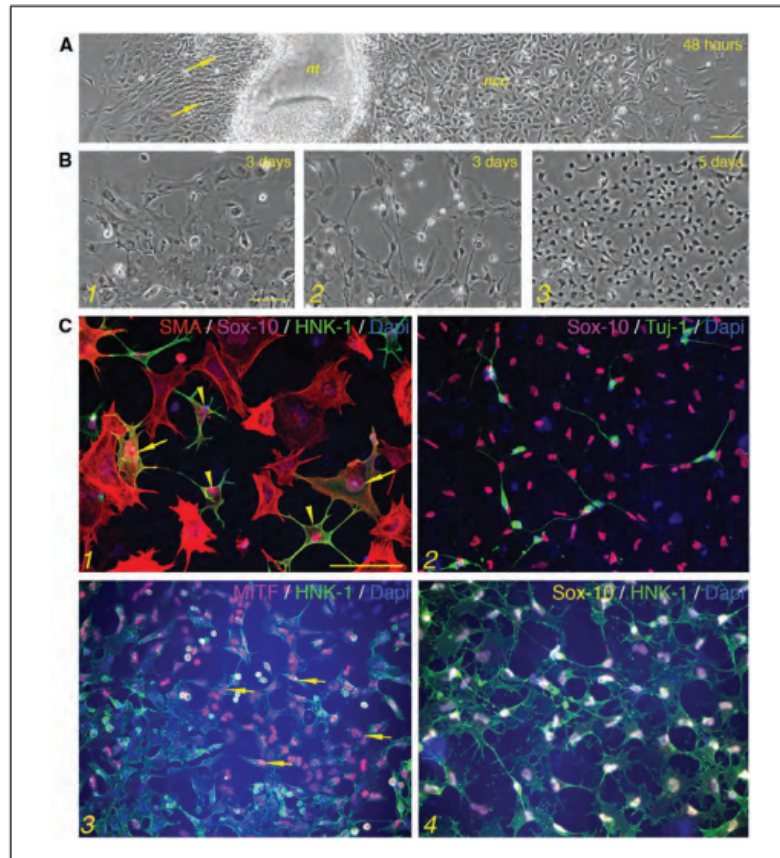


**Figure 8** Phenotypic characterization of neural crest cell cultures after several days in culture with cell lineage markers. **(A)** Phase contrast overview of a 48-hr neural tube explant, showing, on the left, the dense network of neurites (arrows) emerging out of the ventral side of the neural tube and, on the right, the presence of cells with distinct morphologies and shapes among the neural crest cell population. **(B)** Detailed views of the main cell types derived from the neural crest outgrowth after 3 or 5 days in culture: Panel 1, large, well spread myofibroblasts; Panel 2, neurons with long neurites sitting on top of neural crest cells; and Panel 3, little, aster-shaped melanoblasts. Note that these cells are often assembled as separate colonies. **(C)** Immunofluorescence labeling of neural crest-derived cell populations after 3 days in culture with antibodies to Sox-10, HNK-1,  $\alpha$ -SMA,  $\beta$ III-tubulin (Tuj-1), and Mitf revealed by secondary antibodies conjugated to Alexa-488 (green), Cy-3 (red), and Cy-5 (purple in C1-C3 and yellow in C4). Nuclei are visualized with Hoechst staining (blue). Panel 1 shows a group of myofibroblasts characterized by a dense meshwork of  $\alpha$ -SMA in their cytoplasm. Most of them do not express Sox-10 in their nuclei and HNK-1 on their surface but a few cells corresponding possibly to myofibroblasts having not yet completed their differentiation process express all three markers together (arrows). Besides myofibroblasts, a few large cells with an astrocyte-like shape and expressing both HNK1 and Sox-10 represent early differentiating glial cells (arrowheads). Panel 2 shows neurons expressing  $\beta$ III-tubulin but no Sox-10. Panel 3 shows a large group of melanoblasts expressing MITF in their nuclei but no HNK-1. As for myofibroblasts, a few melanoblasts can be seen coexpressing Mitf and HNK-1 (arrows), likely corresponding to early melanoblasts. Panel 4 shows persistent Sox-10 positive, HNK-1 positive undifferentiated neural crest cell progenitors in the outgrowth. Bars in A, B, and C = 100  $\mu$ m.

(Fig. 8C4)—differentiating cells express either Sox-10 (melanoblasts and glial cells) or HNK-1 (neurons) or neither (myofibroblasts), together with their specific differentiation markers. However, occasionally, both Sox-10 and HNK-1 may coexist with SMA or MITF in cells (Fig. 8C1, C3), albeit at lower levels than in undifferentiated neural crest cells. These cells are likely to represent intermediate steps between progenitors to fully differentiated cells.

It should be stressed that although trunk neural crest cell differentiation occurs spontaneously in culture in basic medium with 1% serum, neither the extent of cell differentiation nor the ratio between the various cell types can be mastered easily in these conditions. To this end, it is necessary to add exogenous growth factors or morphogens to the culture medium to help orienting neural crest cell fates toward specific lineages (Dupin et al., 2018). For instance, TGF- $\beta$  promotes a myofibroblastic phenotype at the expense of a neuronal one; BMP-2, neuregulin, endothelin-3, and Shh stimulate differentiation into autonomic neurons, glia, melanocytes, and chondrocytes, respectively; while Wnt-1 and BMP in combination favor maintenance of neural crest cells in a progenitor state. Ideally, to study neural crest cell multipotency and differentiation capacities, in vitro cloning of individual cells on feeder layers and in optimized culture conditions is the best option (Dupin et al., 2018).

### Time Considerations

The timing for preparing neural crest cell cultures depends largely on the number of eggs you have to work with and on the experience and technical skill of the experimenter. Generally consider that 3 hr, maximum 4 hr for beginners, is necessary to collect the embryos from the egg, isolate the trunk fragments, dissect the neural tubes, and transfer them into culture using ~50 eggs. Preferably, start the experiment in the morning; this will give enough time to allow initiation of neural crest cell migration by early afternoon and adequate time to set the experimental conditions for functional studies or for videomicroscopy. (Night owls should not be discouraged, however, and should start at the desired time that is most appropriate for them!)

### Acknowledgments

Work from the authors is supported by Institut National de la Santé et de la Recherche Médicale (INSERM), the Université Paris-

Est Créteil, and the Fondation ARC pour la Recherche contre le Cancer.

### Literature Cited

- Baggiolini, A., Varum, S., Mateos, J. M., Bettosini, D., John, N., Bonalli, M., ... Sommer, L. (2015). Premigratory and migratory neural crest cells are multipotent in vivo. *Cell Stem Cell*, *16*, 314–322. doi: 10.1016/j.stem.2015.02.017.
- Bajpai, V. K., Kerosuo, L., Tseropoulos, G., Cummings, K. A., Wang, X., Lei, P., ... Andreadis, S. T. (2017). Reprogramming postnatal human epidermal keratinocytes toward functional neural crest fates. *Stem Cells*, *35*, 1402–1415. doi: 10.1002/stem.2583.
- Betancur, P., Bronner-Fraser, M., & Saucan-Spengler, T. (2010). Assembling neural crest regulatory circuits into a gene regulatory network. *Annual Review of Cell and Developmental Biology*, *26*, 581–603. doi: 10.1146/annurev.cellbio.042308.113245.
- Calloni, G. W., Glavieux-Pardanaud, C., Le Douarin, N. M., & Dupin, E. (2007). Sonic Hedgehog promotes the development of multipotent neural crest progenitors endowed with both mesenchymal and neural potentials. *Proceedings of the National Academy of Sciences of the USA*, *104*, 19879–19884. doi: 10.1073/pnas.0708806104.
- Carmona-Fontaine, C., Matthews, H. K., Kuriyama, S., Moreno, M., Dunn, G. A., Parsons, M., ... Mayor, R. (2008). Contact inhibition of locomotion in vivo controls neural crest directional migration. *Nature*, *456*, 957–961. doi: 10.1038/nature07441.
- Carmona-Fontaine, C., Theveneau, E., Tzekou, A., Tada, M., Woods, M., Page, K. M., ... Mayor, R. (2011). Complement fragment C3a controls mutual cell attraction during collective cell migration. *Developmental Cell*, *21*, 1026–1037. doi: 10.1016/j.devcel.2011.10.012.
- Cheung, M., Chaboissier, M.-C., Mynett, A., Hirst, E., Schedl, A., & Briscoe, J. (2005). The transcriptional control of trunk neural crest induction, survival, and delamination. *Developmental Cell*, *8*, 179–192. doi: 10.1016/j.devcel.2004.12.010.
- Cohen, A. M., & Konigsberg, I. R. (1975). A clonal approach to the problem of neural crest determination. *Developmental Biology*, *46*, 262–280. doi: 10.1016/0012-1606(75)90104-9.
- Cousin, H., & Alfandari, D. (2018). Cranial neural crest explants. *Cold Spring Harbor Protocols*, *2018*(3), pdb.prot097394. doi: 10.1101/pdb.prot097394.
- Dady, A., & Duband, J. L. (2017). Cadherin interplay during neural crest segregation from the non-neural ectoderm and neural tube in the early chick embryo. *Developmental Dynamics*, *246*, 550–565. doi: 10.1002/dvdy.24517.
- Duband, J.-L., Blavet, C., Jarov, A., & Fournier-Thibault, C. (2009). Spatio-temporal control of neural epithelial cell migration and epithelium-to-mesenchyme transition during neural tube

Duband et al.

23 of 25

- development. *Development, Growth & Differentiation*, 57, 25–44. doi: 10.1111/j.1440-169X.2009.01076.x.
- Duband, J.-L., Dady, A., & Fleury, V. (2015). Resolving time and space constraints during neural crest formation and delamination. *Current Topics in Developmental Biology*, 111, 27–67. doi: 10.1016/bs.ctdb.2014.11.002.
- Duband, J.-L., Rocher, S., Chen, W.-T., Yamada, K. M., & Thiery, J. P. (1986). Cell adhesion and migration in the early vertebrate embryo: Location and possible role of the putative fibronectin-receptor complex. *Journal of Cell Biology*, 102, 160–178. doi: 10.1083/jcb.102.1.160.
- Dupin, E., Calloni, G. W., Coelho-Aguiar, J. M., & Le Douarin, N. M. (2018). The issue of the multipotency of the neural crest cells. *Developmental Biology*, 444(Suppl 1), S47–S59. doi: 10.1016/j.ydbio.2018.03.024.
- Dupin, E., & Coelho-Aguiar, J. M. (2013). Isolation and differentiation properties of neural crest stem cells. *Cytometry. Part A*, 83, 38–47. doi: 10.1002/cyto.a.22098.
- Dupin, E., & Sommer, L. (2012). Neural crest progenitors and stem cells: From early development to adulthood. *Developmental Biology*, 366, 83–95. doi: 10.1016/j.ydbio.2012.02.035.
- Etchevers, H. (2011). Primary culture of chick, mouse or human neural crest cells. *Nature Protocols*, 6, 1568–1577. doi: 10.1038/nprot.2011.398.
- Furlan, A., & Adameyko, I. (2018). Schwann cell precursor: A neural crest cell in disguise? *Developmental Biology*, 444(Suppl 1), S25–S35. doi: 10.1016/j.ydbio.2018.02.008.
- Gonzalez Malagon, S. G., Dobson, L., Munoz, A. M. L., Dawson, M., Barrell, W., Marangos, P., ... Liu, K. J. (2019). Dissection, culture and analysis of primary cranial neural crest cells from mouse for the study of neural crest cell delamination and migration. *Journal of Visualized Experiments*, 152, e60051. doi: 10.3791/60051.
- Hamburger, V., & Hamilton, H. L. (1951). A series of normal stages in the development of the chick embryo. *Journal of Morphology*, 88, 49–92. doi: 10.1002/jmor.1050880104.
- Hockman, D., Chong-Morrison, V., Green, S. A., Gavriouchkina, D., Candido-Ferreira, I., Ling, I. T. C., ... Sauka-Spengler, T. (2019). A genome-wide assessment of the ancestral neural crest gene regulatory network. *Nature Communications*, 10, 4689. doi: 10.1038/s41467-019-12687-4.
- Hong, C. S., & Saint-Jeannet, J. P. (2005). Sox proteins and neural crest development. *Seminars in Cell and Developmental Biology*, 16, 694–703. doi: 10.1016/j.semcdb.2005.06.005.
- Ito, K., & Sieber-Blum, M. (1993). Pluripotent and developmentally restricted neural-crest-derived cells in posterior visceral arches. *Developmental Biology*, 156, 191–200. doi: 10.1006/dbio.1993.1069.
- Kerosuo, L., Nie, S., Bajpai, R., & Bronner, M. E. (2015). Crestospheres: Long-term maintenance of multipotent, premigratory neural crest stem cells. *Stem Cell Reports*, 5, 499–507. doi: 10.1016/j.stemcr.2015.08.017.
- Le Douarin, N. M., & Kalcheim, C. (1999). *The neural crest* (2nd ed.). New York: Cambridge University Press.
- Li, Y., Vieceli, F. M., Gonzalez, W. G., Li, A., Tang, W., Lois, C., & Bronner, M. E. (2019). In vivo quantitative imaging provides insights into trunk neural crest migration. *Cell Reports*, 26, 1489–1500.e1483. doi: 10.1016/j.celrep.2019.01.039.
- Liu, J. A., & Cheung, M. (2016). Neural crest stem cells and their potential therapeutic applications. *Developmental Biology*, 419, 199–216. doi: 10.1016/j.ydbio.2016.09.006.
- Liu, Y., & Labosky, P. A. (2008). Regulation of embryonic stem cell self-renewal and pluripotency by Foxd3. *Stem Cells*, 26, 2475–2484. doi: 10.1634/stemcells.2008-0269.
- Mohlin, S., Kunttas, E., Persson, C. U., Abdel-Haq, R., Castillo, A., Murko, C., ... Kerosuo, L. (2019). Maintaining multipotent trunk neural crest stem cells as self-renewing crestospheres. *Developmental Biology*, 447, 137–146. doi: 10.1016/j.ydbio.2019.01.010.
- Nakagawa, S., & Takeichi, M. (1995). Neural crest cell-cell adhesion controlled by sequential and subpopulation-specific expression of novel cadherins. *Development*, 121, 1321–1332.
- Newgreen, D. F. (1989). Physical influences on neural crest cell migration in avian embryos: Contact guidance and spatial restrictions. *Developmental Biology*, 131, 136–148. doi: 10.1016/S0012-1606(89)80045-4.
- Newgreen, D. F., Gibbins, I. L., Sauter, J., Wallenfels, B., & Wütz, R. (1982). Ultrastructural and tissue-culture studies on the role of fibronectin, collagen and glycosaminoglycans in the migration of neural crest cells in the fowl embryo. *Cell and Tissue Research*, 221, 521–549. doi: 10.1007/BF00215700.
- Newgreen, D. F., Powell, M. E., & Moser, B. (1990). Spatiotemporal changes in HNK-1/L2 glycoconjugates on avian embryo somite and neural crest cells. *Developmental Biology*, 139, 100–120. doi: 10.1016/0012-1606(90)90282-N.
- Nieto, M. A. (2002). The Snail superfamily of zinc-finger transcription factors. *Nature Reviews Molecular Cell Biology*, 3, 155–166. doi: 10.1038/nrm757.
- Nieto, M. A., Sargent, M. G., Wilkinson, D. G., & Cooke, J. (1994). Control of cell behavior during vertebrate development by *Slug*, a zinc finger gene. *Science*, 264, 835–839. doi: 10.1126/science.7513443.
- Park, K. S., & Gumbiner, B. M. (2012). Cadherin-6B stimulates an epithelial mesenchymal transition and the delamination of cells from the neural ectoderm via LIMK/cofilin mediated non-canonical BMP receptor signaling.

- Developmental Biology*, 366, 232–243. doi: 10.1016/j.ydbio.2012.04.005.
- Prescott, S. L., Srinivasan, R., Marchetto, M. C., Grishina, I., Narvaiza, I., Selli, L., ... Wysocka, J. (2015). Enhancer divergence and cis-regulatory evolution in the human and chimp neural crest. *Cell*, 163, 68–83. doi: 10.1016/j.cell.2015.08.036.
- Rovasio, R. A., Delouvé, A., Yamada, K. M., Timpl, R., & Thiery, J. P. (1983). Neural crest cell migration: Requirements for exogenous fibronectin and high cell density. *Journal of Cell Biology*, 96, 462–473. doi: 10.1083/jcb.96.2.462.
- Scarpa, E., Szabo, A., Bibonne, A., Theveneau, E., Parsons, M., & Mayor, R. (2015). Cadherin switch during EMT in neural crest cells leads to contact inhibition of locomotion via repolarization of forces. *Developmental Cell*, 34, 421–434. doi: 10.1016/j.devcel.2015.06.012.
- Sieber-Blum, M., & Cohen, A. M. (1980). Clonal analysis of quail neural crest cells: They are pluripotent and differentiate in vitro in the absence of noncrest cells. *Developmental Biology*, 80, 96–106. doi: 10.1016/0012-1606(80)90501-1.
- Soldatov, R., Kaucka, M., Kastriti, M. E., Petersen, J., Chontorotzea, T., Englmaier, L., ... Adameyko, I. (2019). Spatiotemporal structure of cell fate decisions in murine neural crest. *Science*, 364(6444), eaas9536. doi: 10.1126/science.aas9536.
- Stemple, D. L., & Anderson, D. J. (1992). Isolation of a stem cell for neurons and glia from the mammalian neural crest. *Cell*, 71, 973–985. doi: 10.1016/0092-8674(92)90393-Q.
- Taneyhill, L. A., Coles, E. G., & Bronner-Fraser, M. (2007). Snail2 directly represses cadherin6B during epithelial-to-mesenchymal transitions of the neural crest. *Development*, 134, 1481–1490. doi: 10.1242/dev.02834.
- Thomas, A. J., & Erickson, C. A. (2009). FOXD3 regulates the lineage switch between neural crest-derived glial cells and pigment cells by repressing MITF through a non-canonical mechanism. *Development*, 136, 1849–1858. doi: 10.1242/dev.031989.
- Thomas, S., Thomas, M., Wincker, P., Babarit, C., Xu, P., Speer, M. C., ... Etchevers, H. C. (2008). Human neural crest cells display molecular and phenotypic hallmarks of stem cells. *Human Molecular Genetics*, 17, 3411–3425. doi: 10.1093/hmg/ddn235.
- Thomas, L. A., & Yamada, K. M. (1992). Contact stimulation of cell migration. *Journal of Cell Science*, 103, 1211–1214.
- Trainor, P. (Ed.). (2013). *Neural crest cells: Evolution, development and disease* (pp. 488). San Diego: Elsevier.
- Trichet, L., Le Digabel, J., Hawkins, R. J., Vedula, S. R., Gupta, M., Ribault, C., ... Ladoux, B. (2012). Evidence of a large-scale mechanosensing mechanism for cellular adaptation to substrate stiffness. *Proceedings of the National Academy of Sciences of the USA*, 109, 6933–6938. doi: 10.1073/pnas.1117810109.
- Tucker, G. C., Aoyama, H., Lipinski, M., Tursz, T., & Thiery, J. P. (1984). Identical reactivity of monoclonal antibodies HNK-1 and NC-1: Conservation in vertebrates on cells derived from the neural primordium and on some leukocytes. *Cell Differential*, 14, 223–230. doi: 10.1016/0045-6039(84)90049-6.
- Tucker, G. C., Delarue, M., Zada, S., Boucaut, J.-C., & Thiery, J. P. (1988). Expression of HNK-1/NC-1 epitope in early vertebrate neurogenesis. *Cell and Tissue Research*, 251, 457–465. doi: 10.1007/BF00215855.
- Uchikawa, M., Ishida, Y., Takemoto, T., Kamachi, Y., & Kondoh, H. (2003). Functional analysis of chicken Sox2 enhancers highlights an array of diverse regulatory elements that are conserved in mammals. *Developmental Cell*, 4, 509–519. doi: 10.1016/S1534-5807(03)00088-1.
- Vedula, S. R., Leong, M. C., Lai, T. L., Hensen, P., Kabla, A. J., Lim, C. T., & Ladoux, B. (2012). Emerging modes of collective cell migration induced by geometrical constraints. *Proceedings of the National Academy of Sciences of the USA*, 109, 12974–12979. doi: 10.1073/pnas.1119313109.
- Vincent, M., & Thiery, J. P. (1984). A cell surface marker for neural crest and placodal cells: Further evolution in peripheral and central nervous system. *Developmental Biology*, 103, 468–481. doi: 10.1016/0012-1606(84)90334-8.
- Wang, H. U., & Anderson, D. J. (1997). Eph family transmembrane ligands can mediate repulsive guidance of trunk neural crest migration and motor axon outgrowth. *Neuron*, 18, 383–396. doi: 10.1016/S0896-6273(00)81240-4.
- Weider, M., & Wegner, M. (2017). SoxE factors: Transcriptional regulators of neural differentiation and nervous system development. *Seminars in Cell & Developmental Biology*, 63, 35–42. doi: 10.1016/j.semcdb.2016.08.013.
- Williams, R. M., Candido-Ferreira, I., Repapi, E., Gavriouchkina, D., Senanayake, U., Ling, I. T. C., ... Sauka-Spengler, T. (2019). Reconstruction of the global neural crest gene regulatory network in vivo. *Developmental Cell*, 51, 255–276.e257. doi: 10.1016/j.devcel.2019.10.03.
- Ziller, C., Dupin, E., Brazeau, P., Paulin, D., & Le Douarin, N. M. (1983). Early segregation of a neuronal precursor cell line in the neural crest as revealed by culture in a chemically defined medium. *Cell*, 32, 627–638. doi: 10.1016/0092-8674(83)90482-8.

1 **Submitted version**

2

3

4

5 ***Glucose oxidation and nutrients availability drive neural crest development***

6

7

8 Nioosha Nekooie-Marnany, Redouane Fodil, Sophie Féréol, Marine Depp#, Roberto Motterlini,  
9 Roberta Foresti, Jean-Loup Duband\*, and Sylvie Dufour\*

10

11

12 Institut Mondor de Recherches Biomédicales, INSERM U955, Université Paris-Est Créteil, 94000  
13 Créteil, France

14

15

16 # present address: Institut de Biologie, Ecole Normale Supérieure, Paris, France

17 \* Authors for correspondence: jean-loup.duband@inserm.fr and sylvie.dufour@inserm.fr

18

19

20

21 Running title: Metabolic instruction of neural crest development

22

23 Keywords: neural crest, cellular metabolism, glycolysis, oxidative phosphorylation, nutrient input,  
24 bioenergetics, cell migration, fate decision

25

26

27 **SUMMARY STATEMENT**

28 Here we show that neural crest cell migration and fate decisions rely primarily on glucose oxidation  
29 for energy production and mobilize multiple cooperating metabolic pathways for their biosynthetic  
30 needs and execution of gene programs.

31

32

33 **ABSTRACT**

34 Bioenergetic metabolism is a key regulator of cellular function and signaling activity but the exact  
35 roles of nutrient utilization and energy production in embryonic development remain unknown. Here  
36 we investigated the metabolic pathways and deciphered the role of carbon metabolism required for  
37 the development of neural crest cells (NCC), a migratory stem cell population of the vertebrate  
38 embryo. We uncovered that glucose oxidation constitutes the prominent metabolic signature of trunk  
39 NCC and supports their delamination, migration, and proliferation. Additionally, we found that  
40 glycolysis, mitochondrial respiration and the pentose phosphate pathway are all mobilized  
41 downstream of glucose uptake. These metabolic pathways do not support specific cellular processes  
42 but cooperate and are integrated to accomplish epithelium-to-mesenchyme transition, adhesion,  
43 locomotion and proliferation. Moreover, using different nutrient supplies (glucose vs. pyruvate) we  
44 show that glucose is crucial to modulate NCC migration and adaptation to environmental stiffness,  
45 control NCC stemness and drive their fate decisions through regulation of specific gene expression.  
46 Our data establish that NCC development is instructed by metabolic cues that mobilize defined  
47 metabolic pathways cooperating together in response to nutrient availability.

48

49 **INTRODUCTION**

50 During embryonic development, cell type diversity is generated through migration of progenitor cells  
51 over considerable distances and during long time periods. Neural crest cells (NCC) of the vertebrate  
52 embryo are one remarkable example of such migratory populations (Bronner, 2018; Trainor, 2013).  
53 These cells appear early all along the embryonic rostrocaudal axis in the dorsal part of the neural tube  
54 (NT). Through epithelium-to-mesenchyme transition (EMT), NCC delaminate and disperse away  
55 from the NT to distal sites where they differentiate. Owing to their partition into different populations  
56 (cranial, cardiac, vagal, trunk, and sacral) along the neural axis, NCC give rise to numerous cell types:  
57 skeletal and supportive tissues, endocrine cells, cardiac septum, enteric ganglia as well as peripheral  
58 neurons, glia, and melanocytes. From delamination to differentiation, NCC are confronted with  
59 different environments and are subjected to diverse cues impacting on gene networks and on their  
60 survival, proliferation, shape, adhesion, migration, and fate (Barriga and Mayor, 2019; Chevalier et  
61 al., 2016; Duband et al., 2015; Martik and Bronner, 2017; Soldatov et al., 2019).

62 Cellular metabolism, long regarded as a neutral factor during development, has been proposed  
63 recently to have an instructing role in cell fate (Miyazawa and Aulehla, 2018; Pavlova and Thompson,  
64 2016; Shyh-Chang et al., 2013; Zhang et al., 2018), but the exact roles of nutrient utilization and  
65 energy production in embryonic development still remain to be investigated. The primary function of  
66 cellular metabolism is to provide cells with bioenergetic and biosynthetic supplies from nutrients, e.g.  
67 glucose, pyruvate, amino acids, and fatty acids (Zhu and Thompson, 2019). Glucose constitutes the  
68 major source for ATP production through two pathways occurring in distinct cellular compartments:  
69 glycolysis in the cytoplasm and oxidative phosphorylation (OXPHOS) in mitochondria. Glucose is  
70 also an important source of carbon to produce amino acids, lipids, and nucleotides necessary for  
71 biomass production and generated from metabolic pathways branching from glycolysis. Among  
72 them, the pentose phosphate pathway (PPP) constitutes a major source of nucleotides and NADPH  
73 required during anabolism (Patra and Hay, 2014).

74 Bioenergetic and biosynthetic metabolisms differ among cells and depend on gene regulatory  
75 programs driving expression and activity of metabolic enzymes (Lempradl et al., 2015). For example,  
76 in cell cycle-arrested differentiated cells, metabolism is usually catabolic with high production of  
77 ATP, as a result of pyruvate entry into mitochondria and OXPHOS. In contrast, in proliferating,  
78 undifferentiated cells as well as in cancer cells, metabolic activity is preferably oriented toward  
79 anabolism and ATP production relies mostly on aerobic glycolysis fed by intense glucose uptake,  
80 with high extracellular lactate production, a process known as Warburg effect (Schell et al., 2017;  
81 Vander Heiden et al., 2009). On the other hand, depending on the nature and amount of available

82 nutrients, the metabolic activity of cells varies in time and space to adapt to environmental changes.  
83 For example, the mouse embryo relies essentially on OXPHOS before implantation, while after  
84 implantation aerobic glycolysis predominates until OXPHOS takes over again when blood flow  
85 begins (Johnson et al., 2003; Miyazawa and Aulehla, 2018; Perestrelo et al., 2018; Shyh-Chang et al.,  
86 2013; Zhang et al., 2018). A similar shift from glycolysis to OXPHOS takes place in adult stem cells  
87 leaving quiescence to differentiate and in induced pluripotent stem cells exiting pluripotency (Gu et  
88 al., 2016; Ito and Suda, 2014; Perestrelo et al., 2018; Shyh-Chang et al., 2013).

89       Recently, a study on cranial NCC delamination reported a metabolic shift toward aerobic  
90 glycolysis at initiation of their migration (Bhattacharya et al., 2020), suggesting that NCC can  
91 modulate their metabolic activity to execute different developmental steps. However, cranial NCC  
92 delamination and migration differ strikingly from those of the other NCC populations in their  
93 dynamics, gene regulatory network deployed, and environment (Li et al., 2019; Scully et al., 2016;  
94 Simões-Costa and Bronner, 2015; Simões-Costa et al., 2012; Soldatov et al., 2019; Théveneau et al.,  
95 2007). Therefore, a global view of the NCC metabolic landscape is still lacking, and it remains to be  
96 explored how nutrients support different NCC cellular activities throughout development, which  
97 metabolic pathways are recruited for their bioenergetic and biosynthetic supplies, and to which extend  
98 NCC metabolic activity can drive their behavior and fate.

99       Because investigating NCC metabolic features and their impact on NCC developmental  
100 program cannot be performed directly in intact embryos, we developed an alternative strategy based  
101 on *ex vivo* culture in defined conditions recapitulating the delamination, migration, and differentiation  
102 steps of NCC development, as well as their main features (timing and kinetics of cellular events, rate  
103 of proliferation, cellular interactions) (Duband et al., 2020). We characterized the metabolic traits of  
104 avian trunk NCC, and we modified the activity of some of the key metabolic enzymes or the nutrient  
105 supplies to decipher the role of carbon metabolism in NCC dispersion and differentiation. Our results  
106 indicate that, NCC have a metabolic signature characteristic of glucose oxidation and their  
107 development requires massive mobilization of the glycolytic, OXPHOS and PPP pathways  
108 cooperating together to meet their strong bioenergetic and biosynthetic needs and to adapt to a fast-  
109 changing environment. In addition, our data reveal that nutrient inputs and metabolic pathways can  
110 drive fate decisions in NCC through regulation of gene programs.

111

112

## 113 **RESULTS**

114 We established avian trunk NCC in primary cultures from neural tube (NT) explants in a defined  
115 medium suitable to support their developmental steps, from delamination and dispersion to  
116 differentiation (Fig. S1), at rates and timings comparable to those achieved in classical media (Dupin  
117 et al., 2018; Rovasio et al., 1983; Santiago and Erickson, 2002). This medium, referred as to control  
118 medium, consisted of DMEM containing glucose, pyruvate, and glutamine at 5, 1, and 2 mM,  
119 respectively, as bioenergetic and biosynthetic nutrients and supplemented with only 1% serum to  
120 minimize the contribution of exogenous growth factors and fatty acids.

121

### 122 **Multiple Metabolic Pathways are Mobilized during Trunk NCC Dispersion**

123 We first investigated whether the spread of NCC outgrowth relies on specific metabolic pathways  
124 (Fig. 1A-D). Inhibitors of glycolysis, OXPHOS, and PPP (Fig. 1A) were applied at onset of culture  
125 (except in video microscopy analyses, where they were applied just before recording), and the  
126 behavior of the NCC population over 24 h was compared to that of explants in control medium,  
127 focusing on outgrowth aspect and area at 5 and 24 h (Fig. 1B,C), migration front progression (Fig.  
128 1D) and morphology of cells (Fig. S2A). In the presence of 2-deoxyglucose (2-DG), a potent inhibitor  
129 of upper glycolysis, NCC initially segregated normally from the NT and their progression was close  
130 to that of controls, but cells became less spread and less cohesive, with a spindle shape. Then,  
131 expansion of the population almost completely stalled and NCC started to round up. At 24 h cells  
132 displayed poor survival and were sparse occupying a limited area around the NT, compared with the  
133 large outgrowth with numerous well-spread and dense cells seen in controls. Oligomycin, an inhibitor  
134 of mitochondrial ATP synthase, marginally affected initial NCC progression, but cells were densely  
135 packed, causing a reduction of the outgrowth area. Then, NCC expansion decreased with a  
136 progressive reduction in cell spreading, resulting in a reduced outgrowth of sparse, round cells at 24  
137 h. Rotenone combined with antimycin-A (Rot-AA), blockers of complex I and III of the  
138 mitochondrial electron transport chain, had a similar effect except that reduction in dispersion was  
139 immediate and massive. 6-aminonicotinamide (6-AN), a blocker of PPP, showed no apparent effect  
140 on the initial dispersion of NCC, but the progression of cells slowed down after 5-8 h, and a strongly  
141 reduced outgrowth with many round cells was observed at 24 h. Na-iodoacetate, an inhibitor of lower  
142 glycolysis (Fig. S3A), reduced significantly NCC dispersion after 24 h but less dramatically than 2-  
143 DG (Fig. S3B). Unlike 2-DG, Na-iodoacetate did not alter cell survival but produced sparse  
144 outgrowths containing round to elongated NCC.

145 Thus, all inhibitors of glucose metabolism and OXPHOS affected NCC dispersion even if  
146 with specific kinetic and morphological effects, suggesting that all metabolic pathways downstream  
147 of glucose uptake and utilization are mobilized in a cooperative manner in NCC.

148

### 149 **Nutrient Availability Affects Trunk NCC Dispersion**

150 To investigate whether NCC development is influenced by nutrient availability, we cultured NT  
151 explants in conditions in which, beside glutamine, only pyruvate, glucose, or neither were provided  
152 (Figs. 1E-G, S2B). In the absence of pyruvate and glucose, NCC initiated migration from the NT but  
153 failed to follow their normal progression and dispersion over time, with considerable cell death after  
154 24 h. In the presence of pyruvate, NCC dispersion occurred almost normally at culture onset but  
155 stopped after 5-8 h, with cells exhibiting elongated spindle shaped morphologies, thus mimicking  
156 strikingly the behavior and morphology of NCC treated with 2-DG, except that they did not undergo  
157 cell death in the long term. In the presence of glucose, progression of NCC outgrowths and cell  
158 morphologies were virtually indistinguishable from those observed in controls. Oligomycin exerted  
159 a much more immediate and stronger effect on NCC cultured in pyruvate medium than in glucose,  
160 with the abrogation of cell dispersion (Fig. S2C). Conversely, 6-AN greatly affected NCC dispersion  
161 in glucose medium but had little effect in pyruvate even after 24 h (Fig. S2C). UK-5099, a potent  
162 inhibitor of the mitochondrial pyruvate carrier (Fig. S3A) (Schell et al., 2017) reduced NCC  
163 dispersion and affected their spreading, severely in the presence of pyruvate and more moderately  
164 with glucose (Fig. S3C-F). We also observed that nutrient concentration affects NCC dispersion.  
165 Pyruvate at 1 mM and glucose at 5 mM present in the control medium were the most suitable  
166 conditions for NCC dispersion while either lower or higher concentrations of these nutrients failed to  
167 produce large NCC outgrowths (Fig. S4A). In addition, low concentrations of pyruvate did not  
168 support NCC spreading while at high concentrations it induced extensive NCC flattening (Fig. S4B).  
169 Glucose, in contrast, favored NCC spreading at all concentrations used (Fig. S4B).

170 All together, these results suggest that NCC dispersion relies strongly on nutrient inputs and  
171 downstream metabolic pathways. Specifically, glucose oxidation through glycolysis coupled to  
172 OXPHOS and PPP plays a pivotal role in dispersion. Pyruvate alone, which feeds only OXPHOS, is  
173 in contrast less favorable in the long-term.

174

### 175 **Metabolic Profiling of NCC Reveals a Typical OXPHOS Signature during Migration**

176 We then assessed cellular bioenergetics in NCC and measured mitochondrial respiration and  
177 glycolysis using a Seahorse XF analyzer. Analyses of the bioenergetic profiles of more than 300  
178 individual NT explants combined with MitoStress assays revealed that a great majority of the explants  
179 displayed an OXPHOS signature characterized by high oxygen consumption rate (OCR) and low  
180 extracellular acidification rate (ECAR) at 5 h (Fig. 2A), without notable changes at 24 h (Fig. 2B),  
181 suggesting that their metabolic activity was constant throughout migration. 2-DG or oligomycin

182 caused a sharp drop in OCR with no significant alteration in ECAR (Fig. 2C-E), and they strongly  
183 reduced ATP production (Fig. 2F), but had no effect on the extracellular lactate level (Fig. 2G). In  
184 contrast, 6-AN had no effect on OCR and ATP levels (Fig. 2C-F). Similar to the control condition,  
185 NT explants exposed to glucose or pyruvate only were sensitive to MitoStress (Fig. 2H). Interestingly,  
186 lower values of OCR and ECAR and ATP production were observed in pyruvate condition compared  
187 to glucose (Fig. 2H-K). 2-DG and oligomycin decreased OCR levels (Fig. 2I, J) and sharply reduced  
188 ATP production in both media (Fig. 2K), but they did not affect lactate production (Fig. 2L). Thus, a  
189 better yield in energy production is obtained for glycolysis coupled to OXPHOS than for OXPHOS  
190 fueled by pyruvate alone. Importantly, our results demonstrate that, in explants cultured with control  
191 medium, most of the ATP production relies primarily on glucose oxidation through OXPHOS, and  
192 suggest that OXPHOS inhibition does not cause metabolic rewiring to aerobic glycolysis with  
193 increased lactate production.

194 Finally, we analyzed the topological features of mitochondria network in NCC (Fig. S5). While  
195 in NCC cultured in glucose or in control medium, mitochondria had a large globular structure and  
196 were organized as rings homogeneously distributed throughout the cell body, in pyruvate medium,  
197 they were smaller, elongated, and often organized as chains extending into the cell processes (Fig.  
198 S5A). As expected, mitochondria were small and poorly organized in the absence of nutrients (Fig.  
199 S5A), as observed in the presence of oligomycin or UK-5099 (Fig. S5B), further illustrating the  
200 critical role of mitochondria in NCC.

201

### 202 **Expressions of Glucose Transporter and Glycolysis Enzymes are Regulated at the Time of** 203 **Migration**

204 To probe the link between nutrient supply and metabolic genes expression, we analyzed the  
205 expression of key players of glycolysis in NCC. The glucose transporter *Glut-1* was expressed equally  
206 on the surface of NCC in pyruvate and glucose conditions (Fig. 3A). *Glut-1* mRNA as well as those  
207 for phosphofructokinase *PFK*, a major rate-limiting enzyme of upper glycolysis (Feng et al., 2020),  
208 were clearly expressed in the NT but barely detected in NCC. In addition, they were both up regulated  
209 in the presence of glucose compared to pyruvate (Fig. 3B,C), indicating that their expression relied  
210 on nutrient supply. In contrast, phosphoglycerate kinase-1 (*PGK-1*), an enzyme of lower glycolysis,  
211 was expressed in both the NT and migrating NCC and did not show much differential expression with  
212 nutrients (Fig. 3B). In embryos, *Glut-1* and *PFK* genes were poorly expressed in the caudal trunk  
213 region except in the NT in which they were strongly but transiently up regulated at the time of NCC  
214 delamination (Fig. 3D). *PGK-1* was expressed in all tissues, but was increased in the NT during  
215 delamination.

216           These data indicate that while lower glycolysis is constantly active in migrating NCC, upper  
217 glycolysis is subjected to spatial and temporal regulation at onset of migration, therefore raising the  
218 intriguing possibilities that, in migrating NCC, lower glycolysis may be fed by exogenous metabolic  
219 intermediates possibly provided by the NT; and localized activation of glycolytic enzymes in tissues  
220 may be due to differential distribution of nutrients and metabolites in the embryo.

221

#### 222 **Glucose Metabolism Regulates *Snail-2* Expression during Delamination**

223 NCC dispersion results from multiple cellular processes acting in synergy and in concerted manner:  
224 EMT during delamination, changes of substratum and cell adhesion, activation of the locomotory  
225 machinery, and proliferation. Since higher expression of metabolic enzymes was observed upon NC  
226 emergence, we studied the role of metabolic pathways from the delamination to the migration step  
227 and developed an assay suitable for discriminating delaminated from migrating NCC on 5h NT  
228 explants (Fig. 4A). Interestingly, the number of delaminated cells was halved by addition of 2-DG,  
229 oligomycin, or Rot-AA, as well as in pyruvate medium, while in the presence of 6-AN, it was similar  
230 to control (Fig. 4B). Furthermore, *Snail-2*, a major EMT player (Duband, 2010; Nieto, 2002) was  
231 high in delaminated NCC but declined gradually as cells dispersed away from the NT in control and  
232 in glucose or 6-AN conditions, while in 2-DG or pyruvate, it was strongly diminished in both NCC  
233 compartments (Fig. 4C). In contrast, consistent with an unchanged delamination rate in response to  
234 6-AN, NCC displayed similar *Snail-2* staining under PPP inhibition (Fig. 4C). Intriguingly, with  
235 OXPHOS inhibitors and particularly with Rot-AA, *Snail-2* completely disappeared in delaminated  
236 NCC but remained high in migrating cells. Expression of *Snail-2* messengers in NT explants (Fig.  
237 4D,E) was almost totally abrogated by 2-DG and strongly diminished by oligomycin, and was low in  
238 pyruvate and no nutrient conditions, consistent with the reduction of *Snail-2* protein. Conversely,  
239 *Snail-2* expression was not much altered by Rot-AA, probably as a result of its increase in the  
240 migrating pool.

241           All together, these data indicate that glucose metabolism is required for NCC delamination by  
242 regulating the coordinated expressions of EMT-related genes and that OXPHOS under pyruvate  
243 condition is necessary but not sufficient for this process.

244

#### 245 **Glucose Metabolism is Crucial for Locomotion**

246 Avian trunk NCC display a locomotory behavior different from the ones described for cranial or  
247 enteric NCC populations (Genuth et al., 2018; Kulesa and Fraser, 1998; Li et al., 2019; Rovasio et  
248 al., 1983). Movement of individual cells involves substrate adhesion and intense protrusive activity,  
249 while outward directionality is driven by transient cell adhesion and mechanical forces resulting from

250 high cell density. To better understand the contribution of glucose metabolism to NCC locomotion,  
251 we analyzed by video microscopy the effect of metabolic inhibitors applied after initiation of NCC  
252 migration to avoid any bias due to the delamination process (Figs. 5A,B, S3G,H, S6A,B; see also  
253 Figs. 1, S2). In controls, NCC generally exhibited persistent and directional migration oriented  
254 perpendicular to the NT leading to relatively linear trajectories (Fig. S6A). Both the velocity and  
255 persistence of cells were constant over 18 h, due to maintenance of high cell density (Fig. 5A,B).  
256 With 2-DG, cells trajectories were at first relatively linear but became more random with time. The  
257 most striking effect of 2-DG, however, was a rapid and continuous decrease of velocity over time and  
258 a progressive rounding up, resulting in migration arrest. Unlike 2-DG effect, cell trajectories were  
259 generally not much affected by oligomycin, while velocity was decreased during the first 6 h.  
260 Subsequently cell migration became extremely random with decreased persistence and higher  
261 velocity linked to gradual rounding up of the cells and lack of cell-cell contacts. Interestingly, Rot-  
262 AA showed a much stronger effect than oligomycin. Trajectories were very short because velocity  
263 was almost knocked-out after 2 h and remained weak during 8 h. However, as with oligomycin,  
264 velocity increased with time and persistence decreased coincident with cell rounding up. In UK-5099,  
265 cells trajectories were more random, associated with low persistence (Fig. S3G,H). Lastly, 6-AN  
266 affected velocity strongly and gradually during the first 8 h before stabilizing, and cell trajectories  
267 became less linear (Figs. 5A,B, S6A). NCC locomotion was also impacted by nutrient supply (Figs.  
268 5C, S4C,D, S6B). In absence of nutrients, velocity was consistently low with good persistence,  
269 resulting in very short migration tracks. In glucose condition, NCC displayed long trajectories, with  
270 high and sustained velocity and persistence over time as seen in controls. In contrast, in pyruvate  
271 medium, NCC trajectories exhibited a profile similar to those seen with 2-DG, with a gradually  
272 decreasing velocity and reduced persistence (Fig. 5C, S6B). Velocity peaked for pyruvate at 1 and 2  
273 mM and plateaued for glucose concentrations  $\geq 5$  mM (Fig. S4C), in agreement with the front  
274 progression curves (Fig. 1G). Persistence, in contrast, was greater for pyruvate concentrations  $\geq 2$   
275 mM and constant for glucose concentrations  $> 1$  mM, possibly reflecting the differences observed in  
276 cell spreading (Fig. S4B).

277       These results therefore illustrate the critical contribution of glucose metabolism to NCC  
278 locomotion and also reveal that this process relies on other metabolic processes, notably PPP as well  
279 as non-energetic mitochondrial activities involving TCA metabolites and byproducts.

280

### 281 **Glucose Metabolism Coordinates Substrate and Cell Adhesions**

282 To gain insight into the impact of metabolism on cell adhesions, two pivotal aspects of NCC  
283 delamination and migration, we examined the cellular localization of paxillin and  $\beta$ -catenin, two

284 cytoplasmic partners of integrins- and cadherins-adhesion complexes, respectively (Figs. 5D,E,  
285 S6C,D). Compared to controls, at 5 h, the number of substrate adhesions per NCC was significantly  
286 reduced with 2-DG and increased with oligomycin, consistent with changes in cell spreading (Fig.  
287 5D). In addition, oligomycin increased substantially cell-cell adhesions during the first 5 h (Fig. S6C).  
288 The number of substrate and cell-cell adhesions depended on the nutrient supplies (Fig. 5E, S6D). In  
289 control and glucose medium, NCC exhibited large substrate adhesions with a four- and two-fold  
290 increase in their number at 24 h, respectively (Fig. 5E). In contrast, in pyruvate medium, NCC  
291 displayed more elongated substrate adhesions, which did not increase in number with time. In no  
292 nutrient condition, NCC developed substrate adhesions at 5 h but their number decreased with time.  
293 Quantification of cell-cell adhesions revealed that in control as well as in glucose medium, NCC are  
294 always engaged in transient contacts with 1-3 neighbors while in pyruvate, they remain as individuals  
295 (Fig. S6D).

296         These data indicate that glucose metabolism regulates the balance between substrate and cell-  
297 cell adhesion in NCC, thereby favoring optimal conditions for delamination and migration.

298

### 299 **NCC Mechanics and Response to External Stiffness are Modulated by Nutrient Inputs**

300 NCC are able to sense the extracellular matrix rigidity in their environment, which in turn modulates  
301 their adhesion and migration capacity (Chevalier et al., 2016; Shellard and Mayor, 2021). To  
302 determine whether mechanotransduction activities in NCC are under metabolic control, we  
303 investigated the impact of nutrients on their adhesive and migratory response to fibronectin-coated  
304 polyacrylamide gels with different stiffness in the range of tissue rigidity at early embryonic stages,  
305 from soft (1.2 kPa) to stiff (6.3 kPa) (Chevalier et al., 2016; Discher et al., 2005). We first  
306 characterized and quantified NCC substrate adhesions (Fig. 5F, S6E), velocity and persistence (Fig.  
307 5G), and migration front progression (Fig. 5H). As on glass (Fig. 5D), NCC on stiff and soft gels  
308 developed substrate adhesions irrespective of the nutrient supplied (Fig. S6E). Moreover, we found  
309 important discrepancies in NCC response to gel rigidity with the nutrients (Fig. 5F-H). In glucose  
310 medium, the number of substrate adhesions in individual NCC and the progression of the population  
311 were not significantly different between stiff and soft gels and individual cell velocity and persistence  
312 were only slightly lower on soft gels. In contrast, in pyruvate and control medium NCC displayed  
313 less substrate adhesions on soft gels than on stiff gels, and their velocity and the progression of the  
314 population were significantly lower.

315         We then studied NCC stiffness and traction activity on the gel using atomic force and traction  
316 force microscopy (AFM, TFM) (Fig. 5I-K). Interestingly, measurement of cellular stiffness on gels  
317 revealed that in glucose and control medium NCC adapted their stiffness to that of the substrate in

318 both soft and stiff gels, whereas in pyruvate they failed to increase their stiffness to the level of the  
319 gel when confronted with stiff gel (Fig. 5I). Comparison of NCC traction activity in soft and stiff gels  
320 expressed as force or stress/cell showed that it was constant in glucose whereas in pyruvate and  
321 control medium it was higher in stiff gels, though very heterogeneous (Fig. 5J, K)). Finally, by  
322 calculating the product of the average force and the average displacement per hour, we estimated the  
323 energy produced during NCC displacement on the soft and stiff gels under the different nutrient  
324 conditions. Energy produced was similar in all nutrients on stiff gels, while it was lower on soft gels  
325 in control and pyruvate medium compared to glucose in which it was almost unchanged (Table I).

326 These data indicate that trunk NCC are mechano-responsive as described previously for cranial  
327 and enteric NCC (Chevalier et al., 2016; Shellard and Mayor, 2021), but that their response is  
328 determined by specific metabolic activities. In glucose medium, owing to their capacity to  
329 accommodate their stiffness and energy production to their environment, NCC are endowed with the  
330 ability to migrate in a great diversity of biophysical constraints. In pyruvate medium, NCC are less  
331 prone to modulate their stiffness and negatively respond to modifications in the rigidity of their  
332 environment by decreasing their adhesive and migratory response.

333

#### 334 **Glucose Metabolism is Required for Sustained Proliferation**

335 Contrary to many motile cells, NCC maintain active cell division throughout migration, and although  
336 this process by itself is not the driving force of migration, it is required for delamination (Burstyn-  
337 Cohen and Kalcheim, 2002) and contributes strongly to expansion of the population (Ridenour et al.,  
338 2014). We studied the impact of metabolic inhibitors on NCC proliferation. While, in control  
339 numerous proliferating (EdU<sup>+</sup>) NCC could be identified during their delamination along the NT apical  
340 side, only few proliferative cells were observed with glycolysis or OXPHOS inhibitors (Fig. S7A).  
341 These results indicate the contribution of glycolytic and mitochondrial intermediates in NCC  
342 proliferation during delamination. During migration, all inhibitors decreased both the proportion of  
343 EdU<sup>+</sup> NCC and the EdU-staining intensity (Fig. S7B). Interestingly, unlike other compounds, the  
344 impact of 6-AN on proliferation decreased over time, possibly reflecting the contribution of other  
345 metabolic pathways to the adaptation to PPP inhibition. With no nutrient, proliferation was low at 5  
346 h and was almost abolished after 24 h. Interestingly, consistent with the kinetics of their dispersion  
347 (see Fig. 1G), NCC proliferation observed in glucose was similar to that of controls whereas it was  
348 dramatically reduced after 24 h in pyruvate (Fig. S7C).

349 These data reveal that all metabolic pathways are implicated in a cooperative manner in the  
350 control of NCC proliferation.

351

352 **Pluripotency and Fate Decision are Dictated by Exogenous Nutrient Inputs**

353 To investigate whether metabolic activity affects NCC stem cell capacity and influences their fate,  
354 we analyzed the expression patterns of the transcription factors Sox-10 and Foxd-3, two essential  
355 regulators of NCC pluripotency (Lukoseviciute et al., 2018; Schock and LaBonne, 2020; Simões-  
356 Costa et al., 2012). At 5 h in control, the vast majority of migrating NCC as well as some delaminating  
357 cells exhibited Sox-10<sup>+</sup> nuclei, a pattern that mirrors that of Snail-2 (Fig. 6A, compare with Fig. 4C).  
358 2-DG strongly diminished the number of Sox-10<sup>+</sup> cells leaving a few remaining strongly-expressing  
359 cells while oligomycin and Rot-AA caused an overall reduction of Sox-10 staining intensity in all  
360 NCC (Fig. 6A). Likewise, *Sox-10* and *Foxd-3* mRNA levels dropped strongly with 2-DG and more  
361 moderately with oligomycin and Rot-AA (Fig. 6B). In addition, *Foxd-3* expression was selectively  
362 repressed by 2-DG, oligomycin or Rot-AA in pre-migratory NCC but less so in delaminating and  
363 migrating cells (Fig. 6C). Levels of *Sox-10* and *Foxd-3* messages and proteins were also much  
364 reduced in delaminating and migrating NCC cultured in pyruvate medium or with no nutrient  
365 compared with glucose (Fig. 6A-C). At 24 h (Fig. S8A,B), repression of *Sox-10* and *Foxd-3*  
366 expression was even more pronounced in the presence of metabolic inhibitors, including 6-AN, or in  
367 absence of glucose. These results indicate that sustained glucose metabolism is required for  
368 maintenance of high levels of pluripotency markers during NCC migration.

369 We next searched for the appearance of differentiated cells in culture over time and analyzed  
370 the kinetics of expression of markers of NCC differentiation into the neural, melanocytic, and  
371 myofibroblastic/mesenchymal lineages. Because of the long-term deleterious effects of the metabolic  
372 inhibitors and lack of nutrient on NCC, we only examined cells cultured in the presence of pyruvate,  
373 glucose or both (Fig. 6D, S1C, S8C). In pyruvate medium, expansion of the NCC population stalled  
374 during the first day of culture and cell morphologies gradually shifted predominantly to a large,  
375 flattened fibroblastic shape after 3 days (Fig. S8C). In glucose medium in contrast, the NCC  
376 population steadily expanded, both in the cell number and in the area occupied, accompanied by the  
377 appearance of neurons and other cells presenting a great diversity of morphologies. In addition, the  
378 number of cells with a NCC shape did not decrease as dramatically as in the presence of pyruvate  
379 (Fig. S8C). In glucose medium, the proportion of NCC progenitors (Sox-10<sup>+</sup> and HNK-1<sup>+</sup>) remained  
380 high over time (> 75%) while the number of neurons (Tuj-1<sup>+</sup>, Sox-10<sup>-</sup> and HNK1<sup>+</sup>) and melanoblasts  
381 (MITF<sup>+</sup>, Sox-10<sup>+</sup> and HNK1<sup>-</sup>) increased up to 20% (Fig. 6D). In pyruvate medium, the proportion of  
382 NCC progenitors (Sox-10<sup>+</sup>) dropped to less than 50% at the benefit of myofibroblasts ( $\alpha$ -SMA<sup>+</sup> and  
383 Sox-10<sup>-</sup>), which peaked to about 40%. Of note, the number of melanoblasts did not increase much in  
384 pyruvate medium while the number of HNK1<sup>+</sup> cells was constantly very low. A likely explanation

385 for this persistent absence of HNK-1 staining is that the HNK-1 epitope is a glycoconjugate moiety  
386 and needs glucose for its biosynthesis (Tucker et al., 1984).

387 Our results indicate that NCC differentiation programs are dependent on nutrient inputs, with  
388 glucose favoring neural and melanoblast differentiation, while pyruvate promotes a limited range of  
389 phenotypes where myofibroblasts are predominant.

390

## 391 **DISCUSSION**

392 Our study gives a general view of the metabolic impacts on NC development. We report that trunk  
393 NCC display a typical OXPHOS signature and that glucose oxidation through glycolysis coupled to  
394 OXPHOS plays a critical role in NCC dispersion. Blockers of glycolysis and OXPHOS affected every  
395 aspect of NCC development and caused alterations of mitochondria morphology associated with a  
396 sharp drop in mitochondrial respiration and ATP production. Additionally, our data establish that,  
397 though necessary for trunk NCC development, OXPHOS is not sufficient to support all the cellular  
398 events involved in this process as systematic inhibition of glycolysis compromised NCC dispersion,  
399 even in the presence of pyruvate to support OXPHOS. Likewise, a PPP inhibitor strongly affected  
400 NCC dispersion despite a minimal effect on mitochondrial respiration and ATP production. Finally,  
401 pyruvate alone failed to support complete dispersion, division, survival, and differentiation of NCC,  
402 while glucose could elicit the complete cellular response of NCC, i.e. delamination, adhesion,  
403 migration, proliferation, maintenance of stemness, and widespread differentiation. Glucose also  
404 potentiates NCC stiffness adaptation to that of their microenvironment and supports optimal  
405 dispersion, illustrating the prominent role of glucose metabolism in NCC adaptation to physical  
406 changes in the environment. Thus, contrary to the general assertion that OXPHOS has a bioenergetic  
407 role in differentiated cells and that aerobic glycolysis has a biosynthetic role in proliferating non-  
408 differentiated stem cells (Ito and Suda, 2014; Shyh-Chang et al., 2013), NCC development relies on  
409 the concerted and sustained mobilization of all metabolic pathways dependent on glucose  
410 metabolism, i.e. glycolysis, OXPHOS, and PPP, cooperating together (Fig. 7). These findings  
411 illustrate the necessity for the NCC population to make the most of the potential of the carbon  
412 metabolism route, so that they are endowed with the capacity to meet the high metabolic demands  
413 suitable for the coordinated execution of diverse cellular events, in a minimum of time and in a rapidly  
414 evolving environment.

415 How NCC maintain balanced activities of the different metabolic pathways is currently  
416 unknown. This may be achieved through regulated levels of metabolic enzymes and products of each  
417 pathway, under the control of intrinsic genetic programs as well as extrinsic factors, including nutrient

418 availability and demand (Lempradl et al., 2015). This view is supported by our observations as well  
419 as a recent report (Oginuma et al., 2017) that glycolytic enzymes are not uniformly expressed in the  
420 embryo at the time of NCC dispersion. Alternatively, the uncoupling protein UCP2, the ATPase  
421 inhibitory factor IF1, and the pyruvate dehydrogenate kinase PDK, known to suppress coupling  
422 between glycolysis and OXPHOS or to block mitochondrial activity, may contribute to metabolic  
423 rewiring in pluripotent stem cells (Sánchez-Aragó et al., 2013; Takubo et al., 2013; Zhang et al.,  
424 2011). It will be of interest to investigate whether expression of these players is subjected to  
425 spatiotemporal regulation in NCC.

426 We found no evidence for a significant contribution of a Warburg effect to trunk NCC  
427 development. Indeed, ECAR assessments and lactate measurements both revealed low lactate  
428 production in NCC, demonstrating that glucose is not used for ATP production through lactate  
429 production, but serves to fuel OXPHOS, PPP, and possibly amino acid pathways for biosynthetic  
430 purposes. Moreover, the fact that oligomycin did not increase lactate levels indicate that glucose  
431 metabolism cannot be rewired from OXPHOS to aerobic glycolysis in NCC. Our conclusion contrasts  
432 with a recent report proposing that, similarly to cancer cells, cranial NCC display a Warburg effect  
433 (Bhattacharya et al., 2020). The difference in metabolic activity between cranial and trunk NCC is  
434 likely to reside in the local O<sub>2</sub> concentration in their environment. As for cancer cells in which hypoxia  
435 is known to promote metastatic spread (Semenza, 2012), cranial NCC reside in a hypoxic milieu,  
436 which favors prolonged NCC production from the NT through maintenance of EMT gene expression.  
437 Exposure to high O<sub>2</sub> levels or knockdown of the hypoxia-inducible factor HIF-1 cause strong  
438 reduction of *Snail-2* expression and attenuation of NCC production (Scully et al., 2016). Trunk NCC  
439 dispersion in contrast is intimately associated with blood vasculature (Schwarz et al., 2009; Thiery et  
440 al., 1982), and it is not affected by high O<sub>2</sub> levels or by deletion of the HIF-1 gene (Iyer et al., 1998;  
441 Morriss and New, 1979). Our data therefore indicate that trunk NCC display metabolic requirements  
442 distinct from their cranial counterparts and reveal that, although they possess in common with  
443 metastatic cells a number of cellular and molecular features, such as signaling pathways, EMT,  
444 migration properties and gene circuits, they do not share with them the same metabolic status. This  
445 reflects the strong adaptability of NCC to a great variety of environmental conditions throughout  
446 development, at the origin of the diversity in their migratory behaviors and fates.

447 We could not attribute to any metabolic pathway a specific role in the basic cellular processes,  
448 adhesion, locomotion and division. For example, despite PPP having a well-recognized role in  
449 nucleotide synthesis and maintenance of cellular redox balance (Patra and Hay, 2014), this pathway  
450 was not recruited solely for NCC proliferation but significantly contributed to cell velocity and  
451 persistence of movement as well. Likewise, OXPHOS and ATP production in mitochondria were not

452 exclusively aimed at supporting active migration, but also played a key role in EMT and proliferation.  
453 A likely explanation is that these processes are extremely demanding in both bioenergetic and  
454 biosynthetic supplies (Zanotelli et al., 2021)(Salazar-Roa and Malumbres, 2017). Another reason is  
455 that enzymes, metabolites and byproducts of metabolic pathways are known to influence cellular  
456 programs independently of their canonical bioenergetics and biosynthetic roles (Miyazawa and  
457 Aulehla, 2018). NADH produced through TCA protects cells from oxidative stress (Bigarella et al.,  
458 2014; Khacho et al., 2016). This is illustrated by our observation that Rot-AA exhibit a stronger effect  
459 on NCC than oligomycin. Likewise, similarly to neurons (Herrero-Mendez et al., 2009), the use of  
460 the PPP for metabolizing glucose may ensure NADPH production for the maintenance of a cellular  
461 redox balance. TCA cycle intermediates, in particular acetyl-CoA and  $\alpha$ -ketoglutarate, are involved  
462 in epigenetic regulation through histone acetylation and methylation (Kaelin and McKnight, 2013).  
463 Regulation of gene expression during NCC formation is under tight epigenetic control, involving  
464 DNA methylation, histone modifications, and ATP-dependent chromatin remodelers (Hu et al.,  
465 2014). Our finding of complete reprogramming of gene circuits driving entire developmental  
466 programs such as delamination and maintenance of stemness upon manipulating nutrient availability  
467 and metabolic pathways in NCC is therefore in favor of a direct role of cellular metabolism in  
468 regulation of nuclear transcription programs in NCC through epigenetic regulation.

469 An intriguing finding in our study is related to the effect of pyruvate on NCC differentiation  
470 and fate decision. Consistent with previous studies showing that mitochondrial pyruvate metabolism  
471 represses stem cell state and proliferation (Schell et al., 2017), we found that providing pyruvate to  
472 NCC in absence of glucose caused cell cycle arrest and loss of stem cell markers, but contrary to what  
473 has been reported for many other embryonic and stem cells (Ito and Suda, 2014; Khacho et al., 2016;  
474 Khacho and Slack, 2017; Shyh-Chang et al., 2013), it biased differentiation to a limited range of cell  
475 types where myofibroblasts predominate. In the embryo, myofibroblasts do not normally derive from  
476 trunk NCC but are only provided by cranial NCC. However, in *ex vivo* cultures in the presence of  
477 various hormones and growth factors (Dupin et al., 2018), myofibroblasts were recorded in trunk  
478 NCC progeny, together with skeletogenic and adipogenic cells. These data have been interpreted as  
479 a dormant capacity of trunk NCC to differentiate into non-neural derivatives normally obtained with  
480 cranial NCC. Our observation that myofibroblastic differentiation occurs essentially in pyruvate  
481 conditions in the complete absence of additives suggests that this dormant capacity can be uncovered  
482 by pyruvate, thereby illustrating the key role of metabolism in instructing NCC fate.

483 In conclusion, our data show that, contrary to pluripotent stem cells and cancer cells, NCC in  
484 the embryonic trunk region rely primarily on glucose oxidation through glycolysis and mitochondrial  
485 respiration for energy production and mobilize a large range of metabolic pathways downstream

486 glucose uptake to meet their important bioenergetics and biosynthetic needs as well as to instruct their  
487 gene circuits driving their behavior and fate. These findings therefore reveal the intricate integration  
488 of cellular metabolism to basic cellular processes underlying cell behavior. How these metabolic  
489 pathways are regulated to accommodate the different steps of NCC formation both temporally and  
490 spatially remains to be investigated.

491

## 492 **MATERIALS AND METHODS**

### 493 **Reagents**

494 Bovine plasma fibronectin (1mg/ml stock) was from Sigma (cat. no. F1141). Dispase II at 5 U/ml  
495 stock solution in Hanks' balanced saline was from Stemcell Technologies (cat. no. 07913). The  
496 following chemicals were prepared and used according to the manufacturers' guidelines: 2-deoxy-D-  
497 glucose (2-DG, Sigma, cat. no. D8375), Na-iodoacetate (Sigma, cat. no. I2512), oligomycin-A  
498 (Sigma, cat. no. 75351), rotenone (Sigma, cat. no. R8875), antimycin-A (Sigma, cat. no. A8674),  
499 FCCP (Sigma, cat. no. C2920), 6-aminonicotinamide (6-AN, Cayman Chemicals, cat. no. 10009315),  
500 and UK-5099 (Tocris Biosciences, cat. no. 4186). 2-DG was prepared as a 1 M stock solution in  
501 glucose-, pyruvate- and glutamine-free DMEM and used at 5-10 mM; Na-iodoacetate was prepared  
502 as a 15 mM stock solution in H<sub>2</sub>O and used at 15 μM; oligomycin, rotenone, antimycin-A, and FCCP  
503 were prepared in DMSO as 100 μM stock solutions and used at 1 μM; 6-AN was prepared as 100  
504 mM solution in DMSO and used at 100 μM, except in Seahorse analyses where it was used at 500  
505 μM. UK-5099 was prepared as 100 mM solution in DMSO and used at 100 μM.

506

### 507 **Cell Culture**

508 **Generation of NCC primary cultures:** NCC cultures were produced from NT explants obtained  
509 from quail embryos (*Coturnix coturnix japonica*) as described (Duband et al., 2020). Briefly,  
510 fertilized eggs purchased from a local farm (La Caille de Chanteloup, Corps Nuds, France) were  
511 incubated at 37-38°C for 54 h until the embryos reached stages corresponding to the chick stages 13-  
512 15 of Hamburger and Hamilton (HH) (1951), i.e. comprising 19-25 somite pairs. The eggshell was  
513 opened with curved dissecting scissors and the yolk transferred into phosphate-buffered saline (PBS).  
514 The embryo was cut off from the yolk and transferred into PBS in an elastomer-containing dish. An  
515 embryo portion of about 750-μm long was excised at the level of the last 5 somites with a scalpel  
516 under a stereomicroscope and subjected to mild enzymatic digestion by treatment with dispase II at  
517 2.5 U/ml for 5-10 minutes at room temperature. The NT was dissected out manually using fine  
518 dissection pins under a stereomicroscope, freed from the surrounding tissues, and transferred for 30-

519 60 minutes in DMEM medium (no glucose, no pyruvate, Gibco, cat. no. 11966025) supplemented  
520 with 0.5% fetal bovine serum for recovery from enzyme treatment. NT were explanted onto culture  
521 dishes or coverglasses previously coated with fibronectin at 10  $\mu\text{g}/\text{ml}$  in PBS (i.e. about 5  $\mu\text{g}/\text{cm}^2$ )  
522 for a minimum of 1 h at 37°C. To ensure rapid initiation of NCC migration, NT were positioned with  
523 their dorsal side oriented down toward the substratum. Explants were cultured at 37°C under  
524 normoxic conditions in a humidified 5%-CO<sub>2</sub> incubator in DMEM containing 1% serum, 100 U/ml  
525 penicillin, 100  $\mu\text{g}/\text{ml}$  streptomycin, and 2 mM glutamine, and supplemented or not with 5 mM  
526 glucose and 1 mM pyruvate. The choices of the culture dish, culture medium, and duration of the  
527 culture were determined according to the purpose of the experiment and the method of analysis used  
528 (see below). Throughout each experiment, the morphology of the NT explant, area and progression  
529 of the NCC outgrowth, as well as individual cell shape and viability were evaluated, imaged, and  
530 assessed regularly under an inverted phase contrast Nikon microscope equipped with 6.3X, 10X, and  
531 20X objectives.

532

533 **Delamination assay:** NT explants were cultured for 5 h, a time sufficient to allow NCC segregating  
534 from the dorsal NT to adhere to the substrate. NT was then removed manually from the dish using  
535 fine dissection pins under a stereomicroscope or by gentle flushing of culture medium with a pipet  
536 tip, to uncover delaminated cells.

537

### 538 **Cellular Bioenergetic Analyses**

539 Bioenergetic profiles of NCC primary cultures were determined using a Seahorse Bioscience XF24  
540 Analyzer. A single NT explant was deposited precisely at the center of each well of 24-well Seahorse  
541 plate previously coated with fibronectin in culture medium at 37°C in a humidified 5%-CO<sub>2</sub>  
542 incubator, and NCC were allowed to undergo migration. Before preparation of the plate for Seahorse  
543 analysis, the areas of the NT explants were measured for normalization. Cultures were then rinsed in  
544 Seahorse XF medium (Agilent, cat. no 103575-100) without serum and incubated for 1 h at 37°C in  
545 normal atmosphere. Following incubation, the Seahorse assay was run according to the  
546 manufacturer's instructions. Oxygen consumption rate (OCR) and extracellular acidification rate  
547 (ECAR) values, as readouts of basal mitochondrial respiration and glycolysis respectively, were  
548 assessed regularly every cycle (mix, wait and measurement during 3 minutes), the basal measurement  
549 consisting of 4 cycles and drug injections, 3 cycles during 30 minutes. The key parameters of  
550 mitochondrial respiration (ATP-linked respiration, maximal respiratory capacity and proton leak)  
551 were measured by means of a MitoStress test after sequential additions of oligomycin (1  $\mu\text{M}$ ), FCCP  
552 (0.75  $\mu\text{M}$ ), and Rot-AA (1  $\mu\text{M}$ ) through 3 cycles of measurements in 30 minutes. When appropriate,

553 NCC primary cultures were processed after Seahorse analysis for immunolabeling, qPCR analysis,  
554 or intracellular ATP level and lactate measurement.

555

556 **ATP and lactate measurements:** Intracellular ATP and extracellular lactate levels were measured  
557 for each NCC primary cultures after Seahorse analysis using an ATPlite Bioluminescence assay kit  
558 from PerkinElmer (cat. no. 6016943) and the Lactate Fluorometric Assay kit from BioVision (cat.  
559 no. K607), respectively, according to the manufacturers' instructions.

560

#### 561 **Fluorescence Labeling of NCC Cultures**

562 For immunolabeling, the following primary antibodies were used: Rabbit monoclonal antibody  
563 (mAb) to Snail-2 (clone C19G7, Cell Signaling, 1/300), mouse mAb to Sox-10 (Clone A2, Santa  
564 Cruz, 1/200), mouse mAb to  $\beta$ -catenin (clone 14, BD-Transduction Laboratories, 1/200), mouse mAb  
565 to paxillin (Clone 165, BD-Transduction Laboratories, 1/100), mouse mAb to  $\alpha$ -SMA conjugated to  
566 Cy3 (Clone 1A4, Sigma, 1/300), mouse mAb to  $\beta$ III-tubulin conjugated to Alexa488 (Clone Tuj-1,  
567 R&D Systems, 1/500), mouse mAb to HNK-1 described previously ((Tucker et al., 1984), undiluted  
568 culture supernatant), mouse mAb to MITF (clone C5, Abcam, 1/200), and mouse mAb to Glut-1  
569 (Ab14683, Abcam, 1/50). Filamentous actin was detected using Texas Red<sup>TM</sup>-X Phalloidin  
570 (Molecular probe, cat. no. T7471). NCC primary cultures were performed in 4-well plates or in 8-  
571 well Chambered Coverglass (Nunc, cat. no. 154511) coated with fibronectin, and fixed in 4%  
572 paraformaldehyde (PFA) in PBS for 15 minutes at room temperature for detection of all antigens,  
573 except for Snail-2 (5 minutes in 4% PFA),  $\beta$ -catenin (45 minutes in 1.5% PFA), and Glut-1 (see  
574 below). After permeabilization with 0.5% Triton X-100 in PBS for 15 minutes, cultures were blocked  
575 in PBS-3% BSA and subjected to immunofluorescence labeling using primary antibodies followed  
576 by incubation with appropriate secondary Ab conjugated to Alexa-fluor 488, Cy-3 or Cy-5 (Jackson  
577 Immunoresearch Laboratories), and processed for DAPI or Hoechst staining to visualize cells' nuclei  
578 before mounting in ImmuMount medium (Shandon). For Glut-1 immunolabeling, unfixed NCC  
579 cultures were incubated with the Glut-1 antibody diluted in DMEM for 15 minutes at 15°C to avoid  
580 antibody internalization and immediately fixed in 100% ethanol at -20°C before rinsing in PBS and  
581 secondary antibody treatment. For labeling of mitochondria, MitoTracker Red (Invitrogen, cat. no.  
582 M7512) was added at 1  $\mu$ M to unfixed cultures and incubated for 20-30 minutes at 37°C. After washes  
583 with 37°C pre-warmed PBS, cells were briefly fixed with 4% PFA and mounted. Preparations were  
584 observed with a Zeiss AxioImager M2 epifluorescence microscope equipped with 10X-63X  
585 fluorescence objectives (Acroplan 10X/0.25, 20X/0.45, Plan-Neofluar 40X/0.75 and 63X/1.25 oil)

586 or with a Zeiss LSM 900 confocal microscope equipped with 10X-40X fluorescence objectives (Plan-  
587 Apochrome 40X/1.30 oil). Data were collected using the Zen or Airyscan2 software and processed  
588 using ImageJ software. For each series of experiments, images were acquired using equal exposure  
589 times and settings.

590

### 591 **In Situ Hybridizations for mRNA Detection on NCC Primary Cultures and Whole Mount** 592 **Embryos**

593 The following plasmids for mRNA probe synthesis were used: *Snail-2* from A. Nieto, *Foxd-3* from  
594 C. Erickson, *Sox-10* from P. Scotting, *Glut-1*, *PFK*, *PGK-1* and *PKM* from O. Pourquié. Linearized  
595 plasmid DNA was used to synthesize digoxigenin-UTP (Roche) labeled antisense probes with RNA  
596 polymerases from Promega and RNA probes were purified with Illustra ProbeQuant G-50  
597 microcolumns (GE Healthcare). In situ hybridizations were performed either on NCC primary  
598 cultures produced in fibronectin-coated plastic dishes or on whole mount intact embryos collected at  
599 the appropriate developmental stages, using essentially the same procedure. Samples of embryos and  
600 cultures were fixed in 4% PFA in PBS for 2 h at room temperature or overnight at 4°C. They were  
601 hybridized overnight at 65°C with the digoxigenin-UTP-labeled RNA probes in 50% formamide,  
602 10% dextran sulfate and Denhart's buffer (0.5 µg probe/ml hybridization buffer) and washed twice  
603 in 50% formamide, 1x SSC and 0.1% Tween-20 at 65°C, then 4 times at room temperature in 100  
604 mM maleic acid, 150 mM NaCl pH 7.5 and 0.1% Tween-20 (MABT buffer). After a 1-h pre-  
605 incubation in MABT buffer containing 10% blocking reagent (Roche) and 10% heat-inactivated lamb  
606 serum, samples were incubated overnight at room temperature with the anti-digoxigenin antibody  
607 (Roche). After extensive rinsing with MABT buffer, they were preincubated in 100 mM NaCl, 50  
608 mM MgCl<sub>2</sub>, 1% Tween-20, and 25 mM Tris-HCl, pH 9.5, and stained with NBT-BCIP (Roche)  
609 following manufacturer's guidelines. Preparations were observed and imaged with a Nikon  
610 stereomicroscope and data analyzed with ImageJ software.

611

### 612 **RNA Quantification by Quantitative RT-PCR Analyses**

613 Total RNA of cells from cultures of 5-8 NT explants were extracted using the Ambion PureLink RNA  
614 Mini Kit (Invitrogen, cat. no. 12183018A) following the manufacturer's guidelines. After  
615 quantification of RNA concentration, double-strand cDNA was synthesized from RNA using  
616 SuperScript IV reverse transcriptase (Invitrogen, cat. no. 18090050). Quantitative real time PCR were  
617 performed using the Power Syber Green Master Mix (Applied Biosystems, cat. no. 4368708) in a  
618 StepOne Plus RT-PCR apparatus (Applied Biosystems). Gene expression was assessed by the  
619 comparative CT ( $\Delta\Delta C_t$ ) method with  $\beta$ -actin as the reference gene. The following primers were used:

620 *Snail2fwd* GATGCGCTCGCAGTGATAGT; *Snail2rev* AGCTTTCATACAGGTATGGGGATA;  
621 *Sox10fwd* CGGAGCACTCTTCAGGTCAG; *Sox10rev* CCCTTCTCGCTTGGAGTCAG; *Foxd3fwd*  
622 TCTGCGAGTTCATCAGCAAC; *Foxd3rev* TTCACGAAGCAGTCGTTGAG; *Glut1fwd*  
623 AAGATGACAGCTCGCCTGATG; *Glut1rev* AGTCTTCAATCACCTTCTGCGG; *PFKfwd*  
624 TTGGAATTGTCAGCTGCCCCG; *PFKrev* TGCAGACAACCTTTCATAGGCATCAG;  *$\beta$ Actinfwd*  
625 CTGTGCCCATCTATGAAGGCTA;  *$\beta$ Actinrev* ATTTCTCTCTCGGCTGTGGTG.

626

### 627 **Cell Proliferation Assay**

628 Cell proliferation in culture was monitored using the Plus EdU Cell proliferation kit for imaging from  
629 Life Technologies (cat. no. C10638). Briefly, NCC primary cultures were generated on fibronectin-  
630 coated coverglasses as for immunolabelings and were incubated with EdU at 20  $\mu$ M in culture  
631 medium for 1 h at varying times of NCC development. Immediately after EdU incorporation, cultures  
632 were fixed in 4% PFA in PBS for 15 minutes at room temperature, permeabilized in 0.5 Triton-X100  
633 for 15 minutes and treated for EdU detection using Alexa-555 Fluor azide in accordance with the  
634 manufacturer's guidelines. After DNA staining with Hoechst, cultures were optionally processed for  
635 immunostaining and analyzed as described for immunolabelings.

636

### 637 **Cell Locomotion Assays**

638 NCC primary cultures were performed in 8-well Chambered Coverglass coated with fibronectin. Up  
639 to 4 NT explants were distributed separately into each well, and were maintained at 37°C in a  
640 humidified 5%-CO<sub>2</sub> incubator for about 2 h until the NT adhered firmly to the dish and NCC initiated  
641 migration on the substratum; then the cultures were transferred into a heated chamber (Ibidi) with a  
642 humid atmosphere containing 5% CO<sub>2</sub>/95% air placed on the motorized stage of a Leica DMIRE2  
643 microscope equipped with a CoolSNAP HQ camera (Roper Scientific). Time-lapse video microscopy  
644 was performed with a 10x objective and phase contrast images were captured every 5 minutes during  
645 16-24 h using the Micromanager software. Trajectories and positions of individual NCC in several  
646 explants recorded in parallel were tracked using Metamorph 7 software. The velocity of each cell was  
647 calculated as the ratio between the total length of its trajectory and the duration of the acquisition  
648 time and the persistence of movement as the ratio between the linear distance from the cell's initial  
649 to final positions and the total distance covered by the cell. Evolution of speed and persistence every  
650 hour were determined. The progression of the migratory front of the NCC population every hour was  
651 measured using a custom GUI written in Matlab® (MathWorks®, Natick, Massachusetts, USA).

652

### 653 **Preparation of polyacrylamide gels**

654 Polyacrylamide (PAA) gels were prepared on 32-mm glass coverslips and 8-well Chambered  
655 Coverglass for AFM and TFM experiments, respectively. The surface on which the PAA gels were  
656 polymerized was activated by immersion into a solution of 3-methacryloxypropyltrimethoxysilane  
657 (0.3%, Bind-Silane, Sigma, cat. no. 440159), 10% acetic acid aqueous solution (3%) in absolute  
658 ethanol during 3 minutes to enhance gel adhesion, washed 3 times with ethanol, and air-dried for 45  
659 minutes. Thin sheets of PAA gel of different elastic properties were prepared from concentrations of  
660 acrylamide/bisacrylamide 5%/0.225% and 3%/0.08%, supplemented with 0.5% ammonium  
661 persulfate and 0.05% tetramethylethylenediamine (Sigma) in H<sub>2</sub>O. Practically, for AFM experiments,  
662 81  $\mu$ l of these different mixtures were placed onto the surface of a 32 mm-diameter coverslip and  
663 covered with 14 mm-diameter coverslip. For immunostaining and video microscopy experiments, 2.5  
664  $\mu$ l of the mixtures were placed in the wells of 8-well chambered Coverglass and covered with a 6  
665 mm-diameter coverslip. Top coverslips were treated previously with Repel-Silane ES (Merck, cat.  
666 no. GE17-1332-01) during 5 minutes to prevent PAA gel adhesion. After 30 minutes of  
667 polymerization, the top coverslips were removed and the PAA gels were rinsed 3 times with PBS,  
668 treated twice for 5 minutes with sulfo-SANPAH, UV-photoactivated with Bio-Link Crosslinker  
669 BLX-E254 (Biotech), and rinsed 3 times with 50mM HEPES at pH 8.5. For traction force microscopy  
670 experiments, the gel mixtures contain FluoSpheres from Sigma (TM carboxylate modified, 0.2 $\mu$ m,  
671 red (580/605), cat. no. F8810), at 1/50 dilution. A solution of fibronectin was layered onto the PAA  
672 gels at 30 $\mu$ g/cm<sup>2</sup> and incubated overnight at 4°C under agitation.

673

#### 674 **AFM assessments on polyacrylamide gels and NCC**

675 The elastic modulus for both PAA gels and NCC cultured for 4-6 h was assessed by AFM JPK  
676 NanoWizard Sence+ (Brucker, Billerica, Massachusetts, U.S.A) coupled to a Zeiss Axio-Observer  
677 z1 inverted microscope, as described previously (Ben Bouali et al., 2020) using  $\mu$ Mash CSC38/NO  
678 AL probes (MikroMasch<sup>®</sup>, Sofia, Bulgaria). PAA gels and NCC were set in culture medium  
679 containing 25mM HEPES and maintained at 37°C. For PAA gels, measurements were achieved  
680 considering a measuring point grid with 0.4- $\mu$ m meshes over a 4.8 $\times$ 4.8  $\mu$ m<sup>2</sup> surface set in gel center.  
681 For NCC, measurements were achieved considering a measuring point grid with 1- $\mu$ m mesh over a  
682 12 $\times$ 12  $\mu$ m<sup>2</sup> surface set on cells using visual inspection with a phase contrast microscope. Setting  
683 Poisson's ratio  $\nu = 0.5$  for both PAA gels and NCC, AFM spectroscopy curves were analyzed  
684 according to (Bilodeau, 1992), for quadrilateral pyramid probe using a home written program in  
685 Matlab<sup>®</sup>. The elastic modulus of the PAA gels prepared with proportion of acrylamide/bisacrylamide  
686 5%/0.225% and 3%/0.08% were of 6320 +/- 25 Pa and 1250 +/- 32 Pa (S.E.M), respectively, and  
687 were referred in the text as stiff and soft gels.

688

### 689 **TFM assessments**

690 NT explants were cultured onto bead-embedded PAA gels in various nutrients for 4-6 h and  
691 transferred into a heated chamber with a humid atmosphere containing 5% CO<sub>2</sub>/95% air placed on  
692 the motorized stage of a Zeiss LSM 900 confocal microscope. A specific injector connected to 8-well  
693 Chambered Coverglass was designed for trypsin delivery and installed on the Chambered coverglass.  
694 Images of bead positions were acquired using Plan-Apochrome 40X/1.30 oil objective as follows:  
695 Images with force were acquired with 2-min interval leading to a 12-min observation time (stress  
696 images) and one image was acquired without force (reference image) taken after NCC have detached  
697 by trypsinization and no longer exerting forces on the substrate. Confocal stress and reference images  
698 were aligned using a Matlab<sup>®</sup> script. The gel deformation was measured by the PIV (Particle image  
699 velocimetry) technique using the ImageJ plug-in PIV to get the bead displacement field. Finally, the  
700 ImageJ plug-in FTTC (Fourier Transform traction cytometry) was used to measure the traction force,  
701 exerted by NCC and responsible of PAA gel deformation and bead displacement (Martiel et al.,  
702 2015). The number of NCC in the traction force field was measured by counting NCC nucleus stained  
703 with NucSpot<sup>®</sup> Live 650 and a confocal image was generated before starting TFM measurements.  
704 The stress taken into account is the mean stresses calculated from 6 couples of reference-stress image  
705 corresponding to 2, 4, 6, 8, 10 and 12 minutes TFM assessments. It was observed that between 2 and  
706 12 minutes calculated stress was almost constant. The stress per cell is the stress divided by the  
707 number of nuclei. The force per cell was calculated by multiplying the stress/cell by the area of the  
708 interrogation window used in the PIV.

709

### 710 **Energy estimation**

711 We estimated produced energy during NCC displacement on soft and stiff gels by calculating the  
712 product of the average force F obtained by TFM and the average displacement D per hour obtained  
713 by video microscopy tracking during the time frame of TFM studies. S.D. of the product F by D was  
714 calculated based on the following formula (Goodman, 1960):  $\sigma(F \times D) = \sqrt{(\sigma(F))^2 + (\sigma(D))^2 +$   
715  $(E(D))^2 + (\sigma(F))^2 + (\sigma(F))^2 + (\sigma(D))^2}$ , with  $\sigma$  the S.D. and E(F) and E(D) mean  
716 value of F and D respectively, assuming F and D with normal distribution. To evaluate the statistical  
717 significance of two energy values, i.e.,  $m_1 \pm \sigma_1$  and  $m_2 \pm \sigma_2$ , we calculated Student's *t* and degrees  
718 of freedom,  $n_1 + n_2 - 2$ , assuming  $n_1 = n_2 = 5$  for size of  $m_1$  and  $m_2$ , to obtain *p* values. For this,

719 we considered  $t = \frac{|m_1 - m_2|}{\sqrt{\frac{\sigma_1^2}{n_1} + \frac{\sigma_2^2}{n_2}}}$ , and  $\sigma$  common S.D, given by  $\sigma^2 = \frac{(n_1 - 1) \cdot \sigma_1^2 + (n_2 - 1) \cdot \sigma_2^2}{n_1 + n_2 - 2}$ .

720

## 721 **Statistical Methods**

722 Statistical analyses were performed using Prism 7 (GraphPad). Unless specified, multiple  
723 comparisons were done respective to the control in the same experimental conditions. For statistical  
724 analysis of data we used One-way ANOVA parametric test after the validation of normality and  
725 equality of variances using Shapiro-Wilk and Brown-Forsythe methods, respectively. Otherwise,  
726 non-parametric Krustal-Wallis test was used. For comparison between two conditions we use  
727 unpaired t-test two-tailed test after the validation of normality and equality of using Shapiro-Wilk  
728 and equality of variances. Otherwise, non-parametric Mann-Whitney test was used. For statistical  
729 analysis of qPCR results, the data obtained for each drug or nutrient condition were compared to that  
730 of the control medium using unpaired t-test two-tailed test. Unless specified, at least three  
731 independent experiments were carried out for each procedure. Each NT explants was considered as  
732 an individual sample. The n of samples analyzed is indicated in each graph. Data are expressed as  
733 mean values  $\pm$  S.D. or S.E.M and the P values are \*  $p < 0.05$ , \*\*  $p < 0.01$ ; \*\*\*  $p < 0.001$ ; \*\*\*\*  $p <$   
734  $0.0001$ . Results are considered statistically significantly different when  $p < 0.05$ .

735

## 736 **REFERENCES**

- 737 **Barriga, E. H. and Mayor, R.** (2019). Adjustable viscoelasticity allows for efficient collective cell  
738 migration. *Semin Cell Dev Biol* **93**, 55-68.
- 739 **Ben Bouali, A., Montebault, A., David, L., Von Boxberg, Y., Viallon, M., Hamdi, B., Nothias, F.,**  
740 **Fodil, R. and F  r  ol, S.** (2020). Nanoscale mechanical properties of chitosan hydrogels as revealed by AFM.  
741 *Prog Biomater* **9**, 187-201.
- 742 **Bhattacharya, D., Azambuja, A. P. and Simoes-Costa, M.** (2020). Metabolic reprogramming  
743 promotes neural crest migration via Yap/Tead signaling. *Dev Cell* **53**, 199-211.e6.
- 744 **Bigarella, C. L., Liang, R. and Ghaffari, S.** (2014). Stem cells and the impact of ROS signaling.  
745 *Development* **141**, 4206-18.
- 746 **Bilodeau, G. G.** (1992). Regular pyramid punch problem. *J Appl Mech* **59**, 519-523.
- 747 **Bronner, M.** (2018). Riding the crest for 150 years! *Dev Biol* **444 Suppl 1**, S1-s2.
- 748 **Burstyn-Cohen, T. and Kalcheim, C.** (2002). Association between the cell cycle and neural crest  
749 delamination through specific regulation of G1/S transition. *Develop. Cell* **3**, 383-395.
- 750 **Chevalier, N. R., Gazquez, E., Bidault, L., Guilbert, T., Vias, C., Vian, E., Watanabe, Y., Muller, L.,**  
751 **Germain, S., Bondurand, N. et al.** (2016). How tissue mechanical properties affect enteric neural crest cell  
752 Mmigration. *Sci Rep* **6**, 20927.

753 **Dady, A. and Duband, J. L.** (2017). Cadherin interplay during neural crest segregation from the non-  
754 neural ectoderm and neural tube in the early chick embryo. *Dev Dyn* **246**, 550-565.

755 **Discher, D. E., Janmey, P. and Wang, Y. L.** (2005). Tissue cells feel and respond to the stiffness of  
756 their substrate. *Science* **310**, 1139-43.

757 **Duband, J. L.** (2010). Diversity in the molecular and cellular strategies of epithelium-to-  
758 mesenchyme transitions: Insights from the neural crest. *Cell Adh Migr* **4**, 458-82.

759 **Duband, J. L., Dady, A. and Fleury, V.** (2015). Resolving time and space constraints during neural  
760 crest formation and delamination. *Curr Top Dev Biol* **111**, 27-67.

761 **Duband, J. L., Nekooie-Marnany, N. and Dufour, S.** (2020). Establishing primary cultures of trunk  
762 neural crest cells. *Curr Protoc Cell Biol* **88**, e109.

763 **Dupin, E., Calloni, G. W., Coelho-Aguiar, J. M. and Le Douarin, N. M.** (2018). The issue of the  
764 multipotency of the neural crest cells. *Dev Biol* **444 Suppl 1**, S47-S59.

765 **Feng, J., Li, J., Wu, L., Yu, Q., Ji, J., Wu, J., Dai, W. and Guo, C.** (2020). Emerging roles and the  
766 regulation of aerobic glycolysis in hepatocellular carcinoma. *J Exp Clin Cancer Res* **39**, 126.

767 **Genuth, M. A., Allen, C. D. C., Mikawa, T. and Weiner, O. D.** (2018). Chick cranial neural crest cells  
768 use progressive polarity refinement, not contact inhibition of locomotion, to guide their migration. *Dev Biol*  
769 **444 Suppl 1**, S252-s261.

770 **Goodman, L. A.** (1960). On the exact variance of products. *J Am Statist Ass* **55**, 708-713.

771 **Gu, W., Gaeta, X., Sahakyan, A., Chan, A. B., Hong, C. S., Kim, R., Braas, D., Plath, K., Lowry, W. E.**  
772 **and Christofk, H. R.** (2016). Glycolytic metabolism plays a functional role in regulating human pluripotent  
773 stem cell state. *Cell Stem Cell* **19**, 476-490.

774 **Herrero-Mendez, A., Almeida, A., Fernández, E., Maestre, C., Moncada, S. and Bolaños, J. P.**  
775 (2009). The bioenergetic and antioxidant status of neurons is controlled by continuous degradation of a key  
776 glycolytic enzyme by APC/C-Cdh1. *Nat Cell Biol* **11**, 747-52.

777 **Hu, N., Strobl-Mazzulla, P. H. and Bronner, M. E.** (2014). Epigenetic regulation in neural crest  
778 development. *Dev Biol* **396**, 159-68.

779 **Ito, K. and Suda, T.** (2014). Metabolic requirements for the maintenance of self-renewing stem  
780 cells. *Nat Rev Mol Cell Biol* **15**, 243-56.

781 **Iyer, N. V., Kotch, L. E., Agani, F., Leung, S. W., Laughner, E., Wenger, R. H., Gassmann, M.,**  
782 **Gearhart, J. D., Lawler, A. M., Yu, A. Y. et al.** (1998). Cellular and developmental control of O<sub>2</sub> homeostasis  
783 by hypoxia-inducible factor 1 alpha. *Genes Dev* **12**, 149-62.

784 **Johnson, M. T., Mahmood, S. and Patel, M. S.** (2003). Intermediary metabolism and energetics  
785 during murine early embryogenesis. *J Biol Chem* **278**, 31457-60.

786 **Kaelin, W. G., Jr. and McKnight, S. L.** (2013). Influence of metabolism on epigenetics and disease.  
787 *Cell* **153**, 56-69.

788 **Kerosuo, L. and Bronner, M. E.** (2016). cMyc regulates the size of the premigratory neural crest  
789 stem cell pool. *Cell Rep* **17**, 2648-2659.

790 **Khacho, M., Clark, A., Svoboda, D. S., Azzi, J., MacLaurin, J. G., Meghaizel, C., Sesaki, H., Lagace, D.**  
791 **C., Germain, M., Harper, M. E. et al.** (2016). Mitochondrial dynamics impacts stem cell identity and fate  
792 decisions by regulating a nuclear transcriptional program. *Cell Stem Cell* **19**, 232-247.

793 **Khacho, M. and Slack, R. S.** (2017). Mitochondrial activity in the regulation of stem cell self-renewal  
794 and differentiation. *Curr Opin Cell Biol* **49**, 1-8.

795 **Kulesa, P. M. and Fraser, S. E.** (1998). Neural crest cell dynamics revealed by time-lapse video  
796 microscopy of whole embryo chick explant cultures. *Dev Biol* **204**, 327-44.

797 **Lempradl, A., Pospisilik, J. A. and Penninger, J. M.** (2015). Exploring the emerging complexity in  
798 transcriptional regulation of energy homeostasis. *Nat Rev Genet* **16**, 665-81.

799 **Li, Y., Vieceli, F. M., Gonzalez, W. G., Li, A., Tang, W., Lois, C. and Bronner, M. E.** (2019). In vivo  
800 quantitative imaging provides insights into trunk neural crest migration. *Cell Rep* **26**, 1489-1500 e3.

801 **Lukoseviciute, M., Gavriouchkina, D., Williams, R. M., Hochgreb-Hagele, T., Senanayake, U.,**  
802 **Chong-Morrison, V., Thongjuea, S., Repapi, E., Mead, A. and Sauka-Spengler, T.** (2018). From pioneer to  
803 repressor: bimodal Foxd3 activity dynamically remodels neural crest regulatory landscape in vivo. *Dev Cell*  
804 **47**, 608-628.e6.

805 **Martiel, J.-L., Leal, A., Kurzawa, L., Balland, M., Wang, I., Vignaud, T., Tseng, Q. and Théry, M.**  
806 (2015). Measurement of cell traction forces with ImageJ. *Methods Cell Biol* **125**, 269-287.

807 **Martik, M. L. and Bronner, M. E.** (2017). Regulatory logic underlying diversification of the neural  
808 crest. *Trends Genet* **33**, 715-727.

809 **Miyazawa, H. and Aulehla, A.** (2018). Revisiting the role of metabolism during development.  
810 *Development* **145**.

811 **Morriss, G. M. and New, D. A.** (1979). Effect of oxygen concentration on morphogenesis of cranial  
812 neural folds and neural crest in cultured rat embryos. *J Embryol Exp Morphol* **54**, 17-35.

813 **Nieto, M. A.** (2002). The Snail superfamily of zinc-finger transcription factors. *Nat. Rev. Mol. Cell*  
814 *Biol.* **3**, 155-166.

815 **Oginuma, M., Moncuquet, P., Xiong, F., Karoly, E., Chal, J., Guevorkian, K. and Pourquie, O.**  
816 (2017). A gradient of glycolytic activity coordinates FGF and Wnt signaling during elongation of the body  
817 axis in amniote embryos. *Dev Cell* **40**, 342-353 e10.

818 **Patra, K. C. and Hay, N.** (2014). The pentose phosphate pathway and cancer. *Trends Biochem Sci*  
819 **39**, 347-54.

820 **Pavlova, N. N. and Thompson, C. B.** (2016). The emerging hallmarks of cancer metabolism. *Cell*  
821 *Metab* **23**, 27-47.

822 **Perestrelo, T., Correia, M., Ramalho-Santos, J. and Wirtz, D.** (2018). Metabolic and mechanical  
823 cues regulating pluripotent stem cell fate. *Trends Cell Biol* **28**, 1014-1029.

824 **Ridenour, D. A., McLennan, R., Teddy, J. M., Semerad, C. L., Haug, J. S. and Kulesa, P. M.** (2014).  
825 The neural crest cell cycle is related to phases of migration in the head. *Development* **141**, 1095-103.

826 **Rovasio, R. A., Delouee, A., Yamada, K. M., Timpl, R. and Thiery, J. P.** (1983). Neural crest cell  
827 migration: requirements for exogenous fibronectin and high cell density. *J Cell Biol* **96**, 462-73.

828 **Salazar-Roa, M. and Malumbres, M.** (2017). Fueling the cell division cycle. *Trends Cell Biol* **27**, 69-  
829 81.

830 **Sánchez-Aragó, M., García-Bermúdez, J., Martínez-Reyes, I., Santacatterina, F. and Cuezva, J. M.**  
831 (2013). Degradation of IF1 controls energy metabolism during osteogenic differentiation of stem cells.  
832 *EMBO Rep* **14**, 638-44.

833 **Santiago, A. and Erickson, C. A.** (2002). Ephrin-B ligands play a dual role in the control of neural  
834 crest cell migration. *Development* **129**, 3621-32.

835 **Schell, J. C., Wisidagama, D. R., Bensard, C., Zhao, H., Wei, P., Tanner, J., Flores, A., Mohlman, J.,  
836 Sorensen, L. K., Earl, C. S. et al.** (2017). Control of intestinal stem cell function and proliferation by  
837 mitochondrial pyruvate metabolism. *Nat Cell Biol* **19**, 1027-1036.

838 **Schock, E. N. and LaBonne, C.** (2020). Sorting Sox: Diverse roles for Sox transcription factors during  
839 neural crest and craniofacial development. *Front Physiol* **11**, 606889.

840 **Schwarz, Q., Maden, C. H., Vieira, J. M. and Ruhrberg, C.** (2009). Neuropilin 1 signaling guides  
841 neural crest cells to coordinate pathway choice with cell specification. *Proc Natl Acad Sci U S A* **106**, 6164-9.

842 **Scully, D., Keane, E., Batt, E., Karunakaran, P., Higgins, D. F. and Itasaki, N.** (2016). Hypoxia  
843 promotes production of neural crest cells in the embryonic head. *Development* **143**, 1742-52.

844 **Semenza, G. L.** (2012). Molecular mechanisms mediating metastasis of hypoxic breast cancer cells.  
845 *Trends Mol Med* **18**, 534-43.

846 **Shellard, A. and Mayor, R.** (2021). Collective durotaxis along a self-generated stiffness gradient in  
847 vivo. *Nature* **600**, 690-694.

848 **Shyh-Chang, N., Daley, G. Q. and Cantley, L. C.** (2013). Stem cell metabolism in tissue development  
849 and aging. *Development* **140**, 2535-47.

850 **Simões-Costa, M. and Bronner, M. E.** (2015). Establishing neural crest identity: a gene regulatory  
851 recipe. *Development* **142**, 242-57.

852 **Simões-Costa, M. S., McKeown, S. J., Tan-Cabugao, J., Sauka-Spengler, T. and Bronner, M. E.**  
853 (2012). Dynamic and differential regulation of stem cell factor FoxD3 in the neural crest is Encrypted in the  
854 genome. *PLoS Genet* **8**, e1003142.

855 **Soldatov, R., Kaucka, M., Kastri, M. E., Petersen, J., Chontorotzea, T., Englmaier, L., Akkuratova,**  
856 **N., Yang, Y., Haring, M., Dyachuk, V. et al. (2019).** Spatiotemporal structure of cell fate decisions in murine  
857 neural crest. *Science* **364**.

858 **Takubo, K., Nagamatsu, G., Kobayashi, C. I., Nakamura-Ishizu, A., Kobayashi, H., Ikeda, E., Goda,**  
859 **N., Rahimi, Y., Johnson, R. S., Soga, T. et al. (2013).** Regulation of glycolysis by Pdk functions as a metabolic  
860 checkpoint for cell cycle quiescence in hematopoietic stem cells. *Cell Stem Cell* **12**, 49-61.

861 **Théveneau, E., Duband, J.-L. and Altabef, M. (2007).** Ets-1 confers cranial features on neural crest  
862 delamination. *PLoS ONE* **2**, e1142.

863 **Thiery, J. P., Duband, J.-L. and Delouvé, A. (1982).** Pathways and mechanism of avian trunk neural  
864 crest cell migration and localization. *Develop. Biol.* **93**, 324-343.

865 **Trainor, P. (2013).** Neural Crest Cells: Evolution, Development and Disease: Elsevier.

866 **Tucker, G. C., Aoyama, H., Lipinski, M., Tursz, T. and Thiery, J. P. (1984).** Identical reactivity of  
867 monoclonal antibodies HNK-1 and NC-1: Conservation in vertebrates on cells derived from the neural  
868 primordium and on some leukocytes. *Cell Diff.* **14**, 223-230.

869 **Vander Heiden, M. G., Cantley, L. C. and Thompson, C. B. (2009).** Understanding the Warburg  
870 effect: the metabolic requirements of cell proliferation. *Science* **324**, 1029-33.

871 **Zanotelli, M. R., Zhang, J. and Reinhart-King, C. A. (2021).** Mechanoresponsive metabolism in  
872 cancer cell migration and metastasis. *Cell Metab* **33**, 1307-1321.

873 **Zhang, J., Khvorostov, I., Hong, J. S., Oktay, Y., Vergnes, L., Nuebel, E., Wahjudi, P. N., Setoguchi,**  
874 **K., Wang, G., Do, A. et al. (2011).** UCP2 regulates energy metabolism and differentiation potential of  
875 human pluripotent stem cells. *Embo j* **30**, 4860-73.

876 **Zhang, J., Zhao, J., Dahan, P., Lu, V., Zhang, C., Li, H. and Teitell, M. A. (2018).** Metabolism in  
877 pluripotent stem cells and early mammalian development. *Cell Metab* **27**, 332-338.

878 **Zhu, J. and Thompson, C. B. (2019).** Metabolic regulation of cell growth and proliferation. *Nat Rev*  
879 *Mol Cell Biol* **20**, 436-450.

880

881

## 882 **ACKNOWLEDGMENTS**

883 We deeply thank Chantal Thibert and Sakina Torch for providing advice in cellular metabolism and  
884 critical reading of the manuscript and Frédéric Relaix for constant support. Special thanks to Olivier  
885 Pourquié and Masayuki Oginuma for providing cDNA probes for chicken glycolytic enzymes. We  
886 thank Xavier Decrouy and the IMRB imaging platform.

887

888 **FUNDING**

889 This work was supported by funding from INSERM, Université Paris-Est Créteil, AAP IMRB cross-  
890 teams project, and Fondation ARC (No. PJA 20181207844). Marine Depp was funded by CDE  
891 contract of ANR-12-BSV2-0019. Nioosha Nekooie-Marnany was funded by doctoral fellowship of  
892 Université Paris-Est Créteil and by the Labex REVIVE during the last year of her Ph.D.

893

894 **AUTHOR CONTRIBUTIONS**

895 Nioosha Nekooie-Marnany performed experiments, analyzed data and contributed to the manuscript  
896 Redouane Fodil provided expertise in biomechanics and performed experiments for AFM and TFM  
897 Sophie Féréol provided expertise in biomechanics and prepared the PAA gels. Marine Depp  
898 performed NCC primary culture experiments. Roberta Foresti and Roberto Motterlini provided  
899 expertise in cellular metabolism and Seahorse technology and revised the manuscript. Jean-Loup  
900 Duband conceived and designed the experimental approach, performed experiments, analyzed the  
901 data, and wrote the manuscript. Sylvie Dufour conceived and designed the experimental approach.  
902 performed experiments, analyzed the data, and contributed to the manuscript.

903

904 **COMPETING INTERESTS**

905 The authors declare no competing financial interests.

906

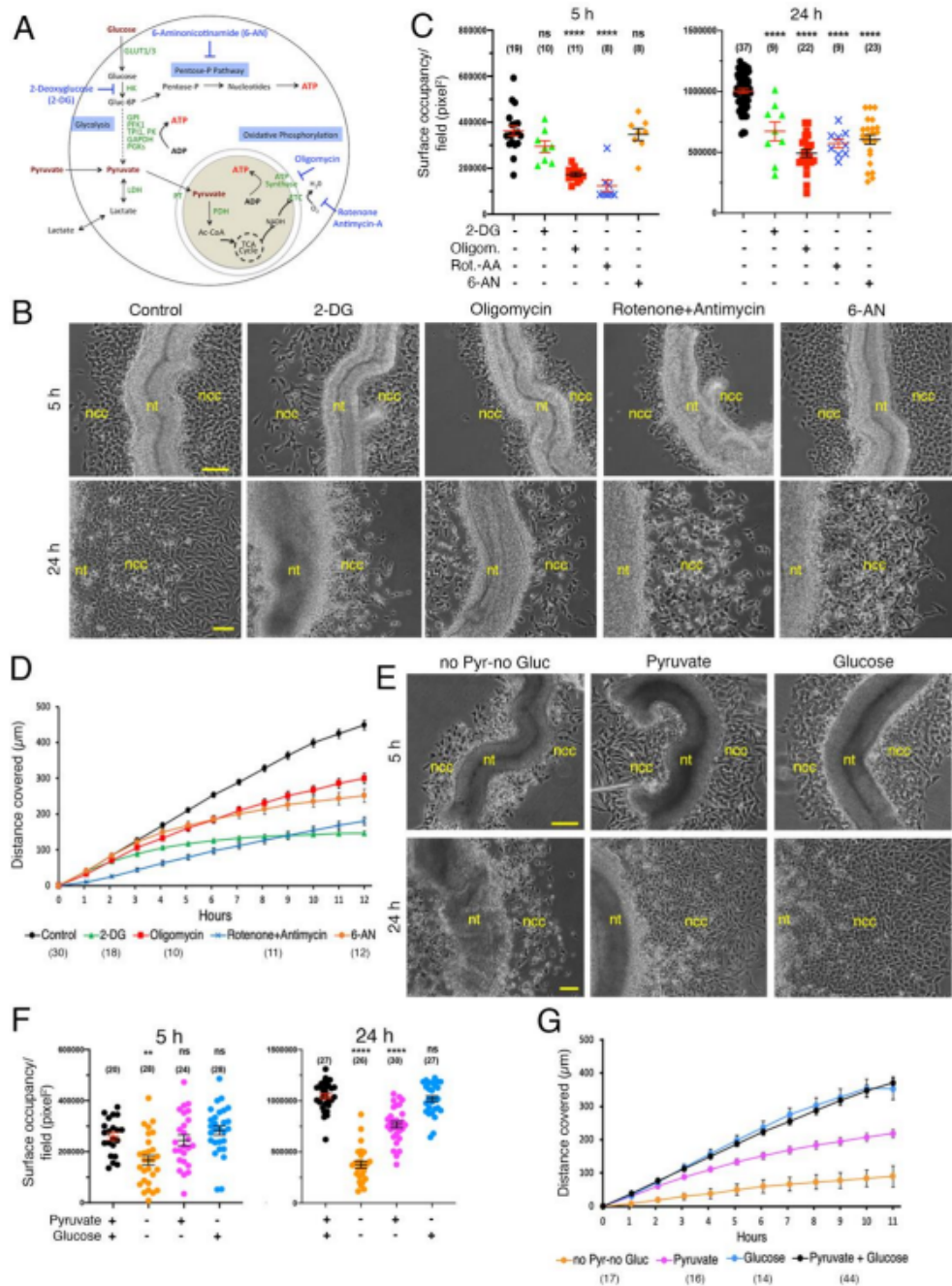


Figure 1: Nekooie-Marnany et al.

909 **Fig. 1. Multiple metabolic pathways are mobilized during trunk NCC dispersion.**  
910 (A) Schematic representation of the main pathways of glucose and pyruvate metabolism indicating  
911 the specific targets of the respective inhibitors of glycolysis (2-DG), ATP synthase (oligomycin),  
912 complex I and III of the electron transport chain (Rot-AA), and PPP (6-AN). (B-G) Effect of  
913 metabolic inhibitors (B-D) and of nutrients on NCC dispersion (E-G): (B, E) Overall aspect of NT  
914 explants; (C, F) NCC outgrowth area; (D, G) Progression of the migratory front of the NCC  
915 population over time. Bars in B and E = 100  $\mu$ m. Error bars = S.E.M.  
916

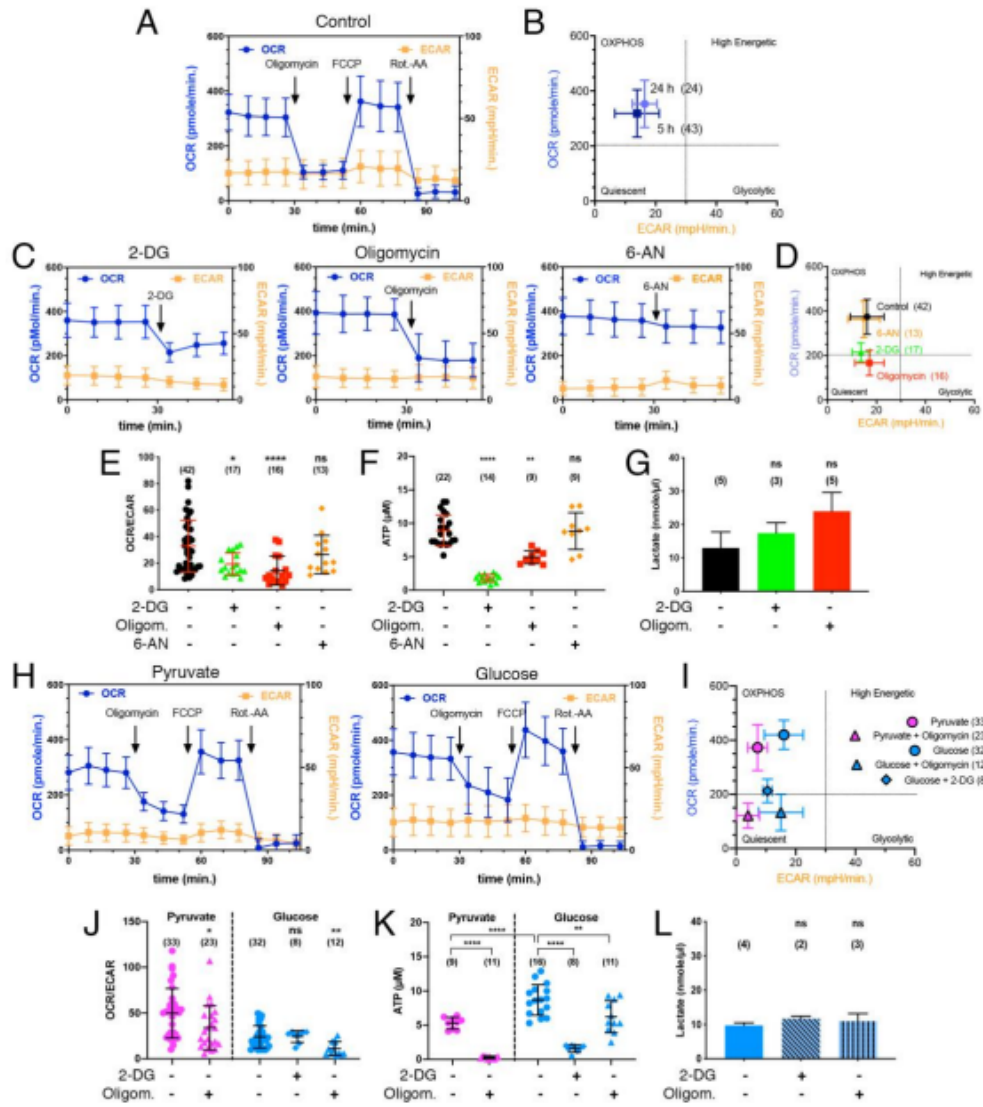


Figure 2: Nekooie-Marnany et al.

918 **Fig. 2. Metabolic profiling of NCC reveals a typical OXPHOS signature during migration.**  
919 Quantitation analyses of O<sub>2</sub> consumption rate (OCR) and extracellular acidification rate (ECAR)  
920 using a Seahorse analyzer, and ATP and lactate productions in individual NT explants cultured for 5  
921 h (and 24 h in B) in control medium after treatment with metabolic inhibitors, and in different  
922 nutrients: (A, H) MitoStress assays; (B, D, I) Energetic maps deduced from OCR and ECAR  
923 measurements; (C) OCR and ECAR profiles over time in explants cultured in control medium in the  
924 presence of metabolic inhibitors; (E, J) Values of OCR/ECAR ratio; (F, K) Intracellular ATP  
925 measurement; (G, L) Extracellular lactate measurement. Error bars = S.D.  
926

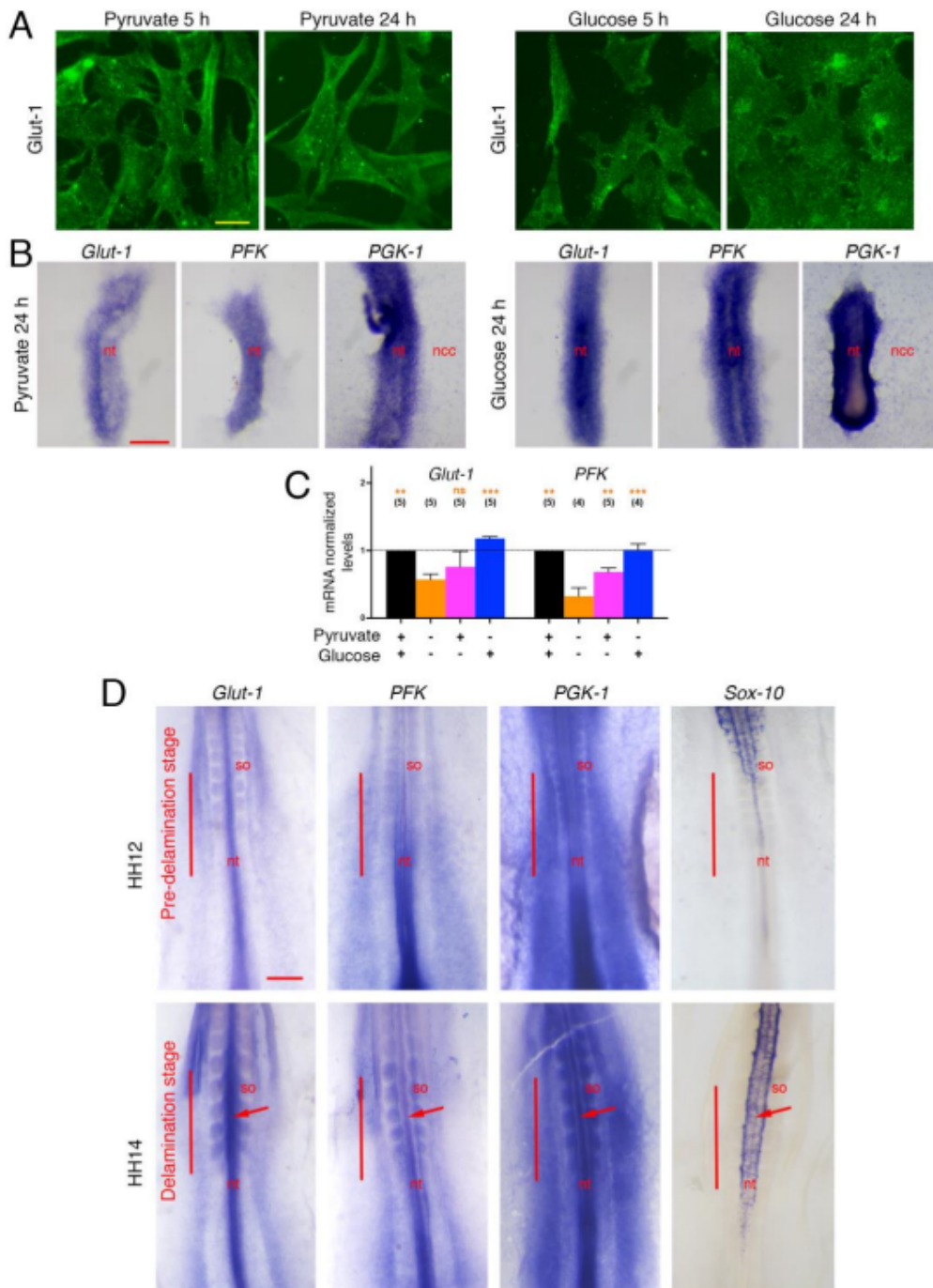


Figure 3: Nekooie-Marnany et al.

928 **Fig. 3. Expressions of glucose transporter and glycolytic enzymes are regulated at the time of**  
929 **NCC migration.**

930 (A-C) Immunostaining (A), in situ hybridization (B), and qPCR (C) analyses of the expression of the  
931 glucose transporter *Glut-1* and of glycolytic enzymes *PFK* and *PGK-1* in NCC and NT explants. (D)  
932 Whole mount in situ hybridization for *Glut-1*, *PFK*, and *PGK-1* and for the migratory NCC marker  
933 *Sox-10* in avian embryos at stage HH12 and 14 (i.e. 17 and 22 somites, respectively), showing the  
934 caudal part of the embryo at the level of the last formed somites (so) and of the unsegmented  
935 mesoderm. The bars indicate the axial levels at which NCC are in the pre-delamination stage at HH12  
936 and in the delamination stage at HH14. Arrows point at the strong staining for *Glut-1*, *PFK*, and *PGK-*  
937 *1* in the NT at levels of delaminating NCC, contrasting with the fainter NT staining in regions of pre-  
938 delaminating NCC. Bars in A = 10  $\mu\text{m}$ , in B = 100  $\mu\text{m}$ , and in D = 200  $\mu\text{m}$ . In C, comparisons were  
939 done respective to the no nutrient condition. Error bars = S.E.M.  
940

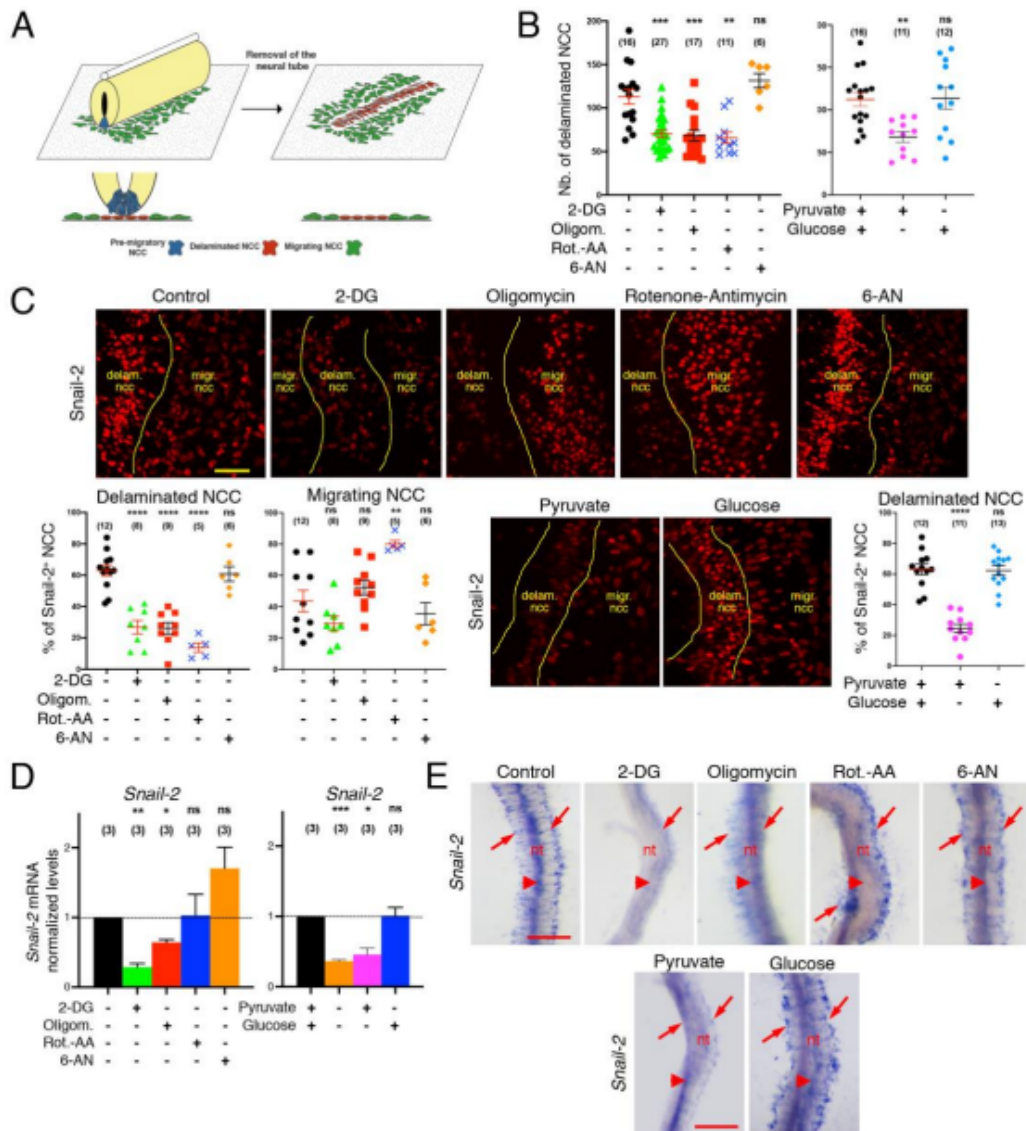


Figure 4: Nekoioie-Marnany et al.

942 **Fig. 4. Glucose metabolism regulates *Snail-2* expression during NCC delamination.**  
943 (A) Schematic representation of the delamination assay. (B, C) Effect of metabolic inhibitors and of  
944 nutrient supplies on the number of delaminated cells per explant (B) and expression of the *Snail-2*  
945 transcription factor (C) in delaminated vs. migrating NCC. (D, E) qPCR (D) and in situ hybridization  
946 (E) analyses of *Snail-2* expression in NT explants. In control medium, in the presence of 6-AN or  
947 with glucose, *Snail-2* messages are distributed in premigratory NCC in the dorsal NT (E, arrowheads)  
948 as well as in the delaminated NCC visible in either sides of the NT (E, arrows). In the presence of 2-  
949 DG, oligomycin, and in pyruvate medium, *Snail-2* is much decreased in both premigratory and  
950 migratory NCC while in the presence of Rot-AA, it drops only in premigratory cells. Bars in C = 50  
951  $\mu\text{m}$  and E = 100  $\mu\text{m}$ . Error bars = S.E.M.  
952

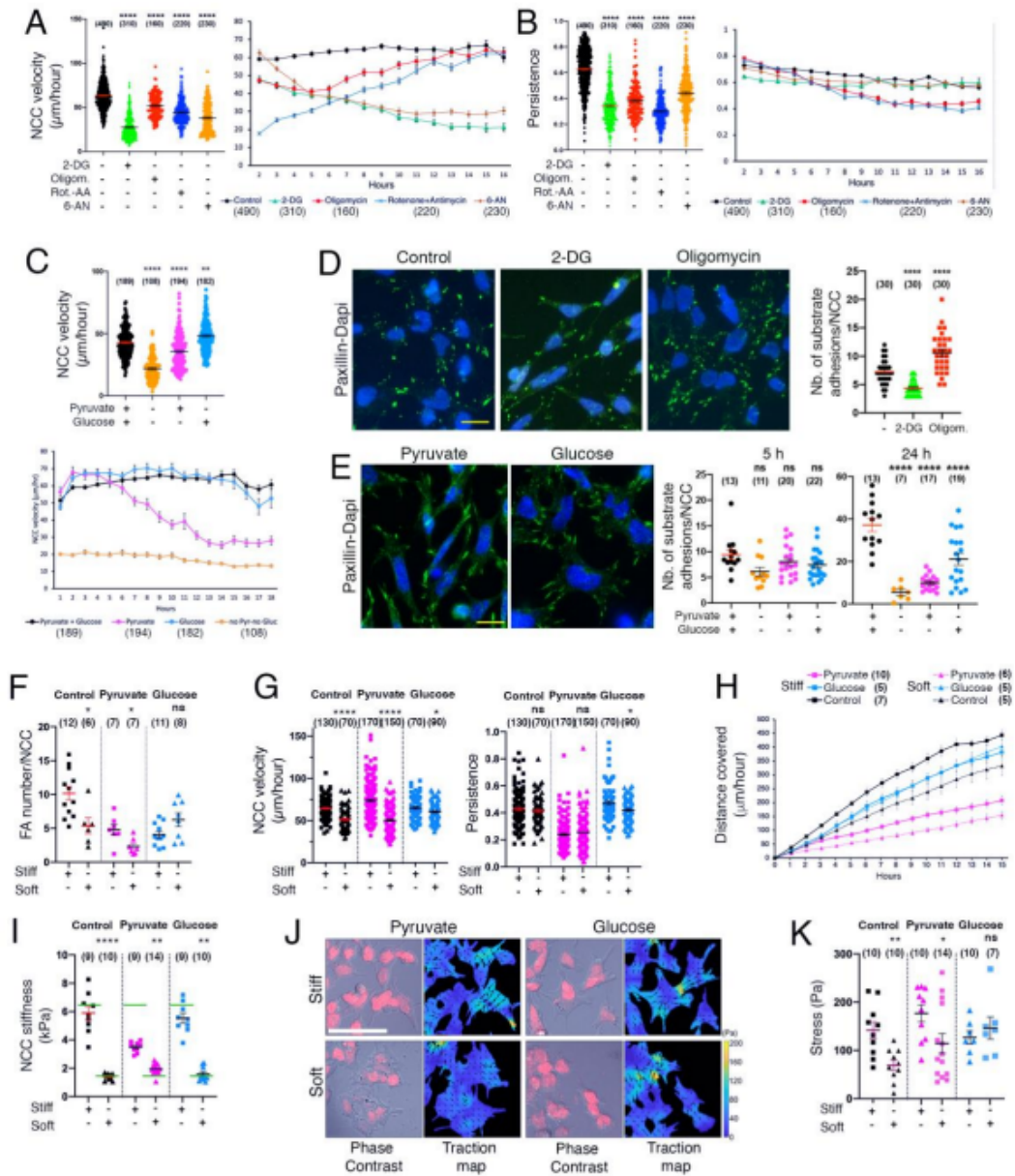


Figure 5: Nekoioie-Marnany et al.

954 **Fig. 5. Glucose metabolism is crucial for NCC locomotion and regulates NCC adhesion and**  
955 **mechanical properties and response to External Stiffness.**

956 (A-E) Effect of metabolic inhibitors and of nutrient supplies on NCC locomotion. (A, C) Velocity of  
957 individual NCC throughout the duration of the video microscopy recording and variation of NCC  
958 velocity over time in culture. (B) Persistence of migration of individual NCC throughout the duration  
959 of the video microscopy recording and variation of the persistence over time in culture. (D) Effect of  
960 metabolic inhibitors and (E) of nutrients on NCC substrate adhesion. Visualization of paxillin (green)  
961 and Dapi (blue) expression and quantification of the number of substrate adhesions in migrating NCC.  
962 (F-H) Effect of nutrient supplies on NCC adhesion and migration on stiff and soft gels in 5-h cultures.  
963 (F) Quantification of substrate/focal adhesions (FA) number per NCC. (G-H) Cell locomotion;  
964 velocity (G, left panel) and persistence of migration (G, right panel) of individual NCC throughout  
965 the duration of the video microscopy recording. (H) Progression of the migratory front of the NCC  
966 population over time. (I-K) Effect of nutrient supplies on NCC mechanical properties. (I) NCC  
967 stiffness on stiff and soft gels. The green bars indicate the stiffness of the gels. (J) Phase contrast and  
968 traction map images. (K) Traction activity of NCC expressed as stress per NCC. Bars in D, E = 20  
969  $\mu\text{m}$ , and in J = 50  $\mu\text{m}$ . Error bars = S.E.M.

970

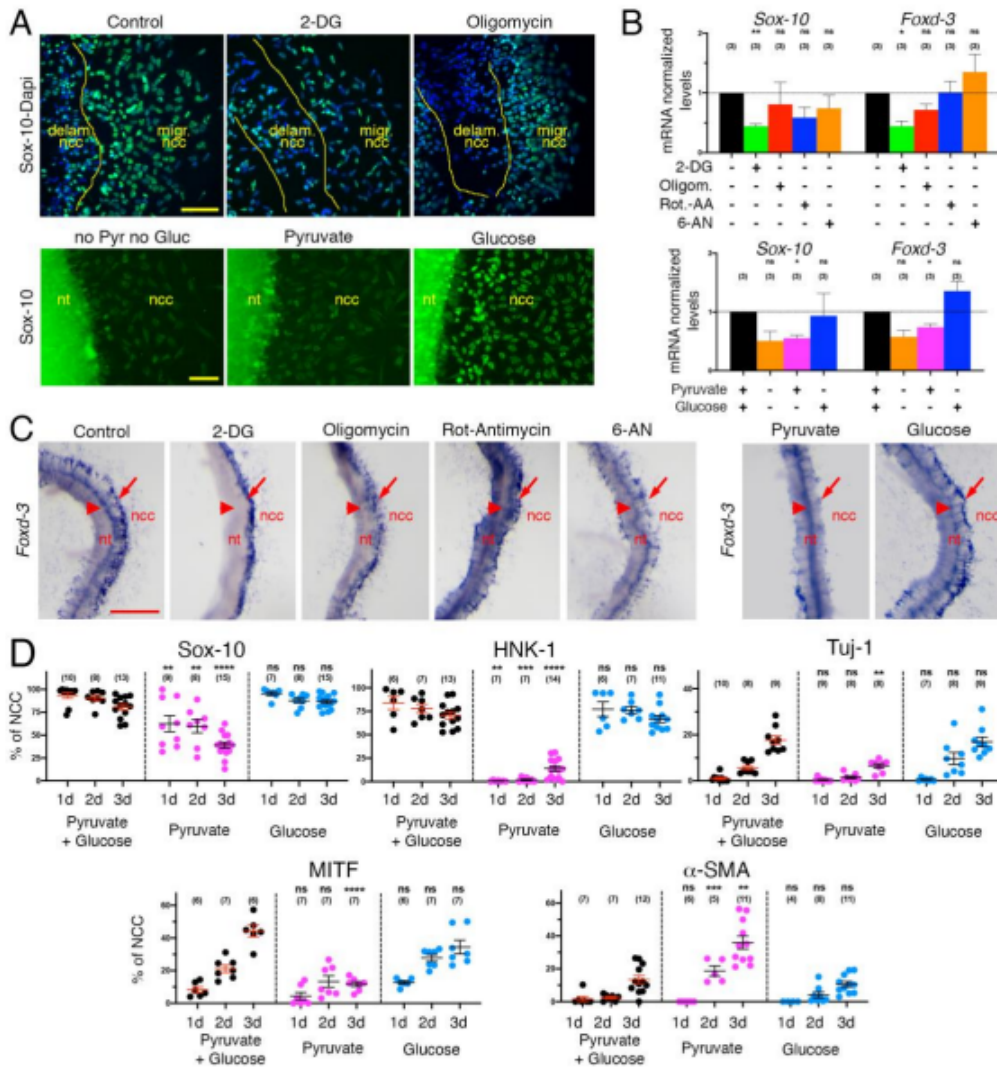


Figure 6: Nekoioie-Marnany et al.

972 **Fig. 6. Glucose metabolism and nutrients supply regulate NCC pluripotency and fate decisions.**  
973 Immunostaining for Sox-10 (A), qPCR (B), and in situ hybridization (C) analyses of the expression  
974 of *Sox-10* and *Foxd-3* transcripts in delaminating and migrating NCC after 5 h. In A, nuclei are  
975 visualized with Dapi. In control and glucose medium, *Foxd-3* messages are distributed in  
976 premigratory NCC in the dorsal NT (C, arrowheads) as well as in the delaminated cells visible in  
977 either sides of the NT (C, arrows) similar to that of *Snail-2*. In 2-DG and oligomycin, it is decreased  
978 essentially in premigratory cells whereas in pyruvate medium it is reduced only in delaminating cells.  
979 (D) Quantification of the proportion of Sox-10<sup>+</sup>, HNK-1<sup>+</sup>, Tuj-1<sup>+</sup>, MITF<sup>+</sup>, and  $\alpha$ -SMA<sup>+</sup> cells in NCC  
980 primary cultures over time under different nutrient conditions. Bar in A = 50  $\mu$ m. Error bars = S.E.M.  
981 Bars in A = 50  $\mu$ m, and C = 100  $\mu$ m. Error bars = S.E.M.  
982

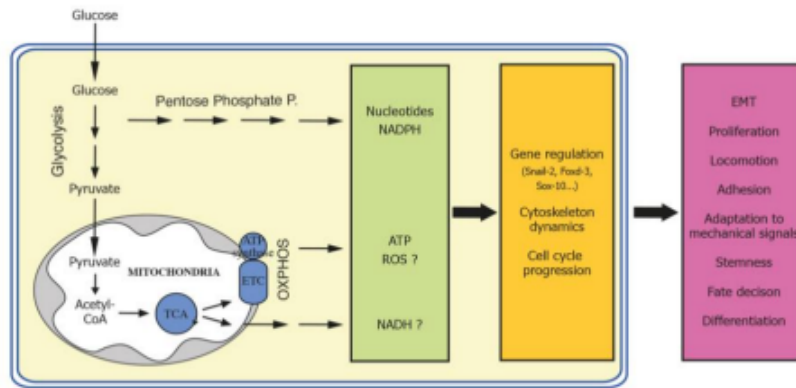


Figure 7: Nekooie-Marnany et al.

983

984 **Fig. 7. Schematic representation of the integration of carbon metabolism in NCC development.**

985 See discussion for details.

	Distance / h $\pm$ S.D. ( $\mu\text{m}$ )		Distance / h $\pm$ S.D. ( $\mu\text{m}$ )
Control (Stiff)	59.49 $\pm$ 7.50	Control (Soft)	47.14 $\pm$ 8.03
Pyruvate (Stiff)	52.11 $\pm$ 3.98	Pyruvate (Soft)	44.46 $\pm$ 1.61
Glucose (Stiff)	69.25 $\pm$ 9.89	Glucose (Soft)	53.27 $\pm$ 9.27
	Force / Cell $\pm$ S.D. (nN)		Force / Cell $\pm$ S.D. (nN)
Control (Stiff)	14.14 $\pm$ 5.41	Control (Soft)	6.90 $\pm$ 3.36
Pyruvate (Stiff)	17.62 $\pm$ 5.48	Pyruvate (Soft)	11.16 $\pm$ 7.25
Glucose (Stiff)	12.66 $\pm$ 3.56	Glucose (Soft)	14.59 $\pm$ 6.08
	Energy / h $\pm$ S.D. (pJ)		Energy / h $\pm$ S.D. (pJ)
Control (Stiff)	0.84 $\pm$ 0.34	Control (Soft)	0.33 $\pm$ 0.17
Pyruvate (Stiff)	0.92 $\pm$ 0.30	Pyruvate (Soft)	0.50 $\pm$ 0.32
Glucose (Stiff)	0.88 $\pm$ 0.28	Glucose (Soft)	0.78 $\pm$ 0.36

986

987 **Table I. Energy produced by NCC on soft and stiff gels in various nutrients.**

988 Energy (expressed in pJ per h) was calculated as the product of the average force/cell in nN  
 989 obtained by TFM and the average distance covered per hour in  $\mu\text{m}$ . P values for control, pyruvate  
 990 and glucose between stiff and soft gels are 0.016, 0.063 and 0.636, respectively.

991

## **Résumé:**

Le métabolisme en tant que clé de voûte du destin des cellules souches fournit non seulement des demandes d'énergie et de molécules précurseurs, mais joue également un rôle dans le remodelage de la chromatine. Dans les embryons de vertébrés, les cellules de la crête neurale (NC) constituent une population remarquable de progéniteurs embryonnaires qui, lors de la délamination du tube neural dorsal, d'une migration et d'une différenciation étendues, donnent lieu à des dérivés neuraux/neuronaux et mésenchymateux. Le potentiel de différenciation des cellules NC nécessite un remodelage épigénétique et des signaux environnementaux. En conséquence, l'intersection du métabolisme et de la plasticité NC fournira des informations essentielles sur la régulation de l'identité et du développement des cellules NC. Ainsi, j'avais l'intention de comprendre le rôle du métabolisme dans l'aspect développemental d'une sous-population de cellules NC, le tronc NC. La première partie de mon étude a abouti à une vision générale des impacts métaboliques sur toutes les étapes de développement de la CN. J'ai mis en évidence que l'oxydation du glucose est un profil métabolique essentiel régissant la délamination, l'adhésion, la migration, la prolifération, le maintien de la tige et la différenciation généralisée des NC. Compte tenu de l'incidence de la transition G1 / S sur l'EMT dans les cellules NC du tronc, l'inhibition de la voie des pentoses phosphates (PPP) n'a pas pu influencer la délamination NC, suggérant une adaptation métabolique pour maintenir les étapes de développement et la survie. Par conséquent, dans l'étape suivante, j'ai cherché à apprécier comment les voies métaboliques s'intègrent dans la délamination NC. Le recâblage de la voie de la glycolyse sous inhibition du PPP au stade de délaminage a fourni un support pour les voies métaboliques multiples recrutées par les progéniteurs NC en réponse au stress métabolique. Mon étude a également élucidé la reprogrammation métabolique du PPP à l'oxydation du glucose dans les cellules NC du tronc, alignée sur la délamination NC à la transition migratoire. De plus, outre le glucose, la glutamine joue un rôle de premier plan dans l'acquisition pluripotente et la délamination des progéniteurs NC qui déclenchent la localisation nucléaire de la glutaminase (GLS) lors de l'étape de délaminage. Par conséquent, la localisation nucléaire du GLS lors de la délamination des cellules NC pré-migratoires suggère la fonction de régulation du gène pour le GLS. Dans l'ensemble, mes résultats ont indiqué l'intersection du métabolisme et de la reprogrammation NC de l'étape pluripotente à l'engagement NC, définis respectivement par le PPP promu et la localisation nucléaire de GLS au phénotype OXPHOS à base de glucose avec localisation GLS cytoplasmique. De plus, l'interaction possible entre le GLS et la B-caténine a favorisé le nouveau concept sur la contribution du GLS à la signalisation Wnt, prometteuse pour comprendre l'étiologie de nombreuses neurocristopathies.

*Mots clés : cellules de la crête neurale, pluripotence, délaminage, métabolisme, glutaminase, OXPHOS, EMT*

## Summary

Metabolism as a keystone of stem cells' fate not only supplies demands for energy and precursor molecules but also has roles in chromatin remodeling. In vertebrate embryos, neural crest (NC) cells constitute a remarkable population of embryonic progenitors, which upon delamination from dorsal neural tube, extensive migration and differentiation give rise to both neural/neuronal and mesenchymal derivatives. The developmental potential of NC cells necessitates epigenetic remodeling and environmental cues. Accordingly, the intersection of metabolism and NC plasticity will provide critical insights into the regulation of NC cell identity and development. Thus, I intended to figure out the metabolism role in the developmental aspect of one sub-population of NC cells, trunk type. The first part of my study resulted in a general view of the metabolic impacts on all developmental NC steps. I evidenced that glucose oxidation is a pivotal metabolic profile governing NC delamination, adhesion, migration, proliferation, maintenance of stemness, and widespread differentiation. Given the incidence of G1/S transition upon EMT in trunk NC cells, the inhibition of pentose phosphate pathway (PPP) was unable to influence the NC delamination, suggesting a metabolic adaptation to maintain developmental steps and survival. Hence, In the next step, I sought to appreciate how metabolic pathways integrate into the NC delamination. The rewiring of glycolysis pathway under PPP suppression in delaminating stage provided support for multi metabolic pathways recruited by NC progenitors in response to the metabolic stress. My study also elucidated the metabolic reprogramming from PPP to glucose oxidation in trunk NC cells, aligned with delaminating to migratory transition of these cells. Additionally, besides glucose, glutamine had a prominent role in pluripotent acquisition and delamination of NC progenitors that triggers the nuclear localization of glutaminase (GLS) upon EMT step. Therefore, the nuclear GLS localization of pre-migratory NC cells in delaminating stage suggests the gene regulatory function for GLS. Altogether, my results indicated the intersection of metabolism and NC reprogramming from pluripotent step to the NC commitment, defined respectively by promoted PPP and nuclear localization of GLS to glucose based OXPHOS phenotype with cytoplasmic GLS localization. Moreover, the possible interaction between GLS and B-catenin fostered the new concept about the contribution of GLS to Wnt signaling, holding promise for understanding the etiology of many neurocristopathies.

*Key words: neural crest cells, pluripotency, delamination, metabolism, glutaminase, OXPHOS, EMT*

## Summary

Metabolism as a keystone of stem cells' fate not only supplies demands for energy and precursor molecules but also has roles in chromatin remodeling. In vertebrate embryos, neural crest (NC) cells constitute a remarkable population of embryonic progenitors, which upon delamination from dorsal neural tube, extensive migration and differentiation give rise to both neural/neuronal and mesenchymal derivatives. The developmental potential of NC cells necessitates epigenetic remodeling and environmental cues. Accordingly, the intersection of metabolism and NC plasticity will provide critical insights into the regulation of NC cell identity and development. Thus, I intended to figure out the metabolism role in the developmental aspect of one sub-population of NC cells, trunk type. The first part of my study resulted in a general view of the metabolic impacts on all developmental NC steps. I evidenced that glucose oxidation is a pivotal metabolic profile governing NC delamination, adhesion, migration, proliferation, maintenance of stemness, and widespread differentiation. Given the incidence of G1/S transition upon EMT in trunk NC cells, the inhibition of pentose phosphate pathway (PPP) was unable to influence the NC delamination, suggesting a metabolic adaptation to maintain developmental steps and survival. Hence, In the next step, I sought to appreciate how metabolic pathways integrate into the NC delamination. The rewiring of glycolysis pathway under PPP suppression in delaminating stage provided support for multi metabolic pathways recruited by NC progenitors in response to the metabolic stress. My study also elucidated the metabolic reprogramming from PPP to glucose oxidation in trunk NC cells, aligned with delaminating to migratory transition of these cells. Additionally, besides glucose, glutamine had a prominent role in pluripotent acquisition and delamination of NC progenitors that triggers the nuclear localization of glutaminase (GLS) upon EMT step. Therefore, the nuclear GLS localization of pre-migratory NC cells in delaminating stage suggests the gene regulatory function for GLS. Altogether, my results indicated the intersection of metabolism and NC reprogramming from pluripotent step to the NC commitment, defined respectively by promoted PPP and nuclear localization of GLS to glucose based OXPHOS phenotype with cytoplasmic GLS localization. Moreover, the possible interaction between GLS and B-catenin fostered the new concept about the contribution of GLS to Wnt signaling, holding promise for understanding the etiology of many neurocristopathies.

*Key words: neural crest cells, pluripotency, delamination, metabolism, glutaminase, OXPHOS, EMT*